Synthesis and characterization of poly(lactic acid) based antimicrobial bio-nanocomposites for potential food packaging applications

A Thesis

Submitted in partial fulfilment of the requirements for the award of the degree of

DOCTOR OF PHILOSOPHY

By

UDANGSHREE BORO

(Roll no. 166107027)

Department of Chemical Engineering

Indian Institute of Technology Guwahati

Guwahati-781039, India

April 2023

Dedicated

to

Almighty, my beloved parents and my loving husband for their endless love, support and encouragement

Department of Chemical Engineering
Indian Institute of Technology Guwahati

DECLARATION

The research work in this thesis entitled "**Synthesis and characterization of poly(lactic acid) based antimicrobial bio-nanocomposites for potential food packaging applications**" has been carried out by me in the Department of Chemical Engineering at Indian Institute of Technology Guwahati, as partial fulfilment for the award of Doctor of Philosophy under the supervision of Prof. Vijayanand S. Moholkar. The results reported in this thesis are achieved by me and has not been submitted to any other institute or university for the award of any degree or diploma.

I further declare that I have faithfully acknowledge and given credits to the research workers wherever their works have been cited in this thesis.

Udangshree Boro

Date: 28-04-2023

(Udangshree Boro)
Roll No: 166107027
Department of Chemical Engineering
Indian Institute of Technology Guwahati
Guwahati-781039, Assam, India

Department of Chemical Engineering
Indian Institute of Technology Guwahati

CERTIFICATE

It is certified that the work contained in thesis entitled "**Synthesis and characterization of poly(lactic acid) based antimicrobial bio-nanocomposites for potential food packaging applications**", by **Udangshree Boro (Roll No. 166107027)**, has been carried out under my supervision and this work has not been submitted either in whole or in part elsewhere for a degree.

Date:

Prof. V. S. Moholkar
HAG Professor, Department of Chemical Engineering
Indian Institute of Technology Guwahati
Guwahati-781039, Assam, India

ACKNOWLEDGEMENTS

With heartfelt gratitude, I express my special thanks to everyone who directly or indirectly helped me in my PhD work. I am really grateful to all of them.

Firstly, I would like to express my sincere gratitude to my thesis supervisor Prof. V. S. Moholkar, for his constant support, guidance and encouragement during my entire PhD time. I must acknowledge the unconditional freedom to think, plan, execute and express that I was given in every step of my research work while keeping faith and confidence in my capabilities. From him, I have learnt how to write a scientific article, which helped me in manuscript and thesis writing. Working under such a flexible, friendly, humble person like him has been a great privilege.

Secondly, I would like to thank my Doctoral Committee members Prof. G. Pugazhenthi, Prof. Pallab Ghosh, Department of Chemical Engineering, IIT Guwahati and Prof. S. Kanagaraj, Department of Mechanical Engineering, IIT Guwahati, for their continuous support, constructive criticism and valuable suggestions during my every progress evaluation seminar.

I express my sincere gratitude to the head, all faculty members and technical staff of the Chemical Engineering Department, IIT Guwahati, for providing all the research and analytical facilities required for my research work. I also want to sincerely thank all non-technical staff of the Chemical Engineering Department for their help and cooperation during this journey. I am indebted to CIF, Centre for the Environment and Centre for Sustainable Polymers, IIT Guwahati, for providing the necessary analytical facilities.

I was fortunate enough to have such friendly and helpful lab mates. My special thanks go to all my lab members, including seniors and juniors: Kajal, Bhaskar, Karan, Kuldeep, Aradhana, Pushpita, Komal, Umesh, Abhinash, Niharika, Maneesh, Arup, Neha, Shyamali, Amit for their help, support and timely assistance whenever I needed. I also thank my close friends inside and

outside the campus, Anjali, Rumi Rani, Pankaj, Pinky, Sumitra, Preetisagar, and Anusuya, who always supported and encouraged me during this journey.

Deep heartedly, I would like to thank my loving parents, supportive and caring husband, in-laws and all my family members for their unconditional love, faith and encouragement. Above all, I would like to thank the Almighty for the blessings he has bestowed on my life. He has always chosen for me the best things in life. He gives me mental strength in tough times and shows me the right path to overcome difficulties.

Udangshree Boro

Abstract

Biopolymers or biodegradable polymers have gained enormous attention worldwide as an alternative to synthetic plastic mainly due to their biodegradability, non-toxic, and renewable resources. Among different biopolymers, poly(lactic acid) (PLA) is the most widely used material in food packaging applications. This may be due to its high transparency, ease of processability, biocompatibility, easy availability, non-toxic nature and comparable physical properties with synthetic polymers such as polypropylene and polyethylene. Moreover, PLA is classified as GRAS (Generally Recognized as Safe) material by the US FDA (United States Food and Drug Administration). Unfortunately, like other biopolymers, PLA has limitations, such as poor thermal, mechanical, and barrier properties compared to synthetic non-degradable plastics. But, storage and transport of any product, especially food, requires a strong, tough material that can be able to withstand any harsh conditions encountered during transportation and storage. Moreover, packaging should preserve food quality, prolonging the product's shelf life. Hence, developing bio-nanocomposite materials containing antimicrobial nanoparticles and other additives is important to reduce environmental problems and maintain the freshness, quality and safety of food products which may get spoiled by food-borne pathogenic microorganisms.

Given the above, the present doctoral work aims to synthesise poly(lactic acid) based bio-nanocomposites by incorporating different nanoparticles/antimicrobial additives with enhanced physiochemical properties for potential food packaging applications. The ultrasound-assisted solvent casting method synthesises PLA-based antimicrobial bio-nanocomposites with four different nanoparticles/additives: ZnO nanoflowers, functionalized ZnO, ZnO@HNT and CEO/alkali treated HNT. The first chapter of the thesis briefly introduces biopolymers, different nanofillers, polymer nanocomposites, synthesis methods of polymer nanocomposites and important properties of food packaging materials. The chapter also reviews the literature available on PLA-based nanocomposites for antimicrobial food packaging applications.

In the second chapter of this thesis, we have presented the ultrasound-assisted synthesis of PLA/ZnO nanocomposites with the special feature of flower-like morphology of ZnO. The ZnO nanoflowers were synthesized via a facile sonochemical method with $Zn(NO_3)_2 \cdot 6H_2O$ as a precursor in different molar concentrations (0.025, 0.05, 0.075 and 0.1 M). The physiochemical characterization of the nanocomposites revealed excellent thermal, optical and mechanical properties at a very low loading of ZnO (0.5 wt%). These properties are attributed to high interfacial interactions between nanofiller and PLA matrix resulting from special morphological features of ZnO nanoflowers and uniform dispersion of ZnO nanoflowers in the PLA matrix under the influence of sonication.

In the third chapter, we have reported the synthesis and surface modification of ZnO nanoparticles with 3-aminopropyltrimethoxysilane coupling agent (APTMS). Thereafter, the nanocomposites of PLA with surface-modified ZnO were synthesized by ultrasound-assisted solvent casting method. When pristine ZnO and functionalized ZnO nanoparticles were incorporated into the PLA matrix, the transmittance values of films at 400 nm decreased from 95% to 70% and 59%, respectively, which means that the nanocomposite films screened higher UV light as compared with the neat PLA film. The water contact angle (WCA) of the neat PLA film was 65.4°; however, it increased significantly after the formation of nanocomposite with pristine ZnO (WCA = 74.8°) and functionalized ZnO (WCA = 85.8°). Surface functionalization reduces the agglomeration of nanoparticles and provides better dispersion in the polymer matrix; hence the properties are improved.

In the fourth chapter, nanocomposites of PLA with ZnO@HNT were synthesized using an ultrasound-assisted solvent casting method. The nanocomposite film PZH2 (consisting of 2 wt% ZnO@HNT) showed the best properties compared to PLA. Moreover, a packaging test was performed on cut apples for 6 days storage period to evaluate the potential efficacy of nanocomposite films for food packaging applications. Overall, incorporating ZnO@HNT in the

PLA matrix improved the physio-chemical properties and imparted antimicrobial properties, enhancing the fruit's shelf life.

In the fifth chapter, nanocomposites of PLA with clove essential oil (CEO) and alkali-treated halloysite nanotubes (NHNT) as fillers were synthesized using a simple ultrasound-assisted solvent casting method. The treatment of halloysite nanotubes with NaOH increased the surface area from 50.16 $m^2 \times g^{-1}$ to 57.01 $m^2 \times g^{-1}$ and pore volume from 0.25 $cm^3 \times g^{-1}$ to 0.32 $cm^3 \times g^{-1}$. Incorporating CEO and NHNT improved the surface hydrophobicity, water vapor barrier properties, thermal stability and mechanical properties (mainly elongation at break) of the PLA-based nanocomposite films. This study has thus demonstrated the potential of PLA films synthesized with functional filler NHNT and bioactive agent CEO for food packaging applications. In the last chapter, we have summarized the major findings from the above studies and presented an outlook for future work.

Contents

List of Figures

List of Tables

Abbreviations

PET	polyethylene terephthalate
LDPE	low density polyethylene
PP	Polypropylene
PS	Polystyrene
PVC	polyvinyl chloride
PLA	poly(lactic acid)
GRAS	generally recognized as safe
US FDA	united states food and drug administration
TiO_2	titanium oxide
ZnO	zinc oxide
HNT	halloysite nanotubes
EMI	electromagnetic interference
NPs	Nanoparticles
TPS	thermoplastic starch
MMT	Montmorillonite
Ag-NPs	silver nanoparticles
Cu-NPs	copper nanoparticles
MgO	magnesium oxide
PCL	Polycaprolactone
PHB	Polyhydroxybutyrate
PHBV	poly(hydroxybutyrate-co-valerate)
LNFs	lysozyme nanofibers
CO_2	carbon dioxide
LA	lactic acid
Ag_2O	silver oxide
CaO	calcium oxide
Fe_2O_3	ferric oxide
CuO	copper oxide
ROS	reactive oxygen species
H_2O_2	hydrogen peroxide
CTAB	cetyltrimethylammonium bromide
KOH	potassium hydroxide
GO	graphene oxide

UV	ultra violet
WVP	water vapor permeability
O_2	Oxygen
Se	Selenium
SiO_2	silicon dioxide
CuS	copper sulfide
PU	Polyurethane
CEO	clove essential oil
CMC	carboxymethyl cellulose
WVTR	water vapor transmission rate
DSC	differential scanning calorimetry
PVA	polyvinyl alcohol
NaOH	sodium hydroxide
HNT	halloysite nanotubes
PBS	poly(butylene succinate)
FE-SEM	field emission scanning electron microscope
$Zn(NO_3)_2 \cdot 6H_2O$	zinc nitrate hexahydrate
APTMS	3-(aminopropyl) trimethoxysilane
BET	brunauer-emmett-teller
H_2S	hydrogen sulfide
FTIR	fourier transform infrared spectroscopy
ATR	attenuated total reflectance
XRD	x-ray diffraction
EDX	energy dispersive x-ray spectroscopy
FE-TEM	Field emission transmission electron microscope
TGA	thermogravimetric analysis
LB	luria broth
NB	nutrient broth
CFU	colony forming unit
FWHM	full width at half maximum
DTG	differential thermogravimetry
DNA	deoxyribonucleic acid
CNT	carbon nanotubes
APTMS	3-aminopropyl trimethoxysilane

$ZnSO_4.7H_2O$	zinc sulfate heptahydrate
IUPAC	International union of pure and applied chemistry
PBAT	poly(butylene adipate-co-terephthalate)

Notations

nm	Nanometer
T_g	glass transition temperature (℃)
T_m	melting temperature (℃)
M_w	molecular weight (g/mol)
kDa	Kilodaltons
meV	mega electron-volt
phr	parts per hundred rubber
MPa	Megapascal
M	Molarity
rpm	rotation per minute
λ	Wavelength
Å	Angstrom
β	full width at half maximum height in radians
k	scherrer constant
kN	Kilonewton
UTS	ultimate tensile strength
A	permeation area (m^2)
W	weight change of bottle with film sample (g)
ΔP	difference in partial vapour pressure between water and dry atmosphere at 25°C
N	Normality
S_{BET}	BET surface area
d	inter-atomic spacing in angstrom
L*	level of light or dark
a*	redness or greenness
b*	yellowness or blueness

CHAPTER 1

Introduction and Literature Review

This chapter deals with a general introduction to biopolymers, different nanofillers, a brief description of polymer nanocomposites, synthesis methods of polymer nanocomposites and finally, their applications in the food packaging sector. The chapter also includes a literature review available on PLA-based nanocomposites for antimicrobial food packaging applications. Thereafter, the objectives of the thesis and the organisation of the thesis have been stated.

1.1 Introduction

Petroleum-based synthetic plastics are the most widely used packaging materials mainly due to their lightweight, low cost and easy processing technologies. Polyethylene terephthalate (PET), low-density polyethylene (LDPE), polypropylene (PP), polystyrene (PS) and polyvinyl chloride (PVC) are the petroleum-based most commonly available packaging plastics. They are generally used as "use and throw" items mainly because of their low cost and low density. Being non-degradable in nature, these plastic waste products cause garbage problems, especially in developing countries with no proper waste management system. In 2016 alone, 23 million tonnes of plastics were discarded in marine ecosystems. This amount is anticipated to double by 2030 (Borrelle et al., 2020), with an estimated rise of 300 – 400% by 2050 (Geyer et al., 2017).

Biopolymers or biodegradable polymers have gained enormous attention worldwide as an alternative to synthetic plastic, mainly due to their biodegradability, non-toxic, and renewable resources (Porta et al., 2020). Moreover, these biopolymers can also act as soil conditioners and fertilizers upon disintegration and composting. Among different biopolymers, poly(lactic acid) (PLA) is the most widely used material in food packaging applications (Shao et al., 2022). This may be due to its high transparency, ease of processability, biocompatibility, easy availability, non-toxic nature and comparable physical properties with synthetic polymers such as polypropylene and polyethylene etc. Moreover, PLA is classified as GRAS (Generally Recognized as Safe) material by the US FDA (United States Food and Drug Administration) (Mulla et al., 2021). Unfortunately, like other biopolymers, PLA has limitations such as poor thermal, mechanical, and barrier properties compared to synthetic non-degradable plastics. But, storage and transporting any product, especially food, requires a strong, tough material that can withstand any harsh conditions encountered during transportation and storage. Moreover, packaging should preserve food quality, prolonging the product's shelf life. Therefore, many research studies have been done to improve the functional properties of biodegradable biopolymers. Bio-nanocomposites represent a new category of materials with enhanced thermal,

barrier, and mechanical properties compared to the base biopolymers (Jafarzadeh et al., 2021). Bio-nanocomposites consist of two major components: one is the matrix (the continuous phase), which is a biopolymer, and another is a reinforcing agent (dispersed phase) having at least one dimension in the nanoscale range (< 100 nm). Due to its high surface area and aspect ratio, the nanofiller plays a vital role in the properties enhancement of the biopolymer matrix. Various reinforcing nanofillers such as silicate (Alvarez Echazú et al., 2018), clay (Orta et al., 2020), lignin nanoparticles (Vijayakumar et al., 2022), cellulose nanocrystals (Nandi & Guha, 2018), TiO_2 (Salahuddin et al., 2020), ZnO (Chong et al., 2022) are added to biopolymers which not only improve the physiochemical properties but also impart other properties such as UV-shielding, antimicrobial activity, and antioxidant activity etc.

Antimicrobial packaging is a new emerging technology to maintain the freshness, quality and safety of food products which may get spoiled by food-borne pathogenic microorganisms. Adding antimicrobial agents to food packaging prevents the development of microorganisms on foodstuffs, thereby increasing its shelf life (R. Sharma et al., 2020). Commonly, antimicrobial agents can be classified into two categories: (a) organic and (b) inorganic materials. Examples of organic antimicrobial agents are naturally occurring biopolymers (chitosan or its derivatives) (Ma et al., 2017), organic acids (Coban, 2020), essential oils (Vergis et al., 2015), enzymes (Corradini et al., 2013) etc. On the other hand, inorganic antimicrobial agents mainly include metals and metal oxides (Dizaj et al., 2014). The advantage of inorganic antimicrobial agents over organic is that they can withstand intense processing conditions such as high pressures and temperatures. Moreover, some of them even contain mineral elements essential to human health. Some common examples of inorganic antimicrobial agents (metals and metal oxide nanoparticles) are ZnO, TiO_2, copper, silver, gold, iron, magnesium and calcium oxide, etc.

Among several reported metal oxide antimicrobial nanoparticles, nano ZnO with varying morphologies shows excellent antimicrobial activity over a broad range of microbial species,

including gram-positive and gram-negative bacteria. ZnO also possesses high UV-light absorption capacity, which is beneficial in antimicrobial activity and used as a UV protector in cosmetics and food packaging applications (Espitia et al., 2012). Moreover, ZnO is considered a GRAS (Generally recognized as safe) material by the USFDA (Food and Drug Administration) and can be used as a food additive. The antimicrobial efficacy of ZnO nanomaterials mainly depends on factors such as particle size, morphology and specific surface (Raghupathi et al., 2011) area. An increase in the surface area of ZnO nanoparticles leads to an enhancement in antimicrobial activity. In literature, various methods are reported for the synthesis of ZnO nanomaterials with different morphologies, such as nanorods, nanowires, nanotubes and nanoflowers etc. In addition, surface functionalization of ZnO surface with polar groups further improves the interactions between the microorganisms and ZnO nanomaterials (Kumar et al., 2017).

There are various types of nano clays (montmorillonite, closite, halloysite nanotubes etc.) available, among which, halloysite nanotubes (HNT) are the most promising in the field of active food packaging due to their non-toxic, low cost and biocompatible nature (Q. Li et al., 2021). Incorporating HNT into the PLA matrix mainly increases its tensile strength and decreases gas and water vapor permeability. Adding HNT provides a tortuous path for permeating molecules through the film matrix, thus reducing the permeability of gas and water molecules. The high specific surface area (50–137 $m^2 \cdot g^{-1}$) and unique hollow tubular structure of HNT make it desirable for sustainable packaging and a suitable carrier for active components. Active components, especially antimicrobial agents, can be incorporated into packaging systems for food preservation purposes (Alkan Tas et al., 2019). The following techniques are used to incorporate active components into HNT: (a) adsorption of active agents onto the external surface of HNT; (b) loading of active agents into HNT lumen; (c) self-grafting on targeted biomolecules. Therefore, nano-interfacial decoration of HNT with ZnO can be a fruitful way to get biopolymers' superior thermo-mechanical and antimicrobial activity.

The nanocomposite films containing essential oils and nanofillers possess antimicrobial and antioxidant properties, which improve the quality and shelf life of food products (da Costa et al., 2020). Different types of essential oils such as clove (Sanuja et al., 2014), thyme (Carvalho et al., 2020), ginger (Alexandre et al., 2016), rosemary (Alizadeh-Sani et al., 2021), and cinnamon (Vahedikia et al., 2019) are being used as active agents in food packaging systems. Among all, clove essential oil (CEO) is known for its excellent UV rays blocking properties and strong antioxidant, antifungal and antibacterial activities. Moreover, incorporating CEO into a polymer matrix improves its flexibility, toughness and hydrophobicity (Lu et al., 2021). Mainly CEO contains 76.8% eugenol, 17.4% β-caryophylene and 2.1% α-humulene (Chaieb et al., 2007). The US Food and Drug Administration (FDA) categorized CEO as GRAS material. Hence, developing bio-nanocomposite materials for food packaging applications containing antimicrobial nanoparticles and other additives is important to reduce environmental problems and improve the functional properties of food packaging materials.

1.2 Bio-nanocomposites

Composite is a multiphase material containing two components, i.e. matrix (continuous phase) and reinforcing filler (dispersing phase). The filler is in the micro or macro size range in composite material. The composite material can be classified depending on the matrix: (a) metal matrix composite, (b) ceramic matrix composite and (c) polymer matrix composite. On the other hand, nanocomposite consists of nano-size filler (at least one dimension <100 nm) and matrix. Compared to composite material, nanocomposite possesses better functional properties like thermal, mechanical, barrier, flame retardant etc., mainly because of the high surface area of nano-size filler. Biopolymers are materials obtained from renewable resources. Unfortunately, they possess several limitations such as brittleness, poor processing ability, poor mechanical, thermal and barrier properties etc., which limits their industrial opportunities. In recent years, various strategies have been followed to overcome such drawbacks. The addition of crosslinking agents (Garavand et al., 2017), physical blending

with other polymers (Arrieta et al., 2017), graft copolymers (Thakur et al., 2013) and inclusion of nanoparticles as reinforcing fillers (Ghanbarzadeh et al., 2015) plays a significant role in improving important properties of biopolymers. Among all, the synthesis of bio-nanocomposites is considered as the most promising methodology to get high-performance, lightweight green materials which can replace petroleum-based non-degradable plastics. Bio-nanocomposites are synthesized from biopolymers with different organic and inorganic nanofillers (1–100 nm). Due to the nanoscale dimension, these fillers have a high surface area and surface-to-volume ratio. So far, the most promising nanofillers in bio-nanocomposites formation are nanoclays, cellulose-based nanofillers, carbon nanotubes, metal oxide nanoparticles etc. Many bio-nanocomposites with improved thermal, barrier, mechanical and other functional properties (antimicrobial, UV-barrier, antioxidant, chemical resistant, EMI shielding etc.) with biodegradable nature were efficiently used in applications such as packaging, sensors, electronics, energy storage etc. Fig. 1.1 shows the difference between polymer composites, nanocomposites and bionanocomposites. The dimensions and consequent aspect ratios of reinforced nanofillers precisely control the final properties of nanocomposites. Furthermore, the proper dispersion of nanofillers and chemical compatibility with the polymeric matrix plays a crucial role in defining the ultimate properties of nanocomposites. The amount of nanofiller also plays an important role in getting optimum properties of nanocomposites. The amount of nanofiller should be such that it can form a homogeneous and continuous structure with a matrix. The optimum nanofiller quantity is called the percolation threshold. At higher loadings, nanofillers tend to agglomerate due to high surface area. To improve the dispersibility, several efforts have been made:

a) Surface modifications of nanofillers to generate desired functional groups, e.g. oxidation of carbon nanotube surface by acid treatment (generate the carboxyl and hydroxyl group).

b) Incorporation of long-chain hydrocarbons or polymer chains onto the nanofiller's surface.

c) Using ultrasound for proper dispersion of nanofillers into the matrix.

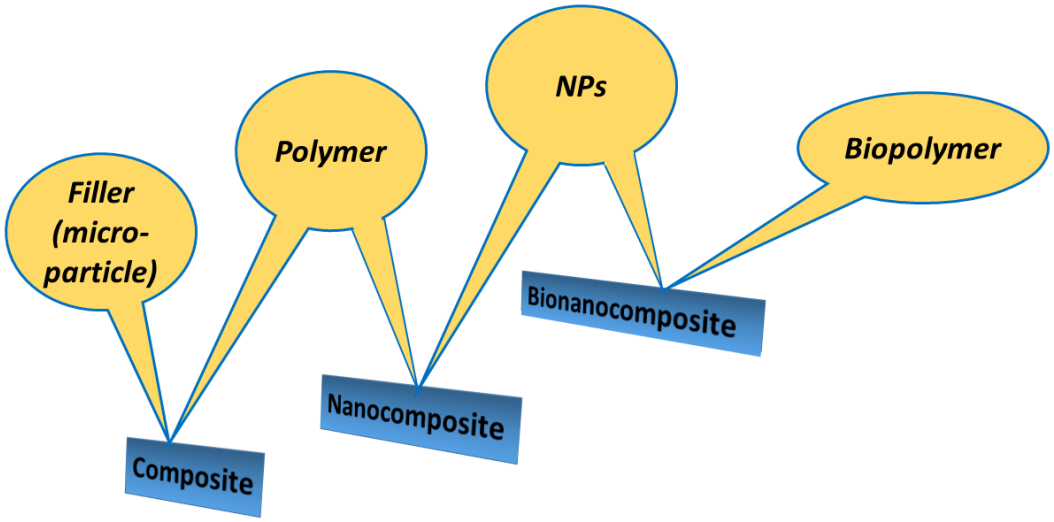

Fig.1.1. Difference between polymer composite, nanocomposite and bionanocomposites

Antimicrobial bio-nanocomposites are newly emerging food packaging materials that are highly useful for inhibiting the growth of microorganisms on food surfaces and maintaining product quality, safety, and shelf life extension. The antimicrobial agents as reinforcing fillers or additives are incorporated into the biopolymer matrix to synthesise antimicrobial bio-nanocomposites. Table 1.1 shows different types of biopolymers and antimicrobial agents for synthesising antimicrobial bio-nanocomposites.

1.3 Biopolymers

The term “biopolymers” usually describes polymers produced by living organisms. Microorganisms’ degradation of these biopolymers occurs under suitable temperature, moisture and oxygen conditions. It leads to the decomposition of the polymer materials with no toxic or harmful residue. Carbohydrates and proteins are the major examples of biopolymers. Among the biopolymers, polysaccharides obtained from linear carbohydrate structures are important in living organisms. Cellulose and chitosan are another important

polymers from the polysaccharide family. Biopolymers can also be produced from monomers obtained from biological resources using conventional chemical processes (poly (lactic acid)), or directly in microorganisms or genetically modified organisms (polyhydroxyalkanoates). Fig. 1.2 describes the classification of the biopolymers.

Biopolymers are classified mainly based on the source of raw materials and their synthesis processes.

- Biopolymers are obtained directly from bioresources (plant or animal origin), such as protein (wheat gluten, gelatin, collagen etc.) and carbohydrates (starch, chitosan, cellulose, carrageenan, agar etc.).
- Biopolymers are obtained by chemical synthesis. Synthetic biodegradable polymer poly(lactic) acid is obtained from bio-based monomer lactic acid. Polycaprolactone and polyvinyl alcohol are obtained from petrochemicals.
- Biopolymers are produced by the fermentation of microorganisms such as polyhydroxyalkanoates (PHA), polyhydroxybutyrate (PHB), polyhydroxyl-valerate (PHV), bacterial cellulose, and pullulan.

Table 1.1. Biopolymers and antimicrobial agents for bio-nanocomposites

Biopolymers	Antimicrobial materials	References
Starch/TPS	Quaternary ammonium salt modified MMT-cloisite 30B/ Ag-NPs	(Abreu et al., 2015)
	Copper nanoparticles (CuNPs)	(Hasanin et al., 2022)
	Layered silicates/Essential oil	(Campos-Requena et al., 2017)
	Chitosan nanoparticles	(Babaee et al., 2022)
Chitosan	Bentonite-Ag-ZnO	(Motshekga et al., 2015)
	ZnO	(D. Li et al., 2022)
	Ag/ZnO	(Ali et al., 2022)
Polylactic acid	ZnO	(Boro et al., 2022)
	TiO_2	(Fonseca et al., 2015)
	MgO	(Swaroop & Shukla, 2018)
Polycaprolactone (PCL)	clay@ZnO	(Maghfoori et al., 2022)
	Cellulose acetate/Copper NPs	(El-Naggar et al., 2022)
Polyhydroxybutyrate (PHB)	Silver nanoparticles	(Castro-Mayorga et al., 2018)
Poly(hydroxybutyrate -co-valerate) (PHBV)	Clay/oregano oil	(da Costa et al., 2020)
Pullulan	lysozyme nanofibers (LNFs)	(Silva et al., 2018)

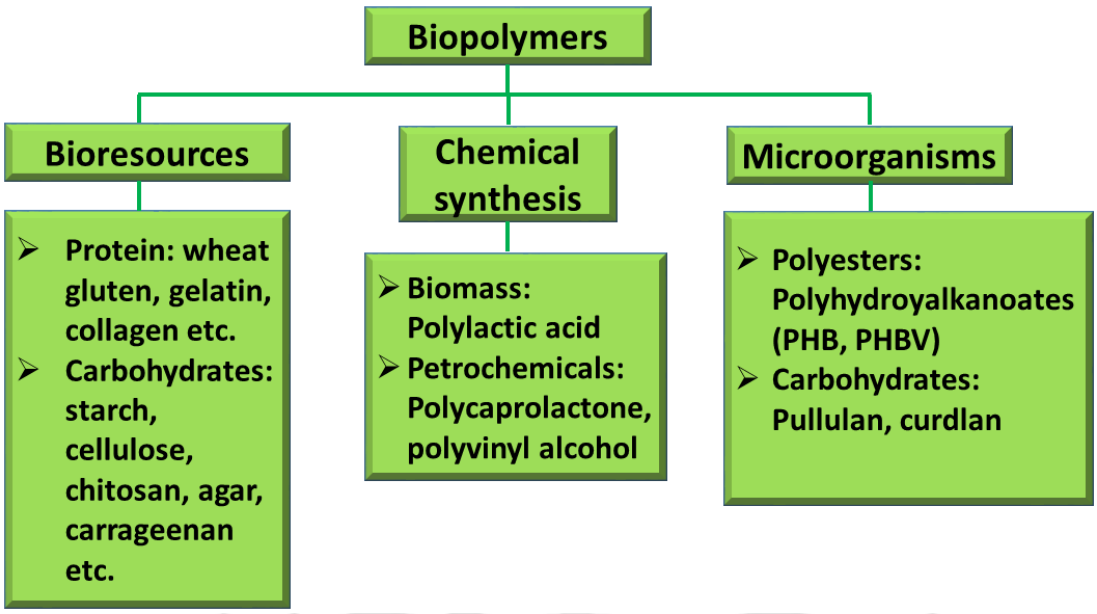

Fig. 1.2. Classification of the biopolymers

1.3.1 Poly (lactic acid)

Poly(lactic acid) is one of the most widely used biopolymers in the family of poly-α-hydroxy acid, a linear aliphatic polyester. It is considered a sustainable substitute for petroleum-based products due to its high mechanical strength, thermal stability, transparency, low carbon footprint, easy processability, etc., compared to other biobased polymers (Taib et al., 2022). It can be easily molded in different-shaped articles by using conventional thermoplastic processing methods such as extrusion, compression molding, blow molding, injection molding and thermoforming etc. Furthermore, after the end of the life cycle, it degrades mainly by hydrolysis after several months of contact with moisture. The degradation of PLA occurs in two steps. Firstly, random non-enzymatic chain scissioning of ester groups of PLA occurs, which causes a reduction in molecular weight. Secondly, the decrease in molecular weight occurs until the formation of lactic acid and low molecular weight oligomers are consumed by microorganisms to produce water, CO_2 and solid biomass. PLA is one of the topmost choices of biobased polymer materials to be used in different applications, including engineering and biomedical (due to its biocompatibility and biodegradability) applications. In contrast, the fields of packaging and fiber technology represent

the primary utilisation sectors. It is considered generally recognized as safe (GRAS) by the United States Food and Drug Administration (FDA) and is safe for all food packaging applications (Garlotta, 2001). Fig. 1.3 depicts the number of publications on PLA-based composites in the last 10 years. The number of papers published on PLA has followed an increasing trend over the last 10 years, showing PLA's significance in composites.

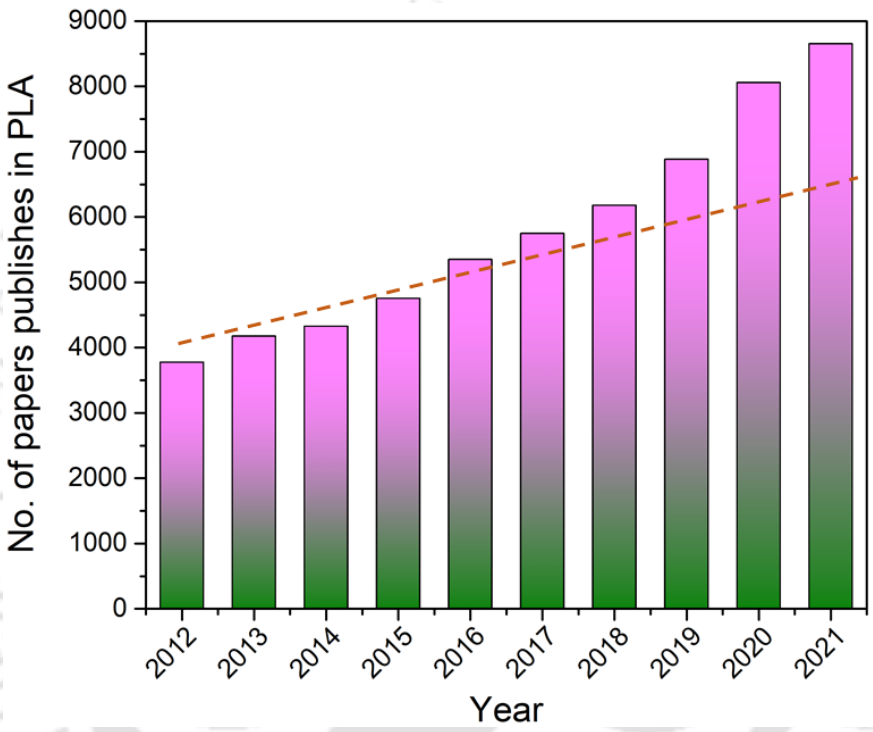

Fig. 1.3. No of paper published on PLA composites (Ranakoti et al., 2022)

1.3.2 Structure and properties of poly(lactic acid)

The biopolymer poly(lactic acid) is obtained from the polymerization of monomer lactic acid (LA). Four different groups are attached to the central carbon atom of LA. Therefore, it is a chiral molecule and exists in three forms: Levorotatory (L-), dextrorotatory (D-) and meso (combination of L- and D-). The formation of L-lactic acid, D-lactic acid or a mixture of L- and D- depends on the source and synthesis method. The lactic acid obtained from the chemical method is a racemic mixture of 50% L- and 50% D-isomers, whereas lactic acid obtained by the fermentation process consists of 99.5% of the L-isomer, and the remaining is D-isomer. The PLA synthesized by using

L-, D- and meso isomers are called poly(L-lactic acid), poly(D- lactic acid) and poly(meso-lactic acid), respectively. The final properties of poly(lactic acid), such as its crystallinity, thermal and mechanical properties, mainly depend on the ratio of L/D content (Ranakoti et al., 2022). The presence of L-lactic acid would produce semi-crystalline PLA (PLLA), while poly (DL-lactide) produces an amorphous polymer (PDLLA). PLA's glass transition temperature (Tg) and melting point (Tm) decrease with decreasing amounts of L-isomers. Physical properties such as heat capacity, density, and mechanical and rheological properties of PLA depend on its T_g. In the case of amorphous PLA, the Tg is an important parameter due to higher changes in polymer chain mobility at and above T_g. Tg and Tm are important parameters for determining PLA behaviour for semicrystalline PLA. Fig. 1.4 shows the chemical structure of lactic acid isomers and poly(lactic acid). The physical, mechanical and thermal properties of commercial PLA grades are shown in Table 1.2.

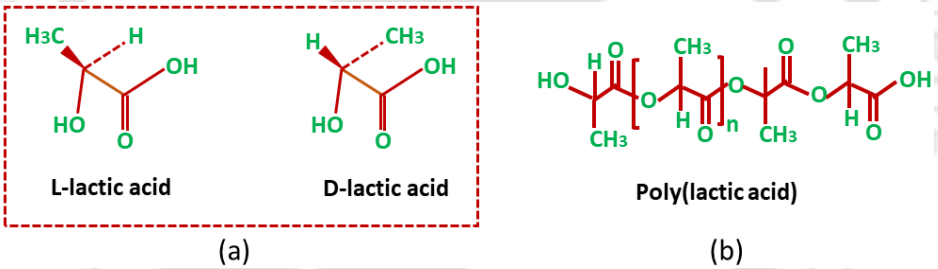

Fig. 1.4. Chemical structure of (a) isomers of lactic acid and (b) poly(lactic acid)

Table 1.2. Physical, mechanical and thermal properties of commercial PLA grades (Farah et al., 2016)

Properties	PLA	PLLA	PDLLA
Density (g/cm^3)	1.21–1.25	1.24–1.30	1.25–1.27
Tensile strength (MPa)	21–60	15.5–150	27.6–50
Elastic modulus (GPa)	0.35–0.5	2.7–4.14	1–3.45
Ultimate strain (%)	2.5–6	3.0–10.0	2.0–10.0
Glass transition temperature (℃)	45–60	55–65	50–60
Melting temperature (℃)	150–162	170–200	Amorphous-no melting point

1.3.3 Synthesis of poly(lactic acid)

Poly(lactic acid) was first synthesized by Carothers (at DuPont) in 1932. He could only synthesize PLA of low molecular weight by simply heating lactic acid under an inert atmosphere with the simultaneous removal of condensed water. The challenge to synthesize high molecular weight PLA was solved by employing ring-opening polymerization of the lactide. Nowadays, different processes are available to produce PLA, but none of them is easy to perform. The PLA synthesis requires proper control of synthesis conditions such as temperature, pressure and pH, choice of catalyst, polymerization time etc. PLA can be synthesized from monomer lactic acid using two different methods: (a) direct condensation process, which involves solvents under high vacuum or in a solvent-free process, a cyclic dimer intermediate called lactide is formed followed by catalytic ring opening polymerization of the cyclic lactide. The direct condensation route is an equilibrium reaction, and there are difficulties in removing water and impurities. Hence, the final product usually has low molecular weights (M_w~1-10 kDa). Because of the problems faced in the direct condensation method, the commercial production processes are based on lactide ring-opening polymerization. Fig. 1.5 shows the synthesis route of polylactic acid.

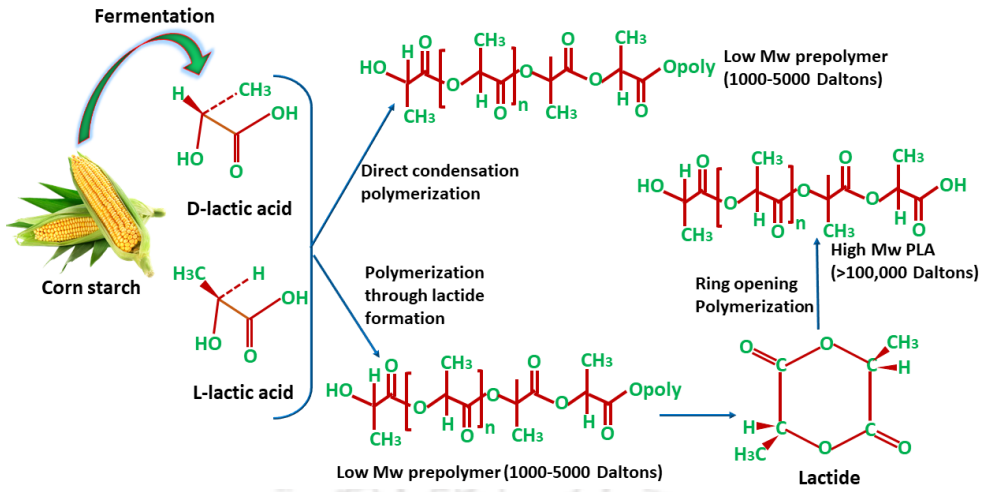

Fig. 1.5. Synthesis route of polylactic acid

Limitations of poly(lactic acid)

Although PLA possesses the prospective to compete with conventional plastics, it is important to highlight the drawbacks, which limit its usage in the packaging application as follows:

a) Highly brittle nature of PLA restricts its applications, such as flexible films.

b) PLA possesses poor thermal stability

c) PLA has a slow crystallization rate.

d) PLA shows poor barrier properties (gas, moisture etc.) compared to conventional polymers.

1.4 Nanofillers/antimicrobial additives for PLA

1.4.1 Zinc oxide nanoparticles (ZnO-NPs)

Among the different nanomaterials used, metal oxides are considered the most promising candidates for antimicrobial applications due to their non-toxic nature, high stability and efficient biological properties, etc. The metal oxides such as Ag_2O, MgO, ZnO, TiO_2, CaO, Fe_2O_3 and CuO are widely explored as antimicrobial agents in various biomedical or food packaging applications. Among variously reported metal oxides, ZnO, a natural n-type semiconductor material, has been widely studied as an antimicrobial agent. The antimicrobial activity of ZnO has received

significant interest through the application of nanotechnology to synthesize ZnO-NPs, which have a far higher surface area as compared to bulk ZnO. Moreover, it is a non-toxic, biocompatible material, which is considered generally recognized as safe (GRAS) material by the U.S. Food and Drug Administration. In addition to its antimicrobial properties, ZnO-NPs exhibit high photocatalytic activity and show high optical absorption in UV-A (315–400 nm) and UV-B (280–315 nm) regions, which is useful in making UV-protector materials (Shi et al., 2014). The antimicrobial properties of ZnO-NPs cover a wide range of Gram-positive and Gram-negative bacteria, including *E. coli*, *B. subtilis*, *S. aureus*, *L. monocytogenes*, *Klebsiella pneumonia*, *P. aeruginosa*, *Salmonella typhimurium*, *E. faecalis*, etc. (Kumar et al., 2017). Various mechanisms, such as the release of Zn^{2+} ion, generation of reactive oxygen species (ROS), and cell membrane destruction caused by the surface defects such as corners and edges of ZnO nanoparticles, etc., have been proposed for explaining the antimicrobial activity of ZnO. ZnO-NPs have a band gap of 3.28 eV and a high exciton binding energy of 60 meV. As a result, the incident of high photon energy radiation (higher than its band gap value) causes the electrons to move from the valence band to the conduction band of ZnO-NPs. The process forms electron holes (h^+) in the valence band and free electrons (e^-) in the conduction band. These holes and free electrons generate reactive oxygen species (ROS) on the surface of ZnO-NPs from adsorbed oxygen and water molecules. These ROS, such as hydroxyl radical ($^{\bullet}OH$), superoxide ($O_2^{\bullet-}$) and hydrogen peroxide (H_2O_2), cause the destruction of cellular components like nucleic acid, proteins, enzymes, membranes, etc. The chemical reactions that take place during the production of ROS on the surface of ZnO-NPs are given as follows:

$$ZnO + h\nu \rightarrow ZnO + e^- + h^+$$

$$h^+ + H_2O \rightarrow O_2^{\bullet-}$$

$$h^+ + H_2O \rightarrow {}^{\bullet}OH + H^+$$

$O_2^{\bullet-} + H^+ \rightarrow HO_2^{\bullet}$

$HO_2^{\bullet} + H^+ \rightarrow e^- \rightarrow H_2O_2$

Fig. 1.6 shows the schematic illustration for mechanism of antimicrobial activity of ZnO nanoparticles. Notably, it has been found that the antimicrobial properties of ZnO-NPs depend on their size, morphology and specific surface area (Lallo da Silva et al., 2019). The nanoparticles with high surface area possess better antimicrobial properties as compared to low surface area material. The morphology of ZnO-NPs is controlled by several factors such as types of Zn precursor used, solvents, synthesis method, temperature, pH and morphology directing agents (surfactants), etc. Table 1.3 shows the synthesis of ZnO nanomaterials using different synthesis methods, precursors, and solvent/morphology directing agents. Research suggested that wires and rod-shaped ZnO-NPs penetrate the bacterial cell wall more easily than spherical-shaped ZnO-NPs (Talebian et al., 2013). Chang et al. (2020) have synthesized three different morphologies of ZnO, including nanorods, nanoplatelets and multi-branched flower-like structures, by varying the pH value of precursor and growth time in hydrothermal reaction (Chang et al., 2020). Results indicated that multibranched flower shape ZnO showed better antifungal activity and significant photodecomposition of organic chemicals present in the soil compared to nanorods and nanoplatelets. Moreover, the functionalization of the ZnO surface with polar groups further improves the interactions between ZnO-NPs and the bacterial cell.

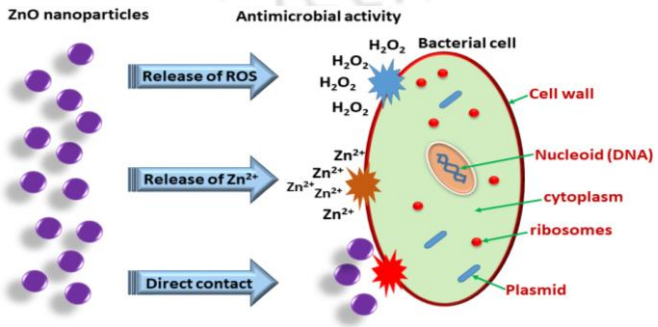

Fig. 1.6. Schematic illustration for mechanism of antimicrobial activity of ZnO nanoparticles

Table 1.3. Synthesis of ZnO nanomaterials by using different synthesis methods, precursor, solvent/morphology directing agents

Method	Precursor	Solvent/morphology directing agents	Size (nm)	Shape	Ref.
Hydrothermal	Zinc nitrate hexahydrate	CTAB	200–250	Nanospheres	(Saleh, 2019)
Hydrothermal	Zince acetate dihydrate	KOH, methyl alcohol	23–150	Nanorods	(V. Kumar et al., 2021)
Thermal decomposition	Zinc acetate dihydrate	-------	86	Nanowires	(Choudhary et al., 2021)
Sonochemical	Zinc nitrate hexahydrate	CTAB	Wide: 200–400	Nanoflowers	(Ghosh et al., 2014)

1.4.1.1 Surface modifications of ZnO nanoparticles

ZnO nanoparticles tend to agglomerate due to their high surface area. When the size of a material is decreased below 100 nm, the number of exposed surface atoms increases, which enhances its reactivity and makes them a highly reactive active material. As the reactivity of the nanomaterial increases, it becomes less stable and has a high tendency to undergo agglomeration. Therefore, the surface modification of ZnO nanoparticles is done to prevent agglomeration and to improve the dispersion of ZnO (hydrophilic) in the polymer matrix (hydrophobic) for their performance enhancement. Various methods are available for modifying metal oxide NPs surfaces, such as physical (physisorption) and chemical (covalent bonding). The physical modification involves the adsorption of surfactants and macromolecules on the surface of ZnO through weak van der Waals forces. Surfactants decrease the interactions between two particles and thus decrease the agglomeration. In the chemical modification, different organic or inorganic low molecular weight compounds or polymers are covalently grafted to nanoparticles. Compared to the physical method, the chemical method is more reliable as it provides better stability and compatibility between

nanoparticles and polymer matrix.

Among different chemical modifiers, silane coupling agents are the most widely used for metal oxide nanoparticles (Ahangaran & Navarchian, 2020). They have two different functional groups; one reacts with organic materials, and another part reacts with inorganic materials. The general formula for representing silane coupling agents is [$X–(CH_2)_n–Si–R_3$]. The 'X' group denotes the organic functional group such as methacryl, epoxy, amino, etc., whereas 'R' denotes hydrolyzable functional groups, for example, ethoxy, methoxy etc. Metal oxides contain –OH groups on their surface, which is a reaction site with trialkoxy groups of silane coupling agent modified the surface of ZnO nanoparticles by treatment with a coupling agent, aminopropyltrimethoxy silane and methacryloxypropyltrimethoxy silane (Mallakpour & Madani, 2015). The reaction mechanism of the silane coupling agent with ZnO is shown in Fig. 1.7.

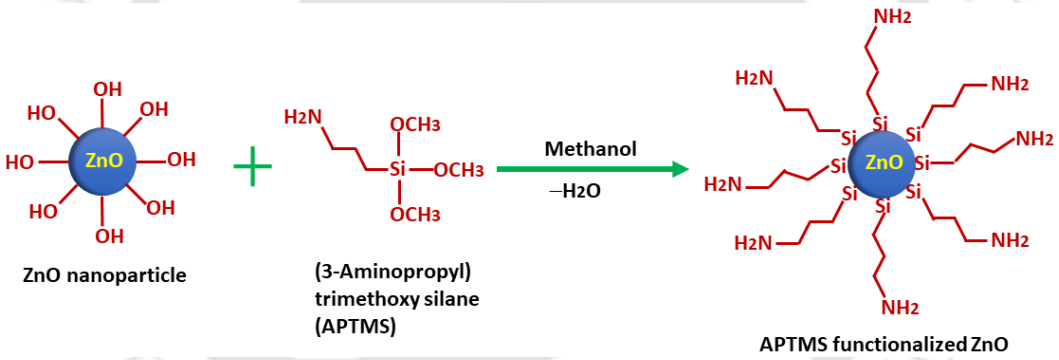

Fig. 1.7. Reaction mechanism of APMTS functionalized ZnO nanoparticles

1.4.2 Halloysite nanotubes (HNT)

HNTs are abundantly available natural aluminosilicate clay minerals. The chemical formula of HNT is $Al_2Si_2O_5(OH)_4$. The internal lumen of HNT containing aluminol (Al–OH) has a positive charge, while the outer surface, siloxane (Si–O–Si), contains negative charges. However, it is chemically similar to kaolinite but is different by the presence of two water molecules between two adjacent HNT nanoclays layers. HNTs are hollow tubular structures with outer diameter ≈ of

50–60 nm, lumen diameter/internal diameter ≈ of 12–15 nm, and ≈ 600–900 nm lengths. The specific surface area of HNT is 48 – 60 m^2 g^{-1} with a pore volume of 0.352 cm^3 g^{-1} (Danyliuk et al., 2020). As compared to other tubular nanostructures such as carbon nanotubes or TiO_2 nanotubes, HNTs are a much cheaper material as they are abundantly available in nature. Some other benefits of HNT include eco-friendliness, non-toxicity and biocompatibility. Due to the high aspect ratio and presence of an empty lumen, HNT can also be used as nanocarriers for loading various drugs and active agents such as essential oil, preservatives, nanoparticles etc. (Saadat et al., 2020). Moreover, due to its high absorption capacity, HNT also finds pesticide and dye removal applications. Fig. 1.8 depicts the chemical structure of halloysite nanotubes.

Currently, adding HNT with different agents (essential oils, antibiotics, preservatives, metal oxides such as ZnO, TiO2, silver nanoparticles etc.) for synthesising nanocomposites with improved antimicrobial activities has attracted the interest of the research community. The main contributions of HNT to antimicrobial nanocomposites include superior mechanical and thermal stability, stability, and prolonged release of the antimicrobial agents in a controlled manner (Barman et al., 2020).

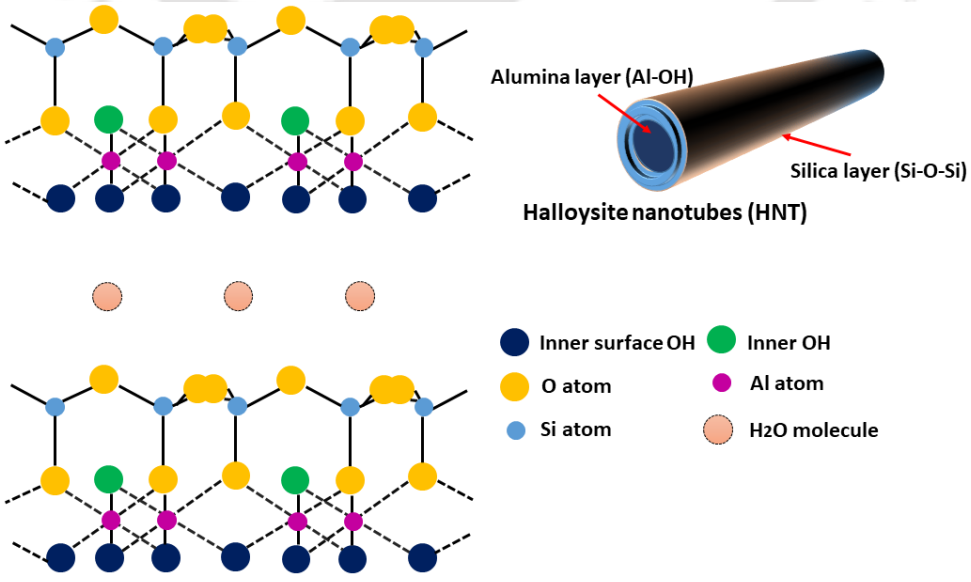

Fig. 1.8. Chemical structure of halloysite nanotubes

1.4.3 Essential oils

Essential oils are aromatic volatile liquids which are extracted from different parts, such as flower, buds, stem, leaves, roots, fruits etc., of plants (Chouhan et al., 2017). Commercially, essential oils are extracted by using steam distillation. Other essential oil extraction techniques include solvent extraction, hydro-distillation, CO2 supercritical, ultrasound-assisted, microwave-assisted extraction, etc. The chemical composition of essential oils depends on the extraction technique used. Generally, essential oils are a complex mixture of different volatile organic compounds containing carbon, oxygen, hydrogen and occasionally nitrogen and sulfur. In nature, essential oils play an important role in plant protection by acting as antivirals, antibacterial, antifungal and insecticides for plants. The antimicrobial activity of essential oils mainly depends on their active components (Hyldgaard et al., 2012). The antimicrobial components present in essential oils can be categorized into four groups depending on their chemical structure: terpens (limonene, p-cymene), terpenoids (carvacrol, thymol), phenylpropenes (eugenol, vanillin) and other compounds such as isothiocyanates (Hyldgaard et al., 2012). Fig. 1.9 shows the chemical structure of bioactive components present in essential oil. The antimicrobial activity of essential oils is mainly due to the presence of phenolic compounds. The acidic characteristics of hydroxyl group of phenolic compounds alter the cell permeability, interfere with the enzymes responsible for energy production and interrupt protein synthesis, which ultimately causes cell death (Khorshidian et al., 2018). Due to its antimicrobial activity, antioxidant property and UV barrier property, essential oil find application in the food industry as a food preservative which helps to extend the shelf life of food products (S. Sharma et al., 2021). Due to its high volatility and instability, essential oils degrade when directly incorporated into the food matrix. Therefore, to prevent the loss of essential oils, various new techniques, such as nano-emulsification and encapsulation of essential oils in nanoparticles, have been used (Hasheminejad et al., 2019).

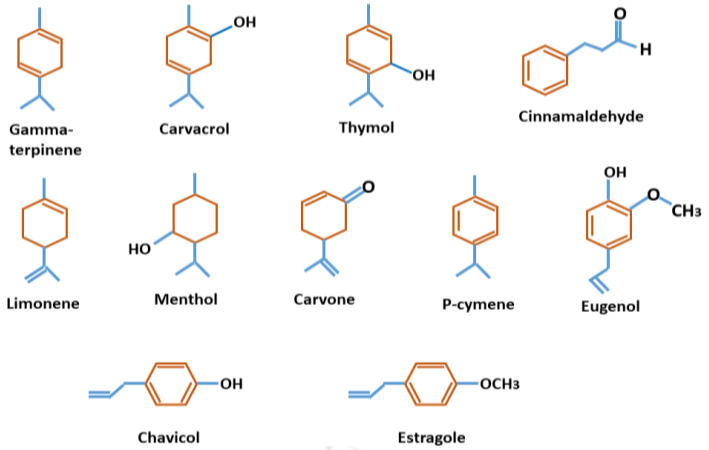

Fig. 1.9. Chemical structure of bioactive components presents on essential oil

1.5 Synthesis method of polymer nanocomposites

The main objective of polymer nanocomposite preparation is to achieve homogenous and thermodynamically stable dispersion of the nanofillers in the polymer matrix. The way in which nanofillers are dispersed in the polymer matrix will influence their level of interaction with the polymer and, thereby, affects the material properties. The applied strategy depends on the compatibility of the nanofillers and the polymer to be used. Different methods of nanocomposite preparation have been used in both intercalated and exfoliated nano-structures. However, the three most widely used methods are generally available for this purpose. These are given below:

a) Solution technique

b) In situ polymerization

c) Melt mixing method

1.5.1 Solvent casting method/solution technique

In solvent casting, solvent molecules swell and disperse the nanofillers into the polymer solution. The application of ultrasonic treatment further enhances the dispersion of the nanofillers. Depending on the intercalation of the solvent and nanofiller, the layers or particles may be delaminated in an adequate solvent due to weak van der Waals forces. This method dissolves the

polymer in the same solvent where the nanofiller is dispersed. Evaporation of the solvent leads to entrapment of polymer chains in-between the nanoparticles. This technique poses difficulties for the commercial production of nanocomposites due to the requirement of large amounts of toxic solvents. Nevertheless, it is an attractive route for water-soluble polymers because, in that case, water is used as a solvent, which has a very low cost and no health and safety risks are involved. A schematic illustration of the solution technique of nanocomposite preparation is shown in Fig. 1.10.

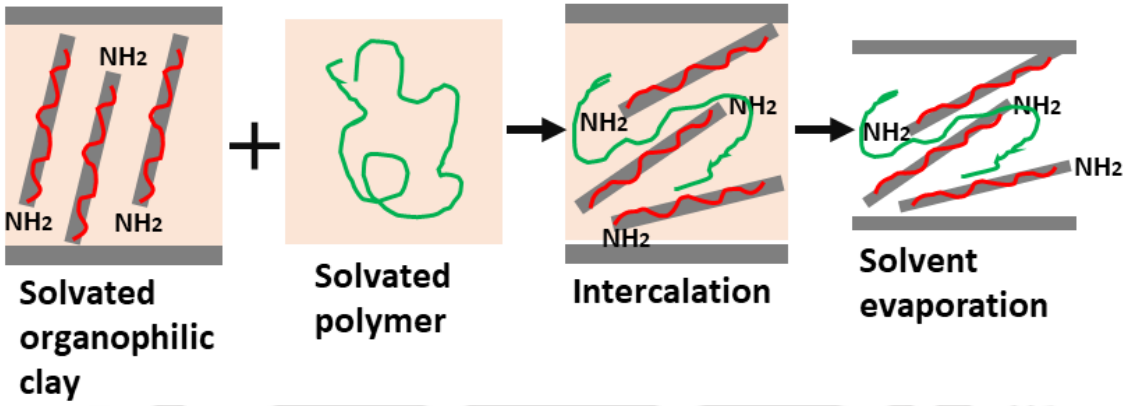

Fig. 1.10. Solution intercalation technique for nanocomposite preparation

1.5.2 In situ polymerization technique

In this method, the nanocomposite is formed during the polymerisation step itself. It involves inserting a polymer precursor (monomer) between nanofiller layers and then dispersing the nanofillers into a polymer matrix by polymerization. In this technique, the low viscosity of monomer or pre-polymer provides better nanofiller dispersion than other techniques. This technique is suitable for raw polymer manufacturers to produce clay/polymer and metal/polymer nanocomposites in the polymerization process itself. Fig. 1.11 represents a schematic illustration of in situ polymerization technique.

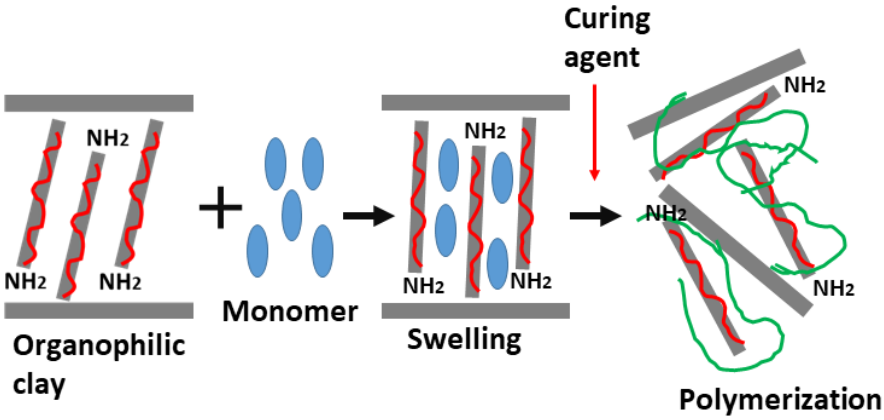

Fig. 1.11. In situ polymerization technique of nanocomposite preparation

1.5.3 Melt mixing method

This method involves the mechanical mixing of a polymer with a nanofiller using, most commonly, extrusion or kneading. In this process, the polymeric material is heated above its softening point, and the nanofiller is inserted into the molten polymer matrix. This technique removes the use of harmful solvents used in the solvent casting technique. Therefore, this process of nanocomposite preparation has played a significant role in spreading up the process for commercial production of polymer nanocomposites. Fig. 1.12 shows the schematic illustration of the melt intercalation or mixing technique.

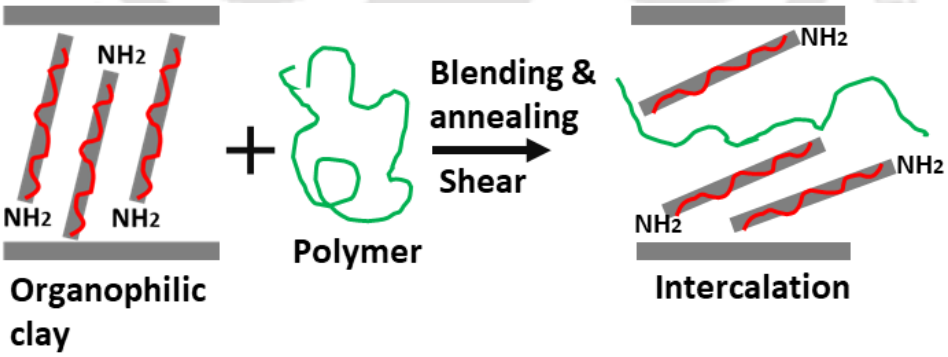

Fig. 1.12. Schematic illustration of melt mixing method

Table 1.4. Literature on PLA based antimicrobial bio-nanocomposites for food packaging applications

Bionanocomposite	Food products	Antimicrobial results	Ref.
PLA/AgNPs/fluorphlogopite		High thermal stability; antibacterial activity against *S. aureus*, *E. faecalis*, and *E. coli*	(Nabgui et al., 2022)
PLA/ZnO/ZEO, PLA/ZnO/MEO	*Otolithes ruber* fish	Shelf life extension up to 16 days; good antioxidant and antimicrobial activity (*E. coli*, *S. enterica*, *P. aeruginosa*, *B. cereus*, *S. aureus*)	(Heydari-Majd et al., 2019)
PLA/TiO_2		Slight increase in thermal degradation temperature; antibacterial activity against *E.coli*	(Segura González et al., 2018)
PLA/NiO supported silica nanoparticles		Tensile strength increases; oxygen and water vapor transmission rate decreases; good antibacterial activity against *L. monocytogenes*, *salmonellae*	(Ramji & Vishnuvarthanan, 2022)
PLA/LCNF-AgNPs, PLA/CHNF-AgNPs, PLA/CNF-AgNPs	Food simulant: ethanol 50% water (v/v)	PLA/LCNF-AgNPs showed higher mechanical and surface hydrophobicity; lower water vapor permeability; antibacterial activity against *S. aureus* and *E. coli*	(Mohammadalinejhad et al., 2021)
PLA/Ag-NPs/vitamin E	Fresh apple and apple juice	Antimicrobial activity against *E. coli*, *L. monocytogenes*, *S. typhymurium* up to 100% growth inhibition; antioxidant activity (94%)	(Munteanu et al., 2014)
PLA/ZnO, PLA/MgO, PLA/TiO_2		Tensile strength decreases at higher concentration than 0.1 phr; thermal degradation temperature decreases in nanocomposites; PLA/ZnO and PLA/MgO showed widest inhibition while PLA/TiO_2 gives smallest inhibition zone against *E. coli*	(Ghozali et al., 2020)
PLA/TiO_2/GO nano fibrous film	Green peppers	Increase tensile strength and elongation at break; improve water barrier properties; significant antibacterial activity against *E. coli* (94.4%) and *S. aureus* (92.6%); nanocomposite maintain the sensory quality and delay the spoilage of green peppers	(Dong et al., 2021)
PLA/chitosan/rosin modified cellulose nanofiber (R-CNF)		Excellent antimicrobial activity against *E. coli* and *B. subtilis*; 8 wt% R-CNF gives optimum mechanical properties	(Niu et al., 2018)
PLA/surface modified ZnO		Excellent antimicrobial activity against *E. coli* and *S. aureus*	(Zhang et al., 2017)

Note: ZEO: Zataria multiflora Boiss; MEO: Menthe piperita L.; LCNF: lignocellulose nanofiber; CHNF: chitosan nanofiber; CNF: cellulose nanofiber

1.6 PLA-based antimicrobial nanocomposites in food packaging applications

Currently, PLA is the most widely used biopolymer for food packaging applications. In the food industry, selecting suitable packaging materials and processes to minimize the damage and spoilage of food products during storage and transportation has always been a major concern. Antimicrobial bionanocomposites belong to a new class of food packaging materials that are extremely useful in minimizing the growth of microorganisms. It helps extend the shelf life of food products and maintain food quality and safety during storage. Table 1.4 provides an overview of different studies on PLA-based antimicrobial bio-nanocomposites for food packaging applications.

1.7 Properties of food packaging materials

The properties of packaging materials have a significant influence on the quality of packaged foods. To obtain good food products (safety and quality) during transportation and storage and to extend food products' shelf-life by avoiding issues such as chemical and microorganism contamination, barrier for oxygen, moisture and light, mechanical damage etc., packaging materials should possess certain properties. The improvements in shelf-life and quality of food products have been achieved mostly by using active food packaging based on antimicrobial bionanocomposites. The presence of nanoparticles reduces gas and water vapor permeability and provides UV-light barrier properties and mechanically strong and tough material along with antimicrobial activity towards various food-borne microorganisms. Important properties that food packaging materials should possess are given in Fig. 1.13.

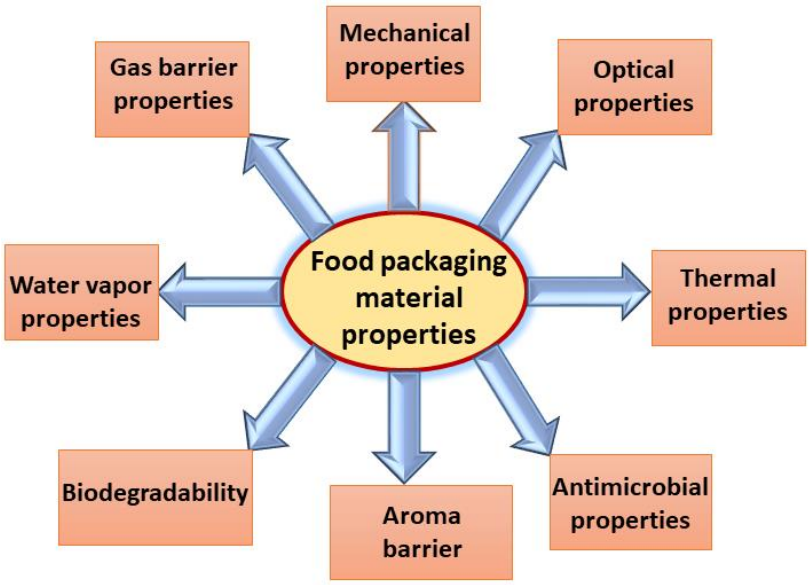

Fig. 1.13. Properties of food packaging materials

1.7.1 Barrier properties

In food packaging applications, barrier properties (against water vapor, gases, and aroma) of packaging material plays an important role in their utilization. During storage and transportation, food quality degrades due to the exchange of moisture, gases, smell, aroma etc., from food products to the surroundings. Therefore, barrier properties of packaging materials play a key role in maintaining weight loss and shrinkage of fruits and vegetables during storage. Incorporation of nanofillers into the polymer matrix changes the barrier properties in two ways: (a) the impermeability of the nanofillers provides a tortuous path for the diffusion of water/gas molecules, and they should move around this path. Hence, the path for the diffusion of water vapor/gas molecules becomes longer and tortuous; (b) the presence of nanofillers also creates some interaction between nanofillers and polymer matrix, which alters the interfacial areas within the polymer matrix. The interfacial interactions between the nanofiller and polymer matrix significantly influence the barrier properties. Fig. 1.14 shows the barrier properties of polymer nanocomposites.

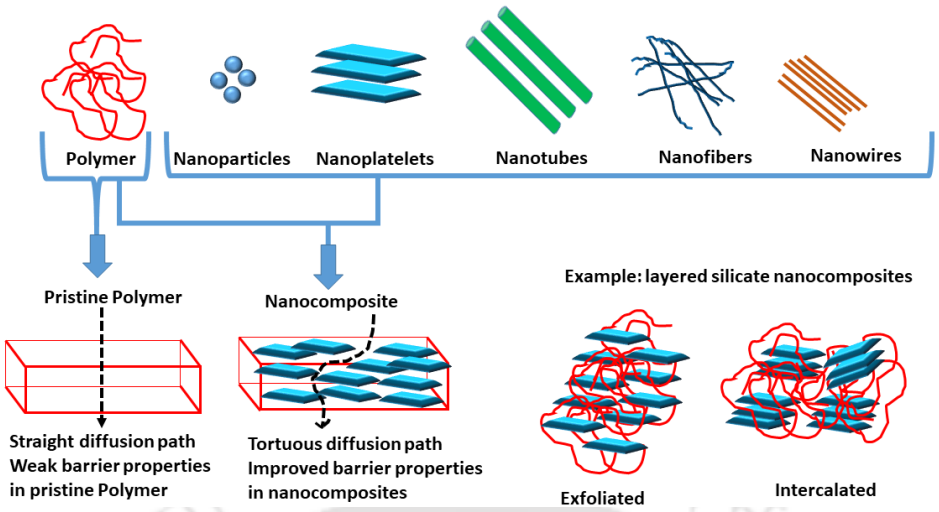

Fig. 1.14. Barrier properties of polymer nanocomposites

Water vapor permeability: One main purpose of packaging material is to reduce moisture diffusion from the surroundings to the food product. Therefore, water vapor permeability (WVP) is an important functional property, and its value should be as low as possible for any packaging film.

Shankar et al. (2018) have reported that the WVP of the alginate films was reduced by 32.4% after the incorporation of alkali-treated HNT/ZnO nanoparticles (Shankar, Kasapis et al., 2018). The reduction in WVP was due to the tortuous path provided by the impermeable alkali-treated HNT/ZnO for the diffusion of water molecules. Meanwhile, Rukmanikrishnan et al. (2020) showed that reinforcement of gellan and xanthan gum films with 5 wt% ZnO reduces the WVP by 39.7% (Rukmanikrishnan et al., 2020). Moreover, Alizadeh-Sani et al. (2021) reported that the nanocomposite film fabricated from sodium caesinate-ZnO-rosemary essential oil had lower WVP (reduced by 16.4%) as compared to pristine sodium caesinate (Alizadeh-Sani et al., 2021).

Oxygen permeability: Monitoring of oxygen transfer ability in food packaging material is important since a higher amount of oxygen diffusion from the surrounding environment into the food products (oily foods such as nuts) causes oxidative rancidity and loss of value, quality, and

nutritional content, and ultimately the shelf life of food products. Van et al. (2012) reported that in the presence of oxygen, ascorbic acid is readily degraded to dehydroascorbic acid, which is prone to further degradation, hereby losing its vitamin C activity (Van Bree et al., 2012). Thus, to minimize the loss of vitamin C and keep the associated non-enzymatic browning as low as possible, oxygen concentration should be minimal. On the other hand, the reduction in O_2 concentration decreases the ethylene production and rates of respiration in fruits, which results in a slow ripening process (Ntsoane et al., 2020). As already stated, the presence of nanofillers in nanocomposite films significantly improve the oxygen barrier properties. Yadav et al. (2021) reported a reduction in the oxygen permeability (OP) value in chitosan film incorporated with gallic acid-loaded ZnO nanoparticles (Yadav et al., 2021). The OP value was significantly reduced by 41.3% in the chitosan-based nanocomposite films. A similar enhancement in OP was also reported with polyethyleneimine-modified mesoporous silica embedded in the polylactic acid film. Here, the OP value was reduced by 46% in nanocomposite film compared to neat PLA (Jacob et al., 2022).

1.7.2 Mechanical properties

The food packaging materials must maintain their integrity during handling, transportation and storage. Therefore, they should possess good mechanical properties (tensile strength, elongation at break and elastic modulus). The incorporation of nanofillers and different additives affects the mechanical properties. The addition of plasticizers into the polymer matrix increases the segmental mobility of polymer chains, reducing the tensile strength with the rise in the elongation at break. Rukmanikrishnan et al. (2020) reported increased tensile strength (TS) by 60.6% for gellan and xanthan gum films incorporated with ZnO nanoparticles (Rukmanikrishnan et al., 2020). In another study, Alizadeh-Sani et al. (2021) reported improved elongation at break (EAB) by 42% for sodium alginate incorporated with 0.5 wt% ZnO and 2 wt% rosemary essential oil, while TS decreased by 27.7% (Alizadeh-Sani et al., 2021).

1.7.3 Optical properties

Maintenance of food quality also depends on the optical properties (UV-light absorbance/ transmission, transparency and color) of the packaging films. The packaging material must have UV-light barrier properties to protect food from lipid oxidation and discoloration and retain nutritional value. Moreover, the color of packaging films also influences the consumers' acceptance of the food product. The color properties of neat alginate films showed they are transparent without any color, while the nanocomposite films were less transparent with a bright and greenish shade. Moreover, the neat alginate film was highly transparent to both UV and visible light; however, the ZnO-incorporated nanocomposite film blocked the UV light (reduced by 87.2%) compared to alginate films) (Shankar, Kasapis, et al., 2018).

1.7.4 Antimicrobial properties

The addition of antimicrobial agents into the food packaging materials prevents the growth of microorganisms on food surfaces and, thus, increases their shelf life. Various types of antimicrobial agents have been studied so far in food packaging applications, including different nanomaterials (Basavegowda et al., 2020), enzymes (Alonso-González et al., 2020), bacteriocins (Verma et al., 2022), antimicrobial polymers (Roy et al., 2020), essential oil (S. Sharma et al., 2021), extracts from plants (Roy & Rhim, 2021) etc. Fig. 1.15 shows different types of antimicrobial agents used in food packaging. Among different nanomaterials, metals and metal oxides, inorganic nanomaterials are most commonly used in food packaging applications due to their superior antimicrobial properties as compared to others. Some examples of commonly used metals and metal oxides antimicrobial nanomaterials are Ag, Cu, Fe, Se, ZnO, TiO_2, SiO_2, CuO, CuS, MgO etc.

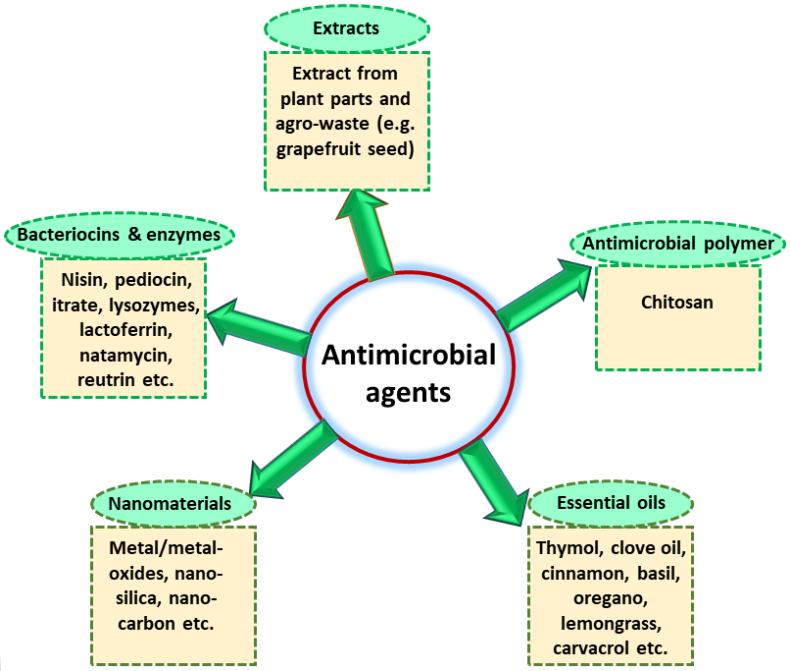

Fig. 1.15. Different types of antimicrobial agents use in food packaging.

1.7.5 Biodegradability

Developing biodegradable polymer-based nanocomposite films for food packaging applications can solve the problem of environmental issues related to synthetic plastic-based packaging materials. Biodegradation (Pires et al., 2022) is the process of breakdown of materials by the action of microorganisms (Fig. 1.16). Firstly, the long polymer chains are broken down into smaller chains and undergo oxidation. This process is initiated by the action of external factors such as heat (slightly higher temperature present in the soil), mechanical stress (wind, compaction in soil), and UV-light (sunlight). The oxidation process makes the molecules small enough and hydrophilic, which can be ingestible by microorganisms. Here, the process of biodegradation begins. Microorganisms secrete specific enzymes or generate free radicals to cleave polymers. Assimilation is the last step of the biodegradation process. The microbial species assimilate the compounds from the fragmentation process, which can stimulate or even inhibit the growth and reproduction of organisms. Monomers are transferred through the cellular membranes with the help of special membrane carriers. Other molecules to which membranes are impermeable can

undergo biotransformation reactions to absorbable products. As microorganisms consume the degraded polymer, carbon dioxide, water, and biomass are produced and returned to nature through the biocycle.

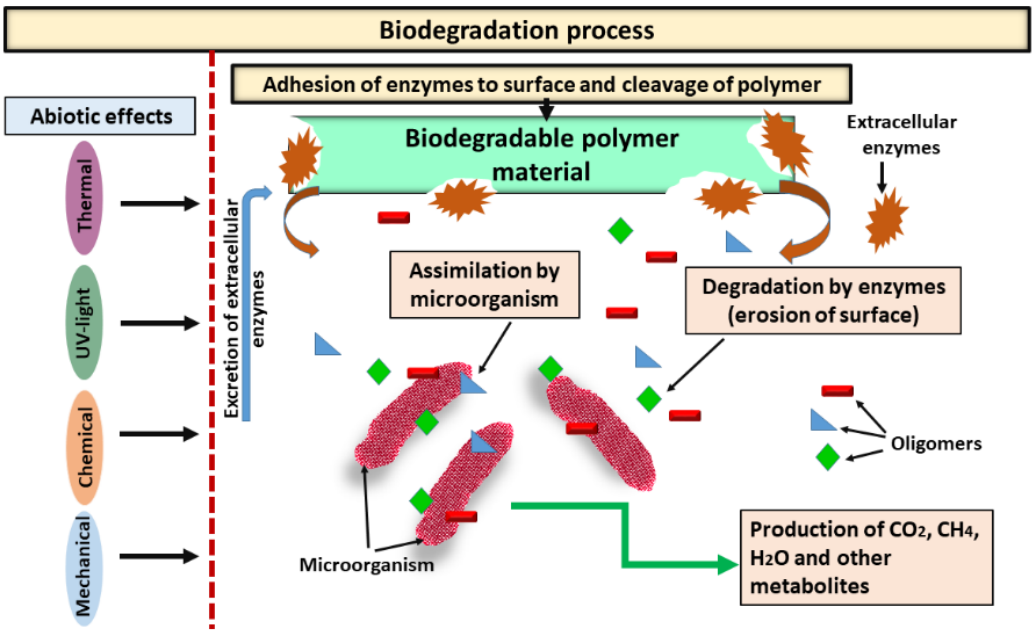

Fig. 1.16. General mechanism of degradation of biodegradable polymer materials

1.8 Literature review on antimicrobial bionanocomposites for food packaging applications

1.8.1 Biopolymer/ZnO nanocomposites

The effects of ZnO nanoparticles on biobased polymer nanocomposites for food packaging applications have been investigated by many researchers as follows:

Marra et al. (2016) have prepared PLA/ZnO nanoparticles (1, 3 and 5 wt%) nanocomposites by the melt mixing method and investigated its effect on barrier, mechanical, and antimicrobial properties (against *E. coli*) (Marra et al., 2016). In this study, ZnO nanoparticles used were of size 100–500 nm. The nanocomposite exhibited good mechanical and gas barrier

(O_2 and CO_2) properties. Most importantly, nanocomposite containing 5 wt% ZnO showed excellent antimicrobial properties against *E. coli* (99.99% reduction in cell growth after 24 h). Kim et al. (2019) have synthesized PLA/ZnO nanocomposites by solvent casting method and studied their physical and antibacterial properties (Kim et al., 2019). They have found that adding 3 wt% of ZnO into PLA completely inhibits the growth of *E. coli*. Therefore, these bionanocomposites could be active food packaging materials with excellent antibacterial properties and UV barrier properties. Shankar et al. (2018) have synthesized cubical-shaped ZnO (50–100 nm) and incorporated them in PLA to fabricate PLA/ZnO nanocomposites (Shankar, Wang, et al., 2018). The nanocomposite film exhibited excellent UV-light barrier properties. Also, the nanocomposites possessed improved tensile strength (37.5%), and WVP was reduced by 30.5%. Moreover, the nanocomposite showed excellent antibacterial activity against *E. coli* and *L. mono-cytogenes*. Further, the storage test revealed that the minced fish paste packed with PLA/ZnO film exhibited strong antibacterial activity. Tajdari et al. (2020) have fabricated PLA-based nanocomposite by incorporating two different morphologies of ZnO (cylindrical and spherical) and their functional properties, such as optical, mechanical, hydrolytic degradation and antibacterial properties (against *E. coli* and *L. monocytogenes*) were investigated (Tajdari et al., 2020). It was observed that the dispersibility of ZnO in a polymer matrix depends on ZnO morphology, and it plays a significant role in enhancing the physiochemical properties of nanocomposites. The cylindrical ZnO showed better mechanical properties (≈20%) as compared to spherical ZnO. On the other hand, in the case of optical properties and degradation, spherical ZnO showed better results (≈60%). Saral Sarojini et al. (2019) fabricated Mahua oil-based polyurethane (PU)/chitosan (CS) incorporated with ZnO nanoparticles (30 nm) (K. et al., 2019). Adding 5 wt% of ZnO into PU/CS exhibited improved tensile strength, barrier properties and hydrophobicity of the film. Moreover, nanocomposite possesses good antimicrobial properties and extends the shelf life of carrot pieces up to 9 days. Ejaz et al. (2018) have synthesized bovine skin gelatin (BSG) based nanocomposite films incorporated with clove essential oil (CEO) and

ZnO nanorods (< 100 nm) (Ejaz et al., 2018). Then the nanocomposite films were used for shrimp packaging. The results showed that nanocomposite possesses improved mechanical, oxygen and UV-barrier properties. The storage test in the refrigerator exhibited that BSG/CEO/ZnO nanorod nanocomposite films with 50% CEO (w/w of protein) showed the highest antibacterial properties against *Salmonella Typhimurium* and *L. monocytogenes*. The results clearly indicate the suitability of the nanocomposite films for active food packaging applications. Mohammadi et al. (2019) have developed bionanocomposite films by using carboxymethyl cellulose (CMC), ZnO nanoparticles and different percentages of okra mucilage (OM) to extend the shelf life of chicken breast meat stored at 4°C (Mohammadi et al., 2019). The antimicrobial activity of nanocomposite was studied using total viable counts, *S. aureus* counts, and *Lactic Acid Bacteria* counts of the chicken breast during the storage period. The results showed that CMC/OM 50%/ZnO gives the best inhibitory results against microorganism growth and exhibited the lowest chemical changes and highest sensory score in the chicken breast during storage. Youssef et al. (2016) have developed a novel nanocomposite film consisting of chitosan, carboxymethyl cellulose (CMC) and ZnO nanoparticles by solvent casting method (Youssef et al., 2016). The nanocomposite film with different concentrations of ZnO (2, 4 and 8 wt%) was studied for physiochemical properties (mechanical, thermal etc.). Moreover, they also investigated the influence of nanocomposite film packaging on the shell life of white soft cheese. The nanocomposite film showed enhanced thermal, mechanical properties and good antibacterial activity against *S. aureus, P. aeruginosa*, and *E. coli* and antifungal activity (*Candida albicans*). Also, the storage test (7°C for 30 days) revealed the improved shelf life of white soft cheese packed in nanocomposite films. Noshirvani et al. (2017) also prepared carboxymethyl cellulose/chitosan/oleic acid (CMC-CH-OL) based nanocomposite containing ZnO nanoparticles (<25 nm) to extend the shelf life of sliced wheat bread (Noshirvani et al., 2017). The presence of ZnO nanoparticles and oleic acid significantly decreased the water vapor transmission rate (WVTR) of nanocomposite film. The results revealed that the nanocomposite film showed excellent antimicrobial properties and could extend the shelf

life of sliced wheat bread from 3–35 days. Moreover, the staling rate of bread was studied by Differential Scanning Calorimetry (DSC) analysis. The results revealed that the nanocomposite film delayed the staling rate of sliced bread, indicating the suitability of nanocomposite film to be used in sliced bread packaging. Petchwattana et al. (2016) have prepared poly(butylene succinate) and ZnO nanoparticles (10 nm) nanocomposite films in the blown-film extruder for food packaging applications (Petchwattana et al., 2016). The antimicrobial activity revealed that 6 wt% of ZnO nanoparticles could inhibit *S. aureus* and *E. coli* with an inhibition zone of 1.25 and 1.31 cm, respectively. The tensile test showed that incorporating ZnO nanoparticles into poly(butylene succinate) film increases the tensile strength while decreasing the elongation at break. Kumar et al. (2019) have synthesized agar-based nanocomposite films containing hexagonal-shaped ZnO nanoparticles (average size: 24 nm) prepared from Mimusops elengi fruit extract (S. Kumar et al., 2019). The nanocomposite film was used as packaging material for the shelf life extension of green grapes. Incorporating ZnO nanoparticles into the nanocomposite film increases the thermal stability, whereas the tensile strength decreases. The storage test of green grapes packaged with nanocomposite films containing 2% (w/w) and 4% (w/w) of ZnO nanoparticles showed a fresh appearance up to 14 to 21 days, respectively, in ambient conditions. Therefore, agar/ZnO nanocomposites film showed promising ability to be used in active food packaging.

1.8.2 Biopolymer/halloysite nanotubes

Meira et al. (2017) have synthesized corn starch-based nanocomposite films reinforced with nisin and pediocin-adsorbed halloysite nanotubes by solvent casting method (Meira et al., 2017). Incorporating halloysite nanotubes containing nisin and pediocin improved thermal and mechanical properties. The nanocomposite film possesses good antimicrobial properties against *Listeria. Monocytogenes* and *Clostridium perfringens*. Huang et al. (2020) fabricated agar-based nanocomposite films with chitosan and halloysite nanotubes by a solution casting technique and studied the physiochemical properties of nanocomposite films (Huang et al. 2020). Results

revealed that with increasing the concentration of chitosan and halloysite nanotubes, the nanocomposite films possess significantly higher tensile strength (35–48 MPa) and elongation at break (14.79–22.62%). The nanocomposite film possesses > 70% transparency in the visible region, which indicates that the presence of chitosan and halloysite nanotubes slightly affected the light transmittance of agar-based nanocomposite films. Bugatti et al. (2017) have synthesized antimicrobial nanocomposites of PLA containing halloysite nanotubes (3, 5, 10 wt%) and lysozyme (antimicrobial agent) (Bugatti et al., 2017). Along with physiochemical properties, they have also studied the controlled release of lysozyme into saline solution using UV spectrophotometry. The nanocomposite possesses improved mechanical properties, especially at low nanofiller loading (3 wt%). At higher loading (10 wt%), elongation at break decreases due to agglomeration. Water vapor barrier properties also improved due to the formation of the nanocomposite. The release kinetics studies of the nanocomposite films were found to be dependent on the nanofiller loading. Abdullah et al. (2019) have synthesized polyvinyl alcohol (PVA)/starch (ST)/glycerol (GL) nanocomposites with the loading of halloysite nanotubes (0.25, 0.5, 1, 3 and 5 wt%) by solvent casting method (Abdullah et al., 2019). The bionanocomposites showed good water and gas barrier properties and increased the shelf life of avocados and peaches. The results demonstrated the potential ability of nanocomposites to be used as active food packaging materials. Dutta et al. (2019) have fabricated ternary nanocomposites of starch/chitosan/halloysite nanotubes by solvent casting method (Devi & Dutta, 2019). The ternary nanocomposite possesses improved water absorption capacity, water vapor transmission rate and water solubility. Water contact results revealed the hydrophilic nature of ternary nanocomposite films. The results showed the suitability of the nanocomposite films for wound dressing applications. Shankar et al. (2018) have prepared alginate-based bionanocomposite films by incorporating ZnO-deposited halloysite nanotubes (1, 3, 5, 7 wt%) (Shankar, Kasapis, et al., 2018). Before the deposition of the ZnO on halloysite nanotubes, the surface was functionalized with NaOH. The nanocomposite films synthesized with 7 wt% of ZnO deposited halloysite nanotubes

showed complete inhibition of *E. coli* and *L. monocytogenes* after 3 and 9 h of the incubation period.

1.8.3 Biopolymer/essential oil/nanoparticles

Gasti et al. (2022) have developed bionanocomposites of chitosan/pullulan containing clove essential oil-loaded chitosan-ZnO hybrid nanoparticles (CZC NPs) (Gasti et al., 2022). The addition of CZC NPs leads to the improvement of nanocomposite films as follows: tensile strength (~39.82%), water vapor barrier (~84.64%), oxygen barrier (~57.66%), film hydrophobicity (~35.36%) and UV light barrier properties as compared to pristine chitosan and pullulan film. The nanocomposite film also possesses good antioxidant and antimicrobial activity against *P. aeruginosa*, *S. aureus*, and *E. coli*. Moreover, the packaging test on chicken meat for 5 days at 8 ± 2℃ revealed an extension of the shelf life of packaged chicken meat. Lee et al. (2018) have synthesized chitosan/clove essential oil/halloysite nanotubes nanocomposites for active food packaging applications (Lee et al., 2018). The nanocomposite film possesses better water vapor barrier properties due to the incorporation of clove essential oil and HNT. This was mainly due to the formation of the tortuous path in the nanocomposite in the presence of HNT. They have also studied the antioxidant activity of the nanocomposite films by total phenolic content, 2,2-diphenyl-1-picrylhydrazyl, and reducing power assays. The nanocomposite films with 15 wt% of HNT exhibit the highest antioxidant activity. The migration studies in food simulant revealed that the release of clove essential oil was higher in 50 % ethanol (simulant for alcoholic food), as compared to 10% (simulant for aqueous food) and 95% ethanol (simulant for fatty food). Alizadeh-Sani et al. (2018) have fabricated whey protein isolate (WPI)/cellulose nanofibers (CNF)/titanium dioxide (TiO_2)/rosemary essential oil (REO) nanocomposites by solvent casting method and characterized for different physiochemical properties (Alizadeh-Sani et al., 2021). The water barrier properties of WPI/CNF nanocomposite films increased significantly with the incorporation of TiO_2 and REO. Loading 7.5 wt% of CNF and 1 wt% of TiO_2 has significantly

increased tensile strength and Young's modulus while decreasing the elongation at break value. The nanocomposite film possesses improved hydrophobicity and strong antibacterial activity against pathogenic bacteria, mainly Gram-positive. Subbuvel et al. (2022) have developed PLA/curcumin/ fenugreek essential oil (FEO) nanocomposites by solvent casting method to improve the functional properties of the nanocomposite films (Subbuvel & Kavan, 2022). Incorporating curcumin and FEO improved tensile strength, thermal stability, UV-barrier properties, surface color, flexibility and water contact angle. The PLA based nanocomposite film possessed good antioxidant and antimicrobial properties (*S. aureus* and *E. coli*). Moreover, a packaging test was done on strawberries as a model food, and the results obtained were compared with commercial polyethylene (PE) film. Cui et al. (2021) have prepared an antimicrobial nanocomposite film of sodium alginate (SA) with the addition of cinnamaldehyde and sulfuric acid-treated HNTs (Cui et al., 2021). The addition of cinnamaldehyde and treated halloysite nanotubes improved the tensile strength, UV barrier and water vapor barrier properties of the SA films. Also, the release of cinnamaldehyde from nanocomposite films containing HNTs to food simulant was delayed by 144 h, compared to polymer film containing only SA and cinnamaldehyde.

1.8.4 Biopolymer/functionalized ZnO nanocomposites

Pantani et al. (2013) fabricated PLA/ZnO nanocomposites using the melt compounding method (Pantani et al., 2013). They used rod-shaped ZnO (0.5–3 wt% with respect to PLA) functionalized with triethoxy caprylsilane. Surface-treated ZnO provides better compatibility with hydrophobic polymers. The nanocomposites exhibited good mechanical, UV barrier and antibacterial properties suitable for application in eco-friendly packaging films. Liu et al. (2013) have studied the surface modification of tetrapod-shaped ZnO whisker (T-ZnO), and nano ZnO was modified with 3-amino propyltriethyloxy silane (Liu et al., 2012). The modified ZnO was then added into

poly(butylene succinate) (PBS) by melt extrusion. The FE-SEM image revealed better interfacial interaction between ZnO and PBS after functionalization of ZnO.

1.9 Outcome of literature review/Research Gap

Detailed literature survey on PLA based bionanocomposites revealed:

- To overcome the inherent limitations of PLA (brittleness, poor barrier properties etc.) and expand its application scope, it is blended with other polymers or nanofillers. The morphology of nanofillers plays an important role in the final properties determination of polymer nanocomposites. Thus, suitable modifications in surface and structural morphologies of the conventional nanofillers may yield even better properties of the nanocomposites.
- The main challenge in polymer nanocomposites is obtaining as uniform nanofiller dispersion in the polymer matrix as possible. Uniform dispersion of the nanofiller results in high surface interactions between the nanofiller and polymer matrix, leading to improved properties.
- Antimicrobial bionanocomposites offer extended protection and preservation of food products. However, the stability of the antimicrobial agents in the polymer matrix is critical.
- The use of essential oil as an antimicrobial additive has limitations, such as high volatility. This limitation requires efforts to reduce the evaporative loss of the antimicrobial agents from the polymer matrix.
- It was observed that very few efforts are made to synthesize PLA-based bionanocomposites by using the ultrasound-assisted solvent casting method. The method of nanocomposite synthesis plays an important role in the dispersion of the nanofiller in the matrix.
- The effect of nanofiller morphology on the PLA matrix has not been studied.
- No literature is available on addressing the improvement of the volatility of essential oil incorporated into PLA matrix to extend the shelf life of food products.

1.10 Objectives of the Thesis

This work aims to synthesize poly(lactic acid) based bionanocomposites by incorporating different nanoparticles/antimicrobial additives with enhanced physiochemical properties for potential food packaging applications. The addition of different antimicrobial agents Inhibits the growth of microorganisms and extends the shelf life and quality of the food products.

Based on the literature review and the broad aim of the thesis, the specific objectives were decided as follows:

1. Sonochemical synthesis of poly(lactic acid) nanocomposites with ZnO nanoflowers: Effect of nanofiller morphology on physical properties.
2. Poly(lactic acid)/functionalized ZnO nanocomposites for antimicrobial food packaging applications.
3. Antimicrobial bionanocomposites of poly(lactic acid)/ZnO deposited halloysite nanotubes for potential food packaging applications.
4. Synthesis and characterization of poly(lactic acid)/clove essential oil/alkali-treated halloysite nanotubes composite films for food packaging applications.

1.11 Organization of the doctoral thesis

This thesis has been organized into six chapters.

Chapter 1 provides a general introduction to biopolymers, different nanofillers, a brief description of polymer nanocomposites, synthesis methods of polymer nanocomposites and their applications in the food packaging sector. The chapter also includes literature on PLA-based nanocomposites for antimicrobial food packaging applications. Finally, the research gap, objectives and the organization of the thesis work are presented.

Chapter 2 reports the ultrasound-assisted synthesis of PLA/ZnO nanocomposites with the special feature of flower-like morphology of ZnO. The ZnO nanoflowers are synthesized via a facile sonochemical method with $Zn(NO_3)_2 \cdot 6H_2O$ as a precursor in different concentrations of 0.025, 0.05, 0.075 and 0.1 M.

In **Chapter 3,** the surface of the ZnO nanoparticles has been modified with silane coupling agent 3-(aminopropyl) trimethoxysilane (APTMS). The effects of surface-modified ZnO on PLA's thermal, mechanical and antimicrobial properties have been investigated. The basic motivation behind this work is to get superior antimicrobial properties of PLA/ZnO nanocomposites with better compatibility of functionalized with PLA.

Chapter 4 reports the synthesis of polylactic acid (PLA) nanocomposites with ZnO@HNT using an ultrasound-assisted solvent casting method. The synthesized PLA/ZnO@HNT films were characterized for physical, thermal, mechanical, UV-shielding, barrier properties and antimicrobial activity for food packaging applications. Moreover, a packaging test was performed on cut apples for 6 days storage period to evaluate the potential efficacy of nanocomposite films for food packaging applications.

Chapter 5 describes the synthesis of nanocomposites of polylactic acid (PLA) with clove essential oil (CEO) and alkali-treated halloysite nanotubes (NHNT) as fillers by using a simple solvent casting method. The as-synthesized nanocomposite films were characterized by the physical, thermal, mechanical and water vapor barrier properties of food packaging material.

Chapter 6 gives an appropriate conclusion based on the findings from the previous chapters. This chapter also gives some suggestions for future work in this field.

References

Abdullah, Z. W., Dong, Y., Han, N., & Liu, S. (2019). Water and gas barrier properties of polyvinyl alcohol (PVA)/starch (ST)/ glycerol (GL)/halloysite nanotube (HNT) bionanocomposite films: Experimental characterisation and modelling approach. *Composites Part B: Engineering*, *174*, 107033. https://doi.org/10.1016/j.compositesb.2019.107033

Abreu, A. S., Oliveira, M., de Sá, A., Rodrigues, R. M., Cerqueira, M. A., Vicente, A. A., & Machado, A. V. (2015). Antimicrobial nanostructured starch based films for packaging. *Carbohydrate Polymers*, *129*, 127–134. https://doi.org/10.1016/j.carbpol.2015.04.021

Ahangaran, F., & Navarchian, A. H. (2020). Recent advances in chemical surface modification of metal oxide nanoparticles with silane coupling agents: A review. *Advances in Colloid and Interface Science*, *286*, 102298. https://doi.org/10.1016/j.cis.2020.102298

Alexandre, E. M. C., Lourenço, R. V., Bittante, A. M. Q. B., Moraes, I. C. F., & Sobral, P. J. do A. (2016). Gelatin-based films reinforced with montmorillonite and activated with nanoemulsion of ginger essential oil for food packaging applications. *Food Packaging and Shelf Life*, *10*, 87–96. https://doi.org/10.1016/j.fpsl.2016.10.004

Ali, H., Ismail, A. M., & Menazea, A. A. (2022). Multifunctional Ag/ZnO/chitosan ternary bio-nanocomposites synthesized via laser ablation with enhanced optical, antibacterial, and catalytic characteristics. *Journal of Water Process Engineering*, 102940. https://doi.org/10.1016/j.jwpe.2022.102940

Alizadeh-Sani, M., Moghaddas Kia, E., Ghasempour, Z., & Ehsani, A. (2021). Preparation of Active Nanocomposite Film Consisting of Sodium Caseinate, ZnO Nanoparticles and Rosemary Essential Oil for Food Packaging Applications. *Journal of Polymers and the Environment*, *29*(2), 588–598. https://doi.org/10.1007/s10924-020-01906-5

Alkan Tas, B., Sehit, E., Erdinc Tas, C., Unal, S., Cebeci, F. C., Menceloglu, Y. Z., & Unal, H. (2019). Carvacrol loaded halloysite coatings for antimicrobial food packaging

applications. *Food Packaging and Shelf Life*, *20*, 100300. https://doi.org/10.1016/j.fpsl.2019.01.004

Alonso-González, M., Corral-González, A., Felix, M., Romero, A., & Martin-Alfonso, J. E. (2020). Developing active poly(vinyl alcohol)-based membranes with encapsulated antimicrobial enzymes via electrospinning for food packaging. *International Journal of Biological Macromolecules*, *162*, 913–921. https://doi.org/10.1016/j.ijbiomac.2020.06.217

Alvarez Echazú, M. I., Olivetti, C. E., Peralta, I., Alonso, M. R., Anesini, C., Perez, C. J., Alvarez, G. S., & Desimone, M. F. (2018). Development of pH-responsive biopolymer-silica composites loaded with Larrea divaricata Cav. Extract with antioxidant activity. *Colloids and Surfaces B: Biointerfaces*, *169*, 82–91. https://doi.org/10.1016/j.colsurfb.2018.05.015

Arrieta, M. P., Samper, M. D., Aldas, M., & López, J. (2017). On the Use of PLA-PHB Blends for Sustainable Food Packaging Applications. *Materials*, *10*(9), Article 9. https://doi.org/10.3390/ma10091008

Babaee, M., Garavand, F., Rehman, A., Jafarazadeh, S., Amini, E., & Cacciotti, I. (2022). Biodegradability, physical, mechanical and antimicrobial attributes of starch nanocomposites containing chitosan nanoparticles. *International Journal of Biological Macromolecules*, *195*, 49–58. https://doi.org/10.1016/j.ijbiomac.2021.11.162

Barman, M., Mahmood, S., Augustine, R., Hasan, A., Thomas, S., & Ghosal, K. (2020). Natural halloysite nanotubes /chitosan based bio-nanocomposite for delivering norfloxacin, an anti-microbial agent in sustained release manner. *International Journal of Biological Macromolecules*, *162*, 1849–1861. https://doi.org/10.1016/j.ijbiomac.2020.08.060

Basavegowda, N., Mandal, T. K., & Baek, K.-H. (2020). Bimetallic and Trimetallic Nanoparticles for Active Food Packaging Applications: A Review. *Food and Bioprocess Technology*, *13*(1), 30–44. https://doi.org/10.1007/s11947-019-02370-3

Boro, U., Kashyap, N., & Moholkar, V. S. (2022). Sonochemical Synthesis of Poly(lactic acid) Nanocomposites with ZnO Nanoflowers: Effect of Nanofiller Morphology on Physical Properties. *ACS Engineering Au*, *2*(1), 46–60. https://doi.org/10.1021/acsengineeringau.1c00018

Borrelle, S. B., Ringma, J., Law, K. L., Monnahan, C. C., Lebreton, L., McGivern, A., Murphy, E., Jambeck, J., Leonard, G. H., Hilleary, M. A., Eriksen, M., Possingham, H. P., De Frond, H., Gerber, L. R., Polidoro, B., Tahir, A., Bernard, M., Mallos, N., Barnes, M., & Rochman, C. M. (2020). Predicted growth in plastic waste exceeds efforts to mitigate plastic pollution. *Science*, *369*(6510), 1515–1518. https://doi.org/10.1126/science.aba3656

Bugatti, V., Sorrentino, A., & Gorrasi, G. (2017). Encapsulation of Lysozyme into halloysite nanotubes and dispersion in PLA: Structural and physical properties and controlled release analysis. *European Polymer Journal*, *93*, 495–506. https://doi.org/10.1016/j.eurpolymj.2017.06.024

Campos-Requena, V. H., Rivas, B. L., Pérez, M. A., Figueroa, C. R., Figueroa, N. E., & Sanfuentes, E. A. (2017). Thermoplastic starch/clay nanocomposites loaded with essential oil constituents as packaging for strawberries − In vivo antimicrobial synergy over Botrytis cinerea. *Postharvest Biology and Technology*, *129*, 29–36. https://doi.org/10.1016/j.postharvbio.2017.03.005

Carvalho, R. A., de Oliveira, A. C. S., Santos, T. A., Dias, M. V., Yoshida, M. I., & Borges, S. V. (2020). WPI and Cellulose Nanofibres Bio-nanocomposites: Effect of Thyme Essential Oil on the Morphological, Mechanical, Barrier and Optical Properties. *Journal of Polymers and the Environment*, *28*(1), 231–241. https://doi.org/10.1007/s10924-019-01598-6

Castro-Mayorga, J. L., Freitas, F., Reis, M. A. M., Prieto, M. A., & Lagaron, J. M. (2018). Biosynthesis of silver nanoparticles and polyhydroxybutyrate nanocomposites of interest

in antimicrobial applications. *International Journal of Biological Macromolecules*, *108*, 426–435. https://doi.org/10.1016/j.ijbiomac.2017.12.007

Chaieb, K., Hajlaoui, H., Zmantar, T., Kahla-Nakbi, A. B., Rouabhia, M., Mahdouani, K., & Bakhrouf, A. (2007). The chemical composition and biological activity of clove essential oil, Eugenia caryophyllata (Syzigium aromaticum L. Myrtaceae): A short review. *Phytotherapy Research*, *21*(6), 501–506. https://doi.org/10.1002/ptr.2124

Chang, T.-H., Lu, Y.-C., Yang, M.-J., Huang, J.-W., Linda Chang, P.-F., & Hsueh, H.-Y. (2020). Multibranched flower-like ZnO particles from eco-friendly hydrothermal synthesis as green antimicrobials in agriculture. *Journal of Cleaner Production*, *262*, 121342. https://doi.org/10.1016/j.jclepro.2020.121342

Chong, W. J., Shen, S., Li, Y., Trinchi, A., Pejak, D., (Louis) Kyratzis, I., Sola, A., & Wen, C. (2022). Additive manufacturing of antibacterial PLA-ZnO nanocomposites: Benefits, limitations and open challenges. *Journal of Materials Science & Technology*, *111*, 120–151. https://doi.org/10.1016/j.jmst.2021.09.039

Choudhary, S., Sahu, K., Bisht, A., Satpati, B., & Mohapatra, S. (2021). Rapid synthesis of ZnO nanowires and nanoplates with highly enhanced photocatalytic performance. *Applied Surface Science*, *541*, 148484. https://doi.org/10.1016/j.apsusc.2020.148484

Chouhan, S., Sharma, K., & Guleria, S. (2017). Antimicrobial Activity of Some Essential Oils—Present Status and Future Perspectives. *Medicines*, *4*(3), Article 3. https://doi.org/10.3390/medicines4030058

Coban, H. B. (2020). Organic acids as antimicrobial food agents: Applications and microbial productions. *Bioprocess and Biosystems Engineering*, *43*(4), 569–591. https://doi.org/10.1007/s00449-019-02256-w

Corradini, C., Alfieri, I., Cavazza, A., Lantano, C., Lorenzi, A., Zucchetto, N., & Montenero, A. (2013). Antimicrobial films containing lysozyme for active packaging obtained by sol–

gel technique. *Journal of Food Engineering*, *119*(3), 580–587. https://doi.org/10.1016/j.jfoodeng.2013.05.046

Cui, R., Zhu, B., Yan, J., Qin, Y., Yuan, M., Cheng, G., & Yuan, M. (2021). Development of a Sodium Alginate-Based Active Package with Controlled Release of Cinnamaldehyde Loaded on Halloysite Nanotubes. *Foods*, *10*(6), Article 6. https://doi.org/10.3390/foods10061150

da Costa, R. C., Daitx, T. S., Mauler, R. S., da Silva, N. M., Miotto, M., Crespo, J. S., & Carli, L. N. (2020). Poly(hydroxybutyrate-co-hydroxyvalerate)-based nanocomposites for antimicrobial active food packaging containing oregano essential oil. *Food Packaging and Shelf Life*, *26*, 100602. https://doi.org/10.1016/j.fpsl.2020.100602

Danyliuk, N., Tomaszewska, J., & Tatarchuk, T. (2020). Halloysite nanotubes and halloysite-based composites for environmental and biomedical applications. *Journal of Molecular Liquids*, *309*, 113077. https://doi.org/10.1016/j.molliq.2020.113077

Devi, N., & Dutta, J. (2019). Development and in vitro characterization of chitosan/starch/halloysite nanotubes ternary nanocomposite films. *International Journal of Biological Macromolecules*, *127*, 222–231. https://doi.org/10.1016/j.ijbiomac.2019.01.047

Dizaj, S. M., Lotfipour, F., Barzegar-Jalali, M., Zarrintan, M. H., & Adibkia, K. (2014). Antimicrobial activity of the metals and metal oxide nanoparticles. *Materials Science and Engineering: C*, *44*, 278–284. https://doi.org/10.1016/j.msec.2014.08.031

Dong, X., Liang, X., Zhou, Y., Bao, K., Sameen, D. E., Ahmed, S., Dai, J., Qin, W., & Liu, Y. (2021). Preparation of polylactic acid/TiO2/GO nano-fibrous films and their preservation effect on green peppers. *International Journal of Biological Macromolecules*, *177*, 135–148. https://doi.org/10.1016/j.ijbiomac.2021.02.125

Ejaz, M., Arfat, Y. A., Mulla, M., & Ahmed, J. (2018). Zinc oxide nanorods/clove essential oil incorporated Type B gelatin composite films and its applicability for shrimp packaging. *Food Packaging and Shelf Life*, *15*, 113–121. https://doi.org/10.1016/j.fpsl.2017.12.004

El-Naggar, M. E., Hasanin, M., & Hashem, A. H. (2022). Eco-Friendly Synthesis of Superhydrophobic Antimicrobial Film Based on Cellulose Acetate/Polycaprolactone Loaded with the Green Biosynthesized Copper Nanoparticles for Food Packaging Application. *Journal of Polymers and the Environment*, *30*(5), 1820–1832. https://doi.org/10.1007/s10924-021-02318-9

Espitia, P. J. P., Soares, N. de F. F., Coimbra, J. S. dos R., de Andrade, N. J., Cruz, R. S., & Medeiros, E. A. A. (2012). Zinc Oxide Nanoparticles: Synthesis, Antimicrobial Activity and Food Packaging Applications. *Food and Bioprocess Technology*, *5*(5), 1447–1464. https://doi.org/10.1007/s11947-012-0797-6

Farah, S., Anderson, D. G., & Langer, R. (2016). Physical and mechanical properties of PLA, and their functions in widespread applications—A comprehensive review. *Advanced Drug Delivery Reviews*, *107*, 367–392. https://doi.org/10.1016/j.addr.2016.06.012

Fonseca, C., Ochoa, A., Ulloa, M. T., Alvarez, E., Canales, D., & Zapata, P. A. (2015). Poly(lactic acid)/TiO2 nanocomposites as alternative biocidal and antifungal materials. *Materials Science and Engineering: C*, *57*, 314–320. https://doi.org/10.1016/j.msec.2015.07.069

Garavand, F., Rouhi, M., Razavi, S. H., Cacciotti, I., & Mohammadi, R. (2017). Improving the integrity of natural biopolymer films used in food packaging by crosslinking approach: A review. *International Journal of Biological Macromolecules*, *104*, 687–707. https://doi.org/10.1016/j.ijbiomac.2017.06.093

Garlotta, D. (2001). A Literature Review of Poly(Lactic Acid). *Journal of Polymers and the Environment*, *9*(2), 63–84. https://doi.org/10.1023/A:1020200822435

Gasti, T., Dixit, S., Hiremani, V. D., Chougale, R. B., Masti, S. P., Vootla, S. K., & Mudigoudra, B. S. (2022). Chitosan/pullulan based films incorporated with clove essential oil loaded chitosan-ZnO hybrid nanoparticles for active food packaging. *Carbohydrate Polymers*, *277*, 118866. https://doi.org/10.1016/j.carbpol.2021.118866

Geyer, R., Jambeck, J. R., & Law, K. L. (2017). Production, use, and fate of all plastics ever made. *Science Advances*, *3*(7), e1700782. https://doi.org/10.1126/sciadv.1700782

Ghanbarzadeh, B., Oleyaei, S. A., & Almasi, H. (2015). Nanostructured Materials Utilized in Biopolymer-based Plastics for Food Packaging Applications. *Critical Reviews in Food Science and Nutrition*, *55*(12), 1699–1723. https://doi.org/10.1080/10408398.2012.731023

Ghosh, S., Majumder, D., Sen, A., & Roy, S. (2014). Facile sonochemical synthesis of zinc oxide nanoflakes at room temperature. *Materials Letters*, *130*, 215–217. https://doi.org/10.1016/j.matlet.2014.05.112

Ghozali, M., Fahmiati, S., Triwulandari, E., Restu, W. K., Farhan, D., Wulansari, M., & Fatriasari, W. (2020). PLA/metal oxide biocomposites for antimicrobial packaging application. *Polymer-Plastics Technology and Materials*, *59*(12), 1332–1342. https://doi.org/10.1080/25740881.2020.1738475

Hasanin, M., Al Abboud, M. A., Alawlaqi, M. M., Abdelghany, T. M., & Hashem, A. H. (2022). Ecofriendly Synthesis of Biosynthesized Copper Nanoparticles with Starch-Based Nanocomposite: Antimicrobial, Antioxidant, and Anticancer Activities. *Biological Trace Element Research*, *200*(5), 2099–2112. https://doi.org/10.1007/s12011-021-02812-0

Hasheminejad, N., Khodaiyan, F., & Safari, M. (2019). Improving the antifungal activity of clove essential oil encapsulated by chitosan nanoparticles. *Food Chemistry*, *275*, 113–122. https://doi.org/10.1016/j.foodchem.2018.09.085

Heydari-Majd, M., Ghanbarzadeh, B., Shahidi-Noghabi, M., Najafi, M. A., & Hosseini, M. (2019). A new active nanocomposite film based on PLA/ZnO nanoparticle/essential oils

for the preservation of refrigerated Otolithes ruber fillets. *Food Packaging and Shelf Life*, *19*, 94–103. https://doi.org/10.1016/j.fpsl.2018.12.002

Huang, D., Zhang, Z., Zheng, Y., Quan, Q., Wang, W., & Wang, A. (2020). Synergistic effect of chitosan and halloysite nanotubes on improving agar film properties. *Food Hydrocolloids*, *101*, 105471. https://doi.org/10.1016/j.foodhyd.2019.105471

Hyldgaard, M., Mygind, T., & Meyer, R. (2012). Essential Oils in Food Preservation: Mode of Action, Synergies, and Interactions with Food Matrix Components. *Frontiers in Microbiology*, *3*. https://www.frontiersin.org/articles/10.3389/fmicb.2012.00012

Jacob, J., Robert, V., Valapa, R. B., Kuriakose, S., Thomas, S., & Loganathan, S. (2022). Poly(lactic acid)/Polyethylenimine Functionalized Mesoporous Silica Biocomposite Films for Food Packaging. *ACS Applied Polymer Materials*, *4*(7), 4632–4642. https://doi.org/10.1021/acsapm.1c01551

Jafarzadeh, S., Mohammadi Nafchi, A., Salehabadi, A., Oladzad-abbasabadi, N., & Jafari, S. M. (2021). Application of bio-nanocomposite films and edible coatings for extending the shelf life of fresh fruits and vegetables. *Advances in Colloid and Interface Science*, *291*, 102405. https://doi.org/10.1016/j.cis.2021.102405

K., S. S., M.p., I., & G.r., R. (2019). Mahua oil-based polyurethane/chitosan/nano ZnO composite films for biodegradable food packaging applications. *International Journal of Biological Macromolecules*, *124*, 163–174. https://doi.org/10.1016/j.ijbiomac.2018.11.195

Khorshidian, N., Yousefi, M., Khanniri, E., & Mortazavian, A. M. (2018). Potential application of essential oils as antimicrobial preservatives in cheese. *Innovative Food Science & Emerging Technologies*, *45*, 62–72. https://doi.org/10.1016/j.ifset.2017.09.020

Kim, I., Viswanathan, K., Kasi, G., Sadeghi, K., Thanakkasaranee, S., & Seo, J. (2019). Poly(Lactic Acid)/ZnO Bionanocomposite Films with Positively Charged ZnO as

Potential Antimicrobial Food Packaging Materials. *Polymers*, *11*(9), Article 9. https://doi.org/10.3390/polym11091427

Kumar, Rajesh, Umar, Ahmad, Kumar, Girish, & Nalwa, H. S. (2017). Antimicrobial properties of ZnO nanomaterials: A review. *Ceramics International*, *43*(5), 3940–3961. https://doi.org/10.1016/j.ceramint.2016.12.062

Kumar, S., Boro, J. C., Ray, D., Mukherjee, A., & Dutta, J. (2019). Bionanocomposite films of agar incorporated with ZnO nanoparticles as an active packaging material for shelf life extension of green grape. *Heliyon*, *5*(6), e01867. https://doi.org/10.1016/j.heliyon.2019.e01867

Kumar, V., Gupta, R., & Bansal, A. (2021). Hydrothermal Growth of ZnO Nanorods for Use in Dye-Sensitized Solar Cells. *ACS Applied Nano Materials*, *4*(6), 6212–6222. https://doi.org/10.1021/acsanm.1c01012

Lallo da Silva, B., Abuçafy, M. P., Berbel Manaia, E., Oshiro Junior, J. A., Chiari-Andréo, B. G., Pietro, R. C. R., & Chiavacci, L. A. (2019). Relationship Between Structure And Antimicrobial Activity Of Zinc Oxide Nanoparticles: An Overview. *International Journal of Nanomedicine*, *14*, 9395–9410. https://doi.org/10.2147/IJN.S216204

Lee, M. H., Kim, S. Y., & Park, H. J. (2018). Effect of halloysite nanoclay on the physical, mechanical, and antioxidant properties of chitosan films incorporated with clove essential oil. *Food Hydrocolloids*, *84*, 58–67. https://doi.org/10.1016/j.foodhyd.2018.05.048

Li, D., Huang, X., Hao, F., Lv, Y., Chen, H., Wu, S., Xiong, W., Liu, P., & Luo, H. (2022). Preparation of organic-inorganic composites with high antibacterial activity based on sepiolite, chitosan and zinc: The study of the active antibacterial sites of chitosan-zinc oxide structure. *Applied Clay Science*, *216*, 106325. https://doi.org/10.1016/j.clay.2021.106325

Li, Q., Ren, T., Perkins, P., Hu, X., & Wang, X. (2021). Applications of halloysite nanotubes in food packaging for improving film performance and food preservation. *Food Control*, *124*, 107876. https://doi.org/10.1016/j.foodcont.2021.107876

Liu, W.-G., Zhang, X.-C., Li, H.-Y., & Liu, Z. (2012). Effect of surface modification with 3-aminopropyltriethyloxy silane on mechanical and crystallization performances of ZnO/poly(butylenesuccinate) composites. *Composites Part B: Engineering*, *43*(5), 2209–2216. https://doi.org/10.1016/j.compositesb.2012.02.021

Lu, W., Cui, R., Zhu, B., Qin, Y., Cheng, G., Li, L., & Yuan, M. (2021). Influence of clove essential oil immobilized in mesoporous silica nanoparticles on the functional properties of poly(lactic acid) biocomposite food packaging film. *Journal of Materials Research and Technology*, *11*, 1152–1161. https://doi.org/10.1016/j.jmrt.2021.01.098

Ma, Z., Garrido-Maestu, A., & Jeong, K. C. (2017). Application, mode of action, and in vivo activity of chitosan and its micro- and nanoparticles as antimicrobial agents: A review. *Carbohydrate Polymers*, *176*, 257–265. https://doi.org/10.1016/j.carbpol.2017.08.082

Maghfoori, F., Najmoddin, N., & Pezeshki-Modaress, M. (2022). Enhancing mechanical and antibacterial properties of polycaprolactone nanocomposite nanofibers using decorated clay with ZnO nanorods. *Journal of Applied Polymer Science*, *139*(30), e52684. https://doi.org/10.1002/app.52684

Mallakpour, S., & Madani, M. (2015). A review of current coupling agents for modification of metal oxide nanoparticles. *Progress in Organic Coatings*, *86*, 194–207. https://doi.org/10.1016/j.porgcoat.2015.05.023

Marra, A., Silvestre, C., Duraccio, D., & Cimmino, S. (2016). Polylactic acid/zinc oxide biocomposite films for food packaging application. *International Journal of Biological Macromolecules*, *88*, 254–262. https://doi.org/10.1016/j.ijbiomac.2016.03.039

Meira, S. M. M., Zehetmeyer, G., Werner, J. O., & Brandelli, A. (2017). A novel active packaging material based on starch-halloysite nanocomposites incorporating

antimicrobial peptides. *Food Hydrocolloids*, *63*, 561–570. https://doi.org/10.1016/j.foodhyd.2016.10.013

Mohammadalinejhad, S., Almasi, H., & Esmaiili, M. (2021). Physical and release properties of poly(lactic acid)/nanosilver-decorated cellulose, chitosan and lignocellulose nanofiber composite films. *Materials Chemistry and Physics*, *268*, 124719. https://doi.org/10.1016/j.matchemphys.2021.124719

Mohammadi, H., Kamkar, A., Misaghi, A., Zunabovic-Pichler, M., & Fatehi, S. (2019). Nanocomposite films with CMC, okra mucilage, and ZnO nanoparticles: Extending the shelf-life of chicken breast meat. *Food Packaging and Shelf Life*, *21*, 100330. https://doi.org/10.1016/j.fpsl.2019.100330

Motshekga, S. C., Ray, S. S., Onyango, M. S., & Momba, M. N. B. (2015). Preparation and antibacterial activity of chitosan-based nanocomposites containing bentonite-supported silver and zinc oxide nanoparticles for water disinfection. *Applied Clay Science*, *114*, 330–339. https://doi.org/10.1016/j.clay.2015.06.010

Mulla, M. Z., Rahman, M. R. T., Marcos, B., Tiwari, B., & Pathania, S. (2021). Poly Lactic Acid (PLA) Nanocomposites: Effect of Inorganic Nanoparticles Reinforcement on Its Performance and Food Packaging Applications. *Molecules*, *26*(7), Article 7. https://doi.org/10.3390/molecules26071967

Munteanu, B. S., Aytac, Z., Pricope, G. M., Uyar, T., & Vasile, C. (2014). Polylactic acid (PLA)/Silver-NP/VitaminE bionanocomposite electrospun nanofibers with antibacterial and antioxidant activity. *Journal of Nanoparticle Research*, *16*(10), 2643. https://doi.org/10.1007/s11051-014-2643-4

Nabgui, A., Follain, N., Vidović, E., El Haskouri, J., Marais, S., El Meziane, A., Lahcini, M., & Thébault, P. (2022). Preparation and study of the thermal, barrier and antibacterial properties of Polylactic acid-Fluorphlogopite-Silver nanoparticles nanocomposite films.

Progress in Organic Coatings, *171*, 107041. https://doi.org/10.1016/j.porgcoat.2022.107041

Nandi, S., & Guha, P. (2018). A Review on Preparation and Properties of Cellulose Nanocrystal-Incorporated Natural Biopolymer. *Journal of Packaging Technology and Research*, *2*(2), 149–166. https://doi.org/10.1007/s41783-018-0036-3

Niu, X., Liu, Y., Song, Y., Han, J., & Pan, H. (2018). Rosin modified cellulose nanofiber as a reinforcing and co-antimicrobial agents in polylactic acid /chitosan composite film for food packaging. *Carbohydrate Polymers*, *183*, 102–109. https://doi.org/10.1016/j.carbpol.2017.11.079

Noshirvani, N., Ghanbarzadeh, B., Rezaei Mokarram, R., & Hashemi, M. (2017). Novel active packaging based on carboxymethyl cellulose-chitosan-ZnO NPs nanocomposite for increasing the shelf life of bread. *Food Packaging and Shelf Life*, *11*, 106–114. https://doi.org/10.1016/j.fpsl.2017.01.010

Ntsoane, M. L., Sivakumar, D., & Mahajan, P. V. (2020). Optimisation of O2 and CO2 concentrations to retain quality and prolong shelf life of 'shelly' mango fruit using a simplex lattice mixture design. *Biosystems Engineering*, *192*, 14–23. https://doi.org/10.1016/j.biosystemseng.2020.01.009

Orta, M. del M., Martín, J., Santos, J. L., Aparicio, I., Medina-Carrasco, S., & Alonso, E. (2020). Biopolymer-clay nanocomposites as novel and ecofriendly adsorbents for environmental remediation. *Applied Clay Science*, *198*, 105838. https://doi.org/10.1016/j.clay.2020.105838

Pantani, R., Gorrasi, G., Vigliotta, G., Murariu, M., & Dubois, P. (2013). PLA-ZnO nanocomposite films: Water vapor barrier properties and specific end-use characteristics. *European Polymer Journal*, *49*(11), 3471–3482. https://doi.org/10.1016/j.eurpolymj.2013.08.005

Petchwattana, N., Covavisaruch, S., Wibooranawong, S., & Naknaen, P. (2016). Antimicrobial food packaging prepared from poly(butylene succinate) and zinc oxide. *Measurement*, *93*, 442–448. https://doi.org/10.1016/j.measurement.2016.07.048

Pires, J. R. A., Souza, V. G. L., Fuciños, P., Pastrana, L., & Fernando, A. L. (2022). Methodologies to Assess the Biodegradability of Bio-Based Polymers—Current Knowledge and Existing Gaps. *Polymers*, *14*(7), Article 7. https://doi.org/10.3390/polym14071359

Porta, R., Sabbah, M., & Di Pierro, P. (2020). Biopolymers as Food Packaging Materials. *International Journal of Molecular Sciences*, *21*(14), Article 14. https://doi.org/10.3390/ijms21144942

Raghupathi, K. R., Koodali, R. T., & Manna, A. C. (2011). Size-Dependent Bacterial Growth Inhibition and Mechanism of Antibacterial Activity of Zinc Oxide Nanoparticles. *Langmuir*, *27*(7), 4020–4028. https://doi.org/10.1021/la104825u

Ramji, V., & Vishnuvarthanan, M. (2022). Influence of NiO Supported Silica Nanoparticles on Mechanical, Barrier, Optical and Antibacterial Properties of Polylactic Acid (PLA) Bio Nanocomposite Films for Food Packaging Applications. *Silicon*, *14*(2), 531–538. https://doi.org/10.1007/s12633-020-00839-x

Ranakoti, L., Gangil, B., Mishra, S. K., Singh, T., Sharma, S., Ilyas, R. A., & El-Khatib, S. (2022). Critical Review on Polylactic Acid: Properties, Structure, Processing, Biocomposites, and Nanocomposites. *Materials*, *15*(12), Article 12. https://doi.org/10.3390/ma15124312

Roy, S., & Rhim, J.-W. (2021). Antioxidant and antimicrobial poly(vinyl alcohol)-based films incorporated with grapefruit seed extract and curcumin. *Journal of Environmental Chemical Engineering*, *9*(1), 104694. https://doi.org/10.1016/j.jece.2020.104694

Roy, S., Van Hai, L., Kim, H. C., Zhai, L., & Kim, J. (2020). Preparation and characterization of synthetic melanin-like nanoparticles reinforced chitosan nanocomposite films. *Carbohydrate Polymers*, *231*, 115729. https://doi.org/10.1016/j.carbpol.2019.115729

Rukmanikrishnan, B., Ismail, F. R. M., Manoharan, R. K., Kim, S. S., & Lee, J. (2020). Blends of gellan gum/xanthan gum/zinc oxide based nanocomposites for packaging application: Rheological and antimicrobial properties. *International Journal of Biological Macromolecules*, *148*, 1182–1189. https://doi.org/10.1016/j.ijbiomac.2019.11.155

Saadat, S., Pandey, G., Tharmavaram, M., Braganza, V., & Rawtani, D. (2020). Nano-interfacial decoration of Halloysite Nanotubes for the development of antimicrobial nanocomposites. *Advances in Colloid and Interface Science*, *275*, 102063. https://doi.org/10.1016/j.cis.2019.102063

Salahuddin, N., Abdelwahab, M., Gaber, M., & Elneanaey, S. (2020). Synthesis and Design of Norfloxacin drug delivery system based on PLA/TiO2 nanocomposites: Antibacterial and antitumor activities. *Materials Science and Engineering: C*, *108*, 110337. https://doi.org/10.1016/j.msec.2019.110337

Saleh, S. M. (2019). ZnO nanospheres based simple hydrothermal route for photocatalytic degradation of azo dye. *Spectrochimica Acta Part A: Molecular and Biomolecular Spectroscopy*, *211*, 141–147. https://doi.org/10.1016/j.saa.2018.11.065

Sanuja, S., Agalya, A., & Umapathy, M. J. (2014). Studies on Magnesium Oxide Reinforced Chitosan Bionanocomposite Incorporated with Clove Oil for Active Food Packaging Application. *International Journal of Polymeric Materials and Polymeric Biomaterials*, *63*(14), 733–740. https://doi.org/10.1080/00914037.2013.879445

Segura González, E. A., Olmos, D., Lorente, M. Á., Vélaz, I., & González-Benito, J. (2018). Preparation and Characterization of Polymer Composite Materials Based on PLA/TiO2 for Antibacterial Packaging. *Polymers*, *10*(12), Article 12. https://doi.org/10.3390/polym10121365

Shankar, S., Kasapis, S., & Rhim, J.-W. (2018). Alginate-based nanocomposite films reinforced with halloysite nanotubes functionalized by alkali treatment and zinc oxide nanoparticles. *International Journal of Biological Macromolecules*, *118*, 1824–1832. https://doi.org/10.1016/j.ijbiomac.2018.07.026

Shankar, S., Wang, L.-F., & Rhim, J.-W. (2018). Incorporation of zinc oxide nanoparticles improved the mechanical, water vapor barrier, UV-light barrier, and antibacterial properties of PLA-based nanocomposite films. *Materials Science and Engineering: C*, *93*, 289–298. https://doi.org/10.1016/j.msec.2018.08.002

Shao, L., Xi, Y., & Weng, Y. (2022). Recent Advances in PLA-Based Antibacterial Food Packaging and Its Applications. *Molecules*, *27*(18), Article 18. https://doi.org/10.3390/molecules27185953

Sharma, R., Jafari, S. M., & Sharma, S. (2020). Antimicrobial bio-nanocomposites and their potential applications in food packaging. *Food Control*, *112*, 107086. https://doi.org/10.1016/j.foodcont.2020.107086

Sharma, S., Barkauskaite, S., Jaiswal, A. K., & Jaiswal, S. (2021). Essential oils as additives in active food packaging. *Food Chemistry*, *343*, 128403. https://doi.org/10.1016/j.foodchem.2020.128403

Shi, L.-E., Li, Z.-H., Zheng, W., Zhao, Y.-F., Jin, Y.-F., & Tang, Z.-X. (2014). Synthesis, antibacterial activity, antibacterial mechanism and food applications of ZnO nanoparticles: A review. *Food Additives & Contaminants: Part A*, *31*(2), 173–186. https://doi.org/10.1080/19440049.2013.865147

Silva, N. H. C. S., Vilela, C., Almeida, A., Marrucho, I. M., & Freire, C. S. R. (2018). Pullulan-based nanocomposite films for functional food packaging: Exploiting lysozyme nanofibers as antibacterial and antioxidant reinforcing additives. *Food Hydrocolloids*, *77*, 921–930. https://doi.org/10.1016/j.foodhyd.2017.11.039

Subbuvel, M., & Kavan, P. (2022). Preparation and characterization of polylactic acid/fenugreek essential oil/curcumin composite films for food packaging applications. *International Journal of Biological Macromolecules*, *194*, 470–483. https://doi.org/10.1016/j.ijbiomac.2021.11.090

Swaroop, C., & Shukla, M. (2018). Nano-magnesium oxide reinforced polylactic acid biofilms for food packaging applications. *International Journal of Biological Macromolecules*, *113*, 729–736. https://doi.org/10.1016/j.ijbiomac.2018.02.156

Taib, N.-A. A. B., Rahman, M. R., Huda, D., Kuok, K. K., Hamdan, S., Bakri, M. K. B., Julaihi, M. R. M. B., & Khan, A. (2022). A review on poly lactic acid (PLA) as a biodegradable polymer. *Polymer Bulletin*. https://doi.org/10.1007/s00289-022-04160-y

Tajdari, A., Babaei, A., Goudarzi, A., & Partovi, R. (2020). Preparation and study on the optical, mechanical, and antibacterial properties of polylactic acid/ZnO/TiO2 shared nanocomposites. *Journal of Plastic Film & Sheeting*, *36*(3), 285–311. https://doi.org/10.1177/8756087919900365

Talebian, N., Amininezhad, S. M., & Doudi, M. (2013). Controllable synthesis of ZnO nanoparticles and their morphology-dependent antibacterial and optical properties. *Journal of Photochemistry and Photobiology B: Biology*, *120*, 66–73. https://doi.org/10.1016/j.jphotobiol.2013.01.004

Thakur, V. K., Thakur, M. K., & Gupta, R. K. (2013). Development of functionalized cellulosic biopolymers by graft copolymerization. *International Journal of Biological Macromolecules*, *62*, 44–51. https://doi.org/10.1016/j.ijbiomac.2013.08.026

Vahedikia, N., Garavand, F., Tajeddin, B., Cacciotti, I., Jafari, S. M., Omidi, T., & Zahedi, Z. (2019). Biodegradable zein film composites reinforced with chitosan nanoparticles and cinnamon essential oil: Physical, mechanical, structural and antimicrobial attributes. *Colloids and Surfaces B: Biointerfaces*, *177*, 25–32. https://doi.org/10.1016/j.colsurfb.2019.01.045

Van Bree, I., Baetens, J. M., Samapundo, S., Devlieghere, F., Laleman, R., Vandekinderen, I., Noseda, B., Xhaferi, R., De Baets, B., & De Meulenaer, B. (2012). Modelling the degradation kinetics of vitamin C in fruit juice in relation to the initial headspace oxygen concentration. *Food Chemistry*, *134*(1), 207–214. https://doi.org/10.1016/j.foodchem.2012.02.096

Vergis, J., Gokulakrishnan, P., Agarwal, R. K., & Kumar, A. (2015). Essential Oils as Natural Food Antimicrobial Agents: A Review. *Critical Reviews in Food Science and Nutrition*, *55*(10), 1320–1323. https://doi.org/10.1080/10408398.2012.692127

Verma, D. K., Thakur, M., Singh, S., Tripathy, S., Gupta, A. K., Baranwal, D., Patel, A. R., Shah, N., Utama, G. L., Niamah, A. K., Chávez-González, M. L., Gallegos, C. F., Aguilar, C. N., & Srivastav, P. P. (2022). Bacteriocins as antimicrobial and preservative agents in food: Biosynthesis, separation and application. *Food Bioscience*, *46*, 101594. https://doi.org/10.1016/j.fbio.2022.101594

Vijayakumar, R., Sivaraman, Y., Pavagada Siddappa, K. M., & Dandu, J. P. R. (2022). Synthesis of lignin nanoparticles employing acid precipitation method and its application to enhance the mechanical, UV-barrier and antioxidant properties of chitosan films. *International Journal of Polymer Analysis and Characterization*, *27*(2), 99–110. https://doi.org/10.1080/1023666X.2021.2016305

Yadav, S., Mehrotra, G. K., & Dutta, P. K. (2021). Chitosan based ZnO nanoparticles loaded gallic-acid films for active food packaging. *Food Chemistry*, *334*, 127605. https://doi.org/10.1016/j.foodchem.2020.127605

Youssef, Ahmed. M., EL-Sayed, S. M., EL-Sayed, H. S., Salama, H. H., & Dufresne, A. (2016). Enhancement of Egyptian soft white cheese shelf life using a novel chitosan/carboxymethyl cellulose/zinc oxide bionanocomposite film. *Carbohydrate Polymers*, *151*, 9–19. https://doi.org/10.1016/j.carbpol.2016.05.023

Zhang, H., Hortal, M., Jordá-Beneyto, M., Rosa, E., Lara-Lledo, M., & Lorente, I. (2017). ZnO-PLA nanocomposite coated paper for antimicrobial packaging application. *LWT*, *78*, 250–257. https://doi.org/10.1016/j.lwt.2016.12.024

CHAPTER 2

Sonochemical synthesis of poly(lactic acid) nanocomposites with ZnO nanoflowers: Effect of nanofiller morphology on physical properties

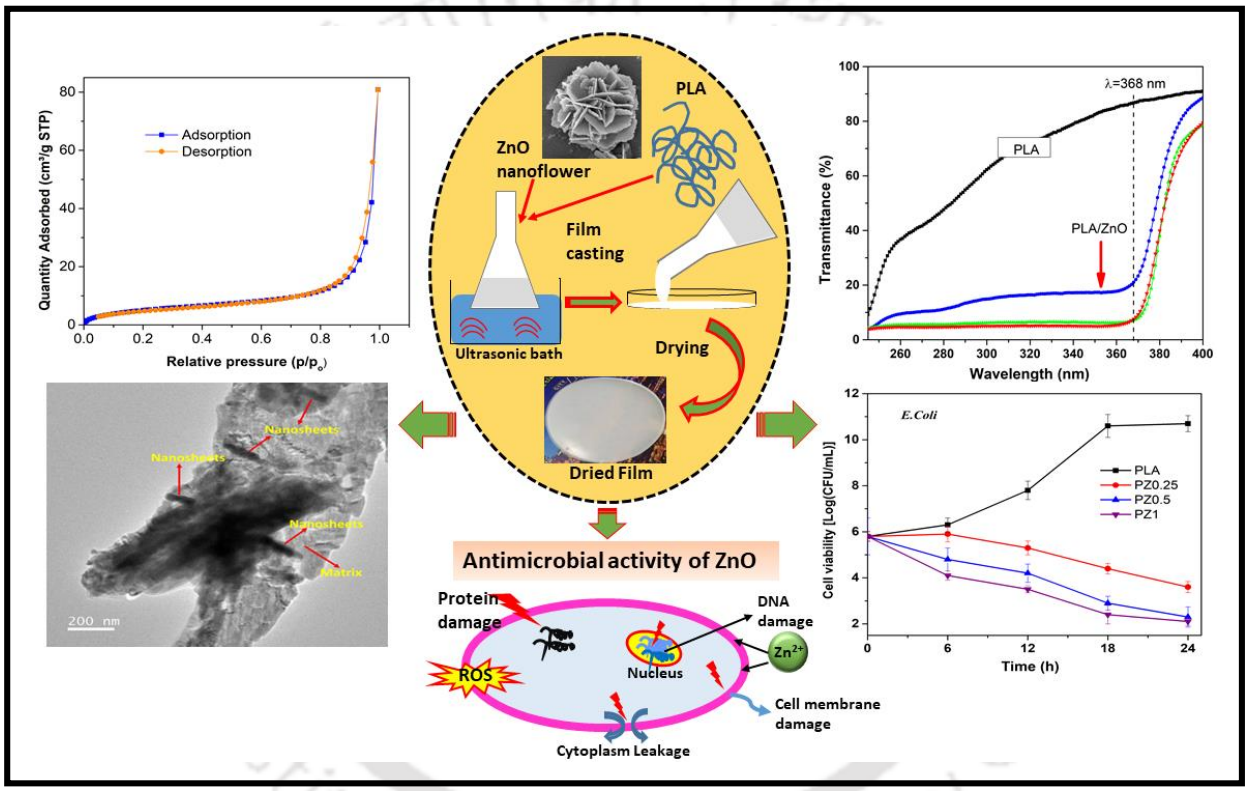

Research output:

U. Boro**, N. Kashyap, V. S. Moholkar, Sonochemical Synthesis of Poly (lactic acid) Nanocomposites with ZnO Nanoflowers: Effect of Nanofiller Morphology on Physical Properties.* ***ACS Engineering Au. *2 (2021) 46–60.*

2.1 Introduction

Due to light weight and low cost, many synthetic polymers based items like polypacks, polyfilms, polycontainers etc. are used for food packaging and disposed after use. These waste products cause garbage disposal problem, especially in developing countries, where there is no proper waste management system. Therefore, there is an urgent need to employ biodegradable natural polymers such as starch, cellulose, chitosan, poly(lactic acid) (PLA), poly(caprolactone) etc. extracted from the renewable natural resources (Kabir et al., 2020; Qasim et al., 2021; Reichert et al., 2020). These bio-polymers have certain limitations such as poor mechanical, thermal, barrier properties etc (Asgher et al., 2020). The properties of bio-polymers can be enhanced using nanoscale reinforcing fillers (dispersed on bio-polymer matrix) to form nanocomposites. Reinforcing fillers not only improves the existing thermal and mechanical properties of the bio-polymers, but depending on their nature also impart certain new properties such as higher conductivity, EMI shielding, antimicrobial activity, UV resistivity etc. (Trifol et al., 2021).

Among the various bio-polymers, the PLA derived from lactic acid is widely used in the development of bionanocomposites, mainly in combination with organically modified silicates, cellulose nanocrystals, carbon based nanofillers and metal oxides etc.(Ghozali et al., 2020). Among various popular nanofillers used in polymer nanocomposites, ZnO in the form of nanowires/nanorods/ nanoparticles have been reported to improve antimicrobial, optical and thermo-mechanical properties of the polymer. The interfacial interactions of ZnO nanofiller with polymer matrix are influenced by the morphology of the nanofiller, which in turn affects the physiochemical properties of the nanocomposites (S. Wang et al., 2020). Many synthesis techniques are available to produce hierarchical (or layered) ZnO, which is suitable for employment as nanofiller in synthesis of nanocomposites. These techniques include electro-deposition (C. Wang et al., 2019), chemical bath deposition (Abdulrahman et al., 2020), microwave methods (Wojnarowicz et al., 2020), chemical vapor deposition (CVD) (Choi et al., 2020), sonochemical method (Bao et al., 2020), hydrothermal methods (Agarwal et al., 2019) etc.

There are previous studies in literature that report synthesis of different hierarchical structures of ZnO such as nanosheets, nanoplates, nanoflowers, disc shaped and star like morphology, etc. (Chang et al., 2020; Zhu et al., 2018). These special morphologies of ZnO affect the physical properties and provide beneficial effect in various applications such as gas sensors, high performing photocatalysts, supercapacitors, EMI shielding, solar cells etc. Guo et al. (Guo et al., 2020) have investigated gas sensing ability of different morphologies of ZnO including nanoparticles, nanosheets and nanoflowers. As compared to other two nanostructures (particles and nanosheets), 3-D hierarchical flower like morphology of ZnO showed the most superior gas sensing properties. This property was attributed to the highest specific surface area of ZnO nanoflowers (BET surface area: 5.7 m^2g^{-1}) against the other nanostructures, viz. nanoparticles (BET surface area: 2.8 m^2g^{-1}) and nanosheets (BET surface area: 4.3 m^2g^{-1}). Fan et al. (2019) synthesized two hierarchical structure of ZnO, viz. fire cracker like ZnO and flower shaped ZnO. They have reported that flower shaped ZnO exhibited higher H_2S sensitivity response (50 ppm H_2S) at 180℃ and shorter response time (14 s) over fire cracker like ZnO (H_2S sensitivity response: 50 ppm H_2S, response time: 19 s) (Fan et al., 2019). Chang et al. (2020) have synthesized three different morphologies of ZnO including nanorods, nanoplatelets and multibranched flower like structures by varying pH value of precursor and growth time in hydrothermal reaction (Chang et al., 2020). Results indicated that multibranched flower shape ZnO showed better antifungal activity and significant photodecomposition of organic chemicals present in the soil, as compared to nanorods and nanoplatelets. Cai et al. (2016) have also fabricated different shape of ZnO nanoflowers viz., rod flowers, fusiform flowers, and petal flowers using hydrothermal process (Cai et al., 2016). Among all petal flowers exhibited highest antibacterial activity (petal flowers > fusiform flowers > rod flowers). This is due to differences in microscopic parameters such as specific surface area (petal flowers: 7.21 m^2g^{-1}, fusiform flowers: 2.72 m^2g^{-1} and rod flower: 3.28 m^2g^{-1}), pore size (petal flowers: 38.31 nm, fusiform flowers: 46.43 nm and rod flower: 42.63 nm) and Zn–polar plane etc. Previous literature has addressed the issue of incorporation of spherical

and rod shape ZnO nanoparticles into different polymer matrix. However, relatively fewer studies have been published on hierarchical ZnO based polymer nanocomposites (Sharma et al., 2020). Pariona et al. (2020) have studied the effect of size and morphology on the antimicrobial activities of ZnO. They have found that ZnO nano platelets showed better antifungal activity than ZnO nanoparticles and nanorods (Pariona et al., 2020).

Polymer nanocomposites can be prepared by using various techniques viz. solution casting, melt mixing, in situ polymerization etc. Among these, solution casting is the simplest technique with least energy requirement and faster kinetics. Uniform dispersion of nanofiller in the polymer matrix is essential for attaining desired enhanced properties. Use of sonication (or ultrasound irradiation) has been attempted by many previous authors for achieving uniform dispersion of nanofiller in the polymer matrix (Hussein et al., 2019; Soltani et al., 2018). Mallakpour et al. (2018) have fabricated nanocomposites of poly(vinyl alcohol) and ZrO_2 nanoparticles by using ultrasound assisted solvent casting method (Mallakpour & Shafiee, 2018). Dhatarwal et al. (2021) also reported ultrasound-assisted synthesis of poly(methyl methacrylate)/MMT nanocomposites using solution casting method (Dhatarwal & Sengwa, 2021). Similarly, nanocomposites with different nanofillers have also been synthesized using ultrasound assisted emulsion polymerization process (Poddar et al., 2016). These nanocomposites possessed superior physical properties (as compared to conventionally synthesized nanocomposites) by virtue of uniform dispersion of nanofillers in the polymer matrix.

In the present study, we report synthesis of polylactic acid/ZnO nanocomposites with a special feature. This feature is in terms of the ZnO with morphology of "nanoflowers". These ZnO nanoflowers have also been synthesized by us using facile sonochemical method with CTAB as a morphology directing agent. Effect of synthesis conditions (such as different molar concentration of the precursor zinc nitrate hexahydrate) on the morphology (or architecture) of flower-like ZnO was also studied. The ZnO nanoflowers were incorporated into PLA matrix by using ultrasound assisted solution casting. The resulting nanocomposite films were characterized for thermal,

mechanical and antimicrobial properties. As a consequence of enhanced interfacial interactions-attributed to special nanoflower morphology of ZnO, these nanocomposites possessed superior physical and antimicrobial properties, as explained in greater details in subsequent sections. To the best of our knowledge, no previous study has reported synthesis of bionanocomposites with flower shaped morphology of ZnO with poly(lactic acid) matrix.

2.2 Materials and Methods

2.2.1 Materials

Zinc nitrate hexahydrate [$Zn(NO_3)_2 \cdot 6H_2O$] and potassium hydroxide (KOH) were obtained from Merck, India. Cetyltrimethylammonium bromide (CTAB) was bought from Sigma Aldrich. Pellets of poly(lactic) acid (code: 4032D) was supplied from Nature Works LLC (USA). Analytical grade chloroform (99.8%) was procured from Merck Chemical Co., Germany, and is used as received. Microbial cultures of *Escherichia coli* and *Listeria monocytogenes* were procured from Biosciences and Bioengineering department of our institute. Luria Bertani Broth (LB) and Nutrient Broth (NB) for cell culture were purchased from Himedia.

2.2.2 Synthesis of ZnO nanoflowers

The main precursor for the synthesis of ZnO nanoflowers was $Zn(NO_3)_2 \cdot 6H_2O$. It was added in different molar concentrations of (0.025, 0.05, 0.075 and 0.1 M) to a mixture of 0.265 M of KOH and 15 mM of CTAB in 250 ml of millipore water. The solution was thoroughly mixed using magnetic stirring for 30 min. Next, the solution was sonicated with a probe type sonicator (Make: Sonics & Material, Model: VCX-500, Frequency: 20 kHz, Power rating: 200 W) for 30 min. The resultant white precipitate was centrifuged (10 min, 4000 rpm) for separation of products from unreacted reactants. The solid residue (i.e. ZnO nanofiller) obtained after discarding the supernatant was vacuum dried at 60 °C for 12 h and stored for further characterization.

2.2.3 Synthesis of PLA/ZnO nanocomposites

For synthesis of PLA/ZnO nanocomposite, ZnO nanofillers obtained with initial concentration of

0.05M $Zn(NO_3)_2 \cdot 6H_2O$ were selected. The exact synthesis procedure is described in the schematic given in Fig. 2.1. Nanocomposite films were prepared by solvent blending method with varying loading of ZnO (0.25, 0.5 and 1 wt%). Firstly, a definite quantity of ZnO was well dispersed in 30 ml of chloroform by magnetic stirring for 20 min at room temperature followed by sonication (frequency: 20 kHz, power: 200 W) for 30 min (solution 1). 4 g of PLA pellets were dissolved in 40 ml of chloroform with magnetic stirring at ambient temperature for 24 h (solution 2). For nanocomposite synthesis, these two solutions (solution 1 and 2) were mixed together with magnetic stirring for 12 h followed by bath sonication for 1 h. (Model: UC-10, 40 kHz, 300 W). For film casting PLA/ZnO nanocomposite solution was poured over a petridish and left for drying under ambient condition for 24 h, followed by vacuum oven drying at 50°C for 12 h. Hereafter, nanocomposites films synthesized with loading of 0.25, 0.5 and 1 wt% ZnO were termed as PZ0.25, PZ0.5 and PZ1, respectively. The blank PLA film was also prepared by applying similar procedure in the absence of ZnO.

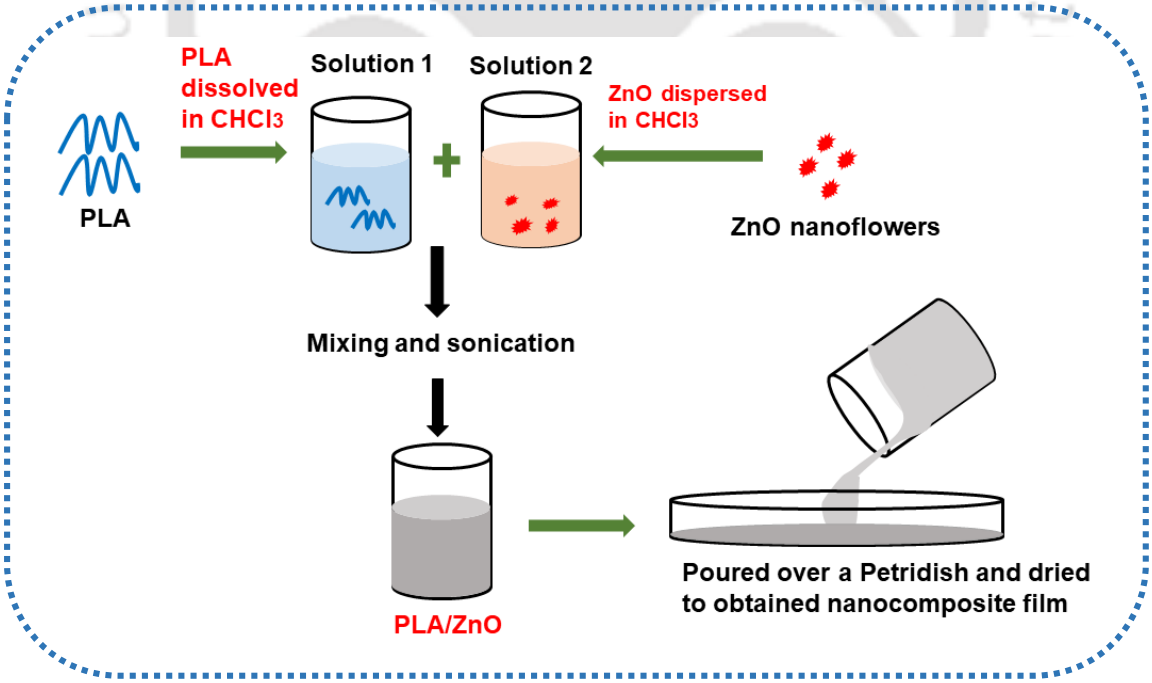

Fig. 2.1. Schematic of experimental protocol of ultrasonic synthesis of PLA/ZnO nanocomposites

2.2.4 Product characterizations

Both ZnO nanofillers and PLA/ZnO nanocomposites were characterized using standard techniques: **(1) FTIR:** FTIR was conducted by using FTIR spectrometer (Make: PerkinElmer, Singapore, Model: Spectrum two) in the frequency range of 4000–400 cm^{-1} at room temperature in Attenuated Total Reflectance (ATR) mode. The nanocomposite film samples were cut into rectangular strips (2 cm×2 cm) and directly placed on the path of infrared ray. **(2) XRD:** The structural characteristics of synthesized materials were analysed using powder X-ray diffractometer (Make: Rigaku Technologies, Japan, Model: Smartlab, $\lambda = 1.5406$ Å) in the angular range of $10° \leq 2\theta \leq 80°$.The crystallite size of the synthesized ZnO was calculated by using Scherrer formula:

crystallite size = $k\lambda/\beta \cos \theta$

Here, k denotes Scherrer constant and β is the full width at half maximum height in radians.

(3) FE-SEM and EDX: Surface morphology and elemental composition of ZnO was examined using Field Emission Scanning Electron Microscope (FE−SEM) (Make: Zeiss, Model: Sigma 300) and Energy Dispersive X-ray Spectroscopy (Make: Zeiss, Model: Sigma 300). For FE−SEM analysis, the ZnO nanoparticles were deposited on the surface of carbon tape, followed by gold-coating using magnetron sputtering device. **(4) Surface area and pore size distribution:** The specific surface area and the pore size distribution of ZnO sample were evaluated via the Brunauer−Emmett-Teller (BET) method and Barret−Joyner-Halenda (BJH) method using BET surface area analyzer (Model No.: Tristar II; Make: M/s Micromeritics, U.S.A.). **(5) TEM:** The internal structure of the synthesized nanocomposites was studied by using Transmission Electron Microscope (TEM) analyzer (Make: JEOL, Model: 2100F). A droplet of diluted PLA/ZnO nanocomposite was deposited on a carbon-coated grid for TEM analysis. **(6) UV-Visible spectroscopy:** UV-Visible spectroscopy study of ZnO and PLA/ZnO nanocomposites were performed using Lambda 35 spectrometer from Perkin Elmer. **(7) Thermal properties:** Thermal

properties of PLA/ZnO nanocomposites were evaluated by DSC and TGA analysis. It was carried out simultaneously using DSC/TGA analyzer (Make: Netzsch model: STA449F3A00) with nitrogen flow rate of 10 mL min^{-1} at a scanning rate of 10 °C min^{-1} in the temperature range 25° to 600 °C. **(8) Mechanical properties:** Mechanical properties were measured by 5 kN Electromechanical Universal Testing Machine (Make: Zwick Roell: Z005TN) at a standard crosshead speed of 1 mm min^{-1}. **(9) Antimicrobial activity test:** The antimicrobial activity of PLA/ZnO nanocomposite films was tested quantitatively by a viable colony count method against two food borne pathogenic bacteria, *Escherichia coli* (Gram negative) and *Listeria monocytogenes* (Gram positive) by using colony count method (Rhim et al., 2009). For the surface sterilization, the film sample (5×5 cm) used for the antimicrobial test was washed with 70% ethanol and then irradiated with UV light for 40 min to prevent any contamination. A colony of *Escherichia coli* and *Listeria monocytogenes* were inoculated in Luria broth (LB) and Nutrient broth (NB), respectively and subsequently incubated at 37 °C for 24 h with mild shaking. The inoculum was diluted and 10 ml of diluted inoculum was aseptically transferred to 100 ml of sterile LB and NB broth containing sterile film samples to attain initial concentration of 10^6 –10^7 CFU/ml and subsequently incubated at 37 °C for 24 h with mild shaking at 200 rpm. The same diluted broth with pristine PLA film was taken as a control. The bacterial culture (1 ml) were taken out at 0, 6, 12, 18 and 24 h of incubation and serial dilutions with sterile water were repeated for each sample. 10 µl diluent of the sample was then spread onto solid agar plates. The cell viability of test microorganisms was calculated by counting bacterial colonies on the plates after 24 h incubation at 37 °C. All experiments were performed in triplicates and results were reported as mean values of CFU/ml. Percentage reduction (% R) of *Escherichia coli* and *Listeria monocytogenes* in contact with PLA and PLA/ZnO nanocomposites for 6, 12, 18 and 24 h can be calculated by using the equation:

$$R\ (\%) = [(B-C)/B]\times 100$$

where, B = CFU of the viable bacterial cells for pure PLA, C = CFU of PLA/ZnO nanocomposite films.

2.3 Results and Discussion

2.3.1 Characterization of ZnO nanoflowers

FTIR spectroscopy was performed in the transmittance mode as shown in Fig. 2.2a. Two absorption peaks occurred at 480 cm^{-1} and 567 cm^{-1}, which correspond to the Zn–O stretching. The absorption peaks at 871 cm^{-1} might arise from C–H out of plane bending, originate from the residual CTAB in the as-synthesized sample. Absence of other peaks such as hydroxyl group (O–H, 3400 cm^{-1}) or methylene group (–CH_3, 2950–3000 cm^{-1}) indicates the purity of the product (Rhim et al., 2009).

Typical XRD patterns of the ZnO samples prepared with different molar concentration of $Zn(NO_3)_2 \cdot 6H_2O$ are shown in the Fig. 2.2b. The diffraction peaks corresponding to ZnO were observed at 2θ = 31.6°, 34.5°, 36.4°, 47.4°, 56.6°, 62.9°, 66.3°, 67.8°, and 69.1°, which are characteristic of (1 0 0), (0 0 2), (1 0 1), (0 0 2), (1 1 0), (1 0 3), (1 1 2), (2 0 1) and (2 0 0) planes of hexagonal wurtzite phase of ZnO (as per JCPDS database no. 36–1451). The diffraction peaks corresponding to (1 0 1) plane become more intense as the molar concentration of $Zn(NO_3)_2 \cdot 6H_2O$ increases from 0.025 M to 0.01 M. Similar trend of result was obtained by Qu et al. (2017) (Qu et al., 2017). They have reported that with increasing the hydrothermal reaction time from 10 min to 4 h, the diffraction peak corresponding to 101 plane becomes more intense. Moreover, the presence of sharp peaks in all ZnO samples indicates high crystallinity of the synthesized material. Table 2.1 depicts the crystallite size of ZnO synthesized with different molar concentration of $Zn(NO_3)_2 \cdot 6H_2O$. It could be observed that the crystallite size increases with increasing the molarity of $Zn(NO_3)_2 \cdot 6H_2O$ (Molefe et al., 2019).

Table 2.1. Crystallite size of ZnO synthesized with different molar concentration of $Zn(NO_3)_2 \cdot 6H_2O$

Concn. of $Zn(NO_3)_2 \cdot 6H_2O$ (M)	2θ	FWHM (radians)	Crystallite size (nm)
0.025	36.25	0.39	21.45
0.05	36.19	0.39	21.62
0.075	36.24	0.26	31.76
0.1	36.24	0.26	32.53

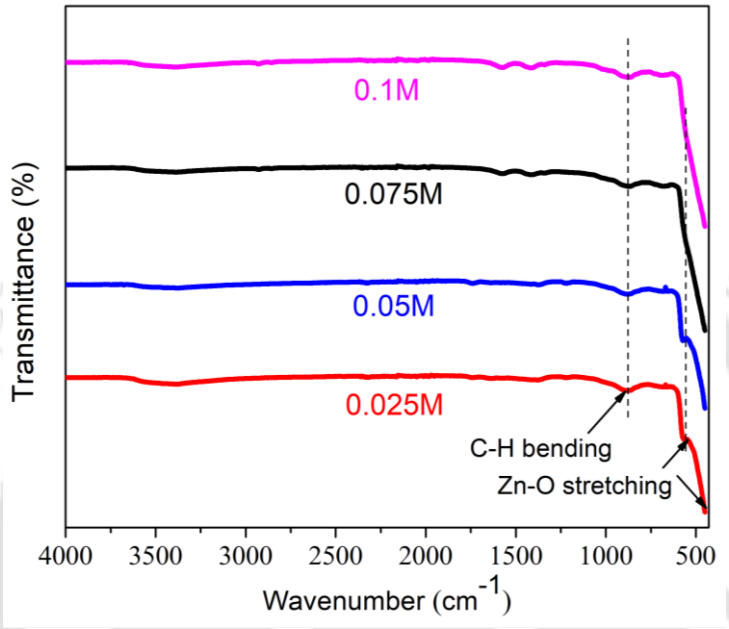

(a)

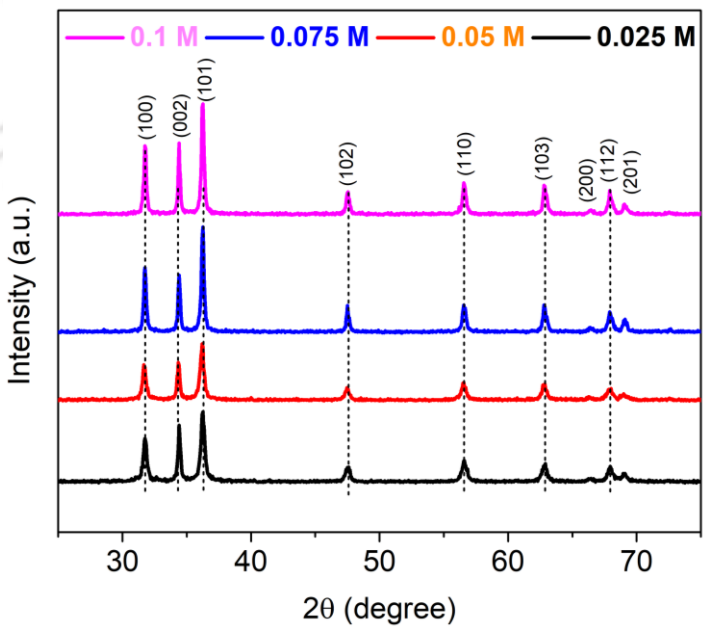

(b)

Fig. 2.2. (a) FTIR spectra, and (b) XRD patterns of ZnO synthesized with different initial concentrations of the precursor $Zn(NO_3)_2 \cdot 6H_2O$

FE–SEM images of ZnO nanostructures are shown in Fig. 2.3a–d. It could be observed that the synthesized ZnO material has flower like morphology. Interestingly, these flower like microstructures were made up of numerous amount of nanosheets (as petals). Nanosheets with thickness of approximately 45, 21, 48 and 64 nm were obtained by adjusting the molar concentration of $Zn(NO_3)_2 \cdot 6H_2O$ from 0.025 M to 0.1 M. With increasing the concentration, aggregation of ZnO nanosheets become denser and at higher concentration the flower-like ZnO microstructures collapsed and formed an irregular structure.

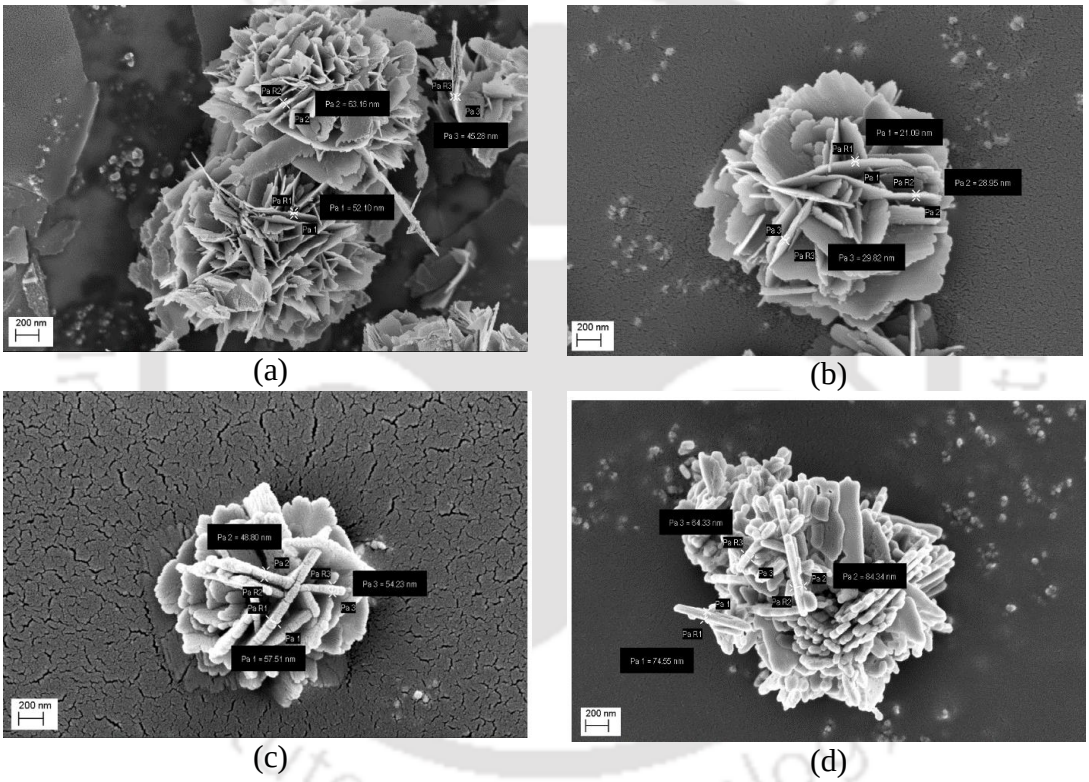

Fig. 2.3. FESEM images of ZnO synthesized with different concentrations of the precursor $Zn(NO_3)_2 \cdot 6H_2O$ (a) 0.025 M, (b) 0.05 M, (c) 0.075 M, and (d) 0.1 M

Adsorption-desorption curve and pore size distribution of ZnO sample are shown in Fig. 2. 4a and b. The surface area of nanomaterial has played a significant role in the final properties determination of polymer nanocomposites. BET surface area obtained for the ZnO nanoflowers (0.05 M) is 19.87 $m^2\ g^{-1}$, that is higher than compare to the commercial ZnO (~ 4–5 $m^2\ g^{-1}$). By employing BJH technique, the pore size distribution of ZnO was determined. The results indicate

that the ZnO possessed mesopores structure with diameters in the range of 6–50 nm. Table 2.2 shows comparison of different morphology of ZnO with BET surface area as the criteria. It was observed that ZnO nanoflower possess higher surface area than ZnO nanorods or nanospheres.

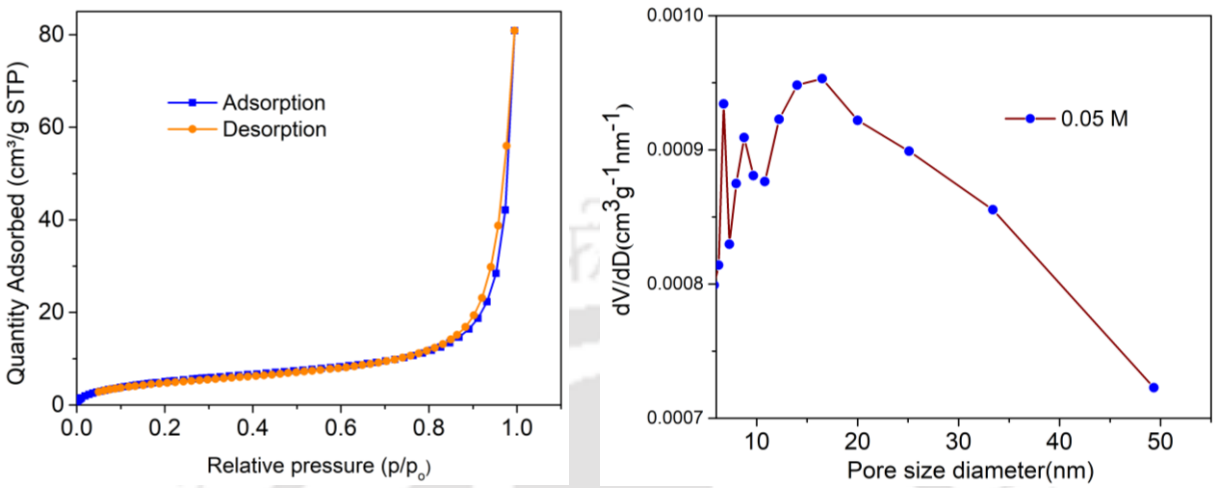

(a) (b)

Fig. 2.4. (a) Adsorption-desorption curve, and (b) pore size distribution curve of ZnO (synthesized with 0.05 M concentration of $Zn(NO_3)_2 \cdot 6H_2O$)

UV-visible spectroscopy was carried out to study the optical transparency of ZnO nanoflowers. As shown in Fig. 2.5, all samples possessed a strong absorption in the UV region (λ= 368 nm) and good transparency in the visible region. Transparency decreases with increasing concentration of $Zn(NO_3)_2 \cdot 6H_2O$. Transparency is related with Zn/O stoichiometric ratio. The transparency improves as the stoichiometric ratio increases. With increasing molar concentration of precursor Zn/O ratio also increases (Table 2.3 and Fig. 2.6). Therefore, transparency increases in the visible range (Soylu & Coskun, 2018). The reduction of transmittance at higher molar concentration may be attributed to the increased scattering of photons due to increase surface roughness.

Table 2.2. Comparison of different morphologies of ZnO nanostructures with BET surface area as the criteria

ZnO morphology	Synthesis method	BET surface area ($m^2 g^{-1}$)	References
Nanorods and Nanodisks	Nanorods: solution precipitation Nanodisks: sol-gel	Nanorods: 8.02 Nanodisks: 14.01	(Fanny Chiat Orou et al., 2018)
Nanorods and Nanorod flowerets	Selective leaching in NaOH solution	Nanorods: 12.5 Nanorods flowerets: 8.4	(Bhushan et al., 2019)
Nanorods	Thermal decomposition under air and vacuum	Nanorods (air): 19.57 Nanorods (vacuum): 15.44	(Rahimi & Yazdani, 2018)
Nanorods	Sol-gel	Nanorods: 6.91	(Nouroozi & Farzaneh, 2011)
Nanospheres, Nanorods and Nanoflowers	Hydrothermal	Nanorods: 2.1, Nanospheres: 4.06 Nanoflower: 14.19	(Suganya Josephine et al., 2021)
Nanorods, Nanoflowers	Hydrothermal	Nanoflower: 15.1 Nanorods: 20	(Garg et al., 2021)
Nanoflowers	Hydrothermal	Nanoflowers: 10.94	(Zou et al., 2022)
Nanorods, Nanospheres	Precipitation (nanospheres), sol gel (nanorods)	Nanorods: 5 Nanospheres: 13	(Uribe-López et al., 2021)
Nanorods	Sol gel (using Hibiscus extract as stabilizing and reducing agent)	Nanorods: 10	(Taha et al., 2020)
Nanoparticles, Nanosheets, Nanoflowers	Hydrothermal	Nanoparticles: 2.8 Nanosheets: 4.3 Nanoflowers: 5.7	(Guo et al., 2020)
Nanoflower	Hydrothermal	Nanoflower: 13	(Ramimoghadam et al., 2013)
Nanoflowers	Sonochemical synthesis	Nanoflowers: 19.87	This study

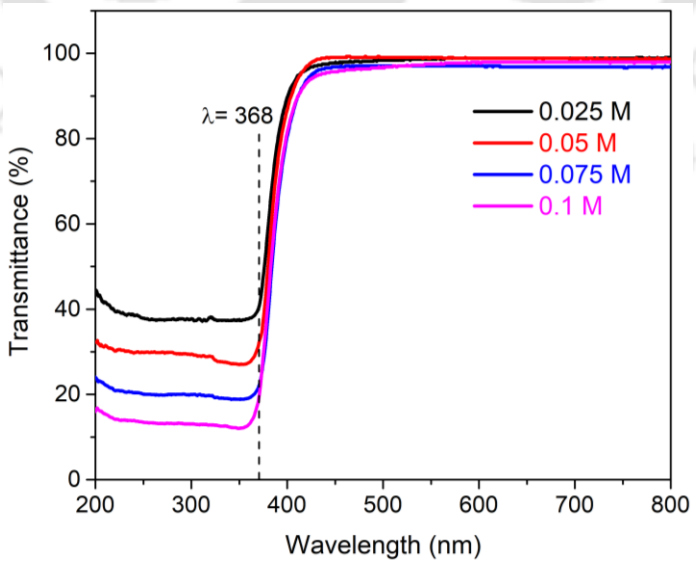

Fig. 2.5. UV-visible spectra of ZnO nanoflowers synthesized with different molar concentration of $Zn(NO_3)_2 \cdot 6H_2O$

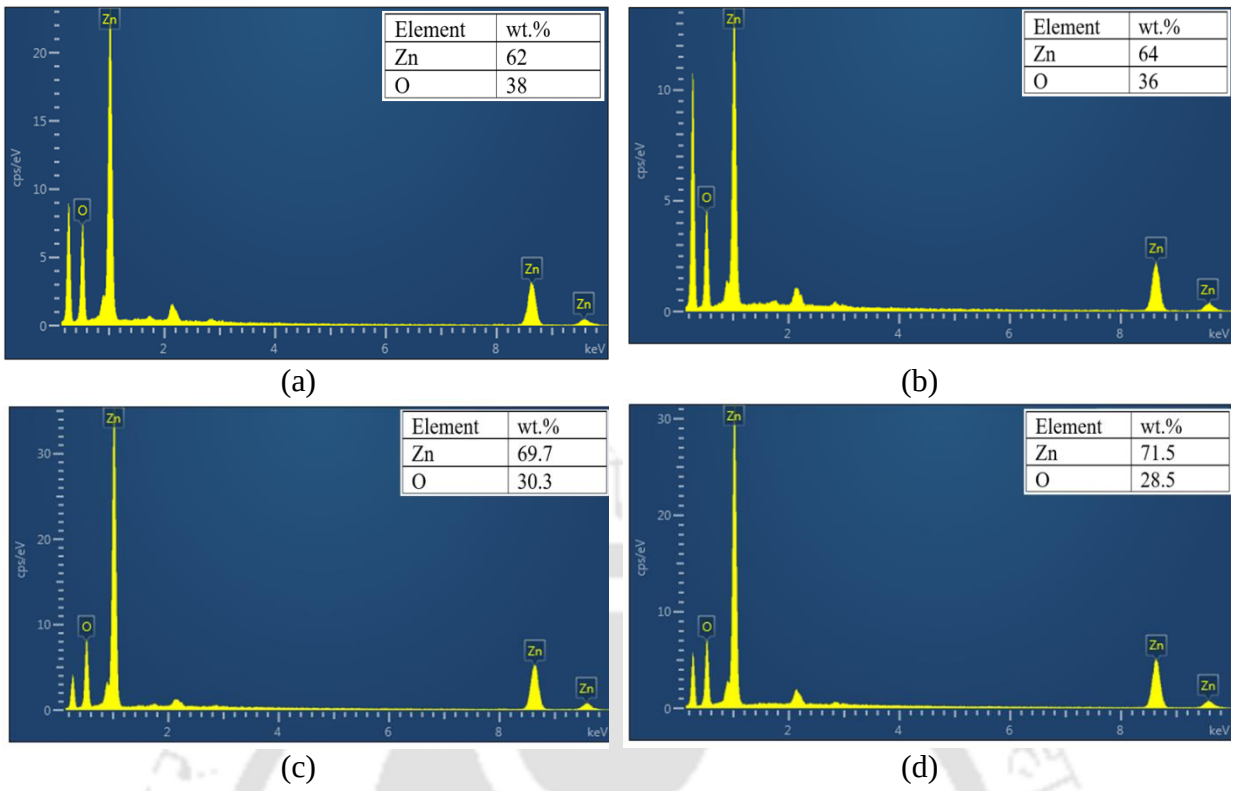

Fig. 2.6. EDX spectra of ZnO with different molar concentration of $Zn(NO_3)_2 \cdot 6H_2O$ (a) 0.025 M, (b) 0.05 M, (c) 0.075 M, and (d) 0.1 M

Table 2.3. Elemental composition and Zn/O of synthesized ZnO nanoflowers by EDX analysis

$Zn(NO_3)_2 \cdot 6H_2O$ (M)	Zn (wt.%)	O (wt.%)	Zn/O
0.025	62	38	1.6
0.05	64	36	1.8
0.075	69.7	30.3	2.3
0.1	71.5	28.5	2.5

2.3.2 Characterization of PLA/ZnO nanoflower nanocomposites

FTIR spectra of the pristine PLA and PLA/ZnO nanoflowers nanocomposite films are shown in Fig. 2.7a. The transmittance peaks at 1451 and 1437 cm^{-1} were assigned to −C−H− symmetric and asymmetric deformations. The bands in the vicinity of 1236–1090 cm^{-1} were associated with the C−O–C stretching vibrations. The bands at 756 and 749 cm^{-1} were attributed to C−H bending. The sharp transmittance band around 1722–1742 cm^{-1} corresponds to the –C=O stretching of the

ester group present in the PLA. The transmittance peaks at 2944 and 3000 cm^{-1} were attributed to the asymmetric and symmetric vibrations of the $-CH_3$ group (Shankar et al., 2018). Presence of a characteristics band at around 480 cm^{-1} (due to Zn–O stretching) in all nanocomposite films confirmed the successful formation of PLA/ZnO nanocomposites (Jayaramudu et al., 2014; Kim et al., 2019). Adding ZnO nanoflowers increased the peak intensities corresponding to 1722–1742 cm^{-1} (–C=O stretching) and 1236–1090 cm^{-1} (C−O–C stretching) due to increase in nucleation rate and density of PLA. These results into destruction of macromolecular structures of PLA generating low molecular weight chains, oligomers and acetaldehyde groups. These results indicate the formation of hydrogen bonding between ZnO and PLA matrix. Use of ultrasonic irradiation in solution casting method provides better dispersion of ZnO in the PLA which further enhance the nucleation rate (Zhang et al., 2021).

XRD is an important tool for the study of structure-property relationship of polymer nanocomposites. The XRD spectra of the virgin PLA and its nanocomposite films with ZnO are shown in Fig. 2.7b. All sample possessed two common diffraction peaks at $2\theta = 17.2°$ and 19.4°, indicating semicrystalline structure of PLA. These peaks were attributed to the crystalline plane (1 1 0)/ (2 0 0) and (2 0 3) of PLA, respectively. In addition, other peaks were observed at $2\theta =$ 31.6°, 34.5° and 36.4° which essentially are characteristics of the crystal planes (1 0 0), (0 0 2), and (1 0 1) of ZnO, respectively. The sharpness of these peaks increases with increase in nanofiller loading. Moreover, the intensity of the peaks associated with PLA ($2\theta = 17.2°$ and 19.4°) also increased with increase in loading, which clearly indicates enhanced crystallinity. This signifies that small amount of ZnO with good dispersion (achieved by ultrasonic irradiation) can act as nucleating agents that enhance the crystallinity of PLA. Further, some of the peaks of nano ZnO were diminished during nanocomposites formation due to the low concentration of nanofiller in the nanocomposites, and also due to interactions between PLA and nano ZnO (Kim et al., 2019).

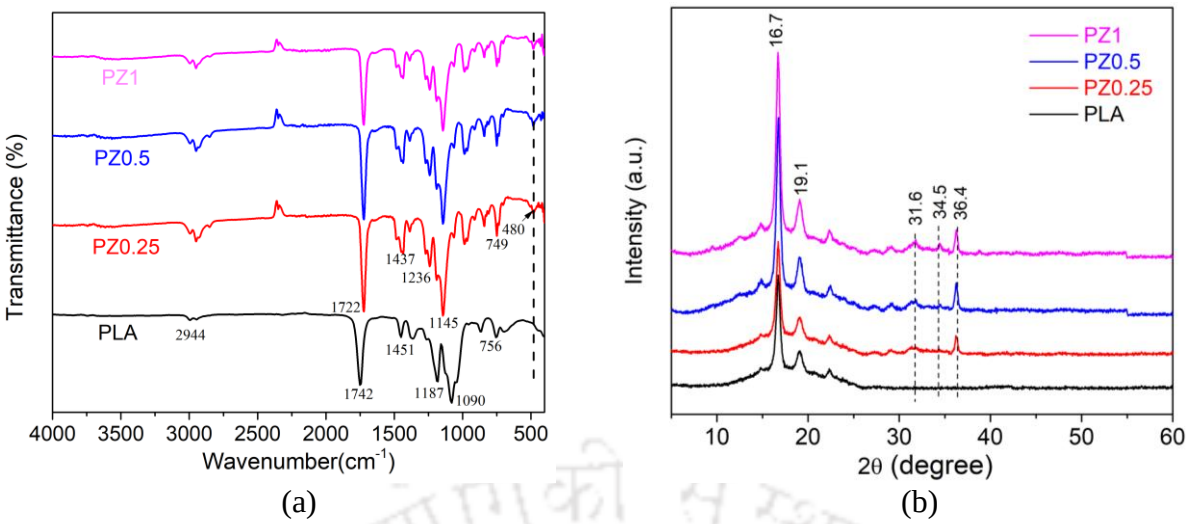

Fig. 2.7. (a) FTIR spectra, and (b) XRD patterns of the neat PLA and PLA/ZnO biocomposite films

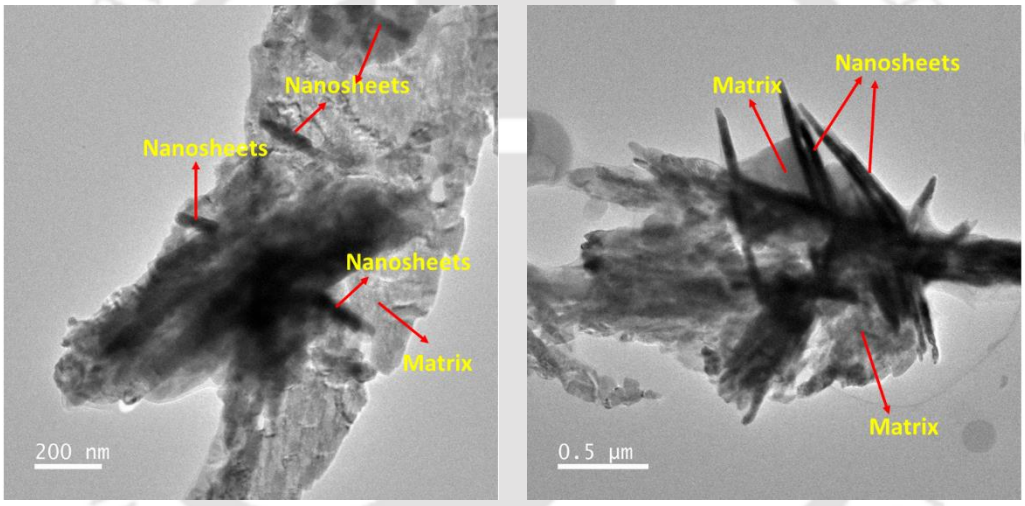

Fig. 2.8. (a) and (b) FE–TEM images of PLA/ZnO nanocomposites (0.5 wt% ZnO) at different magnifications

The internal structure of the nanocomposites and the extent of dispersion of the ZnO nanoflowers in the PLA matrix were studied by using FE–TEM analysis. To obtain an effective nanocomposite material, the reinforcing nanofiller should dispersed homogeneously in the polymer matrix. FE–TEM images of PLA/ZnO nanocomposites (0.5 wt% ZnO) at different magnifications are shown in Fig. 2.8a and b. FE–TEM images of PLA/ZnO nanocomposite at different magnifications reveal disintegration of the nanoflowers after getting embedded in the

PLA matrix that few “petals” detach from nanoflower and get dispersed in the PLA matrix as ZnO nanosheets. Nonetheless, major portion of ZnO nanoflowers (or the flower shape morphology of ZnO) remains intact upon getting embedded in PLA matrix.

2.3.2.1 UV–Visible spectroscopy

UV–Visible spectroscopy was used to study the optical response of polymer nanocomposite films upon exposure to the UV–Vis radiation. Fig. 2.9a and b, shows UV–Visible spectra of pure PLA and its nanocomposites with ZnO nanoflowers. Neat PLA film showed high transparency against both UV (200 – 400 nm) and visible range of light (400 – 700 nm). Incorporation of ZnO significantly reduced the transmittance of PLA/ZnO nanocomposite (Hasan et al., 2021; Soylu & Coskun, 2018) films. This may be due to strong UV radiation absorption capacity of ZnO nanoflowers. It was also observed that decrease in transmittance was a function of nanofiller loading. Low nanofiller loading (0.25 wt.%) had more transparency in UV region than higher loading (0.5 and 1 wt.%). These results encouraged the use of PLA/ZnO nanocomposites films in food packaging sector (such as dairy products) as an UV-preventive packaging films (Hasan et al., 2021).

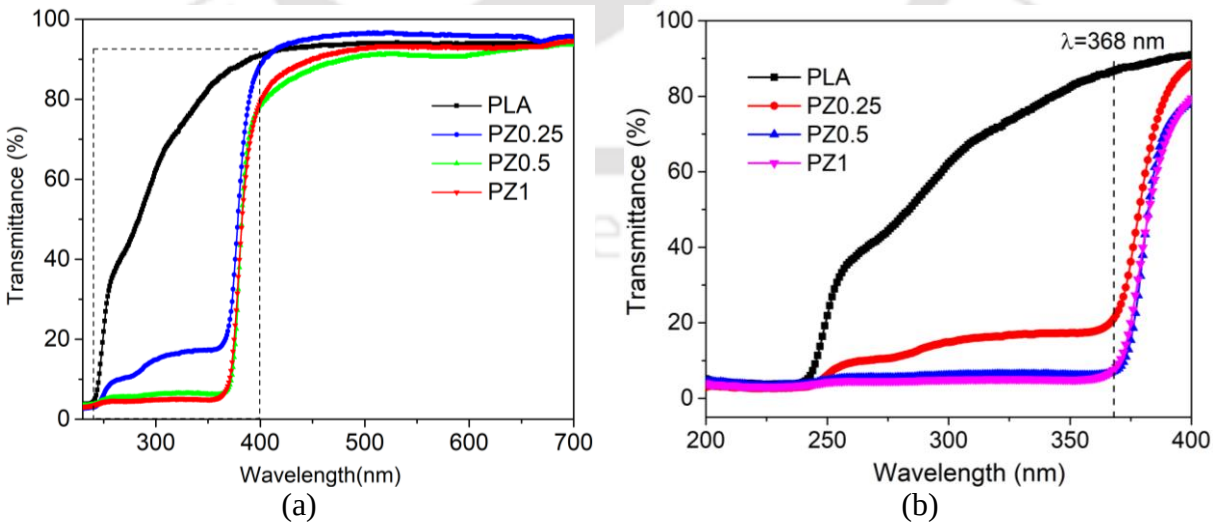

Fig. 2.9. UV–Visible spectra of PLA and PLA/ZnO nanocomposites (a) full wavelength range (200–700 nm), and (b) UV range (200–400 nm)

2.3.2.2 Thermal properties

Thermogravimetric analysis (TGA) and differential thermogravimetry (DTG) curves of PLA and PLA/ZnO nanocomposites are shown in Fig. 2.10a and b, respectively. The result revealed that incorporation of ZnO nanoflowers into PLA continuously decreases the thermal degradation temperatures of the final nanocomposite films. This result well matched with the reported literature (da Cruz Faria et al., 2021; Lizundia et al., 2016; Nonato et al., 2019). This may be due to the catalytic behavior of ZnO, which assists the thermal degradation of the polymer nanocomposite (Murariu et al., 2011; Pantani et al., 2013; Restrepo et al., 2017). Upon exposure to thermal energy, ZnO nanoflowers act as catalyst and initiate unzipping depolymerization /intermolecular transesterification reactions in PLA. This results in chain scissioning of the PLA. TGA curve showed two step degradation of PLA and its nanocomposite films. First step degradation ($t_{5\%}$) for both PLA and PLA/ZnO nanocomposites occurred at 147 and 128 ℃, respectively. This weight loss was due to removal of moisture content present in the sample. Characteristic thermodegradation temperatures of PLA and its nanocomposites with ZnO are shown in Table 2.4. Pristine PLA reached its maximum degradation temperature at (t_{peak}) at 363.1 °C. Conversely, PZ1 nanocomposite attained its maximum degradation temperature at 296.8 °C. In presence of thermally stable ZnO, the char value of the nanocomposite films increases from 0.78 (PLA) to 1.87 (PZ1) percent. The DSC curves for neat PLA and PLA/ZnO nanocomposites are shown in Fig. 2.10c, and the values of glass transition temperature (T_g) and melting temperatures (T_m) are summarized in Table 2.5. DSC results reveal decrease in T_g and T_m values for the PLA/ZnO nanoflowers nanocomposite. The reason is that, ZnO catalyze chain scissioning of PLA matrix, generating PLA with lower molecular weights and leading to formation of monomer lactic acid.

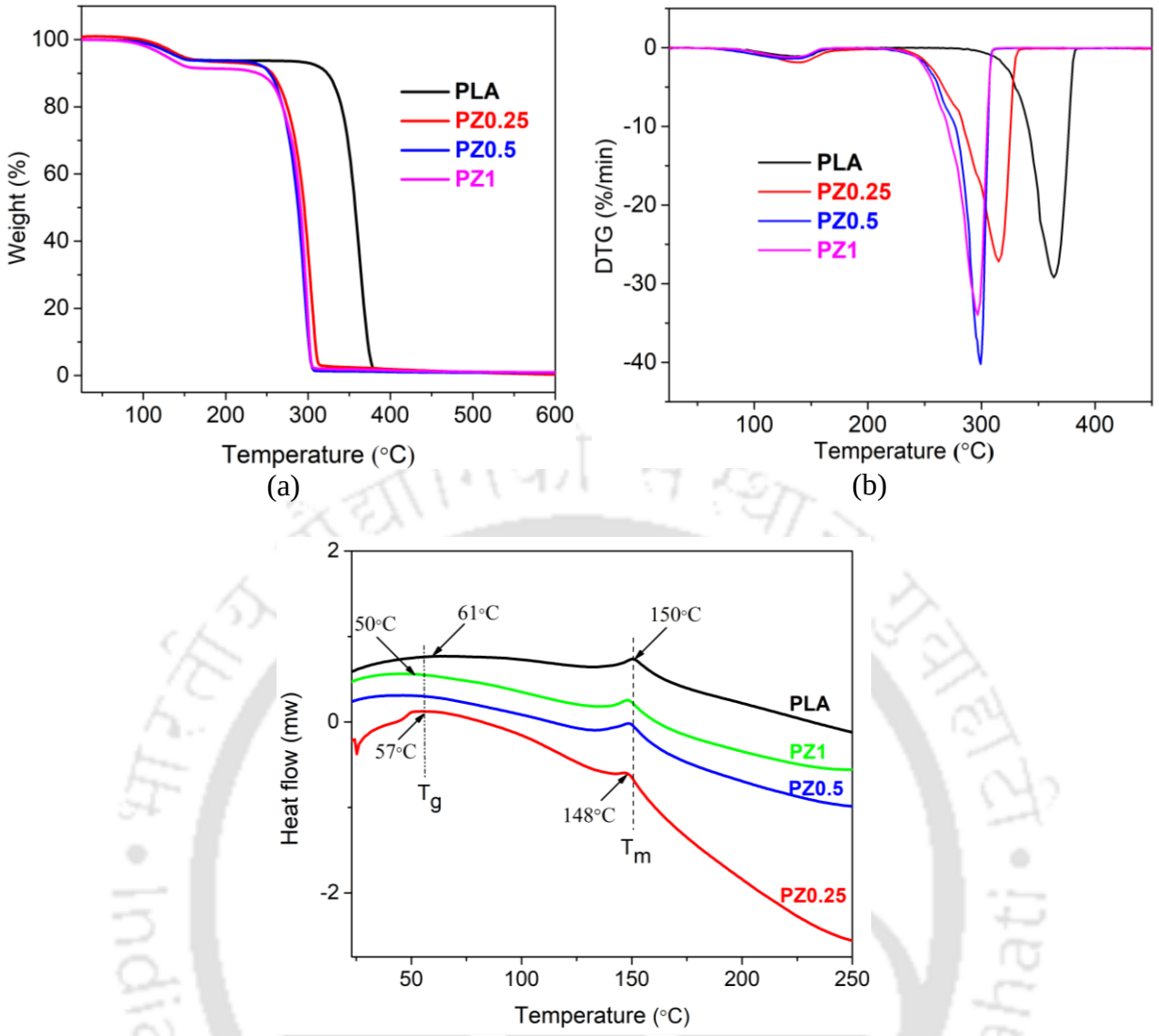

Fig. 2.10. (a) TGA curves, (b) DTG curves and (c) DSC patterns of neat PLA and PLA/ZnO nanocomposites with different loadings of ZnO nanoflowers

Table 2.4. Characteristic thermodegradation temperatures of pristine PLA and its nanocomposites

Specimen	$t_{5\%}$ (°C)	$t_{10\%}$ (°C)	t_{peak} (°C)	Char value (%)
PLA	147.5	323.1	363.1	0.78
PZ0.25	147.5	256.3	315.5	2.94
PZ0.5	141.3	253.7	298.1	1.31
PZ1	128.5	239.2	296.8	1.87

Note: Degradation temperatures for 5 and 10% weight loss are represented by $t_{5\%}$ and $t_{10\%}$, respectively. t_{peak} is the temperature at which maximum degradation occurs.

Table 2.5. Glass transition temperatures (T_g) and melting points (T_m) of PLA and PLA/ZnO nanoflowers composites

Specimen	T_g (°C)	T_m (°C)
PLA	61	150
PZ0.25	57	148
PZ0.5	52	149
PZ1	50	148

2.3.2.3 Mechanical properties

Mechanical properties of polymer nanocomposite depend on many factors such as dispersion of nanofiller in matrix, interfacial interactions between filler and matrix and degree of crystallinity of polymer matrix etc. For food packaging applications the nanocomposite films should have high toughness so that it can resist any kind of handling damages. Mechanical properties (stress vs strain curve, tensile strength, Young's modulus and elongation at break) of PLA and its nanocomposite films were evaluated at ambient temperature by ultimate tensile testing and results are shown in Fig. 2.11a–d and Table 2.6. The maximum tensile strength of pristine PLA was 26.5 MPa, and it increases to 28.3, 32.2 and, 26.1 MPa, respectively, with addition of 0.25, 0.5 and 1 wt% of ZnO nanoflowers (Fig. 2.11b). Nanocomposite films with 0.5 wt% (PZ0.5) showed 22% increment in tensile strength compared to pristine PLA. It was observed that tensile strength of PLA increased at a relatively low loading (0.5 wt%), which could be attributed to flowers shape morphology of ZnO that provides high surface area for filler-matrix interaction. Moreover, use of ultrasonication during synthesis process causes uniform distribution of ZnO nanoflowers in the nanocomposite films. At high loading (1 wt%) a slight decrease in tensile strength was observed. Due to high surface area, the nanofiller tends to agglomerate at high loading and these agglomerates can act as points of stress concentration. The contact surface area between nanofiller-matrix decreases, which in turn reduces the tensile strength. Jayaramudu et al. (2014) and Tang et al. (2020) also reported similar type of results where tensile strength decreases at high loading due to agglomeration (Jayaramudu et al., 2014); (Tang et al., 2020).

Table 2.6. Mechanical properties of pristine PLA and PLA/ZnO nanoflowers composites

Specimen	UTS (MPa)	Young's modulus (MPa)	Elongation at break (%)
PLA	26.5	862.6	2.9
PZ0.25	28.3	856.6	3.6
PZ0.5	32.2	912.2	4.7
PZ1	26.1	783.1	3.2

Note: Thickness of each film samples were approx. 0.25 mm

Young's modulus of nanocomposite films was shown in Fig. 2.11c. It was observed that Young's modulus of nanocomposite films slightly increased (approx. 6 % increase compared to the pristine PLA) when 0.5 wt% of ZnO nanoflowers was added. But relatively at higher loading of ZnO (1 wt%) this value decreases by 9 % than compare to neat PLA. Similar trend of result was also reported in the literature (Nonato et al., 2019; Qu et al., 2017).

The percentage strain at break (Fig. 2.11d), significantly improved (approx. 38% enhancement as compared to pristine PLA) with loading of 0.5 wt% ZnO. Virgin PLA showed minimum strain value of 2.9%, which increased up to 4.7% in PZ0.5. Due to increase in molecular mobility of the segmental polymer chains with incorporation of nanofiller, the strain value increased significantly. More significantly, the present study achieved superior mechanical properties at relatively very low loading (0.5 wt% ZnO) of nanofiller than reported in the literature (Handore et al., 2014; Jayaramudu et al., 2014; Tang et al., 2020). This result is attributed to two factors: high interfacial area between polymer matrix and nanofiller achieved through nanoflower morphology, and secondly, very fine and uniform dispersion of the ZnO nanoflowers in the polymer matrix due to intense microturbulence generated by sonication.

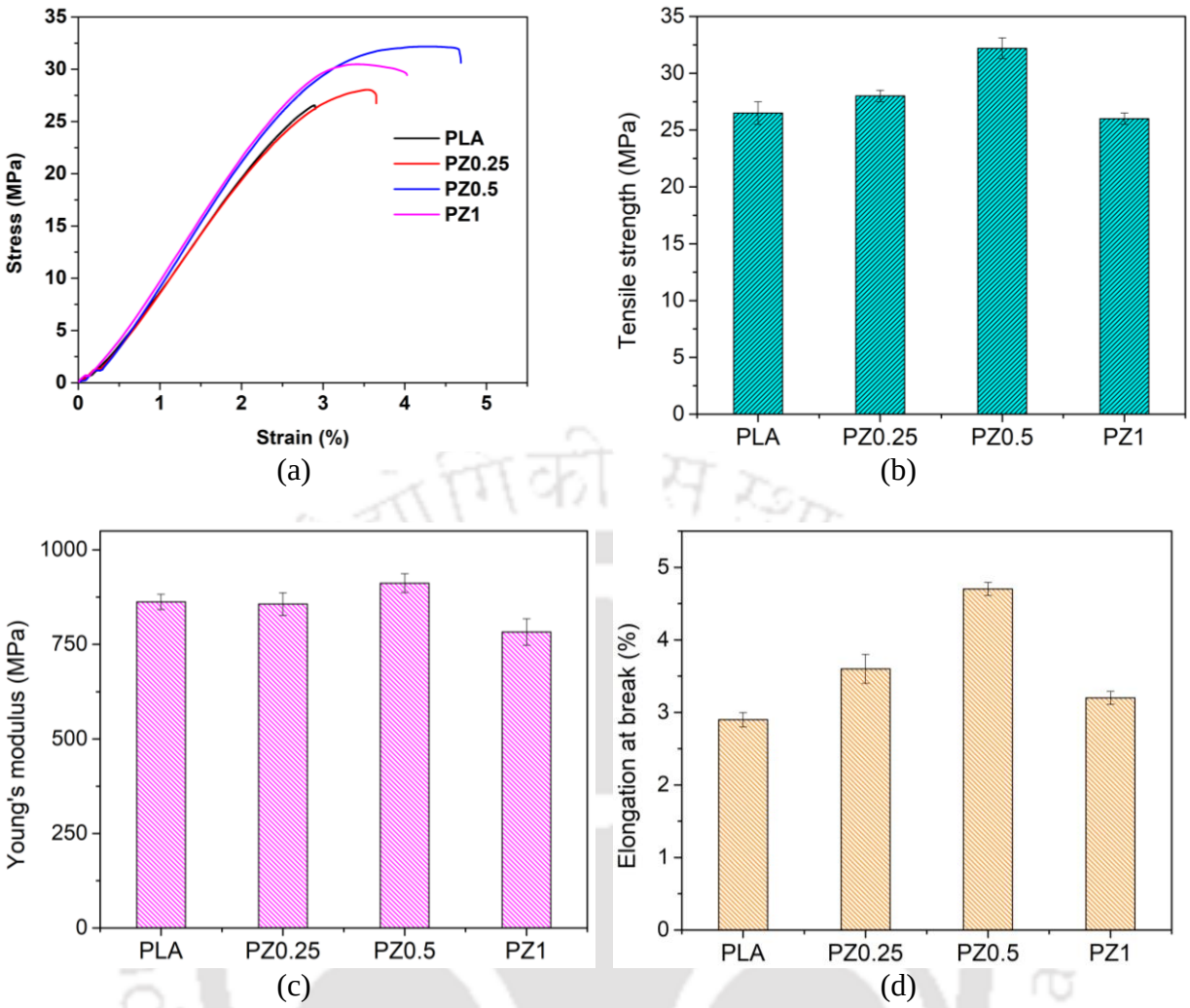

Fig. 2.11. Mechanical parameters of neat PLA and its nanocomposite films (a) stress-strain curve, (b) tensile strength, (c) Young's modulus, and (d) elongation at break

2.3.2.4 Antimicrobial activity

In recent years, addition of antimicrobial agents to food packaging films has been received significant attention. In this regard, polymer nanocomposites containing antimicrobial agents are more promising than compare to polymer micro-composites. This may be due to high aspect ratio (surface to volume) and superior surface reactivity of the nanoscale dimension of antimicrobial agents, which restrict the growth of microorganisms more efficiently than their microscale counterparts (Díez-Pascual & Díez-Vicente, 2014). Various nanoscale metals and metal oxides such as Ag, Cu, Au, ZnO, TiO_2, SiO_2 etc. are used as antimicrobial agents in polymer

nanocomposites. Among various metal oxides, ZnO is well known for antimicrobial efficacy. Here, the antibacterial activity of ZnO incorporated nanocomposite films was studied against two food borne bacteria *Escherichia coli* (gram negative) and *Listeria monocytogenes* (gram positive) and results are shown in Fig. 2.12a and b. Also the values of percentage reduction (% R) of bacterial colonies were summarized in Table 2.7.

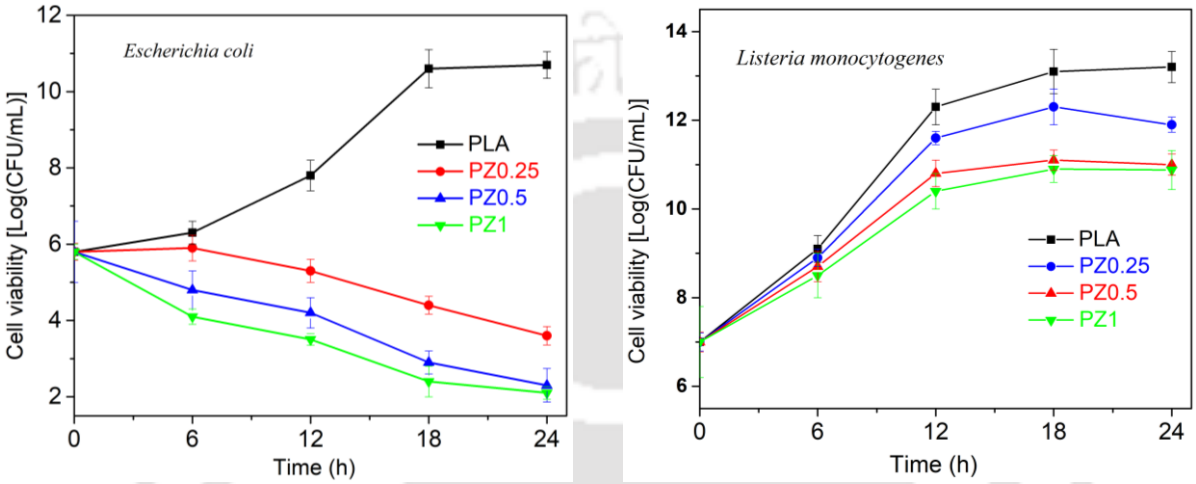

Fig. 2.12. Antimicrobial activity of neat PLA and PLA/ZnO nanocomposite films against two food born bacteria (a) *Escherichia coli*, and (b) *Listeria monocytogenes*

As observed, pristine PLA film did not display any antibacterial activity against *Escherichia coli* and *Listeria monocytogenes*. But, PLA/ZnO nanocomposites possess significant antibacterial activity against *Escherichia coli*, but showed relatively lower antibacterial activity for *Listeria monocytogenes*. As shown in Fig. 2.12a, for *Escherichia coli*, the growth of bacterial cell linearly decreased up to 6 h (% R = 88.9 achieved for PZ1) and completely stopped at 18 h of incubation period (% R = 99 achieved for all nanocomposites). With increasing ZnO loading % R also increases. At 6 h incubation, % R for PZ0.25 was 32.97% which increases up to 88.90% in PZ1. So, it showed the dependency of antibacterial activity of nanocomposite film on incubation time and nanofiller concentration. Release of antimicrobial components such as zinc ions, reactive oxygen species takes time to reach optimum effectiveness. On the other hand, different result was

observed for *Listeria monocytogenes*. The viable cell count increased up to 18 h, and decreased further for all nanocomposites, as depicted in Fig. 2.12b. But these values were lower than neat PLA. At 6 h incubation, % R for PZ0.25 is 18.12%, which increased up to 45.12% in PZ1. After 24 h of incubation it was possible to achieved % R = 90.17ta for PZ1.

The antimicrobial activity of PLA/ZnO nanocomposites on *Escherichia coli* is more prominent than *Listeria monocytogenes*. This result also matched with previous literature that reported higher effectivity of nano ZnO against *Escherichia coli* (gram negative). This may be due to difference in structural and chemical composition of two bacterial cell wall (Roy & Rhim, 2019; Shankar et al., 2018). Gram positive bacteria consist of a thick cell wall containing multiple layers of peptidoglycan, whereas Gram negative bacteria consist of complex cell wall structure with single layer of peptidoglycan surrounded by an outer membrane and cytoplasmic membrane.

Table 2.7. Reduction of *Escherichia coli* and *Listeria monocytogenes* by PLA and PLA/ZnO nanocomposites (in %)

Sample	% R (t = 6 h)	% R (t = 12 h)	% R (t = 18 h)	% R (t = 24 h)
Escherichia coli				
PLA	0	0	0	0
PZ0.25	32.97	91.80	99.80	99.91
PZ0.5	77.70	97.30	99.95	99.98
PZ1	88.90	98.64	99.97	99.98
Listeria monocytogenes				
PLA	0	0	0	0
PZ0.25	18.12	50.34	55.07	72.75
PZ0.5	32.97	77.69	86.47	88.92
PZ1	45.12	85.04	88.92	90.17

Several mechanisms are reported in the literature that explain antibacterial activity of ZnO. Kumar et al. (2017) have given a detailed account of the probable mechanisms underlying the antimicrobial activities of ZnO against gram positive and gram negative bacteria (Kumar et al., 2017). We give herewith a brief summary of these mechanisms. It may, however, be noted that the exact mechanism is not established yet and is still debatable. The antibacterial mechanism of ZnO nanomaterials can be categorized as (1) physical and (2) chemical based on nature of their

interactions with bacterial cells. The principal chemical mechanism are as follows: (a) photocatalytic effect: This is essentially generation of electron-hole pairs when ZnO material is exposed UV/visible light. The oxidation-reduction reactions induced by the electron-hole pairs diffused out to the surface of ZnO generate different oxygen species like, $O_2^{\bullet -}, HO_2^{\bullet}, H_2O_2$ and $^{\bullet}OH$. The oxygen species can attack the lipids in the cell wall, and subsequently rupture the cell wall. ZnO materials also exhibit antimicrobial properties in the dark, which is attributed to the defects present on the surface of ZnO crystal, which induce the reduction reaction resulting in generation of oxidizing species. (b) release of Zn^{2+} ions in solution due to surface leaching of ZnO materials is also a possible mechanism for antibacterial effects. Zn^{2+} ions generate osmosis stress with release of intracellular fluids. (c) production of H_2O_2 as are result of photocatalytic reaction (recombination of $^{\bullet}OH$ radicals generated by the electron-hole pairs) is another possible mechanism. H_2O_2 can penetrate the bacterial cell wall and the intracellular space, where it can induce biocidal effects such as disruption of DNA and oxidation of intracellular proteins.

The physical mechanisms of the antimicrobial activity of ZnO materials are: (a) plasma membrane disruption: The bacterial cell surface is negatively charged while the ZnO nanomaterials are positively charged with zeta potential of ± 24 mV. This induces strong electrostatic attraction between bacterial cells and ZnO nanoparticles. Accumulation of the ZnO nanoparticles on outer surface of plasma membrane results in increased surface tension and membrane depolarization. This can lead to membrane rupture with leakage of intracellular fluids. (b) mechanical damage: ZnO nanomaterials possess surface defects, rough edges and corners on the surface of the particles. This can cause abrasive effects on the microbial cells leading to mechanical damage of the cell membrane.

In the present study, we have not carried out special mechanistic investigations into the antimicrobial activity of PLA/ZnO nanoflower composites. However, the predominant mechanism of the antimicrobial activity of the PLA/ZnO nanoflower nanocomposites can be

conjectured through above discussion. The ZnO nanoflowers are trapped inside the polymer matrix, and thus, physical mechanisms of ZnO accumulation over cell surface or mechanical abrasion and rupture are unlikely. The chemical mechanism of production of oxidizing species seems to be predominant as the solution of nanocomposites and culture media were irradiated with UV light. Among the chemical mechanism, H_2O_2 formation through recombination of $^{\bullet}OH$ radicals seems to be more likely than direct attack of $^{\bullet}OH$ radicals on the cell membrane. The radical species generated on the surface of nanocomposites are highly unstable and do not diffuse much in the liquid medium. Thus the probability of interaction among $^{\bullet}OH$ radicals and bacterial cells is relatively less probable. These radicals can undergo recombination among themselves to form H_2O_2. As noted earlier, H_2O_2 can diffuse inside the cell and induce biocidal effects. More detailed studies are needed for ascertaining of these conjectures. Table 2.8 shows comparative evaluation of antimicrobial properties of PLA/ZnO nanoflowers and other PLA based nanocomposites

Table 2.8. Comparative evaluation of antimicrobial properties of PLA/ZnO nanoflowers and other PLA based nanocomposites

Nanocomposites	Methods	Major findings	References
PLA/ZnO	VC	*E. coli* (gram-negative), 24 h, % R > 70, 7 days % R > 99 *S. aureus* (gram-positive), No activity for 1 and 2 wt% of ZnO. For 3 wt% ZnO loading for 7 days, %R > 99	(Pantani et al., 2013)
PLA/TiO_2/Ag	VC	Incubation time: 24 h, Log reduction: 5.88 (*E. coli*), 5.7 (*Listeria monocytogenes*)	(Li et al., 2017)
PLA/ZnO, PLA/MgO, PLA/TiO_2	IZ	*E. coli*, IZ: 7.66 mm (PLA/ZnO 1 phr), IZ: 7.50 mm (PLA/MgO 1 phr), IZ: 6 mm (PLA/TiO_2 1 phr)	(Ghozali et al., 2020)
PLA/ACNC/ZnO	VC	Incubation time: 24 h, PLA/ACNC/5% ZnO, showed % R = 99.9 against both *E. coli* and *S. aureus*. Antibacterial activity against *E. coli* was higher than *S. aureus*	(Yu et al., 2021)
PLA/CHNF/AgNPs	VC	Incubation time: 24 h, Log reduction: 0.97 (*E. coli*), 1.98 (*S. aureus*)	(Mohammadalinejhad et al., 2021)
PLA/CNTs/CIN	VC	Log reduction: 5.65 (*S. aureus*), 3.07 (*E. coli*)	(Cui et al., 2020)
PLA/CNTs/AgNPs	IZ	IZ = 0.15 cm against *S. haemolyticus*	(Gan et al., 2020)
PLA/Ag/CB	IZ	% R = 99.9 against *S. aureus*	(Nootsuwan et al., 2018)
PLA/ZnO nanoflowers	VC	Incubation time: 24 h, Log reduction: 8.6 (*E. coli*), 2.32 (*Listeria monocytogenes*)	This study

Note: VC: viable colony count method, IZ: inhibition zone method, phr = quantity of additive per 100 unit of base

2.4 Conclusions

In this study, we have reported synthesis and characterization of PLA/ZnO nanocomposites. A peculiar feature of the nanocomposite is the flower like morphology of ZnO, which imparts excellent physical properties to the nanocomposites at very low loading of just 0.5 wt%. The nanoflowers have also been synthesized from precursor of $Zn(NO_3)_2 \cdot 6H_2O$ using a sonochemical method. The enhanced physical properties of the PLA/ZnO nanoflower composites are attributed to high interfacial interactions between ZnO and PLA polymer matrix, in addition to uniform dispersion of the nanofiller in the matrix. These nanocomposites also possessed effective antimicrobial properties, suitable for food packaging applications.

References

Abdulrahman, A. F., Ahmed, S. M., Ahmed, N. M., & Almessiere, M. A. (2020). Enhancement of ZnO Nanorods Properties Using Modified Chemical Bath Deposition Method: Effect of Precursor Concentration. *Crystals*, *10*(5), Article 5. https://doi.org/10.3390/cryst10050386

Agarwal, S., Rai, P., Gatell, E. N., Llobet, E., Güell, F., Kumar, M., & Awasthi, K. (2019). Gas sensing properties of ZnO nanostructures (flowers/rods) synthesized by hydrothermal method. *Sensors and Actuators B: Chemical*, *292*, 24–31. https://doi.org/10.1016/j.snb.2019.04.083

Asgher, M., Qamar, S. A., Bilal, M., & Iqbal, H. M. N. (2020). Bio-based active food packaging materials: Sustainable alternative to conventional petrochemical-based packaging materials. *Food Research International*, *137*, 109625. https://doi.org/10.1016/j.foodres.2020.109625

Bao, Y., Gao, L., Feng, C., Ma, J., Zhang, W., Liu, C., & Simion, D. (2020). Sonochemical synthesis of flower-like ZnO assembled by hollow cones toward water vapor permeability and water resistance enhancement of waterborne film. *Journal of Industrial and Engineering Chemistry*, *82*, 180–189. https://doi.org/10.1016/j.jiec.2019.10.011

Bhushan, B., Murty, B. S., & Mondal, K. (2019). A new approach for synthesis of ZnO nanorod flowerets and subsequent pure free-standing ZnO nanorods. *Advanced Powder Technology*, *30*(1), 30–41. https://doi.org/10.1016/j.apt.2018.10.004

Cai, Q., Gao, Y., Gao, T., Lan, S., Simalou, O., Zhou, X., Zhang, Y., Harnoode, C., Gao, G., & Dong, A. (2016). Insight into Biological Effects of Zinc Oxide Nanoflowers on Bacteria: Why Morphology Matters. *ACS Applied Materials & Interfaces*, *8*(16), 10109–10120. https://doi.org/10.1021/acsami.5b11573

Chang, T.-H., Lu, Y.-C., Yang, M.-J., Huang, J.-W., Linda Chang, P.-F., & Hsueh, H.-Y. (2020). Multibranched flower-like ZnO particles from eco-friendly hydrothermal

synthesis as green antimicrobials in agriculture. *Journal of Cleaner Production*, *262*, 121342. https://doi.org/10.1016/j.jclepro.2020.121342

Choi, S. C., Lee, D. K., & Sohn, S. H. (2020). Effects of Experimental Configuration on the Morphology of Two-Dimensional ZnO Nanostructures Synthesized by Thermal Chemical-Vapor Deposition. *Crystals*, *10*(6), Article 6. https://doi.org/10.3390/cryst10060517

da Cruz Faria, É., Dias, M. L., Ferreira, L. M., & Tavares, M. I. B. (2021). Crystallization behavior of zinc oxide/poly(lactic acid) nanocomposites. *Journal of Thermal Analysis and Calorimetry*, *146*(4), 1483–1490. https://doi.org/10.1007/s10973-020-10166-3

Dhatarwal, P., & Sengwa, R. J. (2021). Superior optical and dielectric properties of ultrasonic-assisted solution-cast prepared PMMA/MMT nanocomposite films. *Functional Composites and Structures*, *3*(2), 025008. https://doi.org/10.1088/2631-6331/ac07f2

Díez-Pascual, A. M., & Díez-Vicente, A. L. (2014). ZnO-Reinforced Poly(3-hydroxybutyrate-co-3-hydroxyvalerate) Bionanocomposites with Antimicrobial Function for Food Packaging. *ACS Applied Materials & Interfaces*, *6*(12), 9822–9834. https://doi.org/10.1021/am502261e

Fan, C., Sun, F., Wang, X., Huang, Z., Keshvardoostchokami, M., Kumar, P., & Liu, B. (2019). Synthesis of ZnO Hierarchical Structures and Their Gas Sensing Properties. *Nanomaterials*, *9*(9), Article 9. https://doi.org/10.3390/nano9091277

Fanny Chiat Orou, S., Hang, K. J., Thuya Thien, M., Ying, Y. L., Foh, L. C., Duong Ngoc Diem, N., Goh, B. H., Pung, S. Y., & Pung, Y. F. (2018). Antibacterial activity by ZnO nanorods and ZnO nanodisks: A model used to illustrate “Nanotoxicity Threshold.” *Journal of Industrial and Engineering Chemistry*, *62*, 333–340. https://doi.org/10.1016/j.jiec.2018.01.013

Gan, L., Geng, A., Jin, L., Zhong, Q., Wang, L., Xu, L., & Mei, C. (2020). Antibacterial nanocomposite based on carbon nanotubes–silver nanoparticles-co-doped polylactic acid. *Polymer Bulletin*, *77*(2), 793–804. https://doi.org/10.1007/s00289-019-02776-1

Garg, R., Gupta, R., Singh, N., & Bansal, A. (2021). Characterization and performance evaluation of synthesized ZnO nanoflowers, nanorods, and their hybrid nanocomposites with graphene oxide for degradation of Orange G. *Environmental Science and Pollution Research*, *28*(40), 57009–57029. https://doi.org/10.1007/s11356-021-14511-3

Ghozali, M., Fahmiati, S., Triwulandari, E., Restu, W. K., Farhan, D., Wulansari, M., & Fatriasari, W. (2020). PLA/metal oxide biocomposites for antimicrobial packaging application. *Polymer-Plastics Technology and Materials*, *59*(12), 1332–1342. https://doi.org/10.1080/25740881.2020.1738475

Guo, W., Liu, W., Xu, L., Feng, P., Zhang, Y., Yang, W., & Shuai, C. (2020). Halloysite nanotubes loaded with nano silver for the sustained-release of antibacterial polymer nanocomposite scaffolds. *Journal of Materials Science & Technology*, *46*, 237–247. https://doi.org/10.1016/j.jmst.2019.11.019

Handore, K., Bhavsar, S., Horne, A., Chhattise, P., Mohite, K., Ambekar, J., Pande, N., & Chabukswar, V. (2014). Novel Green Route of Synthesis of ZnO Nanoparticles by Using Natural Biodegradable Polymer and Its Application as a Catalyst for Oxidation of Aldehydes. *Journal of Macromolecular Science, Part A*, *51*(12), 941–947. https://doi.org/10.1080/10601325.2014.967078

Hasan, M., Altaf, M., Zafar, A., Hassan, S. G., Ali, Z., Mustafa, G., Munawar, T., Saif, M. S., Tariq, T., Iqbal, F., Khan, M. W., Mahmood, A., Mahmood, N., & Shu, X. (2021). Bioinspired synthesis of zinc oxide nano-flowers: A surface enhanced antibacterial and harvesting efficiency. *Materials Science and Engineering: C*, *119*, 111280. https://doi.org/10.1016/j.msec.2020.111280

Hussein, M. A., Alam, M., Asiri, A. M., Al-amshany, Z. M., Hajeeassa, K. S., & Rahman, M. M. (2019). Ultrasonic-assisted fabrication of polyvinyl chloride/mixed graphene-carbon nanotube nanocomposites as a selective Ag+ ionic sensor. *Journal of Composite Materials*, *53*(16), 2271–2284. https://doi.org/10.1177/0021998318825293

Jayaramudu, J., Das, K., Sonakshi, M., Siva Mohan Reddy, G., Aderibigbe, B., Sadiku, R., & Sinha Ray, S. (2014). Structure and properties of highly toughened biodegradable polylactide/ZnO biocomposite films. *International Journal of Biological Macromolecules*, *64*, 428–434. https://doi.org/10.1016/j.ijbiomac.2013.12.034

Kabir, E., Kaur, R., Lee, J., Kim, K.-H., & Kwon, E. E. (2020). Prospects of biopolymer technology as an alternative option for non-degradable plastics and sustainable management of plastic wastes. *Journal of Cleaner Production*, *258*, 120536. https://doi.org/10.1016/j.jclepro.2020.120536

Kim, I., Viswanathan, K., Kasi, G., Sadeghi, K., Thanakkasaranee, S., & Seo, J. (2019). Poly(Lactic Acid)/ZnO Bionanocomposite Films with Positively Charged ZnO as Potential Antimicrobial Food Packaging Materials. *Polymers*, *11*(9), Article 9. https://doi.org/10.3390/polym11091427

Kumar, Rajesh, Umar, Ahmad, Kumar, Girish, & Nalwa, H. S. (2017). Antimicrobial properties of ZnO nanomaterials: A review. *Ceramics International*, *43*(5), 3940–3961. https://doi.org/10.1016/j.ceramint.2016.12.062

Li, W., Zhang, C., Chi, H., Li, L., Lan, T., Han, P., Chen, H., & Qin, Y. (2017). Development of Antimicrobial Packaging Film Made from Poly(Lactic Acid) Incorporating Titanium Dioxide and Silver Nanoparticles. *Molecules*, *22*(7), Article 7. https://doi.org/10.3390/molecules22071170

Lizundia, E., Ruiz-Rubio, L., L. Vilas, J., & M. León, L. (2016). Towards the development of eco-friendly disposable polymers: ZnO-initiated thermal and hydrolytic degradation in

poly(l -lactide)/ZnO nanocomposites. *RSC Advances*, *6*(19), 15660–15669. https://doi.org/10.1039/C5RA24604K

Mallakpour, S., & Shafiee, E. (2018). A simple method for the sonochemical synthesis of PVA/ZrO2-vitamin B1 nanocomposites: Morphology, mechanical, thermal and wettability investigations. *Ultrasonics Sonochemistry*, *40*, 881–889. https://doi.org/10.1016/j.ultsonch.2017.08.039

Mohammadalinejhad, S., Almasi, H., & Esmaiili, M. (2021). Physical and release properties of poly(lactic acid)/nanosilver-decorated cellulose, chitosan and lignocellulose nanofiber composite films. *Materials Chemistry and Physics*, *268*, 124719. https://doi.org/10.1016/j.matchemphys.2021.124719

Molefe, F. V., Mofokeng, S. J., Khenfouch, M., Achehboune, M., Dhlamini, M. S., Mothudi, B. M., & Koao, L. F. (2019). The effect of Zn$\less$sup$\greater$2$\mathplus$$\less$/sup$\greater$ on the anion vacancies in ZnO thin-films grown using chemical bath deposition. *Journal of Physics: Conference Series*, *1292*(1), 012016. https://doi.org/10.1088/1742-6596/1292/1/012016

Murariu, M., Doumbia, A., Bonnaud, L., Dechief, A., Paint, Y., Ferreira, M., Campagne, C., Devaux, E., & Dubois, P. (2011). High-Performance Polylactide/ZnO Nanocomposites Designed for Films and Fibers with Special End-Use Properties. *Biomacromolecules*, *12*(5), 1762–1771. https://doi.org/10.1021/bm2001445

Nonato, R. C., Mei, L. H. I., Bonse, B. C., Chinaglia, E. F., & Morales, A. R. (2019). Nanocomposites of PLA containing ZnO nanofibers made by solvent cast 3D printing: Production and characterization. *European Polymer Journal*, *114*, 271–278. https://doi.org/10.1016/j.eurpolymj.2019.02.026

Nootsuwan, N., Wattanathana, W., Jongrungruangchok, S., Veranitisagul, C., Koonsaeng, N., & Laobuthee, A. (2018). Development of novel hybrid materials from polylactic acid and

nano-silver coated carbon black with distinct antimicrobial and electrical properties. *Journal of Polymer Research*, *25*(4), 90. https://doi.org/10.1007/s10965-018-1484-8

Nouroozi, F., & Farzaneh, F. (2011). Synthesis and characterization of brush-like ZnO nanorods using albumen as biotemplate. *Journal of the Brazilian Chemical Society*, *22*, 484–488. https://doi.org/10.1590/S0103-50532011000300011

Pantani, R., Gorrasi, G., Vigliotta, G., Murariu, M., & Dubois, P. (2013). PLA-ZnO nanocomposite films: Water vapor barrier properties and specific end-use characteristics. *European Polymer Journal*, *49*(11), 3471–3482. https://doi.org/10.1016/j.eurpolymj.2013.08.005

Pariona, N., Paraguay-Delgado, F., Basurto-Cereceda, S., Morales-Mendoza, J. E., Hermida-Montero, L. A., & Mtz-Enriquez, A. I. (2020). Shape-dependent antifungal activity of ZnO particles against phytopathogenic fungi. *Applied Nanoscience*, *10*(2), 435–443. https://doi.org/10.1007/s13204-019-01127-w

Poddar, M. K., Sharma, S., & Moholkar, V. S. (2016). Investigations in two-step ultrasonic synthesis of PMMA/ZnO nanocomposites by in–situ emulsion polymerization. *Polymer*, *99*, 453–469. https://doi.org/10.1016/j.polymer.2016.07.052

Qasim, U., Osman, A. I., Al-Muhtaseb, A. H., Farrell, C., Al-Abri, M., Ali, M., Vo, D.-V. N., Jamil, F., & Rooney, D. W. (2021). Renewable cellulosic nanocomposites for food packaging to avoid fossil fuel plastic pollution: A review. *Environmental Chemistry Letters*, *19*(1), 613–641. https://doi.org/10.1007/s10311-020-01090-x

Qu, X., Wang, M., Sun, W., & Yang, R. (2017). Hierarchical flower-like ZnO microstructures: Preparation, formation mechanism and application in gas sensor. *Journal of Materials Science: Materials in Electronics*, *28*(19), 14702–14710. https://doi.org/10.1007/s10854-017-7338-z

Rahimi, K., & Yazdani, A. (2018). Improving photocatalytic activity of ZnO nanorods: A comparison between thermal decomposition of zinc acetate under vacuum and in

ambient air. *Materials Science in Semiconductor Processing*, *80*, 38–43. https://doi.org/10.1016/j.mssp.2018.02.018

Ramimoghadam, D., Hussein, M. Z. B., & Taufiq-Yap, Y. H. (2013). Synthesis and characterization of ZnO nanostructures using palm olein as biotemplate. *Chemistry Central Journal*, *7*(1), 71. https://doi.org/10.1186/1752-153X-7-71

Reichert, C. L., Bugnicourt, E., Coltelli, M.-B., Cinelli, P., Lazzeri, A., Canesi, I., Braca, F., Martínez, B. M., Alonso, R., Agostinis, L., Verstichel, S., Six, L., Mets, S. D., Gómez, E. C., Ißbrücker, C., Geerinck, R., Nettleton, D. F., Campos, I., Sauter, E., … Schmid, M. (2020). Bio-Based Packaging: Materials, Modifications, Industrial Applications and Sustainability. *Polymers*, *12*(7), Article 7. https://doi.org/10.3390/polym12071558

Restrepo, I., Benito, N., Medinam, C., Mangalaraja, R. V., Flores, P., & Rodriguez-Llamazares, S. (2017). Development and characterization of polyvinyl alcohol stabilized polylactic acid/ZnO nanocomposites. *Materials Research Express*, *4*(10), 105019. https://doi.org/10.1088/2053-1591/aa8b8d

Rhim, J.-W., Hong, S.-I., & Ha, C.-S. (2009). Tensile, water vapor barrier and antimicrobial properties of PLA/nanoclay composite films. *LWT - Food Science and Technology*, *42*(2), 612–617. https://doi.org/10.1016/j.lwt.2008.02.015

Roy, S., & Rhim, J.-W. (2019). Carrageenan-based antimicrobial bionanocomposite films incorporated with ZnO nanoparticles stabilized by melanin. *Food Hydrocolloids*, *90*, 500–507. https://doi.org/10.1016/j.foodhyd.2018.12.056

Shankar, S., Wang, L.-F., & Rhim, J.-W. (2018). Incorporation of zinc oxide nanoparticles improved the mechanical, water vapor barrier, UV-light barrier, and antibacterial properties of PLA-based nanocomposite films. *Materials Science and Engineering: C*, *93*, 289–298. https://doi.org/10.1016/j.msec.2018.08.002

Sharma, S., Kumar, D., & Khare, N. (2020). Hierarchical PANI/ZnO nanocomposite: Synthesis and synergistic effect of shape-selective ZnO nanoflowers and polyaniline sensitization

for efficient photocatalytic dye degradation and photoelectrochemical water splitting. *Nanotechnology*, *31*(46), 465402. https://doi.org/10.1088/1361-6528/abad5b

Soltani, R., Dinari, M., & Mohammadnezhad, G. (2018). Ultrasonic-assisted synthesis of novel nanocomposite of poly(vinyl alcohol) and amino-modified MCM-41: A green adsorbent for Cd(II) removal. *Ultrasonics Sonochemistry*, *40*, 533–542. https://doi.org/10.1016/j.ultsonch.2017.07.045

Soylu, M., & Coskun, M. (2018). Controlling the properties of ZnO thin films by varying precursor concentration. *Journal of Alloys and Compounds*, *741*, 957–968. https://doi.org/10.1016/j.jallcom.2018.01.079

Suganya Josephine, G. A., Jayaprakash, K., Meenakshi, G., Sivasamy, A., Nirmala Devi, G., & Viswanath, R. N. (2021). Photocatalytically active ZnO flaky nanoflowers for environmental remediation under solar light irradiation: Effect of morphology on photocatalytic activity. *Bulletin of Materials Science*, *44*(4), 247. https://doi.org/10.1007/s12034-021-02531-1

Taha, K. K., Modwi, A., Elamin, M. R., Arasheed, R., AL-Fahad, A. J., Albutairi, I., Arasheed, H., Alfaify, M., Anojaidi, K., Algethami, F. K., & Bagabas, A. (2020). Impact of Hibiscus extract on the structural and activity of sonochemically fabricated ZnO nanoparticles. *Journal of Photochemistry and Photobiology A: Chemistry*, *390*, 112263. https://doi.org/10.1016/j.jphotochem.2019.112263

Tang, Z., Fan, F., Chu, Z., Fan, C., & Qin, Y. (2020). Barrier Properties and Characterizations of Poly(lactic Acid)/ZnO Nanocomposites. *Molecules*, *25*(6), Article 6. https://doi.org/10.3390/molecules25061310

Trifol, J., Marin Quintero, D. C., & Moriana, R. (2021). Pine Cone Biorefinery: Integral Valorization of Residual Biomass into Lignocellulose Nanofibrils (LCNF)-Reinforced Composites for Packaging. *ACS Sustainable Chemistry & Engineering*, *9*(5), 2180–2190. https://doi.org/10.1021/acssuschemeng.0c07687

Uribe-López, M. C., Hidalgo-López, M. C., López-González, R., Frías-Márquez, D. M., Núñez-Nogueira, G., Hernández-Castillo, D., & Alvarez-Lemus, M. A. (2021). Photocatalytic activity of ZnO nanoparticles and the role of the synthesis method on their physical and chemical properties. *Journal of Photochemistry and Photobiology A: Chemistry*, *404*, 112866. https://doi.org/10.1016/j.jphotochem.2020.112866

Wang, C., Wang, Z.-G., Xi, R., Zhang, L., Zhang, S.-H., Wang, L.-J., & Pan, G.-B. (2019). In situ synthesis of flower-like ZnO on GaN using electrodeposition and its application as ethanol gas sensor at room temperature. *Sensors and Actuators B: Chemical*, *292*, 270–276. https://doi.org/10.1016/j.snb.2019.04.140

Wang, S., Gao, M., Ma, B., Xi, M., & Kong, F. (2020). Size-dependent effects of ZnO nanoparticles on performance, microbial enzymatic activity and extracellular polymeric substances in sequencing batch reactor. *Environmental Pollution*, *257*, 113596. https://doi.org/10.1016/j.envpol.2019.113596

Wojnarowicz, J., Chudoba, T., & Lojkowski, W. (2020). A Review of Microwave Synthesis of Zinc Oxide Nanomaterials: Reactants, Process Parameters and Morphologies. *Nanomaterials*, *10*(6), Article 6. https://doi.org/10.3390/nano10061086

Yu, F., Fei, X., He, Y., & Li, H. (2021). Poly(lactic acid)-based composite film reinforced with acetylated cellulose nanocrystals and ZnO nanoparticles for active food packaging. *International Journal of Biological Macromolecules*, *186*, 770–779. https://doi.org/10.1016/j.ijbiomac.2021.07.097

Zhang, R., Lan, W., Ji, T., Sameen, D. E., Ahmed, S., Qin, W., & Liu, Y. (2021). Development of polylactic acid/ZnO composite membranes prepared by ultrasonication and electrospinning for food packaging. *LWT*, *135*, 110072. https://doi.org/10.1016/j.lwt.2020.110072

Zhu, L., Li, Y., & Zeng, W. (2018). Hydrothermal synthesis of hierarchical flower-like ZnO nanostructure and its enhanced ethanol gas-sensing properties. *Applied Surface Science*, *427*, 281–287. https://doi.org/10.1016/j.apsusc.2017.08.229

Zou, X., Ke, J., Hao, J., Yan, X., & Tian, Y. (2022). A new method for synthesis of ZnO flower-like nanostructures and their photocatalytic performance. *Physica B: Condensed Matter*, *624*, 413395. https://doi.org/10.1016/j.physb.2021.413395

CHAPTER 3

Poly(lactic acid)/functionalized ZnO Nanocomposites for Antimicrobial Food Packaging Applications

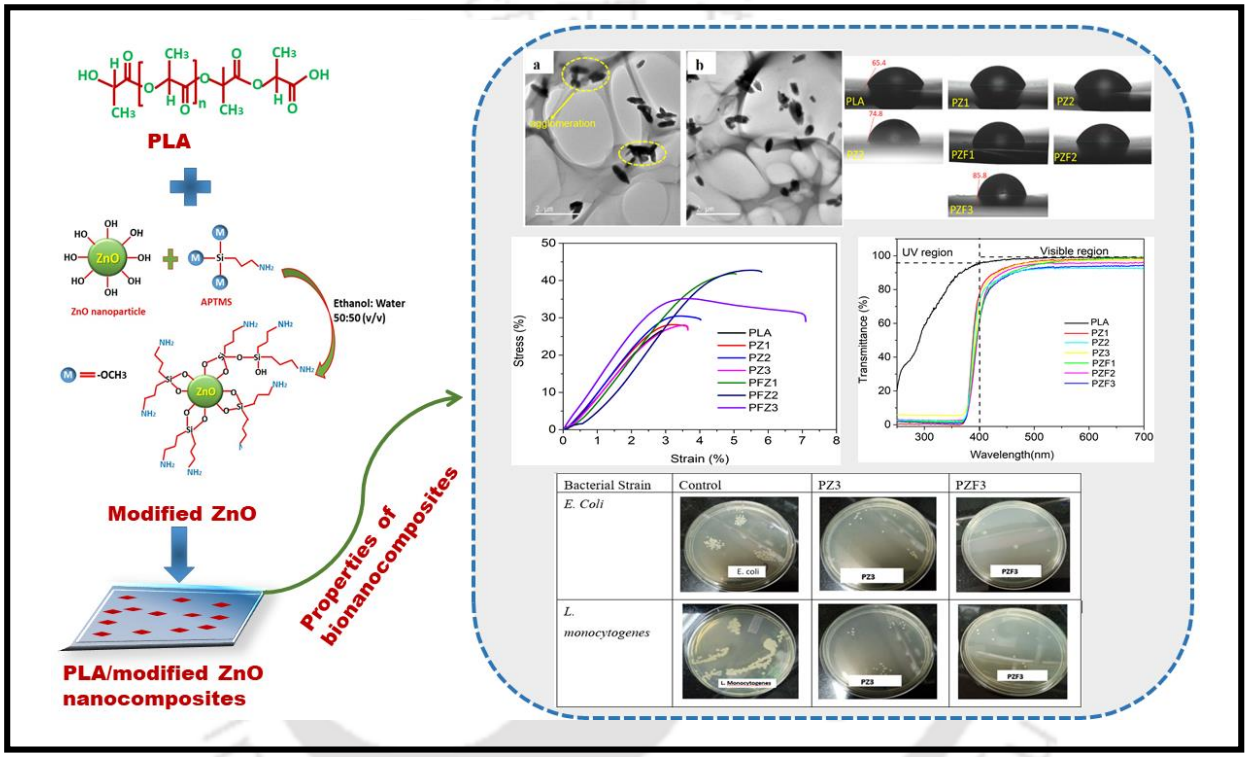

3.1 Introduction

Over the last few years, there is a growing inclination for the use of environmental friendly and degradable biopolymer based nanocomposite films in food packaging sector. Among various biopolymers, biodegradable poly(lactic acid) extracted from corn starch, is extensively used in fabrication of nanocomposite films, mainly in combination with nanoclays, cellulose nanocrystals, carbon based nanofillers and metal oxides etc. Agglomeration and incompatibility with hydrophobic polymers are the two basic limitations of the nanofiller addition in polymer nanocomposites. Owing to its high surface area and aspect ratio, nanoparticles tend to agglomerate in polymer matrix. This agglomeration would hamper the final properties (thermal, mechanical, barrier properties etc.) of polymer nanocomposites (Maghsoudlou et al., 2019; Rong et al., 2006; Zare et al., 2017). Therefore, homogeneous dispersion of nanofillers in polymer matrix is the essential criteria to get the ultimate benefit of polymer nanocomposites. Many methods are available for the enhancement of nanofiller dispersion in polymer matrix. Surface modification of nanofillers with suitable coupling agent is one of them (Kango et al., 2013). Surface modified nanofiller ensure good compatibility with hydrophobic polymers and facilitates the nanofiller dispersion. Many studies have been done on surface modification of nanoparticles by using different modifying agents such as carboxylic acids (Quiñones et al., 2014; Samavini et al., 2018), silanes (Ahangaran & Navarchian, 2020), organophosphorous (Kalska-Szostko et al., 2013; Mohapatra & Pramanik, 2009) etc.

Surface modification of metal oxides are mostly done by using silane coupling agents such as triethoxyvinylsilane, trichlorovinylsilane, γ-aminopropyltrimethoxysilane and γ-mercaptopropyltrimethoxysilane etc. The chemical formula representing silane coupling agent is [$X-(CH_2)_n-Si-R_3$]. Here, 'X' represents organofunctional group and 'R' denotes hydrolyzable group. The organofunctional group reacts with the polymer matrix while the hydrolyzable group form a strong bond with reinforcing filler. The hydroxyl group of metal oxides nanoparticles act

as an active site for the reaction. The surface modification of metal oxides not only improves the compatibility between hydrophilic metal oxide nanoparticles with hydrophobic polymer but also enhances dispersion and reduces the problem of agglomeration (Mallakpour & Madani, 2015).

In this work, the synthesized ZnO nanoparticles has been modified with silane coupling agent 3- (aminopropyl) trimethoxysilane (APTMS). Then the physiochemical properties (thermal, mechanical, antimicrobial properties etc.) of PLA/functionalized ZnO was investigated.

3.2 Experimental

3.2.1 Materials

Zinc sulfate heptahydrate ($ZnSO_4.7H_2O$) and potassium hydroxide (KOH) were supplied from Merck, India. 3-(aminopropyl) trimethoxysilane (APTMS) was procured from Sigma Aldrich. Polylactic acid (PLA) pellets (code PLA 4032D) were obtained from Nature Works LLC (USA).

3.2.2 Synthesis of ZnO nanoparticles

For the preparation of ZnO nanoparticles, zinc sulfate heptahydrate salt (0.05 M) was dissolved in 200 ml of Millipore water. To this solution 0.5 M of KOH was added in dropwise manner. During this reaction, a constant temperature was maintained at 60 °C for 3 h. After completion of the reaction, a white precipitate was obtained. The precipitates were centrifuged and dried at 70 °C overnight to obtain the ZnO nanoparticles. Fig. 3.1. shows the schematic diagram for synthesis of ZnO nanoparticles.

3.2.3 Synthesis of 3-(aminopropyl) trimethoxysilane (APTMS) modified ZnO nanoparticle

Briefly, 1 ml of APTMS was added to 30 ml of ethanol-water (50:50 v/v) mixture. The solution was then continuously stirred at 60 °C for 30 min. To this solution 1.5 g of prepared ZnO was added by maintaining the temperature at 60 °C for 1 h. The precipitate obtained was centrifuged and dried in an oven at 70 °C to get the final functionalized ZnO (f-ZnO) powder. The schematic route for the synthesis of APTMS treated ZnO has been shown in Fig. 3.2.

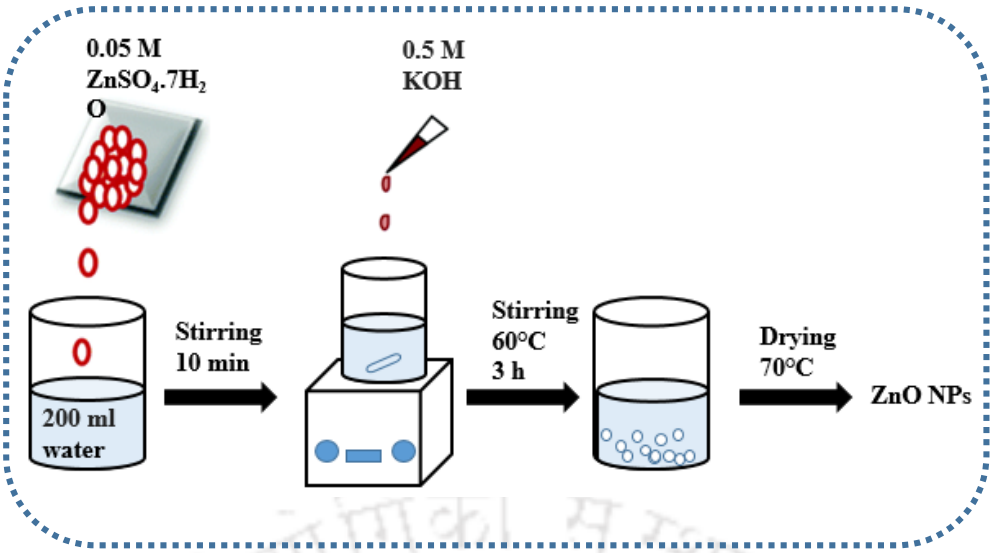

Fig. 3.1. Synthesis of ZnO nanoparticles

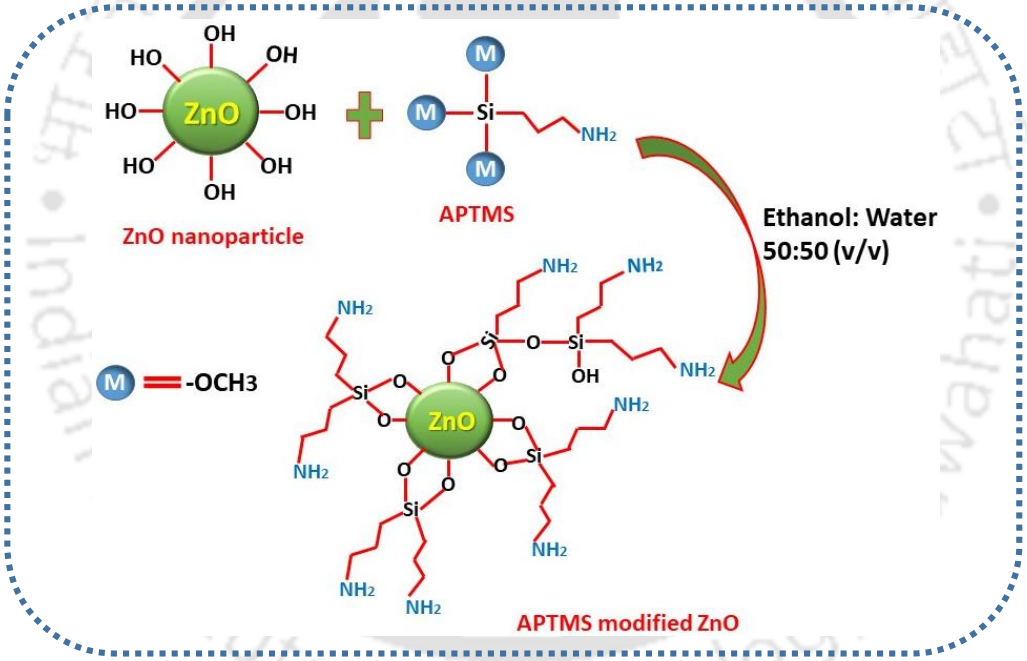

Fig. 3.2. The schematic route for the synthesis of APTMS treated ZnO

3.2.4 Synthesis of PLA/f-ZnO nanocomposites

PLA/f-ZnO nanocomposites were prepared using ultrasound assisted solvent casting method followed by the methodology as described in elsewhere (Chapter 2, Section 2.2.3). PLA based nanocomposite films prepared with 1, 2 and 3 wt% of ZnO were referred as PZ1, PZ2 and PZ3

respectively and nanocomposites prepared with f-ZnO (1, 2 and 3 wt%) were referred as PZF1, PZF2 and PZF3 respectively.

3.2.5 Characterization techniques

ZnO, f-ZnO nanoparticles and PLA/ZnO and PLA/f-ZnO nanocomposites were characterized for composition, structural/morphology and physiochemical properties with following standard techniques: **(1) FTIR:** FTIR was conducted by using FTIR spectrometer (Make: PerkinElmer, Singapore, Model: Spectrum two). **(2) XRD:** The structural characteristics of synthesized materials were analysed using powder X-ray diffractometer (Make: Rigaku Technologies, Japan, Model: Smartlab, $\lambda = 1.5406$ Å). The crystallite size of the synthesized ZnO was calculated by using Scherrer formula:

$$\text{crystallite size} = k\lambda/\beta \cos\theta$$

Here, k denotes Scherrer constant and β is the full width at half maximum height in radians.

(3) FE-SEM and EDX: Surface morphology and elemental composition of ZnO was examined using Field Emission Scanning Electron Microscope (Make: Zeiss, Model: Sigma 300) and Energy Dispersive X-ray Spectroscopy (Make: Zeiss, Model: Sigma 300). **(4) Surface area and pore size distribution:** The specific surface area and the pore size distribution of ZnO sample were evaluated by using BET surface area analyzer (Model No.: Tristar II; Make: M/s Micromeritics, U.S.A.). **(5) TEM:** The internal structure of the synthesized nanocomposites was studied by using Transmission Electron Microscope (TEM) analyzer (Make: JEOL, Model: 2100F). **(6) UV-Visible spectroscopy:** UV-Visible spectroscopy study of ZnO and PLA/ZnO nanocomposites were performed using Lambda 35 spectrometer from Perkin Elmer. **(7) Thermal properties:** Thermal properties of PLA/ZnO nanocomposites were evaluated by using DSC/TGA analyzer (Make: Netzsch model: STA449F3A00). **(8) Mechanical properties:** Mechanical properties were measured by 5 kN Electromechanical Universal Testing Machine (Make: Zwick Roell: Z005TN) at a standard crosshead speed of 1 mm min^{-1}. **(9) Antimicrobial activity test:** The

antimicrobial activity of PLA/ZnO nanocomposite films was tested quantitatively against two food borne pathogenic bacteria, *Escherichia coli* (Gram negative) and *Listeria monocytogenes* (Gram positive) by using colony count method (Rhim et al., 2009) as described in elsewhere (Chapter 2, Section 2.2.4). **(10) Surface color:** The surface color of the nanocomposite films was measured by using colorimeter (Datacolor 550, Datacolor Technology Suzhou Co., Ltd., China). Hunter color values, L^* (lightness/darkness), a^* (redness/greenness), b^* (yellowness/blueness) were measured at five different places of film samples. **(11) Surface wettability:** The surface wettability test of the nanocomposite films was carried by using a contact angle goniometer and associated software (Holmarc, HO-IAD-CAM-01B). The film sample of dimension 20 mm×20 mm was placed on a sample holder and a water droplet of 3 µL was carefully placed on the film surface by using microsyringe and contact angle (CA) was measured. The CA was measured at three different positions of the film surface and the average value was reported. **(12) Water vapor permeability (WVP) test:** The water vapor permeability (WVP) test of the polymer samples were done gravimetrically according to the ASTME00996-00 method with some modifications (Bhat et al., 2021; Yadav et al., 2020). Firstly, 10 mL of distilled water was filled in the glass bottle of inner diameter of 21 mm. By using film samples, the mouth of the bottle was covered and made airtight by wrapping with Teflon tape. For each measurement, dried silica gel was taken in a desiccator and the bottle filled with distilled water was placed inside it after measuring the initial mass of the bottle. The changes in the weight of bottles (to the nearest 0.001 mg) were recorded for three consecutive days. The test was performed in triplicate for each film. The WVP was calculated as:

$$WVP = W \cdot x/(t \cdot A \cdot \Delta P)$$

where W = weight change of bottle with film sample (g), x = film thickness (m), t = time (24 h), A = permeation area (m^2) and ΔP = Difference in partial vapour pressure between water and dry atmosphere at 25°C (2338.9 Pa). The results were expressed as g m^{-1} s^{-1} Pa^{-1}.

3.3 Results and discussion

3.3.1 FTIR and XRD study of ZnO and f-ZnO

FTIR study of ZnO, f-ZnO and APTMS are shown in Fig. 3.3a. The absorption peak at 3421 cm^{-1} and 430 cm^{-1} are attributed to the –OH and Zn–O stretching vibrations of ZnO that indicates successful formation of ZnO nanoparticle (Hang et al., 2015). In case of f-ZnO two newly formed consecutive absorption bands was observed at 2856 cm^{-1} and 2925 cm^{-1} corresponding to the symmetric and asymmetric stretching of alkanes C–H group of the APTMS (Hang et al., 2015; Ma et al., 2008). The absorption band occurred at 1596 cm^{-1} is attributed to the bending vibration of primary N–H group. In addition, the absorption spectra at 874 and 1098 cm^{-1} are attributed to symmetrical vibrations of the Zn–O–Si and Si–O–Si bonds (Ma et al., 2008). Existence of these absorption bonds confirmed the successful functionalization of ZnO surface with APTMS.

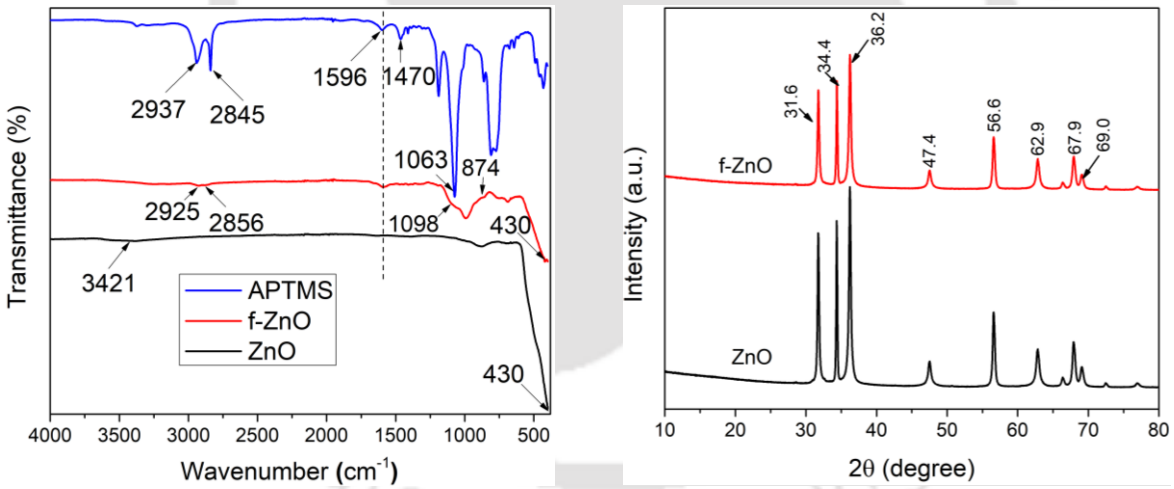

Fig. 3.3. (a) FTIR of ZnO, f-ZnO and APTMS, (b) XRD of ZnO and f-ZnO

Typical XRD patterns of ZnO and f-ZnO nanoparticles are shown in Fig. 3.3b. The synthesized ZnO and f-ZnO nanoparticles are highly crystalline in nature as indicated by its sharp and strong X-ray diffraction peaks. The ZnO and f-ZnO possesses diffraction peaks at 2θ = 31.6° (100), 34.4° (002), 36.2° (101), 47.4° (102), 56.6° (110), 62.9° (103), 67.9° (112) and 69.0° (201).

It is observed that functionalization of ZnO does not change the position of diffraction peaks but the intensity corresponding to crystal plane (101) decrease in f-ZnO. It means that upon functionalization, crystallinity of ZnO slightly decreases (Hang et al., 2015). The silane coupling agent 3-aminopropyl (trimethoxysilane) used for the functionalization of ZnO contain silane group in its structure. Presence of silane group causes irregularity in structure resulting in the reduction of peak intensity. The crystallite size and intensity of ZnO and f-ZnO is shown in Table 3.1. By applying the Debye-Scherrer equation, the average crystallite size was found to be 21.6 nm and 22.6 nm respectively for ZnO and f-ZnO from the FWHM of dominant peak (101). It can be observed from Table 1 that the average crystallite size of the nanoparticles is not affected by much upon functionalization which confirms that functionalization occurs only on the surface.

Table 3.1. Intensity of index peak [101] and the crystallite size of ZnO and f-ZnO

Sample	2Θ (degree)	FWHM	Crystallite size (nm)	Intensity (%)
ZnO	36.2	0.387	21.6	64
f-ZnO	36.2	0.368	22.6	41

3.3.2 Energy dispersive X-ray spectroscopy (EDX)

EDX study was done to determine the elemental compositions of ZnO and f-ZnO (Fig. 3.4a & b). As displayed in Fig. 3.4a, ZnO contain only Zn and O in the weight percentage of 78% and 22% respectively. On the other hand, f-ZnO (Fig. 3.4b) contain Si, Zn and O in the weight percentage of 4.8%, 61.1% and 34.1% respectably. Fig. 3.4c shows the elemental mapping of f-ZnO which also supports the presence of Si in the sample.

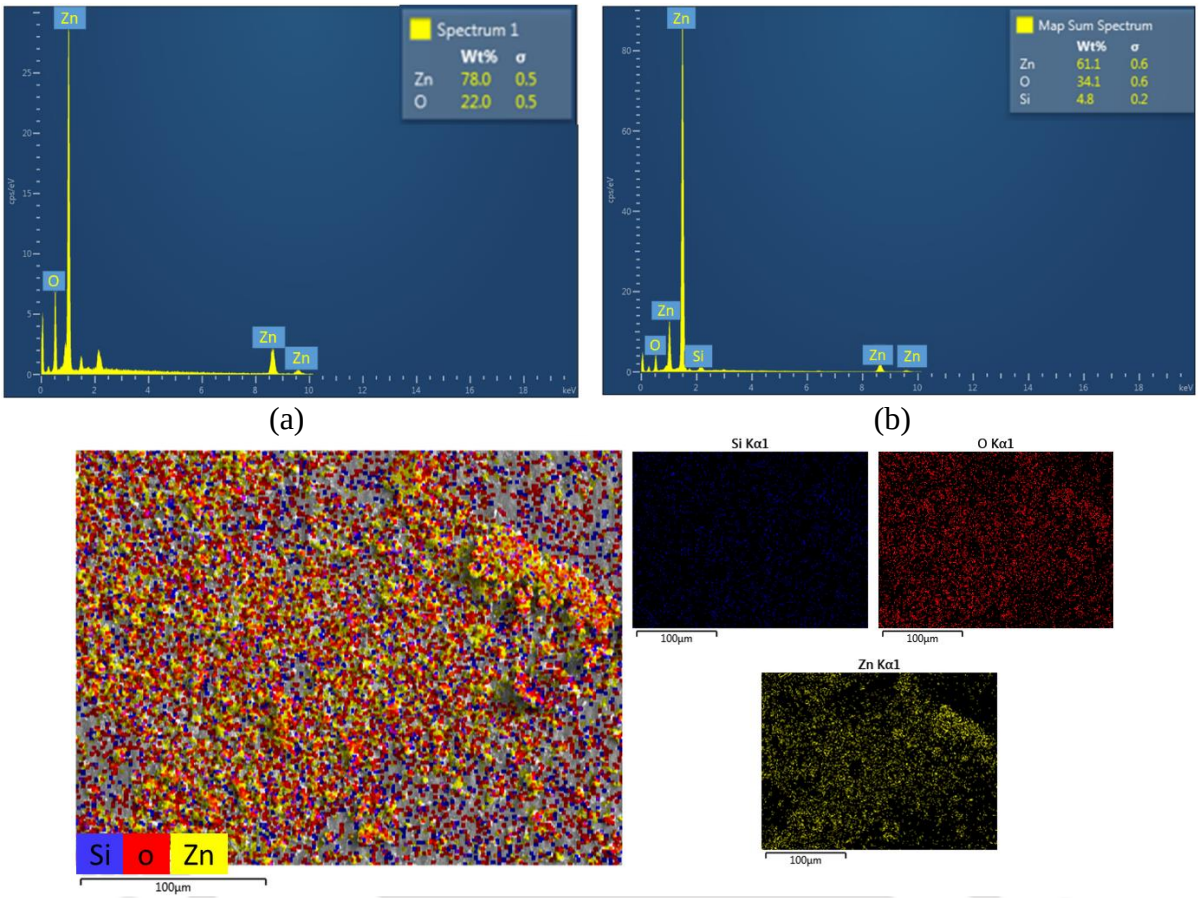

(a) (b)

(c)

Fig. 3.4. EDX spectra of (a) ZnO and (b) f-ZnO, (c) elemental mapping of f-ZnO

3.3.3 FE-SEM analysis

Surface morphology of the prepared ZnO and f-ZnO was studied by using FE-SEM analysis. FE-SEM images of the ZnO nanostructures are shown in Fig. 3.5. It can be seen clearly from the images that both modified and unmodified nanoparticles have rice beads like morphology. The FE-SEM micrograph of f-ZnO suggested non-agglomerated and homogenous distribution of f-ZnO nanoparticles compared to the unmodified ZnO.The agglomeration was reduced due to surface modifiaction of ZnO with silane coupling agent.

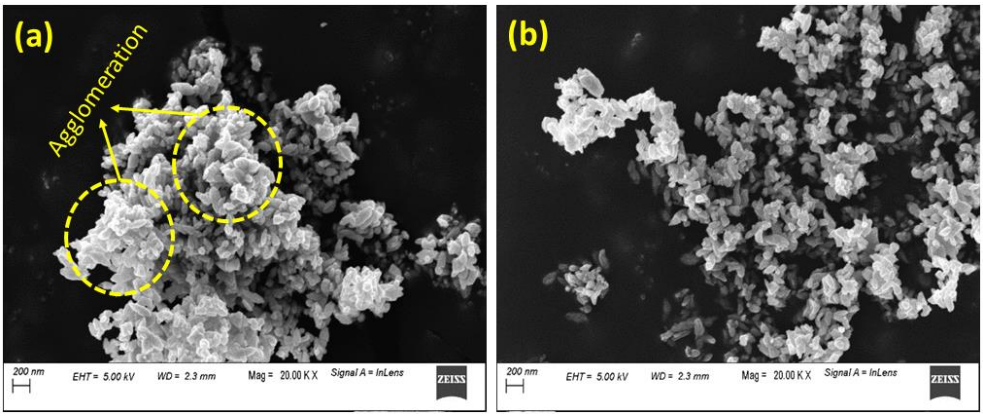

Fig. 3.5. FE-SEM images of (a) ZnO and (b) f-ZnO

3.3.4 BET surface area analysis

The surface area of nanomaterials is an important parameter which plays a major role in the final properties determination of polymer nanocomposites. Fig. 3.6a and b shows N_2 adsorption-desorption curve and BJH (Barrett-Joyner-Halenda) pore size distribution of ZnO and f-ZnO respectively. The BET surface area obtained for the ZnO and f-ZnO are 17.97 $m^2\ g^{-1}$ and 24.18 $m^2\ g^{-1}$ respectively. Pore size distribution (calculated by BJH method) indicates the presence of mesopores in the range of 6–50 nm in both ZnO and f-ZnO samples.

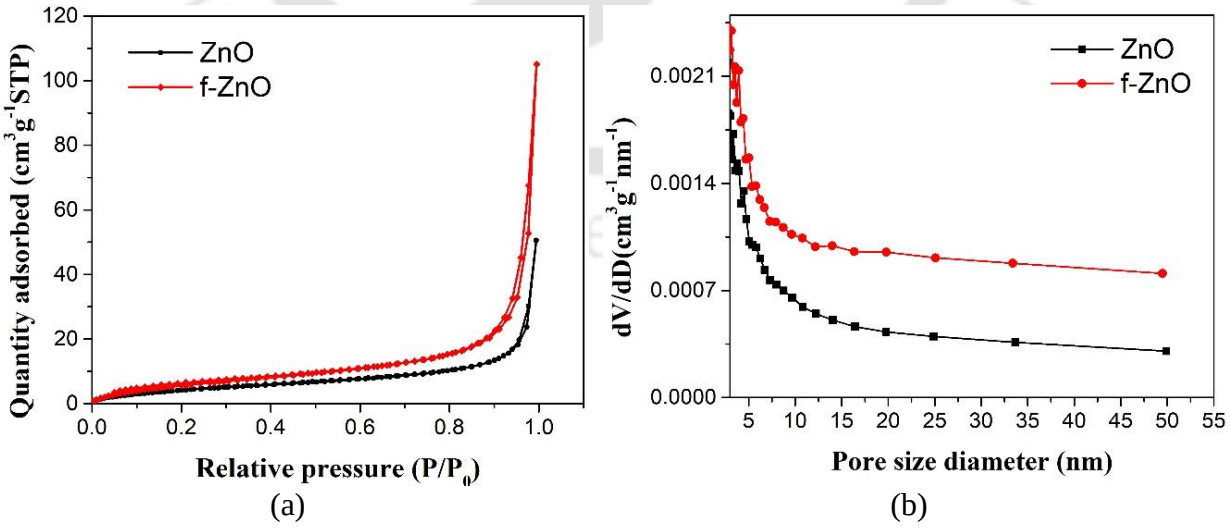

Fig. 3.6. (a) N_2 adsorption-desorption curve, and (b) pore size distribution for ZnO and f-ZnO

3.3.5 FE-TEM analysis of nanocomposites

FE-TEM analysis was done to study the dispersion of ZnO and f-ZnO in PLA matrix. The FE-TEM images are shown in Fig. 3.7a and b. The images revealed more homogeneous dispersion of f-ZnO (PZF2) as compared to ZnO (PZ2) in PLA matrix. In case of PZ2 (Fig. 3.7a) some agglomeration of ZnO are observed, while PZF2 (Fig. 3.7b) shows uniform distribution of the nanoparticles without any agglomeration.

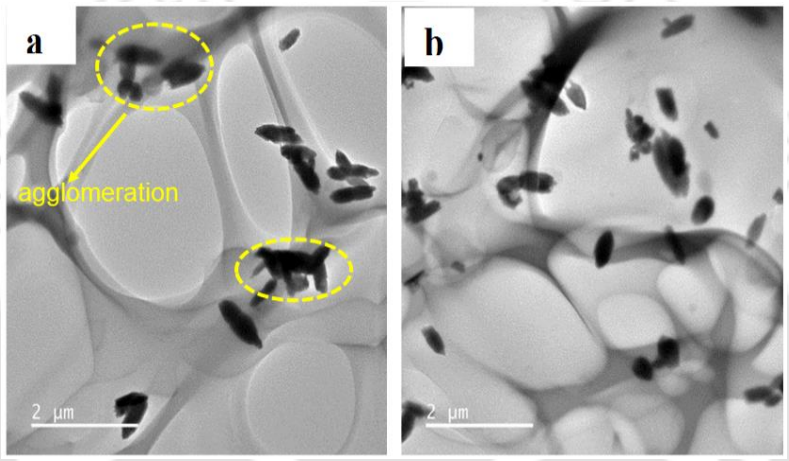

Fig. 3.7. TEM images of (a) PZ2 (2 wt% ZnO) and, (b) PZF2 (2 wt% of f-ZnO)

3.3.6 Thermal properties

Thermogravimetric (TGA) analysis was done to evaluate the thermal stability of PLA and its nanocomposites with ZnO and f-ZnO. The TGA curves are shown in Fig. 3.8a and their characteristic thermodegradation temperatures were summarized in Table 3.2. It could be observed from the result that addition of ZnO nanofillers in the PLA matrix decreases the degradation temperatures of the nanocomposite films resulting a thermally degradable polymer nanocomposite (Kim et al., 2019; Shankar et al., 2018). In presence of thermal energy, ZnO act as a catalyst and starts the unzipping depolymerization/intermolecular transesterification reactions of PLA matrix (Murariu et al., 2011). This results into chain scissioning or the bond dissociation

of PLA chains resulting in decrease in thermal stability of PLA/ZnO nanocomposite films. The pristine PLA showed $T_{5\%}$, $T_{10\%}$ and T_{max} at 147.5℃, 323℃ and 363℃ respectively. Conversely, nanocomposite of PLA with ZnO and f-ZnO begins to degrade at lower temperature as compared to pristine polymer. But the degradation temperature increases in case of nanocomposites with functionalized ZnO surface (Table 3.2). This may be due to homogeneous distribution of f-ZnO in PLA matrix. Clearly, the surface-coating of ZnO nanofiller allows for limiting the decrease in PLA molecular weights and preserving good thermal stability of resulting PLA nanocomposites, improvements that might be ascribed to the shielding effect conferred by the organo-silane layers (Zn-O-Si-R) and –Si-O-Si-O-network (Murariu et al., 2011). As could be seen in Fig. 3.8b, the derivative TGA curve (DTG) of neat PLA and its nanocomposites shows a two-step degradation process. For nanocomposites, the first step of degradation is occurred around 91−181˚C which is related to the decomposition step of PLA close to ZnO surface (Restrepo, I., et al., 2017). The second step degradation, between 297−312˚C could be associated with the degradation of PLA that is far from ZnO.

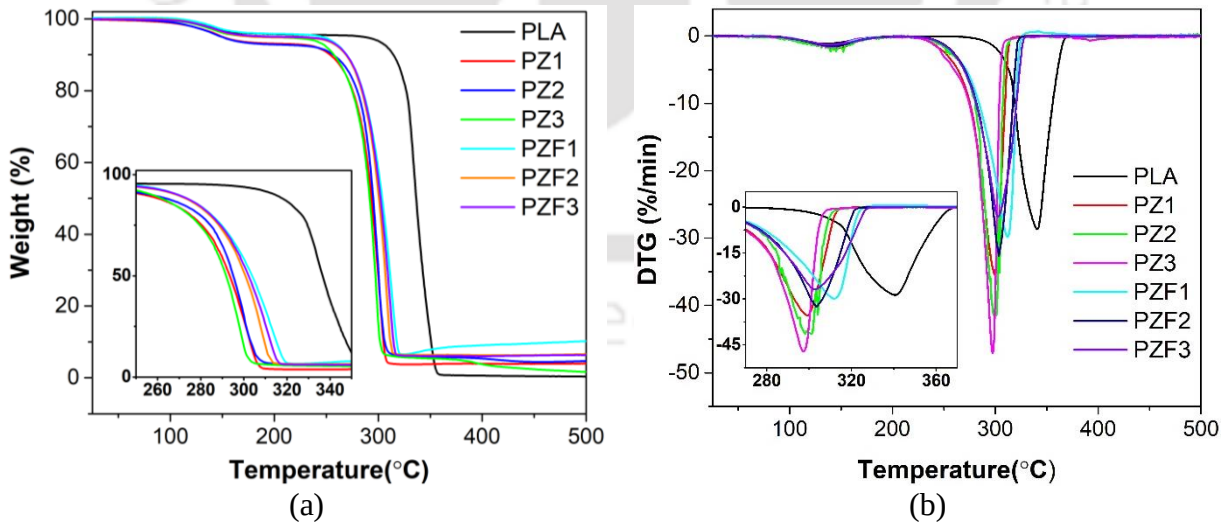

Fig. 3.8. (a) TGA and (b) DTG curve of PLA/ZnO nanocomposites

Table 3.2. Characteristic thermodegradation temperatures of PLA and PLA/ZnO nanocomposites

Sample	$T_{5\%}$ (°C)	$T_{10\%}$ (°C)	$T_{max\%}$ (°C)	Char value at 400 °C (%)
PLA	147.5	323	363	0.78
PZ1	148	254	293	3.70
PZ2	148	256	294	6.03
PZ3	193	256	290	3.73
PZF1	193	270	304	6.20
PZF2	244	270	302	6.02
PZF3	148	269	303	3.00

3.3.7 Mechanical properties

The mechanical properties viz. tensile strength and elongation at break are determined for PLA and its nanocomposite films with ZnO and f-ZnO. The results are shown in Fig 3.9 and Table 3.3. The results showed that incorporation of functionalized ZnO into PLA matrix leads to increase in tensile strength and elongation at break as compared to untreated ZnO based nanocomposites. The tensile strength obtained for PLA, PZ1, PZ2, PZ3, PZF1, PZF2 and PZF3 are 26.5, 28.2, 30.5, 28.0, 41.0, 42.7 and 35.1 MPa respectively. The highest value of tensile strength (42.7 MPa) and elongation at break (5.8%) is obtained for PZF2. These may be due to lower interfacial energy between PLA matrix and f-ZnO and also due to homogeneous dispersion of nanoparticles. The improvement in tensile strength and elongation at break indicates that the interfacial interaction between PLA and ZnO is tuned due to surface modification of ZnO by silane coupling agent. These improvements are generally associated with lower interfacial energy between the polymer matrix and nanofiller as well as finer dispersion of the nanoparticles. Furthermore, one cannot exclude the effect of the –Si–O–Si–O layers that cover the surface of nanofiller and behave as a barrier effectively limiting the catalytic effect of ZnO and allowing for reducing the extent of unzipping/transesterification reactions as aforementioned (Murariu et al., 2011).

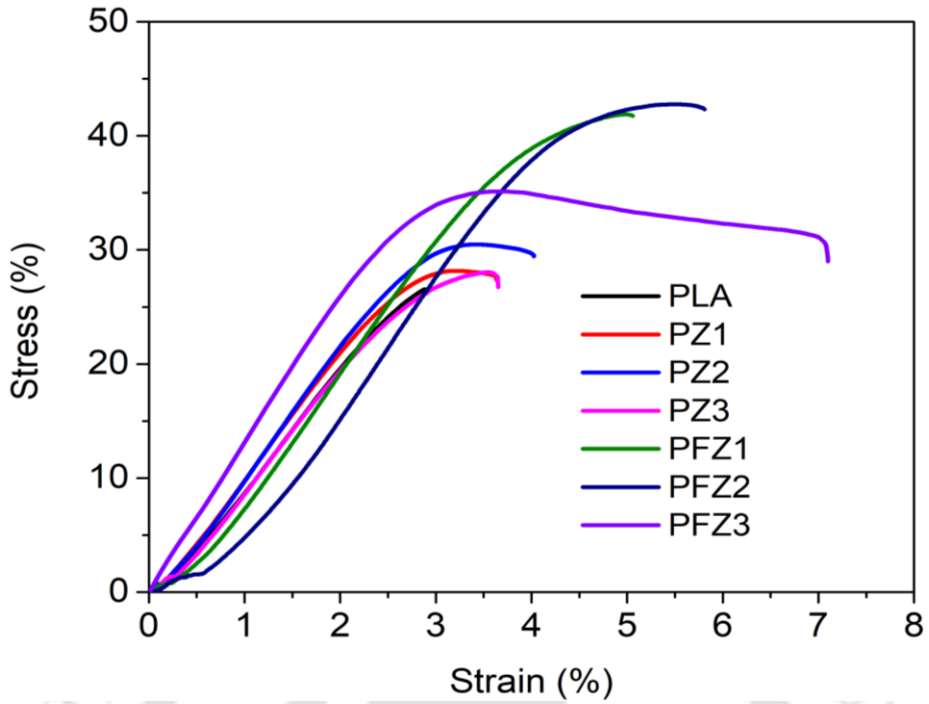

Fig. 3.9. Stress vs strain curve of PLA/ZnO nanocomposites

Table 3.3. Tensile strength and elongation at break of PLA/ZnO nanocomposites

Sample	Tensile strength (MPa)	Elongation at break (%)
PLA	26.5	2.9
PZ1	28.2	3.6
PZ2	30.5	4.2
PZ3	28	3.6
PZF1	41	5.1
PZF2	42.7	5.8
PZF3	35.1	7.1

3.3.8 UV-barrier properties and surface color of the nanocomposites

The UV-light barrier property is an important parameter required in food packaging application. Some components present in food such as fats, lipids and proteins undergo degradation upon exposure to UV-light which reduces the shelf life of food (Ghosh et al., 2019). Therefore, reduction in the transmittance value for UV-light of the packaging material is required in food packaging applications. The UV-Visible spectra of PLA and its nanocomposite with ZnO and f-ZnO are shown in Fig. 3.10 and the transmittance value (%) are displayed in Table 3.4. The results showed that PLA possesses transmittance value 99% in visible range. The addition of ZnO and f-

ZnO reduces the transmittance value especially in UV region (200–400 nm) which indicates the UV barrier property of the nanocomposite films. This may be due to inherent UV-active properties of ZnO (Ekrami et al., 2021; Hari et al., 2021; Pandimurugan & Thambidurai, 2017). The transmittance of PLA, PZ1, PZ2, PZ3, PZF1, PZF2 and PZF3 at 400 nm are 95, 78, 72, 70, 61, 59 and 59% respectively. It can be observed that transmittance value is lower in PLA/f-ZnO nanocomposites as compared to PLA/ZnO nanocomposites. This may be due to uniform dispersion and good interfacial interaction of functionalized ZnO with PLA matrix.

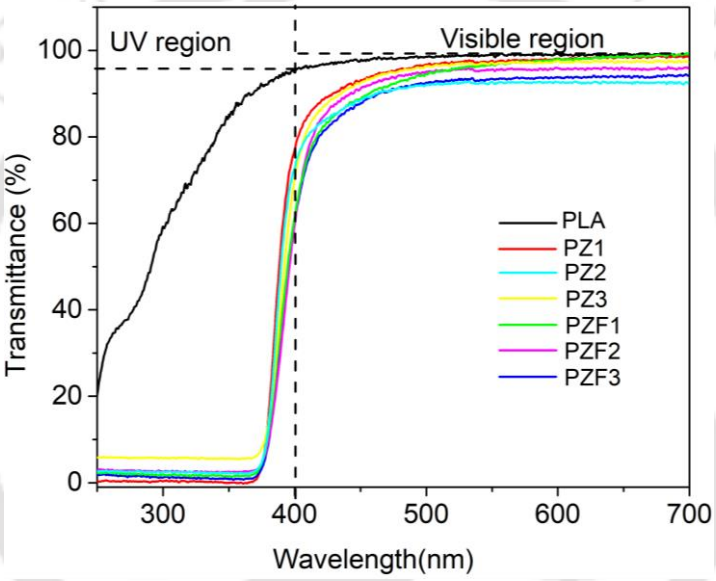

Fig. 3.10. UV-Visible spectroscopy of PLA/ZnO nanocomposite films

Table 3.4. Transmittance (%) of PLA and it PLA/ZnO nanocomposites

	Transmittance (%)	
Specimen	**UV range (300 nm)**	**Visible range (700 nm)**
PLA	62	99
PZ1	0.6	99
PZ2	2.33	92
PZ3	5.7	97
PZF1	1.88	99
PZF2	2.8	96
PZF3	1.26	93

The color parameters of the packaging material affect the consumer's acceptance of the products. The surface color of PLA and its nanocomposite films are shown in Table 3.5. The observed L* value of neat PLA is 86.94, which increases to 87.8, 91.5, 91.6, 90.6, 91.4 and 91.8 for PZ1, PZ2, PZ3, PZF1, PZF2 and PZF3 respectively. These results showed that the nanocomposites are brighter than pristine PLA. Also these nanocomposite films have lower a* and b* values indicating green and blue colorization effect. Moreover, total color difference (ΔE) has been measured for all testing samples. There has been observed a difference in ΔE values for the nanocomposite samples. The color difference in PLA/ZnO and PLA/f-ZnO mainly occurred due to increased brightness as compared to PLA. As shown in Table 3.5, whiteness index (WI) also increases in nanocomposite films.

Table 3.5. Surface color of PLA based nanocomposites

Specimen	L*	a*	b*	ΔE	WI
PLA	85.6	–1.0	8.1	-------	84.4
PZ1	87.8	–1.8	5.9	2.6	86.4
PZ2	91.5	–1.2	5.7	5.4	89.8
PZ3	91.6	–1.3	6.3	5.2	89.4
PZF1	90.6	–1.2	6.1	4.4	88.8
PZF2	91.4	–1.1	6.2	5.1	89.4
PZF90.23	91.8	–0.9	5.3	5.8	90.2

3.3.9 Surface wettability and water vapour permeability

Water contact angle (WCA) measurement was done to measure the surface wettability or surface hydrophobicity of PLA and its nanocomposite films with ZnO and f-ZnO. Generally hydrophobic surface showed higher water contact angle as compared to hydrophilic one. The results are shown in Fig. 3.11a and b. Surface wettability of materials depend on various factors such as surface roughness, chemical affinity (polar/non-polar) etc. The contact angle θ = 65° represents the limiting value between hydrophobic (θ > 65°) and hydrophilic surface (θ < 65°). With incorporation of ZnO and f-ZnO into PLA matrix, WCA increases as similar with several reported biopolymer/ZnO nanocomposites in literature (Kanmani & Rhim, 2014; Lizundia et al., 2016).

WCA obtained for PLA, PZ1, PZ2, PZ3, PZF1, PZF2 and PZF3 are 65.4 ± 1.2, 70.6 ± 1.1, 71.44 ± 0.9, 74.8 ± 1.0, 77.6 ± 1.2, 79.2 ± 1.1 and 85.8 ± 1.2 respectively. The nanocomposite films incorporated with f-ZnO has higher WCA values as compared to unmodified ZnO. These may be due to better compatibility and good interfacial interaction between PLA and functionalized ZnO.

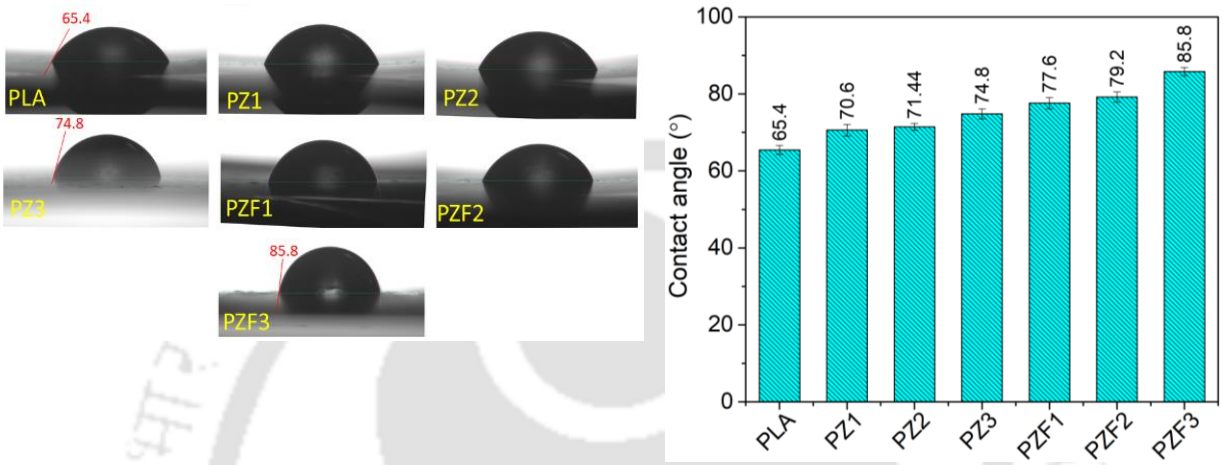

(a) (b)

Fig. 3.11. (a) and (b) water contact angle of PLA/ZnO nanocomposites

The water vapor permeability (WVP) of the PLA, and their nanocomposite films were displayed in Table 3.6. The results revealed that the addition of ZnO and f-ZnO into PLA decreased the WVP of the nanocomposite films. The improved water vapor barrier property is mainly due to the presence of nanoparticles ZnO and f-ZnO which create a tortuous path for the diffusion of water molecules in nanocomposite films. The pristine PLA film showed highest WVP ($8.5 \pm 1.2 \times 10^{-11}$ g/m s Pa) as compared to all nanocomposite films. Kanmani et al. 2014 (Kanmani & Rhim, 2014) also found lower WVP of the nanocomposite films of agar/ZnO (1.92 to 1.73×10^{-9} g/m s Pa) carrageenan/ZnO (1.89 to 1.71 $\times 10^{-9}$ g/m s Pa) and CMC/ZnO (2.23 to 1.86×10^{-9} g/m s Pa) as compared to their pristine polymer.

Table 3.6. Water vapor permeability of PLA based nanocomposite

Specimen	Thickness (mm)	WVP (g/m s Pa)×10^{-11}
PLA	0.285±0.007	8.5±1.2
PZ1	0.315±0.004	7.4±0.9
PZ2	0.320±0.006	6.3±1.1
PZ3	0.333±0.005	6.0±0.8
PZF1	0.314±0.003	5.3±0.7
PZF2	0.322±0.005	4.1±0.8
PZF3	0.337±0.007	3.1±0.9

3.3.10 Antimicrobial properties

The antimicrobial activity of the prepared film was tested against two food-borne bacteria *E. coli* and *L. monocytogenes* by using total viable cell count method. The results are shown in Fig. 3.12 and Fig. 3.13. Results revealed that neat PLA film did not possesses any antimicrobial activity against both *E. coli* and *L. monocytogenes*. However, the nanocomposite films exhibited significant antimicrobial activity against both the bacteria. It was also observed that the antimicrobial activity is dependent on type of bacteria, concentration of ZnO and f-ZnO. The results indicated that nanocomposite films were more active towards Gram negative *E. coli* as compared to Gram positive *L. monocytogenes.* These may be due to difference in cell wall structure of the Gram-negative and Gram-positive positive bacteria. In case of *E. Coli* significant decline in growth of bacteria was observed after 6 h of incubation period. Highest antimicrobial activity was observed for PZF3 sample. The *L. monocytogenes* count increased up to 12 h of incubation, after that the bacterial growth was declined. Surface functionalization will reduce the agglomeration of nanoparticles and hence thereby facilitates the intimate contact of *E. coli* and *L. monocytogenes* with f-ZnO. Therefore, the nanocomposite films with functionalized ZnO showed better antimicrobial results as compared to nanocomposite films with unmodified ZnO.

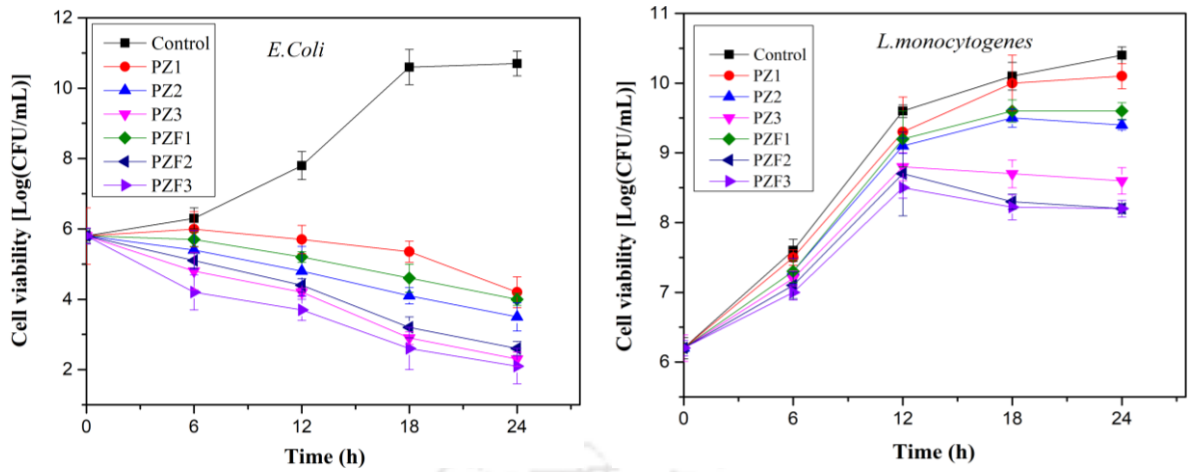

(a) (b)

Fig. 3.12. Antibacterial activity of nanocomposite films against (a) *E. Coli*, (b) *L. Monocytogenes*

Bacterial Strain	Control	PZ3	PZF3
E. Coli	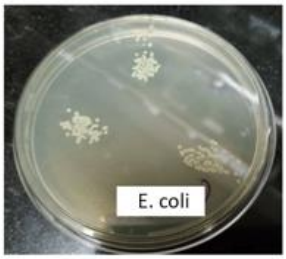	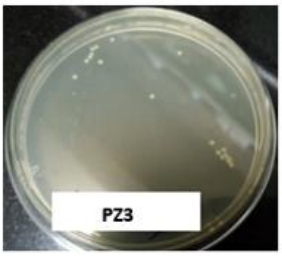	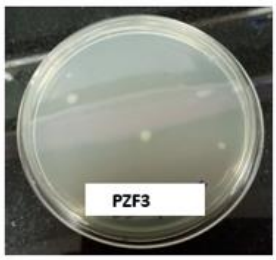
L. monocytogenes		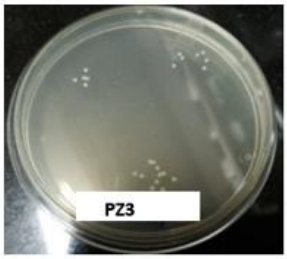	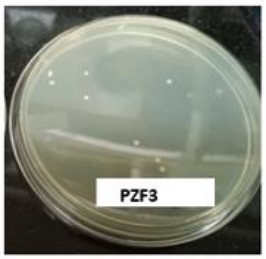

Fig. 3.13. Comparison of bacterial colonies for Gram -negative (*E. Coli*) and Gram- positive (*L. monocytogenes*) in PZ3 and PZF3.

The probable mechanism for antimicrobial activity of ZnO nanoparticles is already explained elsewhere (Chapter 2, Section 2.3.2.4). As shown in Fig. 3.14, mainly two mechanisms are involved: (a) chemical interactions and (b) physical interactions of bacterial cells with ZnO nanoparticles. Chemical interactions include, generation of reactive oxygen species (ROS), release of Zn^{2+} ions and generation of photo induced H_2O_2. Among which most likely mechanism

seems to be generation of ROS in the culture media. The ROS disrupted the DNA and protein synthesis of the bacterial cell, causing bacteriostatic effects toward *E. coli* and *L. monocytogenes*. ZnO nanomaterials possess surface defects, rough edges and corners. This can cause abrasive effects on the microbial cells leading to mechanical damage. Strong electrostatic attraction between bacterial cells and ZnO nanoparticles causes accumulation of the ZnO nanoparticles on outer surface of plasma membrane. Both UV illumination and surface modification involve the alteration of surface properties, which may have a considerable impact on antibacterial activity (Gudkov et al., 2021; Shi et al., 2014; Sirelkhatim et al., 2015).

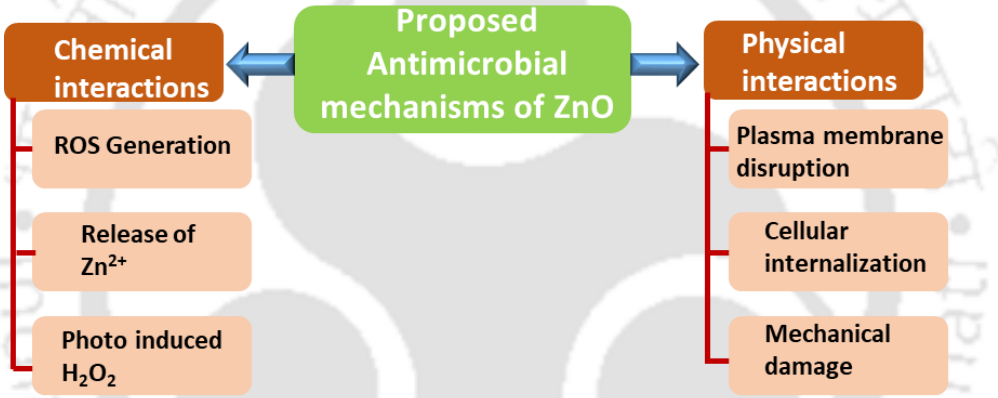

Fig. 3.14. Proposed mechanism for antimicrobial activity of ZnO nanoparticles

3.4 Conclusions

On one side, according to the literature, ZnO and Zn compounds are known to catalyze "unzipping" depolymerisation of PLA. On the other side, this work demonstrates that it is possible to obtain competitive nanocomposites using synthesized ZnO nanofillers and PLA, particularly when polyester/nanofillers interface is adequately tuned, that is, via surface treatment with silane coupling agent. To study the effect of ZnO and f-ZnO on PLA properties, up to 3 wt% of surface-treated or untreated ZnO are incorporated in PLA matrix by using solvent casting method. The study revealed that addition of untreated ZnO to PLA leads to some loss of the thermomechanical

performances. This decrease in properties, in direct correlation with the nanofillers loading is, mainly ascribed to the decrease in PLA molecular weights. Contrary to the untreated nanofillers, surface treated ZnO by (3-aminopropyl trimethoxysilane) is leading to nanocomposites characterized by noticeable thermomechanical performances (e.g. tensile strength in the interval 49 to 53 MPa), whereas good dispersion/distribution of f-ZnO on a nanoscale level was revealed by TEM. The antimicrobial activity test revealed that the nanocomposite films (both ZnO and f-ZnO functionalized) exhibited potent antibacterial activity against food borne pathogenic bacteria *E. Coli* and *L. monocytogenes*. But in compare to unmodified ZnO, surface modified ZnO Showed better antimicrobial properties for both bacterial strains. This may be due to better dispersibility of functionalized ZnO on polymer matrix. It is expected that those findings would open new insights in the use of naturally-available materials for the development of eco-friendly disposable packaging materials.

References

Ahangaran, F., & Navarchian, A. H. (2020). Recent advances in chemical surface modification of metal oxide nanoparticles with silane coupling agents: A review. *Advances in Colloid and Interface Science*, *286*, 102298. https://doi.org/10.1016/j.cis.2020.102298

Ekrami, M., Emam-Djomeh, Z., Joolaei-Ahranjani, P., Mahmoodi, S., & Khaleghi, S. (2021). Eco-friendly UV protective bionanocomposite based on Salep-mucilage/flower-like ZnO nanostructures to control photo-oxidation of kilka fish oil. *International Journal of Biological Macromolecules*, *168*, 591–600. https://doi.org/10.1016/j.ijbiomac.2020.12.013

Ghosh, T., Teramoto, Y., & Katiyar, V. (2019). Influence of Nontoxic Magnetic Cellulose Nanofibers on Chitosan Based Edible Nanocoating: A Candidate for Improved Mechanical, Thermal, Optical, and Texture Properties. *Journal of Agricultural and Food Chemistry*, *67*(15), 4289–4299. https://doi.org/10.1021/acs.jafc.8b05905

Gudkov, S. V., Burmistrov, D. E., Serov, D. A., Rebezov, M. B., Semenova, A. A., & Lisitsyn, A. B. (2021). A Mini Review of Antibacterial Properties of ZnO Nanoparticles. *Frontiers in Physics*, *9*. https://www.frontiersin.org/articles/10.3389/fphy.2021.641481

Hang, T. T. X., Dung, N. T., Truc, T. A., Duong, N. T., Van Truoc, B., Vu, P. G., Hoang, T., Thanh, D. T. M., & Olivier, M.-G. (2015). Effect of silane modified nano ZnO on UV degradation of polyurethane coatings. *Progress in Organic Coatings*, *79*, 68–74. https://doi.org/10.1016/j.porgcoat.2014.11.008

Hari, K. D., Garcia, C. V., Shin, G.-H., & Kim, J.-T. (2021). Improvement of the UV Barrier and Antibacterial Properties of Crosslinked Pectin/Zinc Oxide Bionanocomposite Films. *Polymers*, *13*(15), Article 15. https://doi.org/10.3390/polym13152403

Kalska-Szostko, B., Rogowska, M., & Satuła, D. (2013). Organophosphorous functionalization of magnetite nanoparticles. *Colloids and Surfaces B: Biointerfaces*, *111*, 656–662. https://doi.org/10.1016/j.colsurfb.2013.07.004

Kango, S., Kalia, S., Celli, A., Njuguna, J., Habibi, Y., & Kumar, R. (2013). Surface modification of inorganic nanoparticles for development of organic–inorganic nanocomposites—A review. *Progress in Polymer Science*, *38*(8), 1232–1261. https://doi.org/10.1016/j.progpolymsci.2013.02.003

Kanmani, P., & Rhim, J.-W. (2014). Properties and characterization of bionanocomposite films prepared with various biopolymers and ZnO nanoparticles. *Carbohydrate Polymers*, *106*, 190–199. https://doi.org/10.1016/j.carbpol.2014.02.007

Kim, I., Viswanathan, K., Kasi, G., Sadeghi, K., Thanakkasaranee, S., & Seo, J. (2019). Poly(Lactic Acid)/ZnO Bionanocomposite Films with Positively Charged ZnO as Potential Antimicrobial Food Packaging Materials. *Polymers*, *11*(9), Article 9. https://doi.org/10.3390/polym11091427

Lizundia, E., Ruiz-Rubio, L., Vilas, J. L., & León, L. M. (2016). Poly(l-lactide)/zno nanocomposites as efficient UV-shielding coatings for packaging applications. *Journal of Applied Polymer Science*, *133*(2). https://doi.org/10.1002/app.42426

Ma, S., Shi, L., Feng, X., Yu, W., & Lu, B. (2008). Graft modification of ZnO nanoparticles with silane coupling agent KH570 in mixed solvent. *Journal of Shanghai University (English Edition)*, *12*(3), 278–282. https://doi.org/10.1007/s11741-008-0316-1

Maghsoudlou, M. A., Barbaz Isfahani, R., Saber-Samandari, S., & Sadighi, M. (2019). Effect of interphase, curvature and agglomeration of SWCNTs on mechanical properties of polymer-based nanocomposites: Experimental and numerical investigations. *Composites Part B: Engineering*, *175*, 107119. https://doi.org/10.1016/j.compositesb.2019.107119

Mallakpour, S., & Madani, M. (2015). A review of current coupling agents for modification of metal oxide nanoparticles. *Progress in Organic Coatings*, *86*, 194–207. https://doi.org/10.1016/j.porgcoat.2015.05.023

Mohapatra, S., & Pramanik, P. (2009). Synthesis and stability of functionalized iron oxide nanoparticles using organophosphorus coupling agents. *Colloids and Surfaces A:*

Physicochemical and Engineering Aspects, *339*(1), 35–42. https://doi.org/10.1016/j.colsurfa.2009.01.009

Murariu, M., Doumbia, A., Bonnaud, L., Dechief, A., Paint, Y., Ferreira, M., Campagne, C., Devaux, E., & Dubois, P. (2011). High-Performance Polylactide/ZnO Nanocomposites Designed for Films and Fibers with Special End-Use Properties. *Biomacromolecules*, *12*(5), 1762–1771. https://doi.org/10.1021/bm2001445

Pandimurugan, R., & Thambidurai, S. (2017). UV protection and antibacterial properties of seaweed capped ZnO nanoparticles coated cotton fabrics. *International Journal of Biological Macromolecules*, *105*, 788–795. https://doi.org/10.1016/j.ijbiomac.2017.07.097

Quiñones, R., Rodriguez, K., & Iuliucci, R. J. (2014). Investigation of phosphonic acid surface modifications on zinc oxide nanoparticles under ambient conditions. *Thin Solid Films*, *565*, 155–164. https://doi.org/10.1016/j.tsf.2014.06.057

Rong, M. Z., Zhang, M. Q., & Ruan, W. H. (2006). Surface modification of nanoscale fillers for improving properties of polymer nanocomposites: A review. *Materials Science and Technology*, *22*(7), 787–796. https://doi.org/10.1179/174328406X101247

Samavini, R., Sandaruwan, C., De Silva, M., Priyadarshana, G., Kottegoda, N., & Karunaratne, V. (2018). Effect of Citric Acid Surface Modification on Solubility of Hydroxyapatite Nanoparticles. *Journal of Agricultural and Food Chemistry*, *66*(13), 3330–3337. https://doi.org/10.1021/acs.jafc.7b05544

Shankar, S., Wang, L.-F., & Rhim, J.-W. (2018). Incorporation of zinc oxide nanoparticles improved the mechanical, water vapor barrier, UV-light barrier, and antibacterial properties of PLA-based nanocomposite films. *Materials Science and Engineering: C*, *93*, 289–298. https://doi.org/10.1016/j.msec.2018.08.002

Shi, L.-E., Li, Z.-H., Zheng, W., Zhao, Y.-F., Jin, Y.-F., & Tang, Z.-X. (2014). Synthesis, antibacterial activity, antibacterial mechanism and food applications of ZnO

nanoparticles: A review. *Food Additives & Contaminants: Part A*, *31*(2), 173–186. https://doi.org/10.1080/19440049.2013.865147

Sirelkhatim, A., Mahmud, S., Seeni, A., Kaus, N. H. M., Ann, L. C., Bakhori, S. K. M., Hasan, H., & Mohamad, D. (2015). Review on Zinc Oxide Nanoparticles: Antibacterial Activity and Toxicity Mechanism. *Nano-Micro Letters*, *7*(3), 219–242. https://doi.org/10.1007/s40820-015-0040-x

Zare, Y., Rhee, K. Y., & Hui, D. (2017). Influences of nanoparticles aggregation/agglomeration on the interfacial/interphase and tensile properties of nanocomposites. *Composites Part B: Engineering*, *122*, 41–46. https://doi.org/10.1016/j.compositesb.2017.04.008

CHAPTER 4

Antimicrobial bionanocomposites of poly(lactic acid)/ZnO deposited halloysite nanotubes for potential food packaging applications

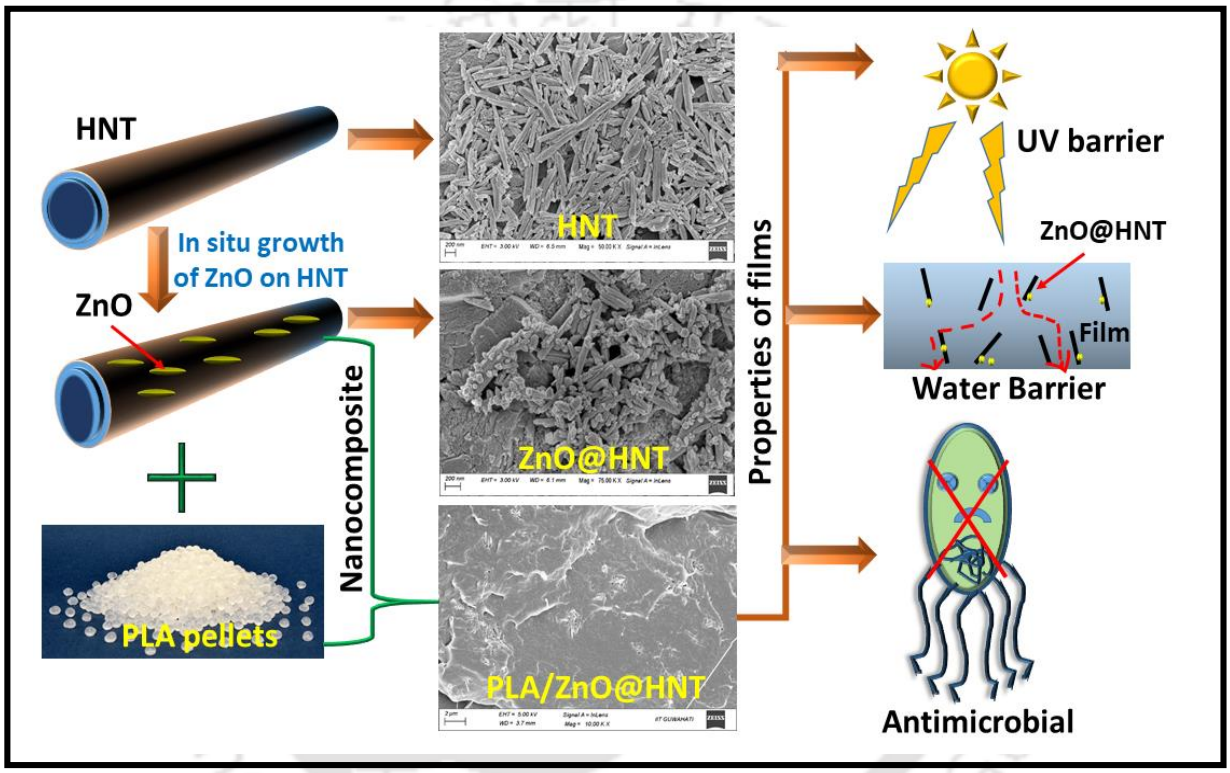

Research output

***U. Boro**, V. S. Moholkar, Antimicrobial Bionanocomposites of Poly (lactic acid)/ZnO Deposited Halloysite Nanotubes for Potential Food Packaging Applications. **Materials Today Communications**, (2022) 104787. https://doi.org/10.1016/j.mtcomm.2022.104787*

4.1 Introduction

In current years, biopolymer based food packaging material has gained much importance as a possible solution to replace the fossil fuel-based synthetic food packaging material (Ciannamea et al., 2018; Yanat & Schroën, 2021). Among different biopolymers, poly(lactic acid) (PLA) is the most widely used material in food packaging applications. This may be due to its high transparency, ease of processability, biocompatibility, easy availability, non-toxic nature and comparable physical properties with that of synthetic polymers such as polypropylene and polyethylene etc. Moreover, PLA is classified as GRAS (Generally Recognized as Safe) material by the US FDA (United State Food and Drug Administration). However, PLA has some limitations such as brittleness, high vapor and gas permeability, which restrict its utilization for food packaging material. Therefore, the development of multifunctional active films of PLA with improved thermo-mechanical and barrier properties, in addition to UV-active and antimicrobial activities is essential (Collazo-Bigliardi et al., 2019; Demchenko et al., 2022; Yu et al., 2021). In this regard, the development of bionanocomposites is most pertinent issue. Bionanocomposite is a material which consists of two phases, viz. a continuous phase or matrix (biopolymer) and a dispersing phase or nanofiller (size < 100 nm). The improvement in functional properties of bionanocomposites can be achieved by formation of good interfacial interaction and hydrogen bonding between nanofillers and matrix (Taherimehr et al., 2021). Previous literature reports use of various nanofillers such as nanoclays (Oliver-Ortega et al., 2021), cellulose nanocrystals (Faraj et al., 2021), silica nanoparticles (Chen et al., 2021), graphene oxides (Ahmed et al., 2021) etc. with PLA for the improvement of thermo-mechanical and barrier properties. Similarly, incorporation of some other nanofillers such as ZnO (Liu et al., 2021), TiO_2 (Dong et al., 2021), silver nanoparticles (Sirotkin et al., 2021), lignin nanoparticles (Cavallo et al., 2021) into PLA matrix imparts the resulting nanocomposite antimicrobial and UV-barrier properties.

There are various types of nanoclays (montmorillonite, halloysite nanotubes etc.) available, among which, halloysite nanotubes (HNT) are the most promising in the field of active food packaging due to its non-toxic, low cost and biocompatible nature (Risyon et al., 2020). There are some studies available on nanocomposites of HNT with biobased polymers, viz. chitosan, alginate, starch, gelatin etc. (Akrami-Hasan-Kohal et al., 2020; Meira et al., 2017; Shankar et al., 2018; Xie et al., 2020). But very few studies are available on PLA/HNT nanocomposites for food packaging applications. Tensile strength and elongation at break are the two important parameters, which define the mechanical properties of packaging films. High toughness is required for food packaging films so that it can sustain the stress during transportation and handling of the products. Also barrier properties, viz. water vapor barrier, gas barrier and thermal barrier properties, are desirable properties for food packaging applications. Incorporation of HNT into PLA matrix mainly increases its tensile strength and decreases gas and water vapor permeability. Addition of HNT provides a tortuous path for permeating molecules through the film matrix, thus reducing the permeability of gas and water molecules (Risyon et al., 2020).

The high specific surface area (50–137 $m^2 \cdot g^{-1}$) and unique hollow tubular structure of HNT makes it not only desirable material for sustainable packaging but also a suitable carrier for active components (Barman et al., 2020). Active components, especially antimicrobial agents, can be incorporated into packaging systems for food preservation purpose. The following techniques are used to incorporate active components into HNT: (a) adsorption of active agents onto the external surface of HNT; (b) loading of active agents into HNT lumen; (c) self-grafting on targeted biomolecules. Recently, loading of different antimicrobial agents such as ZnO, TiO_2, silver nanoparticles etc. on the internal surface as well as on the outer surface of HNT nanotubes has gained researchers' interest (Guo et al., 2020). Antimicrobial agents act as an interfacial material between HNT and pathogenic microorganisms, and form a polymer nanocomposite with enhanced antimicrobial activities. In this type of nanocomposites, HNT provides enhanced thermal and mechanical properties and also facilitates prolong release of the antimicrobial agents from the

nanocomposite films. Among different active agents, ZnO nanoparticles possesses promising antimicrobial properties. It is also listed as GRAS material by the US FDA and are effective against different types of microorganisms. Moreover, it also acts as a source of zinc nutrient which encourages the use of ZnO nanoparticles in food packaging applications. Therefore, nano-interfacial decoration of HNT with ZnO can be a fruitful way to get superior thermo-mechanical and antimicrobial activity of biopolymers. Only a few literatures reported deposition of ZnO on HNT for different applications such as phosphate removal (Wei et al., 2021), sunscreening (Aguzzi et al., 2019), photocatalytic activity (Peng et al., 2017) etc., but not much attention has been paid in the use of ZnO decorated HNT in PLA nanocomposites for potential food packaging applications. Lim et al. (2019) have synthesized ZnO treated HNT by using solvent free method. With incorporation of ZnO treated HNT (loading: 3, 5, 7 wt%), PLA nanocomposite films were synthesized by using melt blending method. The effect of accelerated weathering on PLA/ZnO/HNT nanocomposites were studied. The PLA/ZnO/HNT films exhibited less chain scissioning, and discoloration that indicates its superior photo-stability compared to the PLA/HNT nanocomposites (Lim et al., 2019). Silva et al. (2015) synthesized ZnO deposited HNT by using two step solvothermal method and incorporated them (loading: 2.5, 5, 7.5 and 10 mass%) in PLA matrix to synthesize PLA/ZnO-HNT nanocomposites They have found that addition of ZnO-HNT into PLA matrix enhanced the tensile strength (30%) and elastic modulus (65%) of the nanocomposite along with excellent antimicrobial activity against *E. coli* and *S. aureus* (R. T. De Silva et al., 2015).

The present study has dealt with the synthesis and characterization of ZnO deposited halloysite nanotubes (ZnO@HNT) and incorporation of ZnO@HNT into PLA matrix as reinforcing nanofillers for potential antimicrobial food packaging application.

4.2 Materials and methods

4.2.1 Materials

Halloysite nanotubes were purchased from Sigma-Aldrich. Zinc acetate dihydrate and NaOH were obtained from Merck, India. Poly(lactic) acid (Ingeo^{TM} 4032D) was purchased from Natureworks. Poly(lactic) acid pellets were dried at 55℃ for 12 h before use. Chloroform (99.8%) was supplied by Merck Chemical Co., Germany. The microorganisms, *E. coli* and *L. monocytogenes* were kindly supplied by Department of Biosciences and Bioengineering (I.I.T. Guwahati). Nutrient Broth (NB) and Luria Broth (LB) were obtained from HiMedia.

4.2.2 Fabrication of ZnO deposited halloysite nanotubes (ZnO@HNT)

In brief, 0.05 M zinc acetate dihydrate were added in 100 mL of Millipore water. To this solution, 2 g of HNT was added. The solution was sonicated in bath sonicator for 30 min. Now 0.5 M NaOH was added slowly by maintaining the temperature of the solution at 60 °C. The reaction was carried out for 3 h. Finally, a white precipitate was obtained. It was centrifuged and dried at 70 °C for 12 h. As-obtained dried powder was named as ZnO@HNT. For comparison purpose, ZnO was synthesized without adding HNT. The schematic diagram of *in situ* synthesis of ZnO on HNT (ZnO@HNT) is shown in Fig. 4.1.

4.2.3 Synthesis of PLA/ZnO@HNT nanocomposites

PLA/ZnO@HNT and PLA/HNT were synthesized by simple sonication assisted solvent blending technique followed by the methodology as described in elsewhere **(Chapter 2, Section 2.3)**. The nanocomposites synthesized with 1, 2 and 3 wt % of HNT were referred as PH1, PH2 and PH3, respectively, and nanocomposites prepared with 1, 2 and 3 wt% of ZnO@HNT were referred as PZH1, PZH2 and PZH3, respectively.

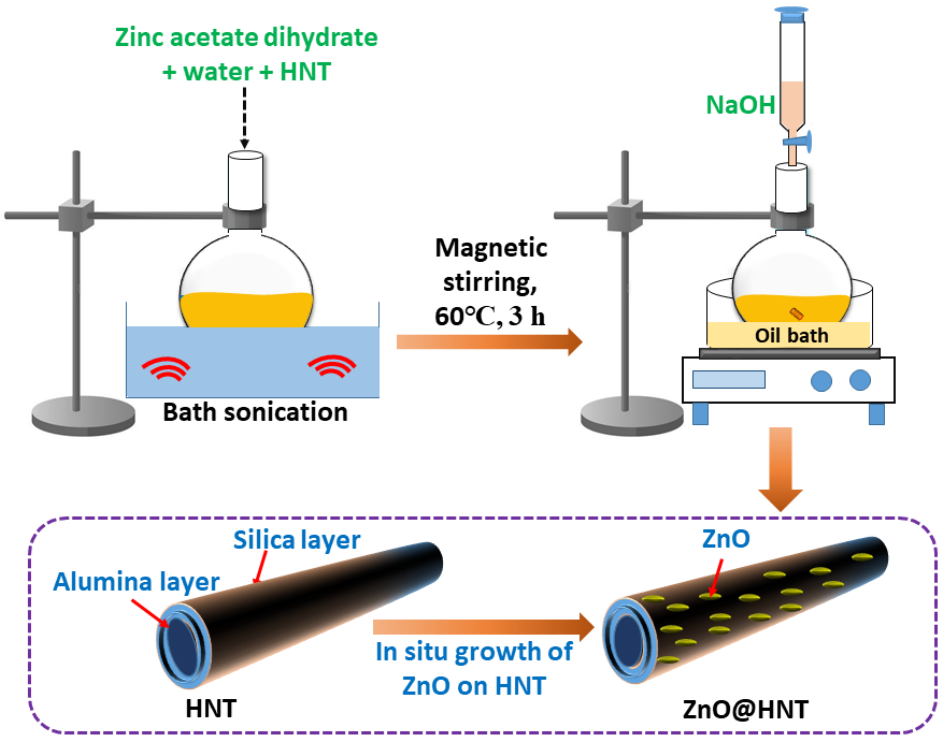

Fig. 4.1. Schematic diagram of in situ synthesis of ZnO on HNT (ZnO@HNT)

4.3 Characterization of ZnO@HNT and its nanocomposite films

(1) FE-SEM and FE-TEM analysis: The surface morphology and internal structure of HNT and ZnO@HNT were examined by using FE-SEM (ZEISS Sigma 300) and FE-TEM analysis (JEOL 2100F), respectively. **(2) BET surface area and XRD analysis:** The specific surface area and the pore size distribution of ZnO, HNT and ZnO@HNT samples were determined by using BET surface area analyzer (Model No.: Tristar II; Make: M/s Micromeritics, USA). X-ray Diffraction analysis was done by using powder X-ray diffractometer (Make: Rigaku Technologies, Japan, Model: Smartlab, $\lambda = 1.5406$ Å) in the range of $10° \leq 2\theta \leq 80°$. **(3) Thermal and mechanical properties:** Thermal stability of PLA/ZnO@HNT nanocomposites was studied by Thermogravimetric (TGA) analysis. It was done by using Differential Scanning Calorimetry/Thermogravimetric (DSC/TGA) analyzer (Make: Netzsch model: STA449F3A00) at heating rate of 10°C min^{-1} (25°C - 600°C) with 10 mL min^{-1} nitrogen flow rate. The Mechanical properties were determined by using 5 kN Electromechanical Universal Testing Machine (Make:

Zwick Roell: Z005TN) following ASTM D-882 at crosshead speed of 10 mm min^{-1}. **(4) UV light barrier properties and surface color parameters:** The UV light barrier properties of PLA/ZnO@HNT nanocomposites were measured using UV-vis spectrophotometer (PerkinElmer, Lambda 35). The film samples were cut into dimension of 25 × 25 mm and placed in the UV cell for spectrum measurement in the wavelength range of 250–800 nm. The UV blocking capacity (%) was measured by using following equation:

$$UV\ blocking\ (\%) = 100 - (\int_a^b T(\lambda)\, d\lambda)/(\int_a^b d\lambda)$$

Where, $T(\lambda)$ = Spectral transmittance of the films, $d\lambda$ = bandwidth, λ = incident wavelength, a, b are the integral upper and lower limit which is basically the absorbance range of UV-B and UV-A.

The surface color of the nanocomposite films was measured by using colorimeter (Datacolor 550, Datacolor Technology Suzhou Co., Ltd., China). Hunter color values, L^* (lightness/darkness), a^* (redness/greenness), b^* (yellowness/blueness) were measured at different five places of film samples. **(5) Surface wettability and Water vapor permeability (WVP) test:** The surface wettability test of the nanocomposite films was carried by using a contact angle goniometer and associated software (Holmarc, HO-IAD-CAM-01B). The water vapor permeability (WVP) test of the polymer samples were done gravimetrically according to the ASTME00996-00 method with some modifications (Bhat et al., 2021; Yadav et al., 2020) as described in elsewhere (Chapter 3, section 3.2.5). (**6) Antimicrobial activity test**: The antimicrobial efficacy of PLA based nanocomposite films was determined against a gram positive bacteria (*Listeria monocytogenes*) and a gram negative bacteria (*Escherichia coli)* by viable colony count technique followed by the same methodology as described in elsewhere (Chapter 3, section 3.2.5).

4.4 Application of PLA/ZnO@HNT nanocomposites on fresh cut apples

4.4.1 Preparation of the packaged samples

To evaluate the effectiveness as a packaging material, PLA/ZnO@HNT nanocomposite films

were used in packaging of cut apples. For the experiment, the defect free apples were purchased from the market complex at I.I.T. Guwahati. First, the apples were washed with distilled water and air dried. The pristine PLA film, PLA/HNT, PLA/ZnO@HNT and commercial poly(ethylene) films were tested for their efficiency for food packaging. The pouches were prepared by heat sealing of nanocomposite films of dimension 100 mm × 75 mm. Cut apples were placed in each pouch and stored at room temperature for 6 days. The apples were taken out from the pouch every day and various properties were measured.

4.4.2 Weight loss

The weight loss of the cut apples during storage was determined by using a digital weighing balance. The initial weight of each of cut apple pieces (M_i) was weighed before wrapping in the nanocomposite films. The samples were stored at room temperature for 6 days. The final weight (M_f) of each sample was determined on each sampling day. The measurements were done with three replicates. The weight loss (%) of the cut apples was calculated as: = $(M_i - M_f) / M_i \times 100$, where M_i = initial weight of cut apples (at day 0), M_f = final weight of cut apples on each sampling day.

4.4.3 Total soluble solids (TSS)

Total soluble solids (TSS) is an important parameter of fruit quality. TSS value affects the taste as it indicates the level of sweetness of the fruit. For the measurement of TSS, the apple juice was extracted using domestic mixer grinder and filtered by using muslin cloth. The TSS of the filtered juice was measured three times using a hand held refractometer (Bombay Scientific ERMA with ATC, range: 0 – 32 °Brix).

4.4.4 Titratable acidity (TA) and pH

Titratable acidity (TA) measures the total acid concentration present in food item (also called as total acidity). The TA was determined by standard titration AOAC (Association of Official Analytical Chemists) method. 2 mL apple juice was taken in a conical flask and was diluted with 20 mL Millipore water. This solution was titrated against 0.1 N NaOH. Titration was repeated

three times for each sample. The results were presented with respect to maleic acid. The pH of the juice was measured using pH meter (Eutech pH 700 Meter).

4.4.5 Firmness

The firmness of cut apples was tested by a penetration test using penetrometer (ACUCAL Fruit Pressure Tester 1–24 kg/cm^2 ACSY3 Penetrometer, India). The measurements were done in triplicates.

4.5 Results and discussion

4.5.1 Characterization of ZnO@HNT

The surface morphology of HNT and ZnO@HNT nanoparticles were characterized by FE-SEM analysis and results are shown in Fig. 4.2. As depicted in Fig. 4.2a and b, HNT consist of cylindrical tubular structure with length up to 1 μm and outer diameter of about 70–80 nm. Fig. 4.2c and d clearly depict the presence of ZnO nanoparticles on HNT surface. The ZnO nanoparticles are ellipsoidal in shape with a length of 200–300 nm and a diameter of about 40–60 nm. In ZnO@HNT composites, HNT retained their cylindrical tubular morphology but the surface became more rough due to presence of ZnO nanomaterial.

FE-TEM image of HNT and ZnO@HNT are shown in Fig. 4.3a and b. These images also suggested the successful formation of ZnO nanoparticles on the surface of HNT nanotubes. The Energy Dispersive X-ray spectroscopy (EDX) spectra and elemental mapping of ZnO@HNT nanocomposites was shown in Fig. 4.4a and b respectively. Both images clearly showed the presence of elemental Zinc (Zn) in ZnO@HNT nanocomposites. According to EDX spectra the weight % of Zn in the nanocomposite is 18.3% and others elements such as O, Si and Al are 48.5, 16.9 and 16.3%, respectively (Fig. 4.4a).

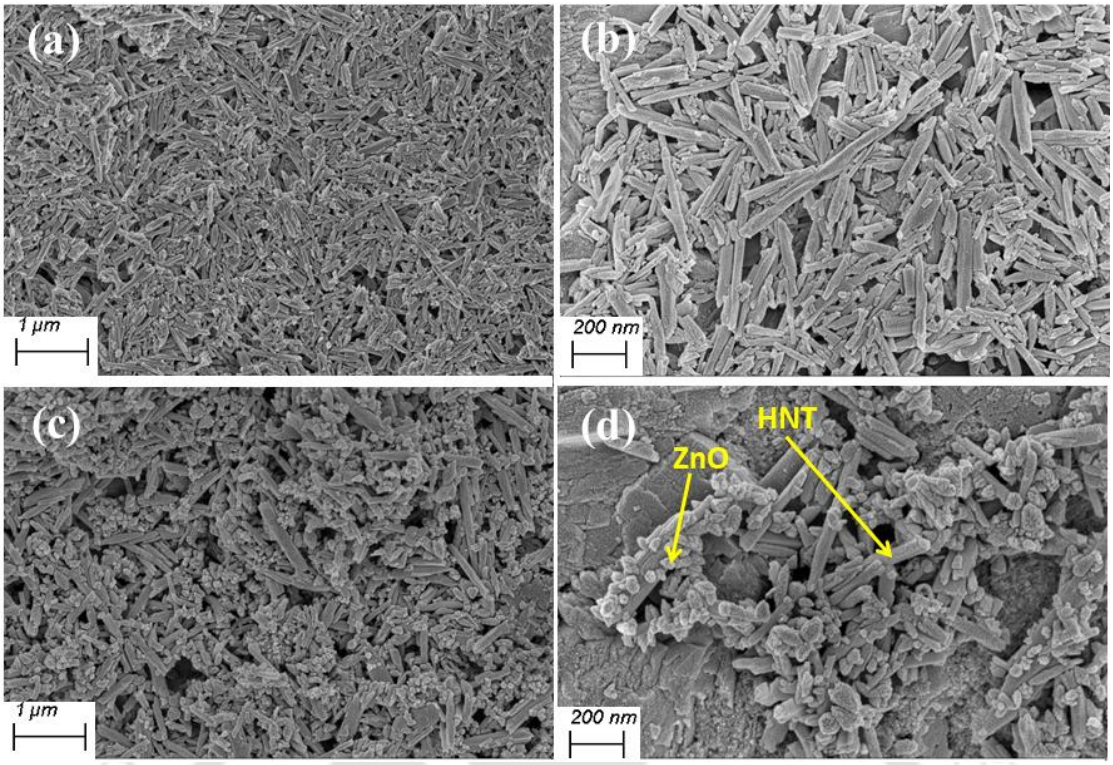

Fig. 4.2. FE-SEM images of (a–b) HNT, and (c–d) ZnO@HNT at magnification of 1 µm and 200 nm

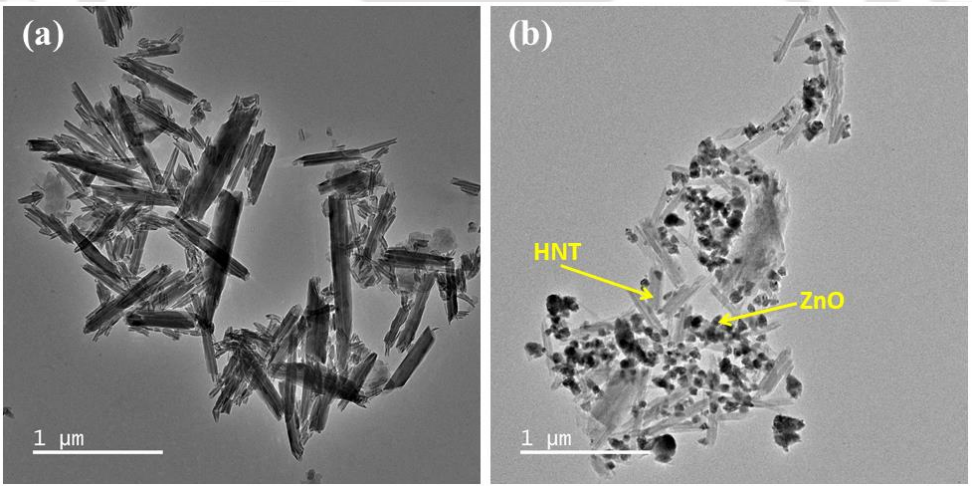

Fig. 4.3. FE-TEM images of (a) HNT, and (b) ZnO@HNT

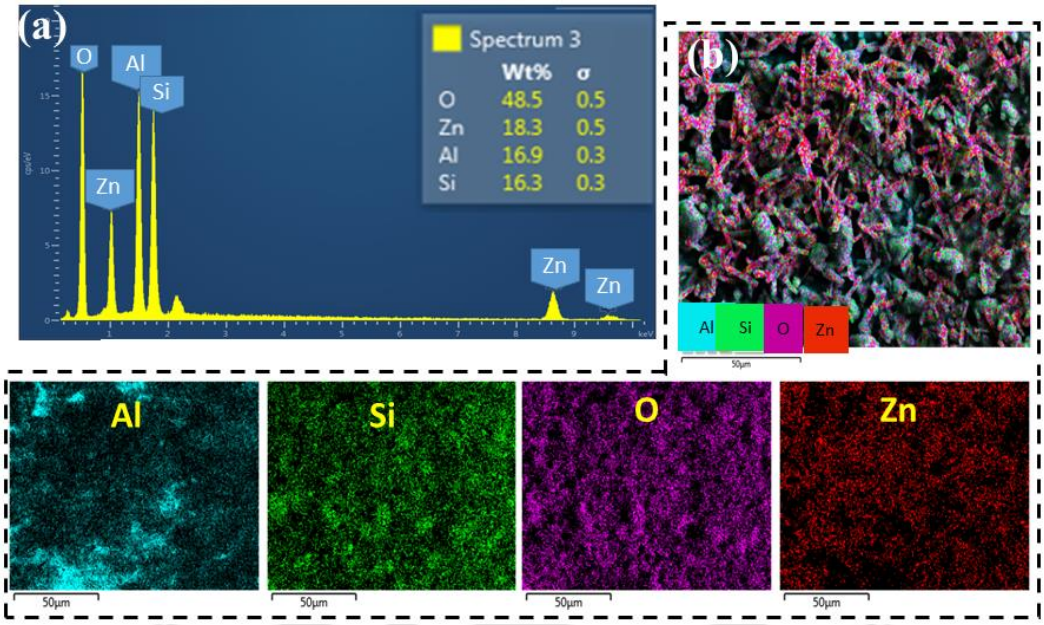

Fig. 4.4. (a) EDX spectra of ZnO@HNT (inset: elemental composition in weight fractions) and (b) elemental mapping of ZnO@HNT (Aluminum in sky blue, Silicon in green, Oxygen in violet, and Zinc in red)

The BET analysis was done to find out the specific surface area, pore size and pore volume of the synthesized materials. Fig. 4.5a shows nitrogen adsorption-desorption isotherms (inset: pore size curves) of HNT and ZnO@HNT. The pristine HNT have surface area of 50.16 ± 0.86 $m^2 g^{-1}$. The deposition of ZnO nanoparticles on HNT (ZnO@HNT) led to decrease in BET surface area, from 50.16 ± 0.86 $m^2 \cdot g^{-1}$ to 30.43 ± 0.77 $m^2 \cdot g^{-1}$, with a reduction in the total pore volume, from 0.25 ± 0.02 cm^3/g for HNT to 0.23 ± 0.01 cm^3/g for ZnO@HNT. The presence of ZnO on the surface of HNT covered the pores of HNT which reduces the adsorption of nitrogen. Reduction in surface area of HNT by the presence of ZnO nanoparticles are also reported elsewhere (De Silva R. T. et al. 2015; Wei et al. 2021). According to IUPAC (The International Union of Pure and Applied Chemistry)-classification, the nitrogen adsorption–desorption isotherms of HNT and ZnO@HNT are type IV isotherms featuring H3 hysteresis loops. This type of isotherm is a typical one of mesoporous structures. Table 4.1 shows the BET surface area, pore volume and pore size of ZnO, HNT and ZnO@HNT.

Table 4.1. BET surface area, pore volume and pore size of ZnO, HNT and ZnO@HNT

Nanomaterials	S_{BET} (m^2 g^{-1}) [a]	Pore volume (cm^3 g^{-1}) [b]	Pore size (nm) [c]
ZnO	17.97± 1.01	0.07± 0.01	15.61± 0.97
HNT	50.16± 0.86	0.25± 0.02	20.24± 0.96
ZnO@HNT	30.43± 0.77	0.23± 0.01	30.93± 0.96

Values are represented as mean ± standard deviation, [a] BET surface area. [b] Single point adsorption total pore volume of pores less than 1,952.438 Å width at p/p° = 0.990. [c] Adsorption average pore diameter (4V/A by BET)

The results of X-ray diffraction (XRD) study of HNT and ZnO@HNT are shown in Fig. 4.5b. In XRD spectra of HNT, the observed diffraction peaks can be indexed to the typical characteristic peaks of HNT (JCPDS card no. 09-0453). The diffraction peaks at 2θ = 11.8° (*d* = 7.49 Å), 19.9° (*d* = 4.45 Å) and 24.7° (*d* = 3.60 Å) (marked as ■ in Fig. 4.5b) are attributed to the crystal orientations of (0 0 1), (0 2 0) and (0 0 2), respectively. The XRD peak at 2θ = 11.8° depicts the basal spacing of 7.5 Å, which reflects the dehydrated form of HNT (Aguzzi et al., 2019) [24]. As shown in Fig. 4.5b, apart from the typical XRD peaks of HNT, ZnO@HNT exhibits the diffraction peaks of ZnO at 2θ = 31.7° (*d* = 2.82 Å), 34.4° (*d* = 2.60 Å), 36.2° (*d* = 2.47 Å), 47.5° (*d* = 1.91 Å), and 68.0° (*d* = 1.37 Å) (marked as ● in Fig. 4.5b), which are attributed to the crystallographic orientations of (1 0 0), (0 0 2), (1 0 1), (1 0 2), (1 1 0), (1 0 3) and (1 1 2), respectively. The XRD results suggested successful crystallization of ZnO on the surface of HNT.

Table 4.2. TGA results of ZnO, HNT and ZnO@HNT

Specimen	$T_{5\%}$ (°C)	$T_{10\%}$ (°C)	T_{max} (°C)	Ash content @ 600°C (%)
ZnO	–	–	–	1.5
ZnO@HNT	438	479	474	15
HNT	312	474	470	20

[**Note**: Degradation temperature for 5%, 10% and maximum weight loss (from DTG curve) are represented by- $T_{5\%}$, $T_{10\%}$ and $T_{max\%}$ respectively]

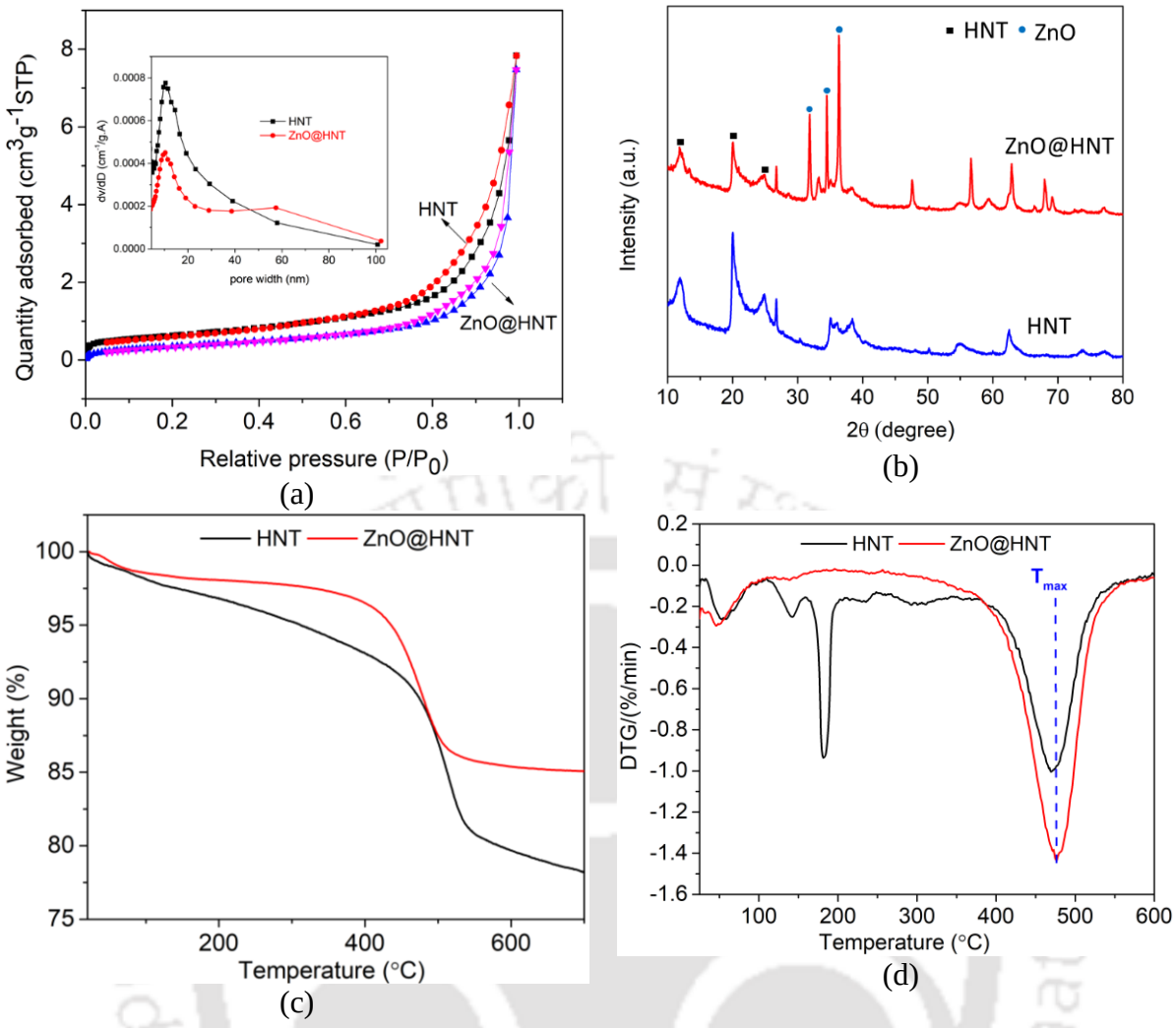

Fig. 4.5. (a) Nitrogen adsorption–desorption isotherms (inset: pore size curves), (b) XRD spectra, (c) TGA, and (d) DTG curves of HNT and ZnO@HNT

TGA and Derivative Thermogravimetric (DTG) curves of HNT and ZnO@HNT are shown in Fig. 4.5c and d. The HNT showed two step degradation process. The first stage of degradation occurred at 100–290 °C with weight loss of 4.6% (at 290°C). This weight loss occurred was due to the removal of interlayer trapped water and adsorbed water present on the surface of HNT. The second step of degradation occurred at 400–600 °C with weight loss of 20.4% (at 600°C). This weight loss was mainly due to the dehydroxylation (loss of hydroxyl groups attached to the intralayer cations) of Al–OH groups of HNT (Hu et al., 2020; Lim et al., 2019). The weight loss of ZnO@HNT decreased due to the formation of ZnO nanoparticles on HNT. The

maximum decomposition temperatures, T_{max} (obtained from DTG curve), of HNT and ZnO@HNT are 470 °C and 474°C, respectively, which clearly revealed the better thermal stability of ZnO@HNT over pristine HNT. The degradation temperatures of 5% ($T_{5\%}$), 10% ($T_{10\%}$), maximum weight loss (T_{max}), and the final residual ash content at 600°C are given in Table 4.2.

4.6 Characterization and properties evaluation of PLA/HNT and PLA/ZnO@HNT nanocomposites

4.6.1 FE-SEM study

Fig. 4.6 shows the FE-SEM images of PLA and PLA/ZnO@HNT nanocomposite films. As expected, PLA film possessed a smooth surface (Fig. 4.6a); while, the incorporation of ZnO@HNT in PLA matrix made the surface rough. High agglomeration of nanofiller, ZnO@HNT was observed at relatively high loading of 3 wt% (Fig. 4.6d). It is well known that increasing the nanofiller loading caused agglomeration due to its high surface area. For PZH2, we observed good dispersion of nanofiller with very less agglomeration (Fig. 4.6c).

4.6.2 XRD study

XRD spectra of PLA, PH3 (3 wt% of HNT), and PZH3 (3 wt% of ZnO@HNT) are shown in Fig. 4.7. All three samples possessed a strong diffraction peak at $2\theta = 16.5°$, which is assigned for PLA. The diffraction peaks at $2\theta = 24.6°$, 31.7°, 34.4° and 36.2° are ascribed to the characteristics peak of HNT and ZnO. Presence of characteristics peaks of both HNT and ZnO in the X-ray diffractogram of PLA-based nanocomposite films confirms the successful formation of PLA/HNT and PLA/ZnO@HNT nanocomposites. The XRD spectra of nanocomposite films also revealed their crystalline nature.

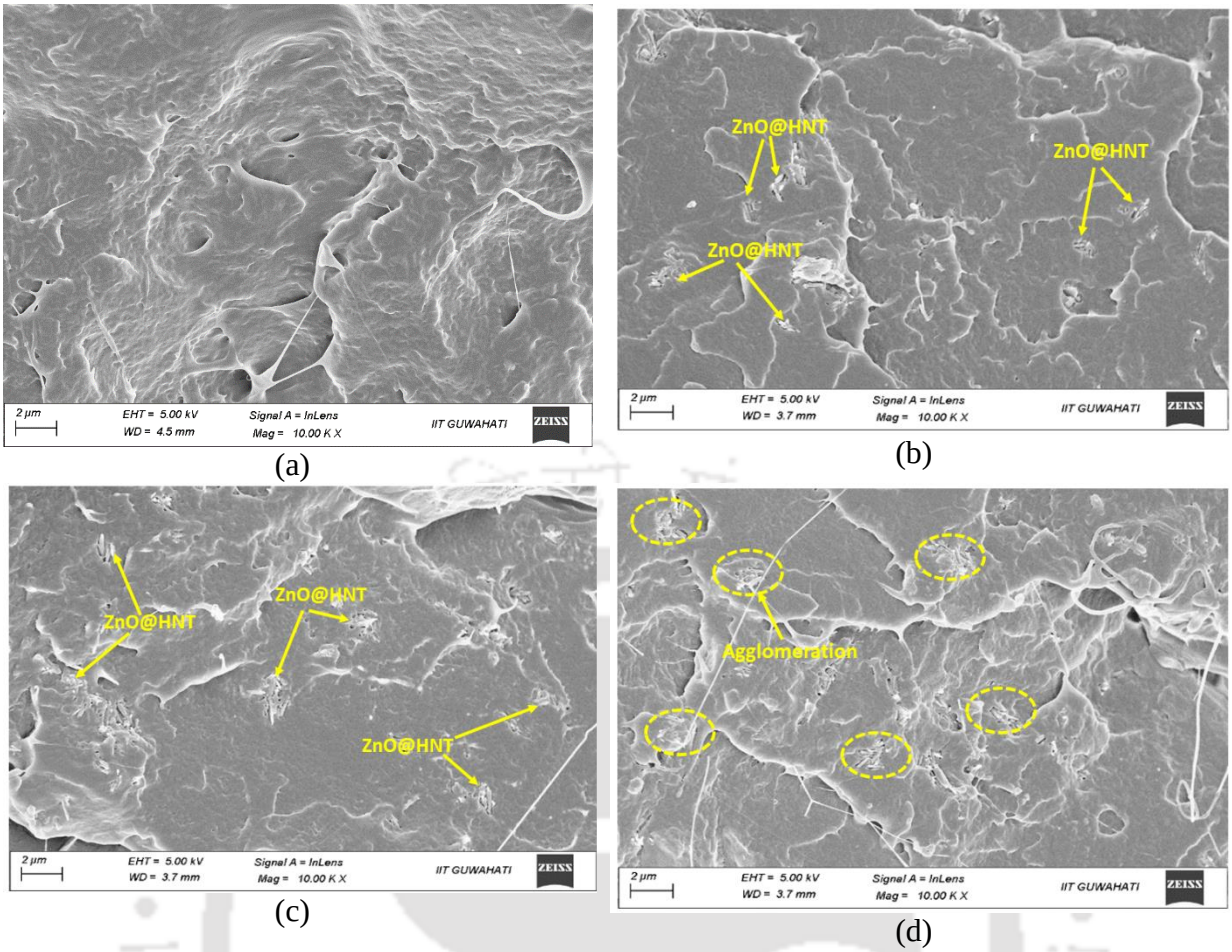

Fig. 4.6. FE-SEM images of (a) PLA, (b) PZH1, (c) PZH2, and (d) PZH3

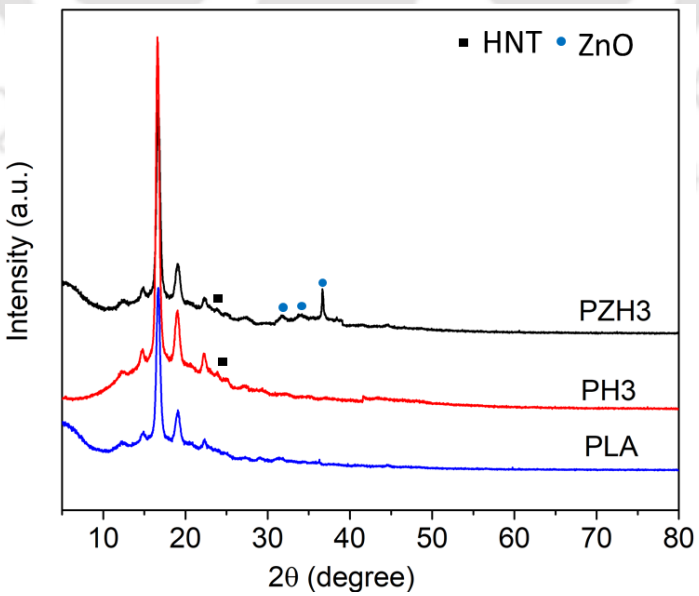

Fig. 4.7. XRD spectra of PLA, PH3 and PZH3 nanocomposites

4.6.3 Surface wettability and water vapor permeability (WVP)

The surface wettability is an important parameter of food packaging materials. The function of packaging material is to protect foods from external environment such as humidity during handling, transportation and storage. Surface wettability or water absorption capacity of nanocomposite films were determined by measuring water contact angle on the surface. The results are shown in Fig. 4.8a. The contact angle θ° = 65 represents the limiting value between hydrophobic (θ° > 65°) and hydrophilic surface (θ° < 65°) (Pal & Katiyar, 2017). Surface wettability of a material depends on its surface morphology, roughness and chemical affinity etc. Mainly, chemical affinity (polar/nonpolar) and surface roughness plays an important role. As observed in Fig. 4.8a, all film samples possess contact angle higher than 65°, which indicates its poor affinity towards water and highlighting their suitability as food packaging material. The pure PLA has water contact angle of 65.4°, which is similar with the values reported in the literature (Arrieta et al., 2014). Incorporation of HNT and ZnO@HNT in PLA significantly enhanced the water contact angle of PH3 (3 wt% of HNT) and PZH3 (3 wt% of ZnO@HNT) by ~6.4% and ~20.5%, respectively. The HNT contains a polar Si – OH group on its surface. Addition of 1 wt% of HNT (PH1) into PLA matrix tends to slightly decrease the contact angle (PLA: 65.4° to PH1: 64.0°). The presence of hydrophilic groups (Al–OH and Si–OH) in the structure of HNT increase the surface energy of nanocomposite films. Therefore, the contact angle of nanocomposite film decreases which concurs with previous literature on polymer–nanoclays composites (Nizar et al., 2018). By increasing the loading of HNT to 2 wt% (PH2) and 3 wt% (PH3), the contact angle slightly increases to 68.4° and 69.6°, respectively, which may be due to increase in surface roughness of the nanocomposite films. As a result, the interfacial tension between water and nanocomposite films reduces, which in turn reduces the surface energy of the material and enhances its hydrophobicity (R. De Silva et al., 2014).

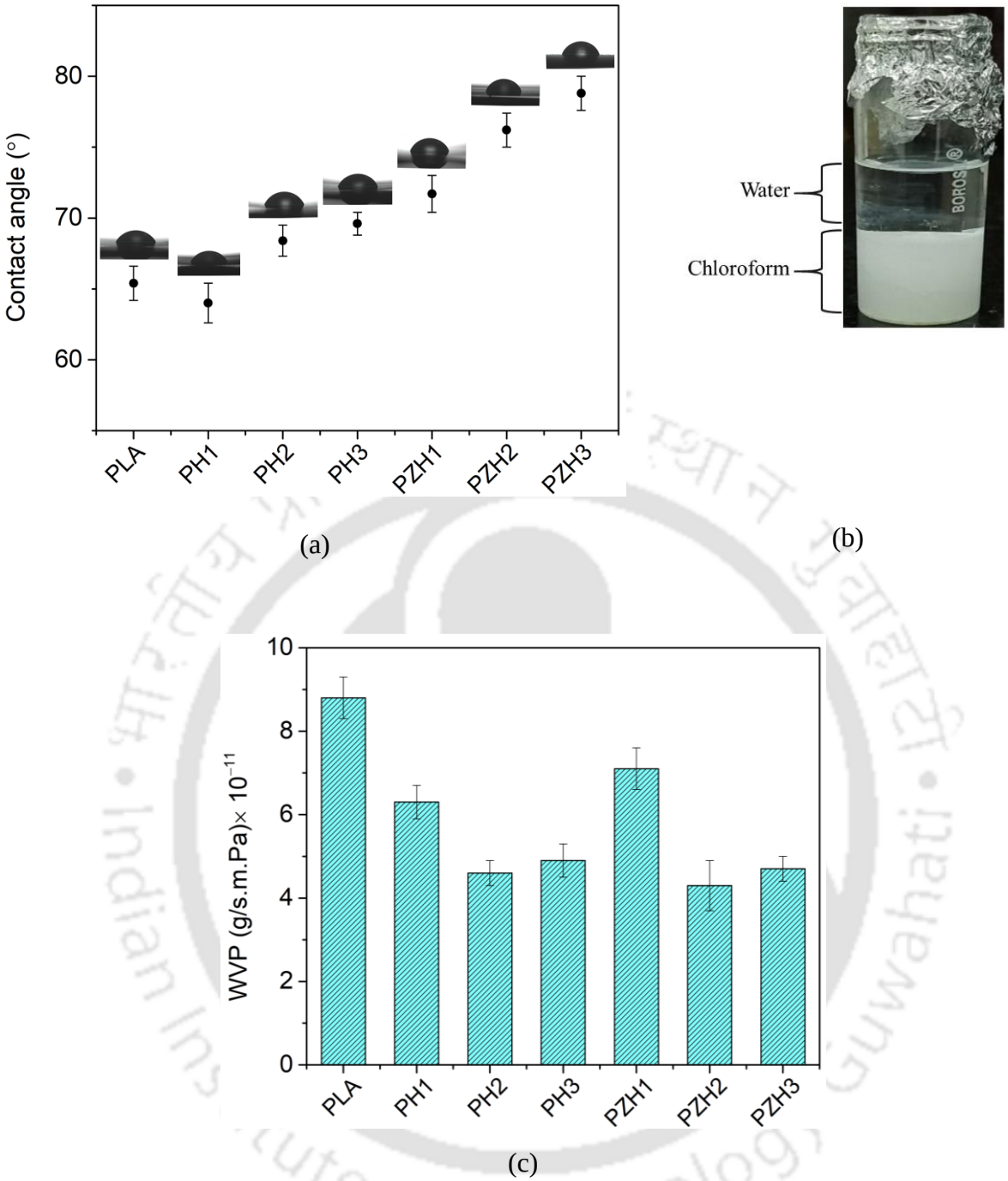

Fig. 4.8. (a) Water contact angle of nanocomposites films; (b) Dispersion of ZnO in a chloroform/water binary system; and (c) WVP of nanocomposite films

In case of PLA/ZnO@HNT nanocomposites, the water contact angles obtained for 1, 2 and 3 wt% of ZnO@HNT are 71.7°, 76.2° and 78.8°, respectively. It is observed that the water contact angle increased with increasing ZnO@HNT loading from 1 wt% to 3 wt%, which indicates rise in hydrophobicity of the nanocomposite films. ZnO nanoparticles possess two types of dominant

surfaces: polar (0 0 0 1) and non-polar (1 0 1 0), (1 1 2 0) surfaces. Polar surfaces are either zinc terminated, (0 0 0 1)-Zn, or oxygen terminated, (0 0 0 1)-O. The (1 0 1 0) planes consist of equivalent Zn^{2+} and O^{2-} ions at the same planes, signifying non-polar planes having the lowest surface energy (Boro et al., 2022). In this study, ZnO nanoparticles were well dispersed in chloroform phase (Fig. 4.8b), as compared to water, which signifies the non-polar surface and hydrophobic nature of ZnO. Moreover, higher loading of ZnO@HNT increases the surface roughness, and hence, the contact angle increases. Also, water vapor permeability (WVP) decreases (Fig. 4.8c) as the concentration of HNT and ZnO@HNT increases from 1 wt% to 3 wt% in PLA matrix. The WVPs of PLA, PH1, PH2, PH3, PZH1, PZH2 and PZH3 are 8.8×10^{-11}, 6.3×10^{-11}, 4.6×10^{-11}, 4.9×10^{-11}, 7.1×10^{-11}, 4.3×10^{-11}, 4.7×10^{-11} g. s^{-1} m^{-1} Pa^{-1}, respectively. The increase in water vapor barrier properties of the nanocomposite film as compared to pristine PLA is mainly due to the tortuous path for diffusion of water vapor due to the dispersion of HNT and ZnO@HNT in the PLA matrix.

4.6.4 UV-barrier properties

The UV-barrier properties in food packaging material are desirable to protect the food products from degradation upon exposure to UV light. Some components in food such as lipids, proteins and fats undergo oxidation with exposure to light, and thereby, reduce the shelf life of food. Therefore, the reduction in the transmittance value of the packaging material can be beneficial for the food packaging application. The transmittance value of the synthesized nanocomposite films is shown in Fig. 4.9a. The result revealed that pure PLA showed transmittance value of more than 90% in visible range (400–800 nm). The addition of HNT in PLA matrix decreases the transmittance value specially in UV region (200–400 nm) which signifies the enhancement of UV-barrier properties of the films. The presence of nanoparticles HNT and ZnO@HNT in polymer matrix might diffract/block the UV-visible light, which reduces the transmittance. Moreover, the inherent UV-shielding capacity of ZnO possesses also contributes to UV barrier

property of PLA based nanocomposites. The transmittances of PLA, PH1, PH2, PH3, PZH1, PZH2 and PZH3 at 600 nm are 95.1, 84.5, 80.5, 82.7, 72.6, 67.5 and 67.7%, respectively. The UV blocking capacity (%) and transmittance (%) at two representative wavelengths in UV region, viz. UV-B (300 nm) and UV-A (360 nm), are shown in Fig. 4.9b. It can be observed that transmittance values of PLA, PH1, PH2, PH3, PZH1, PZH2 and PZH3 at 300 nm are 62.2, 41,9, 30.7, 35.4, 8.8, 3.9 and 6.8%, respectively. The transmittance values of PLA, PH1, PH2, PH3, PZH1, PZH2 and PZH3 at 360 nm are 85.4, 75.4, 71.4, 74.5, 10.8, 4.0 and 8.0, respectively. It can be seen that in both wavelengths the transmittance value is lower in PLA/ZnO@HNT nanocomposites than PLA/HNT nanocomposites. On the other hand, the UV blocking capacity is higher in both nanocomposites than pure PLA, which signifies their UV barrier properties. The homogeneous dispersion and the strong interfacial interaction of nanofiller with PLA matrix is an important criterion to get optimum UV-shielding properties. It was reported that the presence of ZnO nanoparticles on HNT surface effectively improved the dispersion of ZnO by avoiding agglomeration.

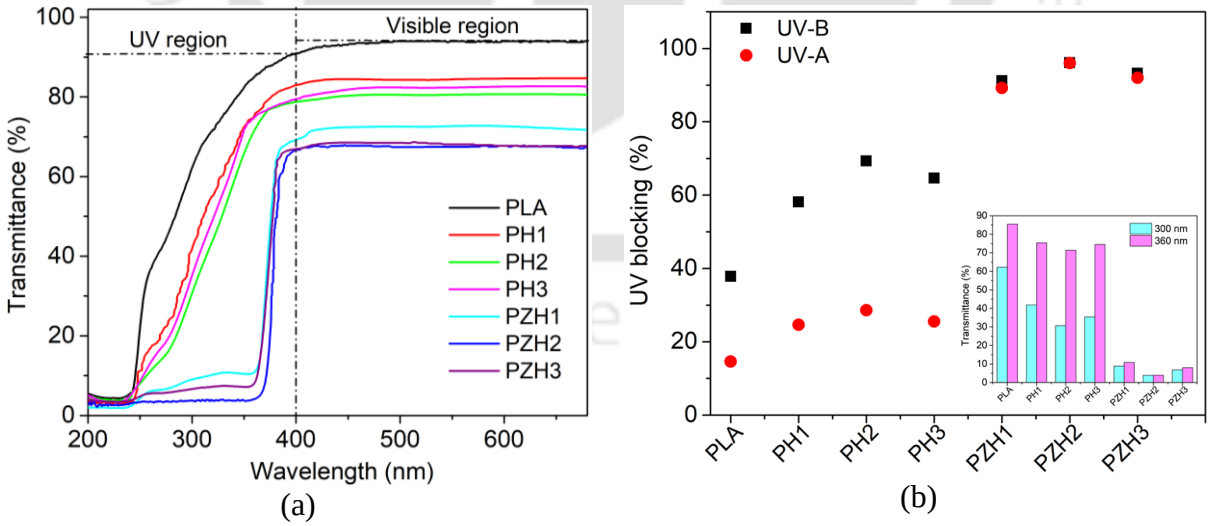

Fig. 4.9. (a) UV-visible spectra, and (b) UV blocking efficiency of PLA based nanocomposites

Table 4.3. Surface color of PLA/HNT and PLA/ZnO@HNT nanocomposites

Specimen	L*	a*	b*	Chroma	Hue (°)
PLA	86.94	–0.91	8.72	8.77	96.05
PH1	85.73	–0.97	8.51	8.56	96.15
PH2	86.04	–1.05	7.83	7.90	97.79
PH3	86.15	–1.06	7.78	7.85	97.82
PZH1	87.90	–0.99	8.44	8.50	96.78
PZH2	88.29	–1.18	7.73	7.82	98.79
PZH3	88.39	–1.56	7.11	7.27	102.52

The color factors are greatly affected by the incorporation of filler materials in the polymer matrix. The surface colors of pristine PLA and nanocomposite films are shown in Table 4.3. The observed *L* value of neat PLA film is ~86.94, which reduced to 85.73, 86.04, 86.15 for PH1, PH2, PH3, respectively. This result indicates that the nanocomposites of PLA/HNT were darker than pristine PLA. Also these nanocomposites have lower *a** and *b** values than PLA that indicate green and blue coloration effect. On the other hand, incorporation of ZnO@HNT in PLA increased *L** values to 87.90, 88.29 and 88.39 for PZH1, PZH2 and PZH3, respectively. These results indicate that the nanocomposite films are brighter than pure PLA. Here also, the nanocomposite films have lower *a** and *b** values than PLA that represent green and blue coloration effect. The *a** values vary inversely with amounts of filler materials, and impart green coloration effect to the films. Similarly, the *b** value for neat PLA film is ~8.72, which reduced to 8.44, 7.73 and 7.11 for PZH1, PZH2, and PZH3, respectively. This variation indicates reduction in yellow coloration of nanocomposite films as compared to pristine PLA. The hue angle indicates the dominant color of the material. The hue angle of 90° indicates yellow coloration effect. Pristine PLA have hue angle of 96.05° which shows rise in all nanocomposites. The hue angles of PH1, PH2, PH3, PZH1, PZH2 and PZH3 are 96.15°, 97.79°, 97.82°, 96.78°, 98.79° and 102.52°, respectively. Chroma refers to the intensity/strength of the color or degree of saturation of a particular hue. The chroma of PLA is 8.77 that reduces to 8.56, 7.90, 7.85, 8.50, 7.82 and 7.37 for PH1, PH2, PH3, PZH1, PZH2 and PZH3, respectively.

4.6.5 Thermal properties

Thermal properties of pristine PLA, PLA/HNT and PLA/ZnO@HNT bionanocomposites were studied by using TGA analysis. The results are shown in Figs. 4.10a, and Table 4.4. The TGA thermographs revealed two step thermal degradation process of the polymer films. The first step of degradation occurs at around 74–160 ℃, and is attributed to removal of water and volatile components from the samples. The second step of degradation occurs at around 315°–370 ℃. The weight loss in this temperature range is due to chemical debonding/degradation of PLA chains. Risyon et al. (2020) also reported second step degradation temperature in the range of 330° – 350℃ (Risyon et al., 2020). Table 4.4 shows $T_{10\%}$, $T_{50\%}$, $T_{max\%}$ and ash content (%) of all nanocomposite films. The TGA thermographs revealed that presence of HNT decreases the thermal stability of PLA. This might be due to presence of Brønsted acid sites (Al–OH and Si–OH) on the surface of HNT. It provides a catalytic role for degradation of PLA chains. The pristine PLA, PH1, PH2, and PH3 showed $T_{10\%}$ at 323.2, 306.5, 286.3 and 277.4℃, respectively, while nanocomposites of ZnO@HNT with PLA had $T_{10\%}$ values of 240.5, 240.6, 241℃ for PZH1, PZH2 and PZH3, respectively. Maximum degradation temperature $T_{max\%}$ was obtained from DTG curve (Fig. 4.10b).

Table 4.4. Thermal properties of PLA, PLA/HNT and PLA/ZnO@HNT based nanocomposites

Specimen	$T_{10\%}$ (℃)	$T_{50\%}$ (℃)	T_{max} (℃)	Ash content (%) @ 500℃
PLA	323.2	357.3	362.6	1.05
PH1	306.5	343.5	351.5	0.97
PH2	286.3	330.6	342.5	1.52
PH3	277.4	315.6	323.2	2.34
PZH1	240.5	279.9	288.5	0.65
PZH2	240.6	278.0	286.9	1.87
PZH3	241	276.7	285.4	3.35

[**Note**: Degradation temperature for 10%, 50 % and, maximum weight loss (from DTG curve) are represented by- $T_{10\%}$, $T_{50\%}$ and $T_{max\%}$, respectively]

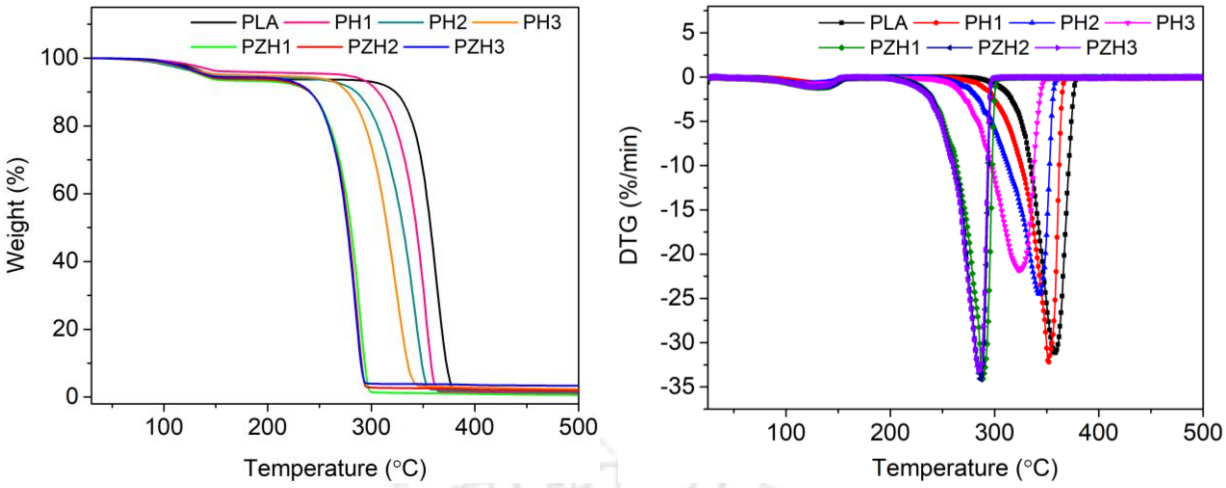

(a) (b)

Fig. 4.10. (a) TGA and (b) DTG curves of PLA and PLA based nanocomposite films

4.6.6 Mechanical Properties

The mechanical properties (tensile strength, elastic modulus and elongation at break) of pristine PLA and PLA based nanocomposites are depicted in Fig. 4.11 and Table 4.5. The stress vs strain curve is shown in Fig. 4.11a. Incorporation of HNT and ZnO@HNT into PLA matrix results in significant enhancement in tensile strength (Fig. 4.11b). The tensile strengths of PLA, PH1, PH2, PH3, PZH1, PZH2 and PZH3 are 26.5, 40.8, 41.9, 38.1, 34.7, 36.8 and 32.7 MPa, respectively. The addition of ZnO@HNT into PLA matrix causes enhancement in tensile strength, where the highest value is obtained for PZH2 (2 wt% of ZnO@HNT). For this composition the enhancement in tensile strength is 58.1%. This may be due to homogeneous dispersion of the ZnO@HNT that results in strong interfacial interaction with PLA. The tubular structure of HNT could also be another reason for enhancement in tensile strength, since tubular shape nanoparticles are more efficient in stress transfer between matrix and filler as compared to spherical particles. The tensile strength of PLA/HNT (PH2 = 41.9 MPa) is higher than PLA/ZnO@HNT (PZH2 = 36.8 MPa). This is plausibly attributed to availability of more hydroxyl and siloxane groups of pristine HNT as compared to ZnO@HNT (BET results also confirm higher surface area of HNT than ZnO@HNT) that boost interfacial interactions with PLA matrix. The tensile strength reduces at higher loading of HNT (PH3) and ZnO@HNT (PZH3). This may be due to agglomeration of

nanoparticles that reduces the interfacial area between HNT / ZnO@HNT and PLA and generates weaker points for crack formation under the application of external force. Incorporation of HNT and ZnO@HNT also improves elastic modulus of the PLA based nanocomposites. The elastic moduli of PLA, PH1, PH2, PH3, PZH1, PZH2 and PZH3 are 0.86, 5.46, 5.50, 5.38, 4.66, 5.24 and 3.00 GPa, respectively. The enhancement in elastic modulus of the nanocomposite films is essentially attributed to strong interfacial interactions that restricted the mobility of the polymer chains and increased the structural rigidity of the PLA matrix. The elongation at break (EB) reduced for PH1, PH2 and PH3 as compared to pristine PLA. The EB values for PLA, PH1, PH2, PH3, PZH1, PZH2 and PZH3 are 2.9, 1.8, 1.4, 1.1, 2.7, 5.2 and 3.6 % respectively. Reduction in the EB values of PH1, PH2 and PH3 is possibly due to addition of HNT nanoparticles. The presence of HNT improves the rigidity of the PLA chains that results in reduction of the EB values. On the other hand, different result is observed for PLA/ZnO@HNT nanocomposites. The EB values increases in case of PZH1, PZH2 and PZH3. This enhancement could be due to lower surface area of ZnO@HNT as compared to HNT. Low surface area of PLA/ZnO@HNT (as compared to PLA/HNT) leads to lower interfacial interactions with PLA matrix, which in turn facilitated more space and free volume for mobility of PLA chains. As a consequence, the EB values are higher for PLA/ZnO@HNT as compared to PLA/HNT and pristine PLA.

Table 4.5. Tensile strength (TS), elastic modulus (EM) and elongation at break (EB) of PLA, and PLA based nanocomposite films containing ZnO@HNT

Specimen	TS (MPa)	EM (MPa)	EB (%)
PLA	26.5	0.86	2.9
PH1	40.8	5.46	1.8
PH2	41.9	5.50	1.4
PH3	38.1	5.38	1.1
PZH1	34.7	4.66	2.7
PZH2	36.8	5.24	5.2
PZH3	32.7	3.01	3.6

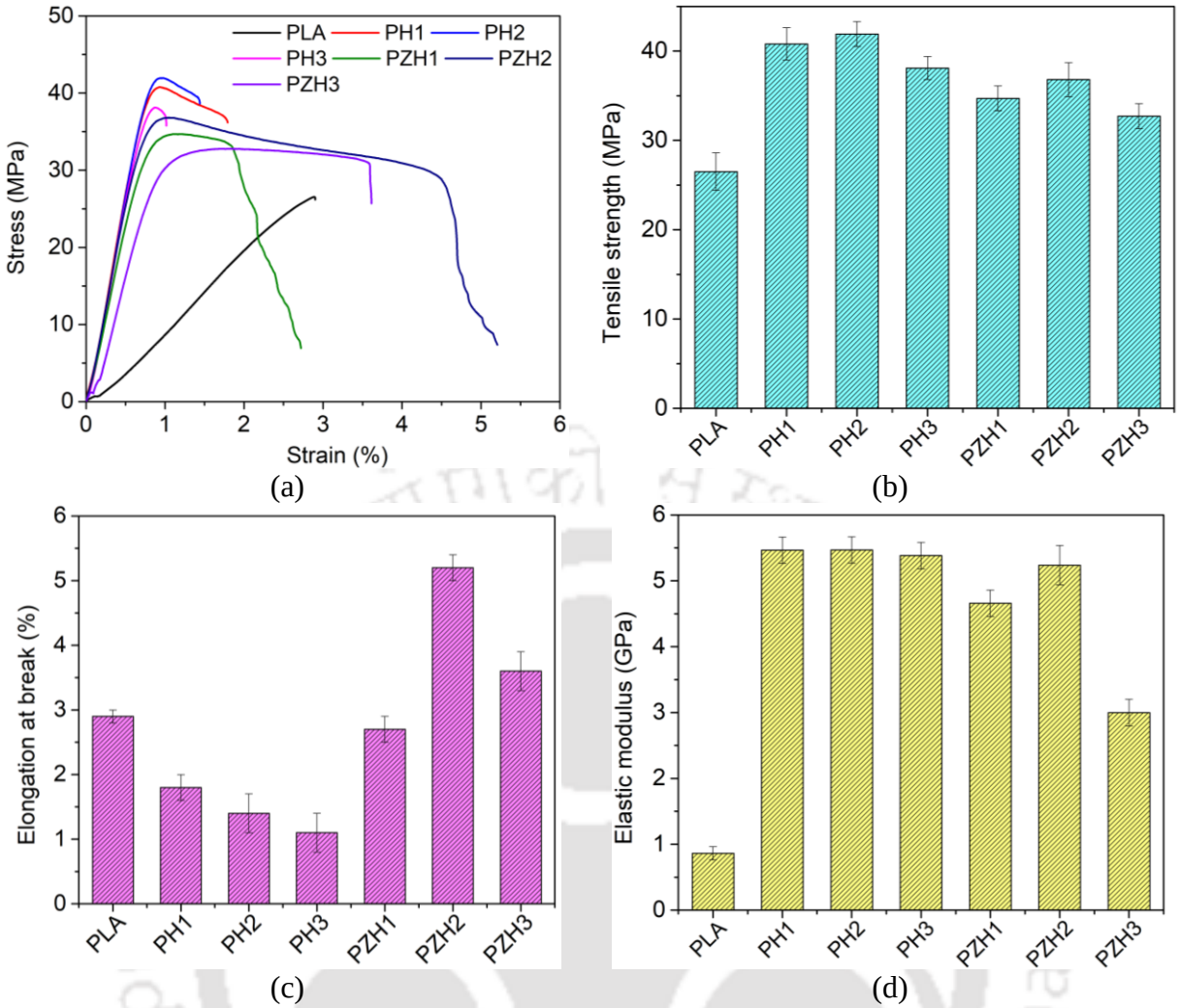

Fig. 4.11. (a) Stress vs strain curve, (b) tensile strength, (c) elongation at break and (d) elastic modulus

4.6.7 Antimicrobial properties

The antimicrobial efficacy of PLA based nanocomposites against two food born bacterial, a gram positive (*Listeria monocytogenes*) and a gram negative (*Escherichia coli*) bacteria is shown in Fig. 4.12a and b, and the percentage reduction (%R) of bacterial colonies are summarized in Table 4.6. The pristine PLA did not possess any antimicrobial activity towards *Escherichia coli* (Fig. 4.12a). During the testing period (0–48 h), the bacterial count obtained for pristine PLA was in the range of 6.1–8.1 log(CFU/mL). The addition of HNT in PLA matrix did not show any antibacterial activity against both *E. coli* and *Listeria monocytogenes*. But the inhibition on bacterial growth

was affected by the presence of ZnO on HNT surface (ZnO@HNT). The incorporation of ZnO@HNT on PLA matrix showed significant antimicrobial efficacy compared to pure PLA films. The nanocomposite films with 2 wt% of ZnO@HNT showed reduction in bacterial count (%R) of *E. coli* by 97% within 24 h of incubation period, and it further reduced to 99% after 48 h. At higher loading of ZnO@HNT (3 wt%), the antimicrobial activity of nanocomposite is more significant. The antimicrobial efficacy of % Reduction = 95% is achieved within just 12 h of incubation period for PZH3. The antimicrobial efficacy of PLA based nanocomposite films against gram positive bacteria *Listeria monocytogenes* is shown in Fig. 4.12b. It was observed that the antimicrobial activity of PLA/ZnO@HNT nanocomposites against *E. coli* is more effective than *Listeria monocytogenes* especially after 12 h of incubation period. For PZH3, % Reduction for *E. coli* and *Listeria monocytogenes* were 95% and 99%, respectively. At higher incubation period (24 and 48 h). the antimicrobial activity against *Listeria monocytogenes* also improved and significant reduction in bacterial colonies (>99%) was observed. As per results, the antimicrobial efficacy of PLA based nanocomposites against *E. coli* and *Listeria monocytogenes* showed the dependency on both incubation period and concentration of ZnO@HNT. Moreover, the different antimicrobial responses of *E. coli* and *Listeria monocytogenes* to PLA/ZnO@HNT nanocomposites are due to the differences in the structural and chemical composition of cell wall. The PLA nanocomposite films with 1, 2 and 3 wt% of HNT (PH1, PH2 and PH3) did not possess any reduction in the bacterial count, which confirms that HNT lacks antimicrobial property. So, the antimicrobial mechanism of the PLA based nanocomposite was solely governed by the presence of ZnO nanoparticles on the surface of HNT. Similar results are reported in previous literature (R. T. De Silva et al., 2015). Various mechanisms have been proposed in the literature for the antimicrobial activity of ZnO. However, the exact mechanism is not known yet. Mainly two mechanisms are involved in antimicrobial activity of ZnO nanomaterials: (i) physical, and (ii) chemical mechanism. Physical mechanism mainly involves plasma membrane disruption in which positively charged ZnO nanoparticles (zeta potential ± 24 mV) induce strong electrostatic force

between ZnO nanomaterials and bacterial cells that could lead in cell membrane damage with intracellular fluid leakage. The chemical mechanism involves: (a) generation of different oxygen species such as superoxide, hydrogen peroxide, OH radicals etc. by photocatalytic effect (when ZnO is exposed to visible and UV light). This species can damage the cell wall by attacking on lipid cell wall, (b) generation of Zn^{2+} ions due to surface leaching of ZnO is also another mechanism for antimicrobial activity (Boro et al., 2022).

Table 4.6. Summary of the antimicrobial properties of PLA nanocomposites

Sample	**% R (t = 12 h)**	**% R (t = 24 h)**	**% R (t = 48 h)**
Escherichia coli			
PLA	–	–	–
PZH1	83.47	94.49	98.64
PZH2	91.79	97.26	98.99
PZH3	95.02	98.50	99.32
Listeria monocytogenes			
PLA	–	–	–
PZH1	99.54	99.92	99.98
PZH2	99.75	99.94	99.99
PZH3	99.81	99.99	99.99

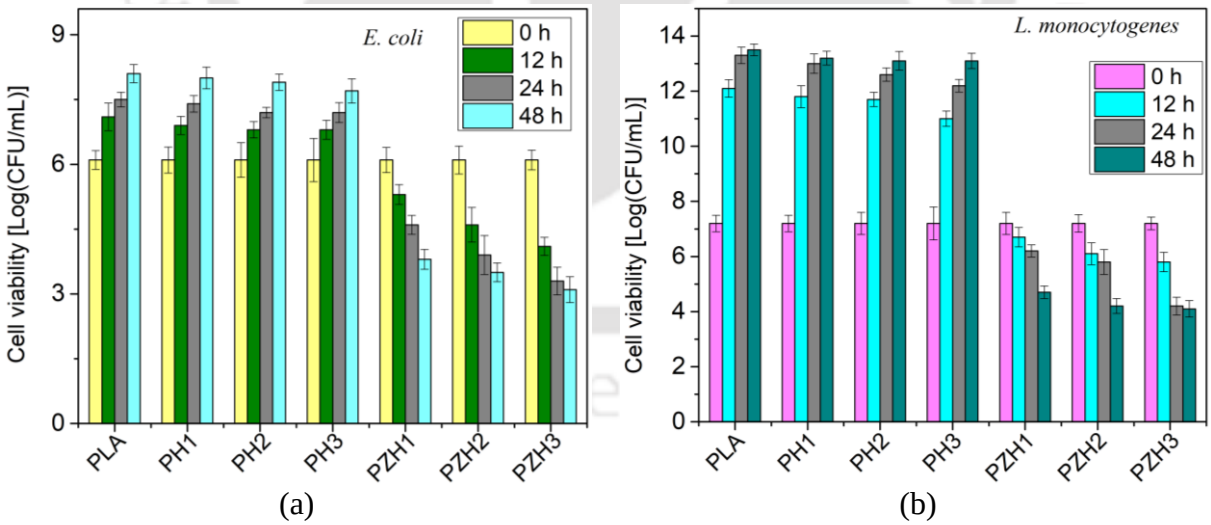

Fig. 4.12. Antimicrobial activity of PLA/HNT and PLA/ZnO@HNT nanocomposites

In the current study, the ZnO@HNT are trapped inside the PLA matrix, and thus, the physical mechanism is not likely to contribute to the antimicrobial activity. Therefore, the possible

chemical mechanism could be the production of different oxidizing species, since the nanocomposite films were exposed with UV light prior to the antimicrobial activity test. More detailed studies are needed in this area to establish exact mechanism of anti-microbial activity of PLA/ZnO@HNT nanocomposites.

4.7 Study of the potential ability of the PLA based nanocomposite films for packaging of fresh cut apples

To study the suitability of the fabricated PLA based nanocomposite films for food packaging purpose, the fresh cut apples were packaged with the polymer films and various properties such as weight loss, total soluble solids, *pH* and fruit firmness were investigated over 6 days of storage period.

4.7.1 Weight loss

During the storage period, the weight loss of fruits and vegetables basically indicates its deterioartion. Weight loss mainly occurs due to post harvest transpiration. Generally, a weight loss > 5% would cause a reduction in the market value of fruits and vegetables (Punia Bangar et al., 2022). The weight losses of cut apples stored in pure PLA, commercial polyethylene (PE) and nanocomposite films are compared in Fig. 4.13a. For all pacakging films, the weight loss of cut apples increased from 0 to 6^{th} day of stoarge period due to the continuous water evaporation from cut apples to the surroundings. The cut apples packaged with PE and pure PLA films showed higher weight loss of 5.5% and 5.6%, respectively up to the 6^{th} day as compared to the nanocomposite films. The PLA film reinforced with HNT and ZnO@HNT significantly lowered the weight loss with concurrent rise in storage period. The weight losses of 4.8%, 4.3%, 4.6%, 4.8%, 4.1% and 4.2% were obtained for PH1, PH2, PH3, PZH1, PZH2 and PZH3, respectively. Among all nanocomposite films, PZH2 exhibited minimum weight loss and preserved the freshness of the cut apples for longer period. The presence of HNT and ZnO@HNT in PLA matrix created a tortuous path and hindered in the transport of gases (O_2, CO_2) and water vapor across the nanocomposite film. Due to the hindrance, water molecules takes longer path for diffusion that

results in reduction in weight loss of cut apples during storage.

4.7.2 Total soluble solids (TSS)

Due to metabolic activity and respiration, the TSS decreased during storage of fruits and vegetables. The decrease in TSS values might be due to degradation of sugars and organic acid consumptions as the main respiratory substrates during storage. The main role of TSS is in fruit flavour, and thus, maintanance of TSS in fruit produce is associated with fulfillment of consumer expectations. The TSS of cut apples stored in PE, PLA, PLA/HNT and PLA/ZnO@HNT nanocomposites for day 0 to 6 at room temperature are shown in Fig. 4.13b. The results revealed that the cut apples packed in PLA/HNT and PLA/ZnO@HNT films retain relatively higher amounts of TSS, as compared to PE and PLA at the end of 6^{th} day of storage. The lowest values of TSS 10.0 and 10.2 °Brix were obtained for fruits packed in PE and PLA respectively, while the highest value of TSS 10.9 °Brix was observed for PZH2.

4.7.3 pH

The pH value of apple juice significantly increased in control experiments (i.e. packaging with PE and PLA) and test experiments (packaging with all nanocomposite films) as depicted in Fig. 4.13c. The initial pH of juice on day 0 for PE and PLA were 3.87, 3.89, respectively, which increased up to 4.08 and 4.09 on day 6. In case of nanocomposite films at 0 day the pH values were 3.90, 3.90, 3.91, 3.93, 3.91, and 3.89, which increased up to 4.02, 4.01, 4.02, 4.01, 4.0 and 4.17 for PH1, PH2, PH3, PZH1, PZH2 and PZH3, respectively on day 6. Variation in the pH depend on metabolic activities and respiration rate of the fruit. The results showed that PZH2 was the most effective packaging film in maintaining the change of pH during storage period. This might be due to the lower respiration rate of cut apples packaged in PZH2, which result into lower metabolic activities. Moreover, incorporation of ZnO@HNT into PLA could probably modify the pattern of fruit respiration by possible interaction of ZnO@HNT with cell membranes, which in turn affect the fruit metabolic pattern and senescence.

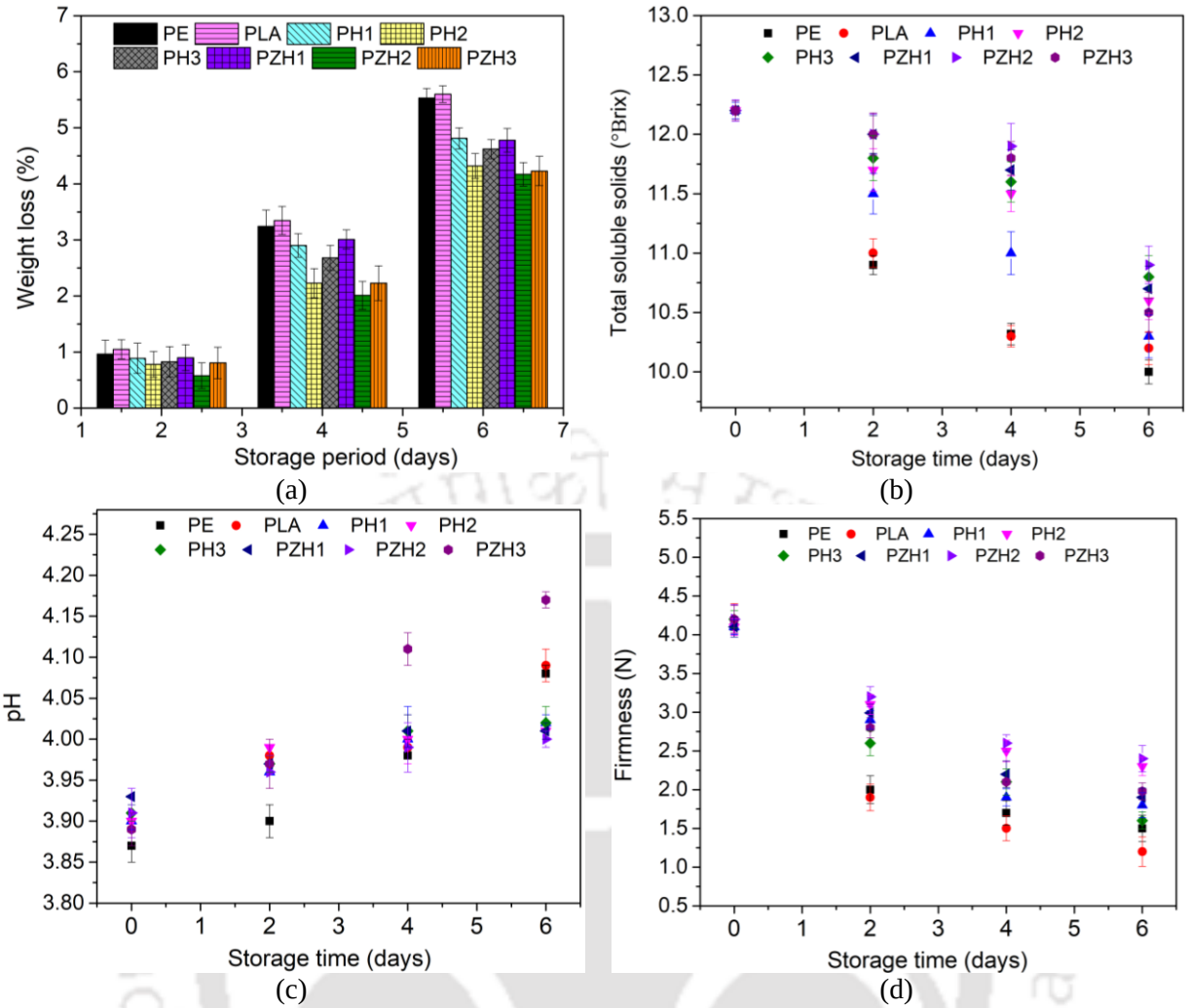

Fig. 4.13. (a) weight loss, (b) total soluble solids, (c) pH and (d) Firmness of cut apples packaged in PLA/ZnO@HNT nanocomposite films at room temperature for 6 days

4.7.4 Fruit firmness

Firmness indicates the crispiness of fruits. It is an important parameter for consumer acceptability of the product. As shown in Fig. 4.13d, the firmness of the cut apples decreases during storage period for all films. The weight loss that occurred during storage period causes reduction in fruit firmness. The changes in firmness (from day 0 to 6) of cut apples stored in packaging films were: 4.1 – 1.5 N (PE), 4.2 – 1.2 N (PLA), 4.1 – 1.8 N (PH1), 4.1 –2.3 N (PH2), 4.2 – 1.6 N (PH3), 4.1 –1.9 N (PZH1), 4.2 –2.4 N (PZH2), and 4.2 – 2.0 N (PZH3). The results revealed that among all films, PZH2 is the most efficient in maintaining the higher value of firmness during storage period. This might be due to homogeneous dispersion of ZnO@HNT (2 wt%) which creates additional

resistance for water vapor diffusion through nanocomposite film, which reduces the moisture loss from fruit. This finding was also supported by the low WVP value of PZH2 as compared to PLA, PE as discussed in earlier section.

4.8 Safety issues and migrations of nanoparticles

Bionanocomposites have high potential to be used in food packaging sector with functional properties that can preserve the food quality and improved the shelf life. However, there are some major concerns regarding the use of nanocomposites when it is used in direct contact with food items. Due to tiny size (< 100 nm) the nanoparticles may migrate from nanocomposite to food items. The high surface area of nanoparticles increases their reactivity and provides a better contact with cell, as well as facilities higher absorption and migration. Nanoclays are categorized as generally recognized as safe (GRAS) material, while organomodified clay viz. octadecylamine and aminopropyltriethoxysilane exhibited toxicity. The U.S. FDA (Food and Drug Administration) and EFSA (European Food Safety Authority) have made guidelines regarding the migration of nanoparticles from packaging materials (He et al., 2014). The nanoclays and ZnO are mainly incorporated into polymer matrix to improve its mechanical and antimicrobial properties. Study revealed that migration of nanoclays are dependent on temperature and contact time (Huang et al., 2015). Echegoyen et al. (2016) have studied the migration of nanoclays into 3% acetic acid and 10% ethanol (Echegoyen et al., 2016). Farhoodi et al. (2014) also studied the migration of Al (aluminum) and silicon (Si) from PET/nanoclays based packaging material into acidic food simulant over a period of 7–90 days (Farhoodi et al., 2014). They have found that migration of Si was 23% higher as compare to migration of Al. Moreover, they also revealed dependency of rate of migration of nanoparticles on storage time and temperature. The ZnO nanoparticles are considered as a biocompatible material with low toxicity as human body requires Zn trace (~10 mg of Zn^{2+} per day is recommended) (Zhang et al., 2013). Although, ZnO nanoparticles provides excellent antimicrobial activity to the packaging materials but the consideration of its migration and toxicity is also an equally important. Six important factors can

be studied regarding the migration of nanoparticles from packaging material to food (Jokar et al., 2017): (1) selection of food simulant, (2) migration rate, (3) how to analyze the trace, (4) mechanism of migration, (5) how to predict migration modeling, and (6) risk of the migration on human health. The migration behavior of nanofillers are still not clear and more studies and investigations are required on exposure, toxicity, and effects of bionanocomposites for the commercial and social acceptance.

4.9 Conclusions

In this study, PLA based nanocomposite films with HNT and ZnO@HNT were synthesized with ultrasound-assisted solution casting method and various functional properties of the films were studied. FE-TEM, FE-SEM and XRD results indicated effective deposition of ZnO nanoparticles on surface of HNT nanotubes, i.e. ZnO@HNT composite nanofiller. The incorporation ZnO@HNT in PLA matrix yielded PLA based nanocomposite films with enhanced surface hydrophobicity, water vapor barrier properties, UV-shielding properties, mechanical properties (mainly tensile strength), and antimicrobial activity. The addition of 2 wt% of ZnO@HNT was found to be the optimum loading that provides maximum toughness to the nanocomposite films in terms of mechanical properties. The addition of HNT to PLA matrix did not show any antibacterial activity against both *E. coli* and *Listeria monocytogenes*. On the other hand, incorporation of ZnO@HNT showed significant antimicrobial efficacy against both type of bacteria. As per results, the antimicrobial efficacy of the nanocomposite film was dependent on incubation period and concentration of ZnO@HNT. The packaging results indicated that storage of cut apples for 6 days inside the pouches prepared from nanocomposites films delayed weight loss and retained firmness of the cut apples. Overall, the incorporation of ZnO@HNT in PLA matrix improves the physio-chemical properties and also imparts antimicrobial properties which enhances the shelf life of the fruit. This study has thus exhibited the suitability of PLA films synthesized with ZnO@HNT for food packaging applications.

References

Aguzzi, C., Donnadio, A., Quaglia, G., Latterini, L., Viseras, C., & Ambrogi, V. (2019). Halloysite-Doped Zinc Oxide for Enhanced Sunscreening Performance. *ACS Applied Nano Materials*, *2*(10), 6575–6584. https://doi.org/10.1021/acsanm.9b01482

Ahmed, J., Mulla, M. Z., Vahora, A., Bher, A., & Auras, R. (2021). Morphological, barrier and thermo-mechanical properties of high-pressure treated polylactide graphene oxide reinforced composite films. *Food Packaging and Shelf Life*, *29*, 100702. https://doi.org/10.1016/j.fpsl.2021.100702

Akrami-Hasan-Kohal, M., Ghorbani, M., Mahmoodzadeh, F., & Nikzad, B. (2020). Development of reinforced aldehyde-modified kappa-carrageenan/gelatin film by incorporation of halloysite nanotubes for biomedical applications. *International Journal of Biological Macromolecules*, *160*, 669–676. https://doi.org/10.1016/j.ijbiomac.2020.05.222

Arrieta, M. P., Castro-López, M. del M., Rayón, E., Barral-Losada, L. F., López-Vilariño, J. M., López, J., & González-Rodríguez, M. V. (2014). Plasticized Poly(lactic acid)–Poly(hydroxybutyrate) (PLA–PHB) Blends Incorporated with Catechin Intended for Active Food-Packaging Applications. *Journal of Agricultural and Food Chemistry*, *62*(41), 10170–10180. https://doi.org/10.1021/jf5029812

Barman, M., Mahmood, S., Augustine, R., Hasan, A., Thomas, S., & Ghosal, K. (2020). Natural halloysite nanotubes /chitosan based bio-nanocomposite for delivering norfloxacin, an anti-microbial agent in sustained release manner. *International Journal of Biological Macromolecules*, *162*, 1849–1861. https://doi.org/10.1016/j.ijbiomac.2020.08.060

Bhat, V. G., Narasagoudr, S. S., Masti, S. P., Chougale, R. B., & Shanbhag, Y. (2021). Hydroxy citric acid cross-linked chitosan/guar gum/poly(vinyl alcohol) active films for food packaging applications. *International Journal of Biological Macromolecules*, *177*, 166–175. https://doi.org/10.1016/j.ijbiomac.2021.02.109

Boro, U., Kashyap, N., & Moholkar, V. S. (2022). Sonochemical Synthesis of Poly(lactic acid) Nanocomposites with ZnO Nanoflowers: Effect of Nanofiller Morphology on Physical Properties. *ACS Engineering Au*, *2*(1), 46–60. https://doi.org/10.1021/acsengineeringau.1c00018

Cavallo, E., He, X., Luzi, F., Dominici, F., Cerrutti, P., Bernal, C., Foresti, M. L., Torre, L., & Puglia, D. (2021). UV Protective, Antioxidant, Antibacterial and Compostable Polylactic Acid Composites Containing Pristine and Chemically Modified Lignin Nanoparticles. *Molecules*, *26*(1), Article 1. https://doi.org/10.3390/molecules26010126

Chen, Y., Han, L., Zhang, H., & Dong, L. (2021). Improvement of the strength and toughness of biodegradable polylactide/silica nanocomposites by uniaxial pre-stretching. *International Journal of Biological Macromolecules*, *190*, 198–205. https://doi.org/10.1016/j.ijbiomac.2021.08.218

Ciannamea, E. M., Castillo, L. A., Barbosa, S. E., & De Angelis, M. G. (2018). Barrier properties and mechanical strength of bio-renewable, heat-sealable films based on gelatin, glycerol and soybean oil for sustainable food packaging. *Reactive and Functional Polymers*, *125*, 29–36. https://doi.org/10.1016/j.reactfunctpolym.2018.02.001

Collazo-Bigliardi, S., Ortega-Toro, R., & Chiralt, A. (2019). Using grafted poly(ε-caprolactone) for the compatibilization of thermoplastic starch-polylactic acid blends. *Reactive and Functional Polymers*, *142*, 25–35. https://doi.org/10.1016/j.reactfunctpolym.2019.05.013

De Silva, R., Pasbakhsh, P., Goh, K., Chai, S.-P., & Chen, J. (2014). Synthesis and characterisation of poly (lactic acid)/halloysite bionanocomposite films. *Journal of Composite Materials*, *48*(30), 3705–3717. https://doi.org/10.1177/0021998313513046

De Silva, R. T., Pasbakhsh, P., Lee, S. M., & Kit, A. Y. (2015). ZnO deposited/encapsulated halloysite–poly (lactic acid) (PLA) nanocomposites for high performance packaging films with improved mechanical and antimicrobial properties. *Applied Clay Science*, *111*, 10–20. https://doi.org/10.1016/j.clay.2015.03.024

Demchenko, V., Kobylinskyi, S., Iurzhenko, M., Riabov, S., Vashchuk, A., Rybalchenko, N., Zahorodnia, S., Naumenko, K., Demchenko, O., Adamus, G., & Kowalczuk, M. (2022). Nanocomposites based on polylactide and silver nanoparticles and their antimicrobial and antiviral applications. *Reactive and Functional Polymers*, *170*, 105096. https://doi.org/10.1016/j.reactfunctpolym.2021.105096

Dong, X., Liang, X., Zhou, Y., Bao, K., Sameen, D. E., Ahmed, S., Dai, J., Qin, W., & Liu, Y. (2021). Preparation of polylactic acid/TiO2/GO nano-fibrous films and their preservation effect on green peppers. *International Journal of Biological Macromolecules*, *177*, 135–148. https://doi.org/10.1016/j.ijbiomac.2021.02.125

Echegoyen, Y., Rodríguez, S., & Nerín, C. (2016). Nanoclay migration from food packaging materials. *Food Additives & Contaminants: Part A*, *33*(3), 530–539. https://doi.org/10.1080/19440049.2015.1136844

Faraj, H., Sollogoub, C., Guinault, A., Gervais, M., Bras, J., Salmi-Mani, H., Roger, P., Le Gars, M., & Domenek, S. (2021). A comparative study of the thermo-mechanical properties of polylactide/cellulose nanocrystal nanocomposites obtained by two surface compatibilization strategies. *Materials Today Communications*, *29*, 102907. https://doi.org/10.1016/j.mtcomm.2021.102907

Farhoodi, M., Mousavi, S. M., Sotudeh-Gharebagh, R., Emam-Djomeh, Z., & Oromiehie, A. (2014). Migration of Aluminum and Silicon from PET/Clay Nanocomposite Bottles into Acidic Food Simulant. *Packaging Technology and Science*, *27*(2), 161–168. https://doi.org/10.1002/pts.2017

Guo, W., Liu, W., Xu, L., Feng, P., Zhang, Y., Yang, W., & Shuai, C. (2020). Halloysite nanotubes loaded with nano silver for the sustained-release of antibacterial polymer nanocomposite scaffolds. *Journal of Materials Science & Technology*, *46*, 237–247. https://doi.org/10.1016/j.jmst.2019.11.019

He, X., Aker, W. G., Leszczynski, J., & Hwang, H.-M. (2014). Using a holistic approach to assess the impact of engineered nanomaterials inducing toxicity in aquatic systems. *Journal of Food and Drug Analysis*, *22*(1), 128–146. https://doi.org/10.1016/j.jfda.2014.01.011

Hu, D., Zhang, Z., Liu, M., Lin, J., Chen, X., & Ma, W. (2020). Multifunctional UV-shielding nanocellulose films modified with halloysite nanotubes-zinc oxide nanohybrid. *Cellulose*, *27*(1), 401–413. https://doi.org/10.1007/s10570-019-02796-0

Huang, J.-Y., Chieng, Y. Y., Li, X., & Zhou, W. (2015). Experimental and Mathematical Assessment of Migration from Multilayer Food Packaging Containing a Novel Clay/Polymer Nanocomposite. *Food and Bioprocess Technology*, *8*(2), 382–393. https://doi.org/10.1007/s11947-014-1408-5

Jokar, M., Pedersen, G. A., & Loeschner, K. (2017). Six open questions about the migration of engineered nano-objects from polymer-based food-contact materials: A review. *Food Additives & Contaminants: Part A*, *34*(3), 434–450. https://doi.org/10.1080/19440049.2016.1271462

Lim, K., Chow, W. S., & Pung, S. Y. (2019). Accelerated Weathering and UV Protection-Ability of Poly(lactic acid) Nanocomposites Containing Zinc Oxide Treated Halloysite Nanotube. *Journal of Polymers and the Environment*, *27*(8), 1746–1759. https://doi.org/10.1007/s10924-019-01464-5

Liu, W., Wang, T., Tao, Y., Ling, Z., Huang, C., Lai, C., & Yong, Q. (2021). Fabrication of anti-bacterial, hydrophobic and UV resistant galactomannan-zinc oxide nanocomposite films. *Polymer*, *215*, 123412. https://doi.org/10.1016/j.polymer.2021.123412

Meira, S. M. M., Zehetmeyer, G., Werner, J. O., & Brandelli, A. (2017). A novel active packaging material based on starch-halloysite nanocomposites incorporating antimicrobial peptides. *Food Hydrocolloids*, *63*, 561–570. https://doi.org/10.1016/j.foodhyd.2016.10.013

Nizar, M. M., Hamzah, M. S. A., Razak, S. I. A., & Nayan, N. H. M. (2018). Thermal Stability and Surface Wettability Studies of Polylactic Acid/Halloysite Nanotube Nanocomposite Scaffold for Tissue Engineering Studies. *IOP Conference Series: Materials Science and Engineering*, *318*, 012006. https://doi.org/10.1088/1757-899X/318/1/012006

Oliver-Ortega, H., Tresserras, J., Julian, F., Alcalà, M., Bala, A., Espinach, F. X., & Méndez, J. A. (2021). Nanocomposites Materials of PLA Reinforced with Nanoclays Using a Masterbatch Technology: A Study of the Mechanical Performance and Its Sustainability. *Polymers*, *13*(13), Article 13. https://doi.org/10.3390/polym13132133

Pal, A. K., & Katiyar, V. (2017). Melt processing of biodegradable poly(lactic acid)/functionalized chitosan nanocomposite films: Mechanical modeling with improved oxygen barrier and thermal properties. *Journal of Polymer Research*, *24*(10), 173. https://doi.org/10.1007/s10965-017-1305-5

Peng, H., Liu, X., Tang, W., & Ma, R. (2017). Facile synthesis and characterization of ZnO nanoparticles grown on halloysite nanotubes for enhanced photocatalytic properties. *Scientific Reports*, *7*(1), Article 1. https://doi.org/10.1038/s41598-017-02501-w

Punia Bangar, S., Whiteside, W. S., Ozogul, F., Dunno, K. D., Cavender, G. A., & Dawson, P. (2022). Development of starch-based films reinforced with cellulosic nanocrystals and essential oil to extend the shelf life of red grapes. *Food Bioscience*, *47*, 101621. https://doi.org/10.1016/j.fbio.2022.101621

Risyon, N. P., Othman, S. H., Basha, R. K., & Talib, R. A. (2020). Characterization of polylactic acid/halloysite nanotubes bionanocomposite films for food packaging. *Food Packaging and Shelf Life*, *23*, 100450. https://doi.org/10.1016/j.fpsl.2019.100450

Shankar, S., Kasapis, S., & Rhim, J.-W. (2018). Alginate-based nanocomposite films reinforced with halloysite nanotubes functionalized by alkali treatment and zinc oxide nanoparticles. *International Journal of Biological Macromolecules*, *118*, 1824–1832. https://doi.org/10.1016/j.ijbiomac.2018.07.026

Sirotkin, N. A., Gurina, D. L., Khlyustova, A. V., Costerin, D. Yu., Naumova, I. K., Titov, V. A., & Agafonov, A. V. (2021). Experimental and computational investigation of polylactic acid/silver-NP nanocomposite with antimicrobial activity prepared by plasma in liquid. *Plasma Processes and Polymers*, *18*(2), 2000169. https://doi.org/10.1002/ppap.202000169

Taherimehr, M., YousefniaPasha, H., Tabatabaeekoloor, R., & Pesaranhajiabbas, E. (2021). Trends and challenges of biopolymer-based nanocomposites in food packaging. *Comprehensive Reviews in Food Science and Food Safety*, *20*(6), 5321–5344. https://doi.org/10.1111/1541-4337.12832

Wei, Y., Liang, X., Wu, H., Cen, J., & Ji, Y. (2021). Efficient phosphate removal by dendrite-like halloysite-zinc oxide nanocomposites prepared via noncovalent hybridization. *Applied Clay Science*, *213*, 106232. https://doi.org/10.1016/j.clay.2021.106232

Xie, M., Huang, K., Yang, F., Wang, R., Han, L., Yu, H., Ye, Z., & Wu, F. (2020). Chitosan nanocomposite films based on halloysite nanotubes modification for potential biomedical applications. *International Journal of Biological Macromolecules*, *151*, 1116–1125. https://doi.org/10.1016/j.ijbiomac.2019.10.154

Yadav, S., Mehrotra, G. K., Bhartiya, P., Singh, A., & Dutta, P. K. (2020). Preparation, physicochemical and biological evaluation of quercetin based chitosan-gelatin film for food packaging. *Carbohydrate Polymers*, *227*, 115348. https://doi.org/10.1016/j.carbpol.2019.115348

Yanat, M., & Schroën, K. (2021). Preparation methods and applications of chitosan nanoparticles; with an outlook toward reinforcement of biodegradable packaging. *Reactive and Functional Polymers*, *161*, 104849. https://doi.org/10.1016/j.reactfunctpolym.2021.104849

Yu, F., Fei, X., He, Y., & Li, H. (2021). Poly(lactic acid)-based composite film reinforced with acetylated cellulose nanocrystals and ZnO nanoparticles for active food packaging.

International Journal of Biological Macromolecules, *186*, 770–779. https://doi.org/10.1016/j.ijbiomac.2021.07.097

Zhang, Y., R. Nayak, T., Hong, H., & Cai, W. (2013). Biomedical Applications of Zinc Oxide Nanomaterials. *Current Molecular Medicine*, *13*(10), 1633–1645.

CHAPTER 5

Synthesis and characterization of poly(lactic acid)/clove essential oil/alkali-treated halloysite nanotubes composite films for food packaging applications

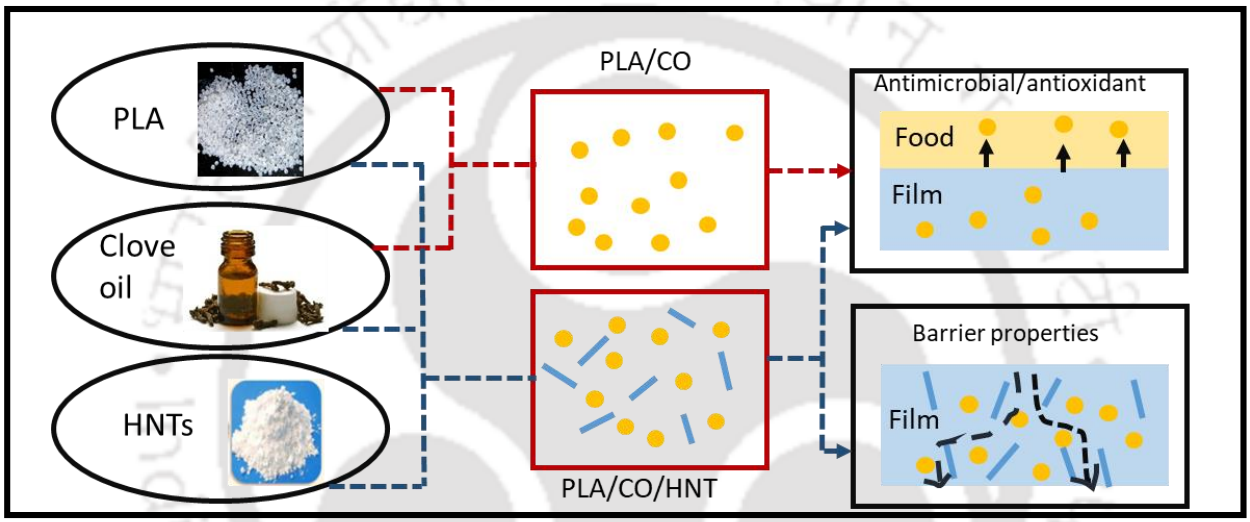

Research output

***Boro, U.**, Priyadarsini, A., & Moholkar, V. S. (2022). Synthesis and characterization of poly (lactic acid)/clove essential oil/alkali-treated halloysite nanotubes composite films for food packaging applications. **International Journal of Biological Macromolecules**, 216, 927-939*

5.1 Introduction

In recent years, mainly the environmental issues and human health concerns have encouraged the use of biopolymers in place of petroleum based, non-degradable, synthetic polymers as food packaging material (Popa et al., 2022; Sadeghi et al., 2022). Hence, biobased polymers obtained from natural resources such as proteins (Hadidi et al., 2022), chitosan (Riaz et al., 2018), cellulose (Liu et al., 2021), starch (Vianna et al., 2021) and their derivatives are used for the synthesis of biodegradable food packaging films. Among different biopolymers, poly(lactic acid) (PLA) extracted from corn starch, potato starch and sugar beet is the most widely used material for food packaging applications because of its superior physical (mechanical or thermal) properties as compared to other bio-polymers. Moreover, PLA has been declared as "Generally Recognized as Safe" (GRAS) material by US Food and Drug Administration (FDA) (Villegas et al., 2017). However, PLA has certain limitations such as poor toughness, low flexibility, and low water and gas barrier properties etc. Significant research has been carried out in past few years for improvement of physiochemical properties of PLA. The incorporation of nanoparticles, such as ZnO, nanoclays, nano silver, nano copper, TiO_2, and SiO_2 not only improves the thermal, water vapor barrier and mechanical properties but also add some other functional properties such as antimicrobial, UV-light barrier properties to the PLA films (Bao et al., 2020; Batool et al., 2022; Chi et al., 2019; Chu et al., 2017; M. Z. Mulla et al., 2021).

In food industry, maintenance of food products shelf life and freshness is the key challenge. In this regard, use of biopolymer-based food packaging films containing natural extracts such as essential oils are known to be beneficial. In food packaging sectors, essential oils are used as a natural preservative due to their antimicrobial, antioxidant effect, which helps to extend the shelf-life of foods (Falleh et al., 2020; Saeed et al., 2022; Vergis et al., 2015). The nanocomposite films containing essential oils and nanofillers possess antimicrobial and antioxidant properties which improve the quality and shelf life of food products (Alizadeh-Sani et al., 2021; Arfat et al., 2018; Javaherzadeh et al., 2020; Y. Liu et al., 2017). Different types of

essential oils such as clove, thyme, ginger, rosemary, cinnamon, and garlic oils are being used as active agents in food packaging systems. Among all, clove essential oil (CEO) is known for their excellent UV rays blocking properties and strong antioxidant, antifungal and antibacterial activities (Acosta et al., 2016; Chen et al., 2017; M. Mulla et al., 2017). Moreover, incorporation of CEO into polymer matrix improves its flexibility, toughness and hydrophobicity (Lee et al., 2018; Lu et al., 2021). Mainly CEO contains 76.8% eugenol, 17.4% β-caryophylene and 2.1% α-humulene (Chaieb et al., 2007). The US Food and Drug Administration (FDA) has categorized CEO as GRAS material. In literature, several groups have reported incorporation of CEO into polymer matrix as an additive for the extension of shelf life of foods. Sharma et al. have found that incorporation of clove and thyme oil in PLA/PBAT blend influences the final film properties. Here, clove oil gives higher UV barrier, antibacterial properties as compared to thyme oil. Therefore, clove oil loaded PLA/PBAT can be used as active food packaging materials (Sharma et al., 2020). Qin et al. (2017) have fabricated plasticized PLA by incorporation of four different essential oils, viz. clove oil, lemongrass, bergamot, and rosemary (Qin et al., 2017). Among these, bergamot oil provides the highest plasticizing activity than others. The synthesized bio-composites exhibited good antimicrobial activity against *B. subtilis* and *E. coli.* However, the use of essential oils in packaging system has some limitations. High volatility is the major drawback of essential oils as active agents. Due to its volatility, the chances of losing the essential oils from the packaging system increases. To get better stability, essential oils are first loaded into nanoparticles and then added into polymer matrix. In light of these facts, techniques like nano emulsification and encapsulation of essential oils on nanoparticles have been used (Gasti et al., 2022; Lu et al., 2021).

Halloysite nanotube (HNT) is a kind of nanoclay having hollow tubular structure with a chemical formula of $Al_2Si_2O_5(OH)_4$ (Saadat et al., 2020). Due to nontoxic, low price, high aspect ratio, encapsulation capacity, and suitability for incorporation into different biopolymers, HNTs are considered as an excellent nanofiller material for the development of bio-nanocomposite films

suitable for food packaging applications. HNTs contains a positive inner lumen of alumina and a negative outer surface of silica allowing its selective functionalization, and facilitates the encapsulation of chemically and biologically active agents. In polymer nanocomposites HNTs can be used as nanocarriers which facilitates the control release of the active agents (Yuan et al., 2015). Moreover, HNTs are also categorized as GRAS material for food packaging by the US FDA (Lee et al., 2017). Several research reports have suggested the use of essential oils and HNTs as filler material into various biopolymers. Lee et al. (2018) have studied the effect of HNTs and clove essential oil (CEO) on chitosan based films (Lee et al., 2018). Here, HNTs act as stabilizing agents for essential oil droplets. In absence of HNTs, CEO agglomerates and floats during the drying process with formation of some porous structure, which causes the loss of CEO. The water vapor barrier properties improved with addition of CEO and HNTs. This might be due to the formation of tortuous path by HNTs and hydrophobic nature of CEO. Cui et al. (2021) have prepared an antimicrobial nanocomposite film of sodium alginate (SA) by addition of cinnamaldehyde and sulfuric acid treated HNTs. Addition of cinnamaldehyde and treated halloysite nanotubes improved the tensile strength, UV barrier and water vapor barrier properties of the SA films. Also, the release of cinnamaldehyde from nanocomposite films containing HNTs to food simulant was delayed by 144 h as compared to polymer film containing only SA and cinnamaldehyde (Cui et al., 2021). Since the treatment with acidic or alkaline solutions changes the structure of HNTs, these methods have been used for increasing the lumen size and adsorption capacity of HNTs, which facilities the loading of active agents (Boonsiriwit et al., 2020).

Considering the review of previous literature on applications of HNTs and also the biopolymer PLA, it seems a good idea to combine these for possible nanocomposite, which is likely to have excellent properties by virtue of merits of both HNTs and PLA. To the best of our knowledge, no previous study has addressed synthesis of PLA based films incorporated with HNTs and essential oils. In this paper, we report synthesis of PLA based nanocomposite films incorporated with CEO and alkali treated HNTs (NHNT). We have also characterized

physiochemical properties (contact angles, WVP, thermal and mechanical properties etc.) of these nanocomposite films. Moreover, the PLA/CEO/NHNT nanocomposite films have been tested for shelf life of cut apples on the basis of properties like weight loss, titratable acids, total soluble solids, pH, firmness and mesophilic count.

5.2 Materials and Methods

5.2.1 Materials

Poly(lactic) acid (Ingeo 4032D, 98.6% L-lactic acid) were procured from Nature Works LLC (USA). Chloroform (analytical grade, purity: 99.8%) was purchased from Merck Chemical Co., Germany. Halloysite nanotubes were procured from Sigma-Aldrich and NaOH were obtained from Merck, India. Luria Bertani broth (LB) and agar powder (bacteriological grade) were obtained from Himedia. Clove essential oil was purchased from aromazotika essential oils. All the chemicals were used as received.

5.2.2 Synthesis of alkali treated halloysite nanotubes (NHNTs)

Surface activation of HNTs for loading of clove essential oil was done as follows: The raw HNTs (5 g) was dispersed in 5 M NaOH by using 30 min of bath sonication followed by 24 h magnetic stirring. Then the solution containing NHNT was repeatedly washed with water by using centrifugation process (rpm: 6000, time: 10 min) until it becomes neutral. After that it was dried at 60 ℃. The alkali treated HNT was named as NHNT.

5.2.3 Synthesis of PLA based nanocomposites with NHNT and clove essential oil (CEO)

PLA based nanocomposites with NHNT and CEO were synthesized by using solvent casting method. Essentially, 4 g of PLA was dissolved on 40 ml chloroform and after complete dissolution, 200 µl (5 wt% w.r.t PLA) of CEO was added on it. Ultrasonic treatment (bath sonication, power: 100 W, frequency: 40 kHz) was used for 30 min followed by magnetic stirring (rpm: 350, room temperature) for 6 h. Then, 0.25, 0.5 and 1 wt% of NHNT (w.r.t PLA) were added to PLA/CEO solution. After stirring for 24 h, the solution of PLA/CEO/NHNT was

obtained, and it was casted on the petridish and allowed to dry. As-synthesized nanocomposites with 0.25, 0.5 and 1 wt% of NHNT and CEO were named as PCOH0.25, PCOH0.5 and PCOH1. For comparison (or as base case), PLA with CEO was also synthesized and named as PCO. Fig. 5.1 shows the schematic illustration of molecular interaction during synthesis of PLA/CEO/NHNT nanocomposites.

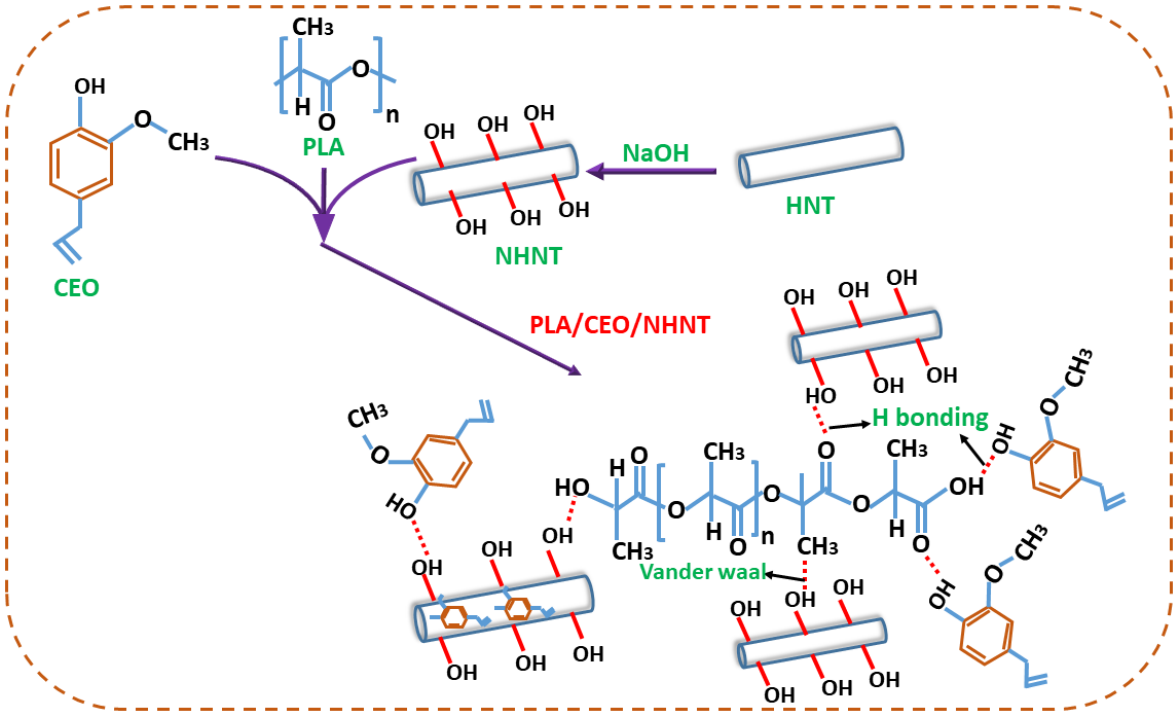

Fig. 5.1. Schematic illustration of molecular interaction during synthesis of PLA/CEO/NHNT nanocomposites

5.3 Characterizations of nanoparticles and nanocomposite films

(1) BET analysis: The specific surface area, pore volume and the pore size distribution of HNT and NHNT samples were determined by using BET surface area analyzer (Model No.: Tristar II; Make: M/s Micromeritics, U.S.A.). **(2) TEM analysis:** TEM analysis of HNT and NHNT was done by using Transmission Electron Microscope (TEM) analyzer (Make: JEOL, Model: 2100F). **(3) X-ray diffraction and FT-IR spectroscopy:** The structural characteristics of HNT and NHNT were analysed using powder X-ray diffractometer (Make: Rigaku Technologies, Japan, Model: Smartlab, $\lambda = 1.5406$ Å) in the range of $10° \leq 2\theta \leq 80°$. To study the functional group present in

the samples FT–IR study was done by using FTIR spectrometer (Make: PerkinElmer, Singapore, Model: Spectrum two) in the wavelength range of 4000–400 cm^{-1}. **(4) Film thickness:** The thickness of each nanocomposite film was measured randomly at five different places using a digimatic micrometer (Mitutoyo Co. Ltd., Tokyo, Japan) with 0.001-mm accuracy. The average thickness was used during the calculation of water vapor permeability and mechanical properties testing. **(5) Surface wettability/contact angle analysis:** The surface wettability test of the nanocomposite films was carried by using a contact angle goniometer and associated software (Holmarc, HO-IAD-CAM-01B). **(6) water vapor permeability test:** The water vapor permeability (WVP) test of the polymer samples were done gravimetrically according to the ASTME00996-00 method with some modifications (Bhat et al., 2021; Yadav et al., 2020). The detailed methodology is already described in elsewhere (Chapter 3, section 3.2.5). (**7) Thermal and mechanical properties**: The thermal stability of the prepared nanocomposite films was evaluated by using TGA analyzer (Make: Netzsch model: STA449F3A00) and the mechanical properties, viz. tensile strength, elongation at break and elastic modulus of the films were measured by using 5 kN Electromechanical Universal Testing Machine (Make: Zwick Roell: Z005TN) following the ASTM D-882. (**8) UV-barrier properties**: The UV-barrier properties of PLA based nanocomposites were performed using UV-vis spectrophotometer (PerkinElmer, Lambda 35).

5.4 Application of PLA based nanocomposites on fresh cut apples

5.4.1 Preparation of the packaged samples

To evaluate the effectiveness of the nanocomposite films, the synthesized halloysite nanotubes and clove oil loaded PLA based nanocomposite films were used in packaging of cut apples. For the experiment, the defect free apples were purchased from the market complex in IIT Guwahati. First, the apples were washed with distilled water and air dried. The pristine PLA film, PCO, PCOH0.25, PCOH0.5, PCOH1 and commercial poly(ethylene) films were tested for their efficiency for food packaging. The pouches were prepared by heat sealing of nanocomposite films

of dimension 10 cm × 7.5 cm. Cut apples were placed in each pouch and stored at room temperature for 6 days. The apples were taken out from the pouch every day and various properties were measured.

5.4.2 Weight loss

The weight loss of the cut apples during storage was determined by using a digital weighing balance. The initial weight of each cut apples (M_i) were weighed and wrapped in nanocomposite films. The samples were stored at room temperature for 6 days. The final weight (M_f) of each sample was determined on each sampling day. The measurements were done with three replicates. The weight loss (%) of the cut apples was calculated as (Boonsiriwit et al., 2020): = $(M_i - M_f) / M_i \times 100$, where M_i = initial weight of cut apples (at day 0), M_f = final weight of cut apples on each sampling day.

5.4.3 Total soluble solids (TSS)

For the measurement of TSS, the apple juice was extracted using domestic mixer grinder and filtered by using muslin cloth. The TSS of the filtered juice was measured three times using a hand held refractometer (Bombay Scientific ERMA with ATC, range: 0 – 32 °Brix).

5.4.4 Titratable acidity (TA) and pH

Titratable acidity (TA) measures the total acid concentration present in food item (also called as total acidity). The determination of TA was done by standard titration AOAC method (Sadler et al., 2010). 2 mL apple juice was taken in a conical flask and was diluted with 20 mL Millipore water. A few drops of phenolphthalein were added to this solution before titrated against 0.1 N NaOH. Titration was repeated for three times for each sample. The results were presented with respect to maleic acid. The pH of the juice was measured using pH meter (Eutech pH 700 Meter). The formula for TA (%) is given below:

TA (%) = [(ml of NaOH consumed)× (normality of NaOH)×m_{eq} factor×100]/sample volume (ml)

m_{eq} factor of maleic acid = 0.067

5.4.5 Firmness

The firmness of cut apples was tested by a penetration test using penetrometer (ACUCAL Fruit Pressure Tester 1–24 kg/cm^2 ACSY3 Penetrometer, India). The measurements were done in triplicates.

5.4.6 Microbial analysis

The microbiological analysis of the stored packaged cut apples was done in terms of aerobic mesophilic count (Chi et al., 2019). The cut apples (2.5 g) were crushed inside the pouch and aseptically transferred to the 20 mL of sterile water. Then, 100 µL of the sample was taken for serial dilution and total mesophilic count was cultivated by spreading 10 µL of diluted sample on agar plate. The plates were incubated at 28 °C for 24 h and the number of colonies were counted. The result obtained were expressed in terms of log (CFU/mL). The experiments were done on duplicates.

5.5 Statistical analysis

The experiments were carried out in triplicate (n = 3) and the results were reported as mean value ± standard deviation. A single factor or one-way ANOVA (analysis of variance) was used to analyze a significant difference between mean values followed by Tukey's test. This analysis was done using Microsoft Excel Office 2016. The differences between mean values were considered significant at $p<0.05$.

5.6 Results and discussion

5.6.1 Characterization of HNT, NHNT and PLA/CEO/NHNT

The primary objective of treating HNTs with NaOH was to increase its specific surface area to obtain better contact of HNTs with PLA. To assess this expectation, the surface area and total pore volume of NaOH-treated HNTs was determined by using BET technique and the results are presented in Fig. 5.2 and Table 5.1. The N_2 adsorption-desorption isotherms of HNT and NHNT exhibit type II isotherms with H3 hysteresis loop in the relative pressure (P/P_0). This type of isotherms reveals the presence of mesopores and macropores in the material (Lun et al., 2014).

The surface area of HNT increased from 50.16 to 57.01 m^2/g with NaOH treatment (NHNT). The treatment with NaOH leads to the formation of $Al(OH)_3$ nanosheets by collapsing and dissolution of HNT structures (Akbari et al., 2019). The removal of $Al(OH)_3$ nanosheets from internal tubes and aggregation on the outer surface of HNT causes wall thinning and surface roughening of the material. The higher BET surface area achieved was attributed to the increase in internal diameter of the HNTs lumen and the introduction of extra surfaces and pores by the roughness treatment. Previous studies have demonstrated that alkali treatment of HNT lead to an increase in surface area and pore volume of the tubes (Li et al., 2016; Shankar et al., 2018). Fig. 5.2 (inset) shows the pore size distribution (PSD) of HNT and NHNT. The PSD curve of the samples indicate existence of mainly mesoporous structures (2–50 nm) in the sample. The average pore size of HNT and NHNT are calculated by BJH absorption method and it was found to be 16.9 nm and 15.7 nm respectively (Table 5.1). The total pore volume of NHNT (0.32 $cm^3\ g^{-1}$) is found to be higher than HNT (0.25 $cm^3\ g^{-1}$). The removal of Al^{3+} ions during alkali treatment causes the formation of voids, which increases the total pore volume of NHNT and enhanced the adsorption capacity for CEO.

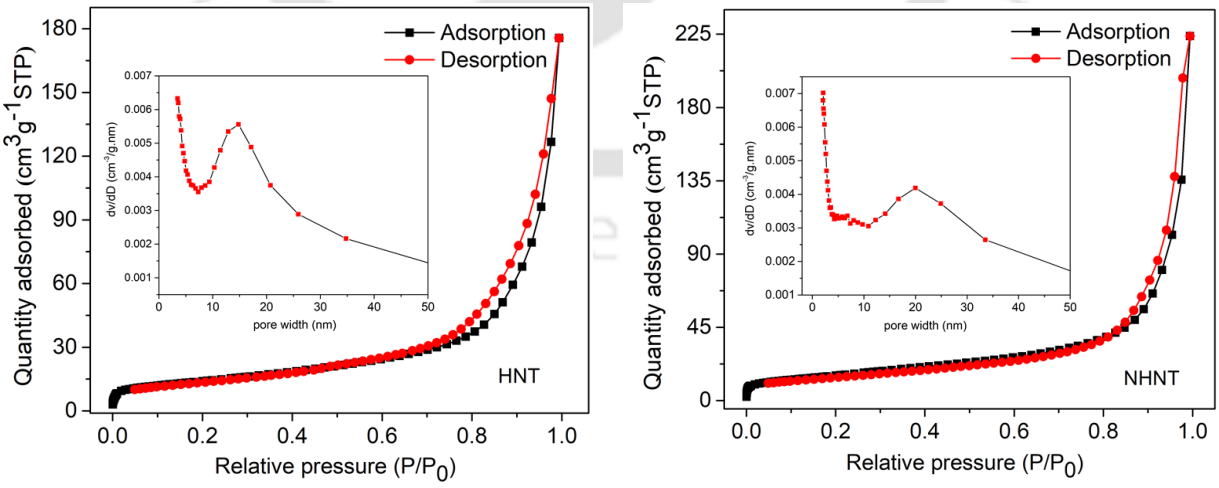

(a) (b)

Fig. 5.2. BET surface area of (a) HNT (inset: pore size distribution of HNT), (b) NHNT (inset: pore size distribution of NHNT)

Table 5.1. BET surface area, pore volume and pore size of HNT and NHNT

Sample	S_{BET} (m^2 g^{-1}) [a]	Total pore volume (cm^3 g^{-1}) [b]	Average pore width (nm) [c]
HNT	50.16	0.25	16.9
NHNT	57.01	0.32	15.7

[a] BET surface area. [b] Single point adsorption total pore volume of pores less than 1,952.438 Å width at p/p_0 = 0.99.
[c] BJH Adsorption average pore width (4V/A).

TEM images of raw HNT and NHNT were shown in Figs. 5.3a and b respectively. The images revealed that HNT possess smooth surface with lesser internal diameter, while NHNT had rough surface with higher internal diameter. The raw HNT had an average internal diameter of 15 nm with thickness of 14 nm. After treatment with NaOH, the average internal diameter increased up to 27 nm and wall thickness decreased up to 11 nm. TEM image also revealed marginal (~ 30%) rise in the external diameter of NHNT after alkali treatment. This rise in external diameter is mainly contributed by change in internal diameter of NHNT after alkali treatment. The wall thickness of the NHNT tubes also undergoes minor changes after treatment.

Fig. 5.4a shows the X-ray diffraction patterns of HNTs and NHNTs. For HNTs, the observed diffraction peaks can be indexed to the characteristic peaks of halloysite nanotubes (7 Å) (JCPDS card no. 09-0453). The diffraction peak at 2θ value of 11.79° (d001 = 7.5 Å) was corresponding to the multilayer wall packing of HNTs. The intense peak at 2θ = 20.07° (d100 = 4.42 Å) is attributed to other characteristic peaks of the HNTs. The diffraction peaks of NHNTs agree well with that of HNTs. But the peak intensity of NHNT at 11.79° and 20.07° decreases, which might be due to etching of HNTs wall by NaOH treatment. Further, it can be observed that NHNT possess the same crystal phase as HNTs, which indicate that tubular structure of HNTs remain unchanged on alkali treatment.

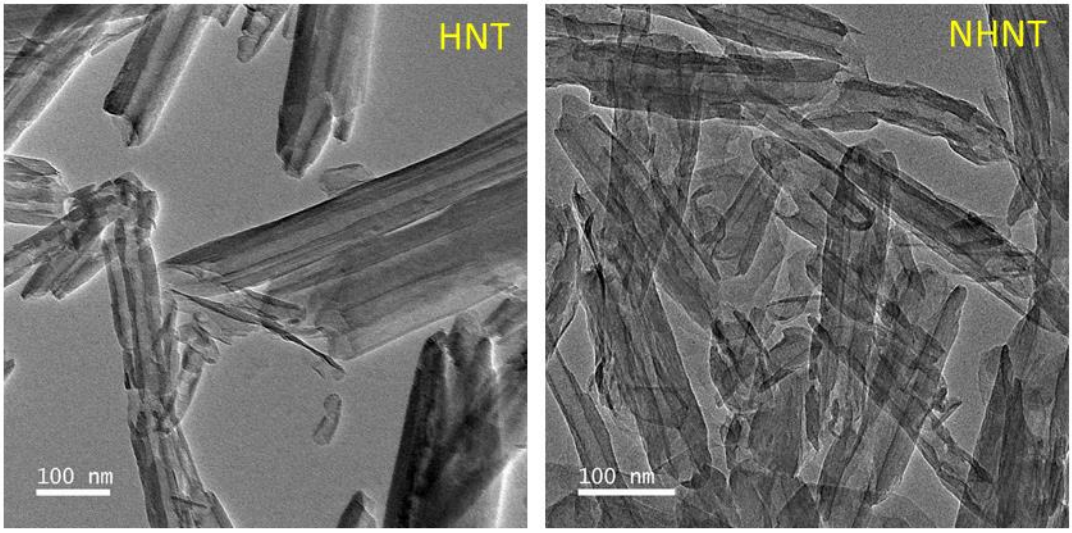

Fig. 5.3. TEM images of (a) HNT, and (b) NHNT

The FTIR spectra of HNT and NHNT were displayed in Fig. 5.4b. The spectra at 3697 and 3622 cm^{-1} are ascribed to –OH stretching and band at 903 cm^{-1} is corresponding to the bending vibration of the inner OH. The absorption band at 1643 cm^{-1} is ascribed for adsorbed water molecules. The peak at 1122 cm^{-1} and 1013 cm^{-1} are assigned to the Si–O stretching vibration (M. Liu et al., 2013; Wei et al., 2021). The band at 752 cm^{-1} is ascribed to Si–O–Al stretching vibrations. The band at 527 cm^{-1} is occurred due to Si–O bending vibration and that at 458 cm^{-1} to Al–O stretching mode. Reduction in the peak intensities at 1013, 527 and 458 cm^{-1} might be due alkali treatment of HNT, which could remove some Si–OH and Al–OH groups from raw HNT (Wang et al., 2013).

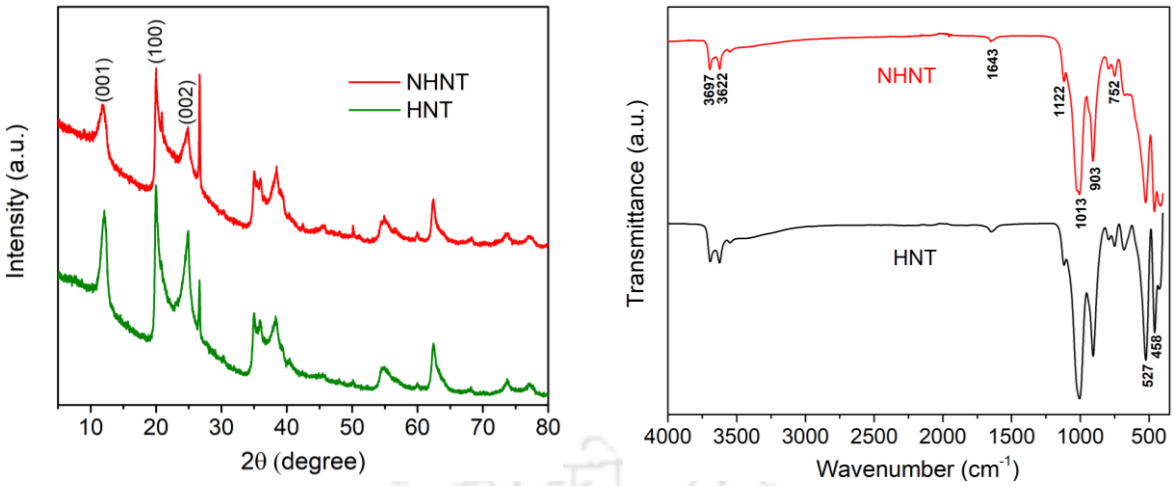

(a) (b)

Fig. 5.4. (a) XRD and, (b) FTIR spectra of HNT and NHNT

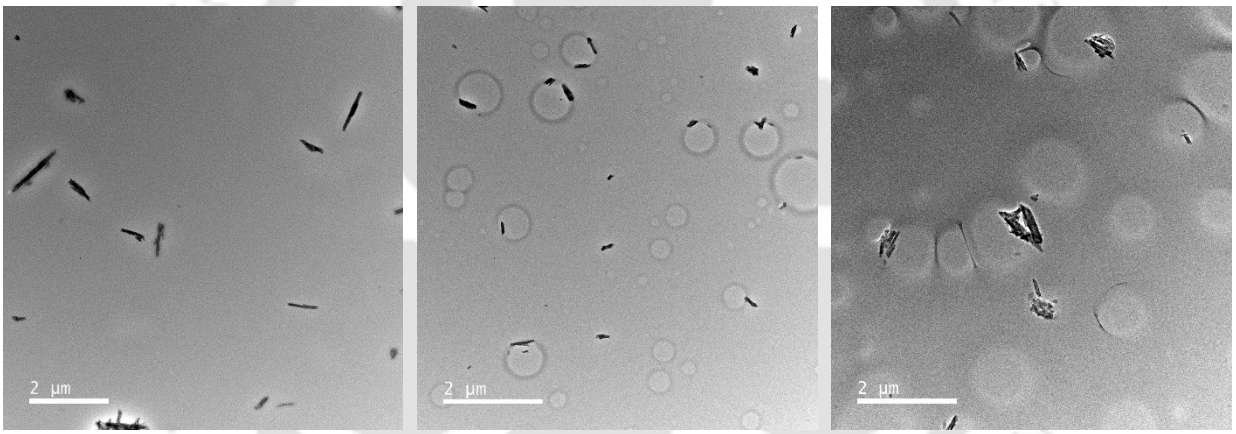

(a) (b) (c)

Fig. 5.5. TEM images the nanocomposite films (a & b) PCOH0.5, (c) PCOH1. The oil globules and the halloysite nanotubes dispersed in the PLA matrix are clearly visible. For PCOH1, agglomeration of the halloysite nanotubes is also seen

TEM images of PCOH0.5 (0.5 wt% NHNT) and PCOH1 (1 wt% of NHNT) was shown in Fig. 5.5. It shows the presence of CEO, and homogeneity of oil droplets was detected in the PLA matrix. Also uniform dispersion of NHNT was observed on PLA/CEO/NHNT composites (PCOH0.5) which indicate the formation of PLA/CEO/NHNT nanocomposite.

5.6.2 Properties of nanocomposite films

5.6.2.1 Surface wettability

The surface wettability of the nanocomposite film was evaluated by water contact angle analysis (WCA). This property is an indicator of hydrophobic/hydrophilic nature of the material. The nanocomposite films having WCA < 65° and > 65° are considered as hydrophilic and hydrophobic respectively (Gasti et al., 2022; Shankar et al., 2018). The WCA of pure PLA and its nanocomposite films with clove essential oil and halloysite nanotubes are shown in Figs. 5.6a and b. The WCA obtained for pure PLA film was 65.4° (Subbuvel & Kavan, 2022). The hydrophobicity of PLA film was increased from 65.4° to the highest value of 85.2° for nanocomposite films after incorporation with clove essential oil and halloysite nanotube (1 wt% wrt PLA). The surface hydrophobicity of the materials depends on the surface topography and chemical properties. Presence of hydrophobic clove essential oil increased the hydrophobicity of the film surface (Sharma et al., 2020). Moreover, due to presence of nanoparticles (NHNTs) film surface become rough, which is the another reason for higher hydrophobicity of the nanocomposite films. The hydrophobic nature of bionanocomposite films facilitates their potential use in the food packaging applications by maintaining high water barrier and moisture retention capacity. It should be mentioned that all bionanocomposites had WCA > 65°, showing hydrophobic surface, highlighting their suitability for food packaging purposes.

5.6.2.2 Water vapor permeability (WVP) test

The water vapor barrier property is an important criteria of food packaging films. The main function of packaging film is to decrease the exchange of moisture between the surroundings and the foods. The packaging film should have low values of WVP, so that it can maintain the quality and shelf life of the foods. The WVP of pure PLA and its nanocomposite films with NHNT and CEO are displayed in Table 5.2. The WVP of the bionanocomposite film is greatly affected by the addition of CEO and NHNT. The WVP of the pure PLA is 4.13×10^{-10} g/m s Pa, which decreases up to 12.8% by incorporation of CEO. The addition of CEO into PLA decreases the water vapor

permeability by increasing hydrophobicity. The result is consistent with previous literature (Gasti et al., 2022; Mohamad et al., 2020), which report reduction in WVP with the addition of different essential oil into PLA matrix. The WVP values further reduce by addition of NHNT on PCO composites. The WVP values for PCOH0.25, PCOH0.5 and, PCOH1 are 3.12×10^{-10}, 2.39×10^{-10} and 2.67×10^{-10} g/m s Pa, respectively.

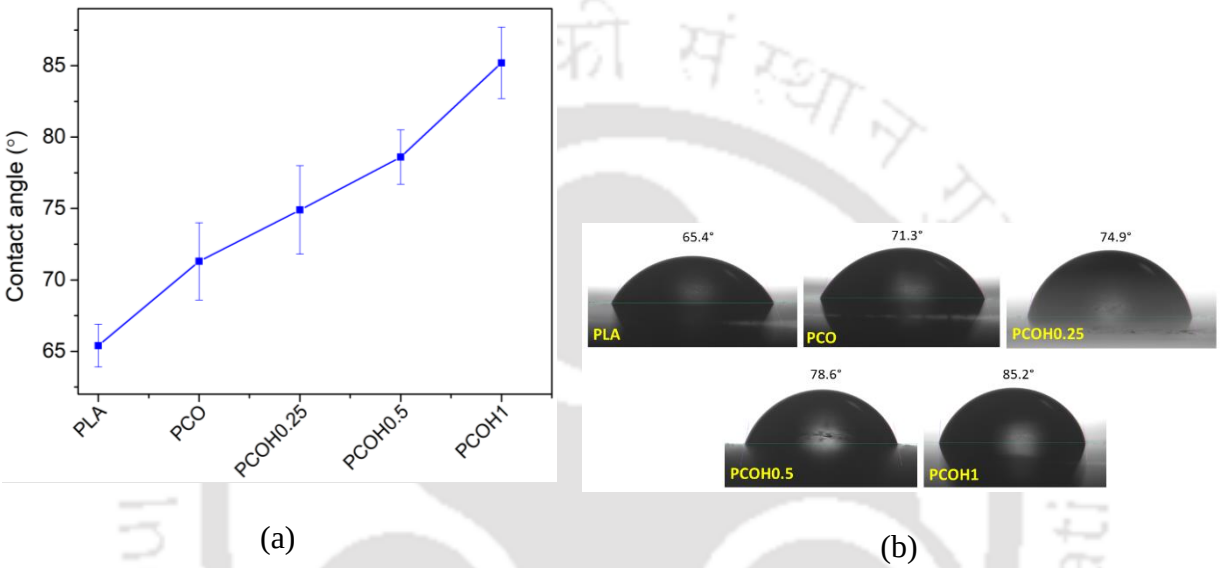

(a) (b)

Fig. 5.6. (a) and (b) Water contact angles of PLA and prepared nanocomposite films

Different factors influence the WVP of the polymer films, viz. hydrophobicity, mobility of the polymer chains, structure and nanofiller concentration etc. The inherent hydrophobic properties of CEO could affect the ratio of hydrophilic/ hydrophobic of the films, which results in decrease of WVP. The aluminosilicate NHNT dispersed in PLA matrix might create a tortuous path which hinders the passage of water molecules, by creating longer path lengths through the polymer matrix (Saadat et al., 2020; Shankar et al., 2018). Moreover, the homogeneously dispersed NHNT nanoclays in the PLA matrix restrict the movement of polymer chains. At 1 wt% of NHNT loading (PCOH1), WVP increases due to agglomeration of nanoparticles. Overall, the nanocomposite film incorporated with 0.5 wt% of NHNT and CEO (PCOH0.5) exhibited superior water vapor barrier properties as compared to other nanocomposites. The WVP tests results are in

good agreement with the WCA analysis results.

Table 5.2. Water vapor permeability of PLA, PCO and nanocomposite films incorporated with CEO and HNT

Sample	NHNT loading (wt%)	Thickness (mm)* ($p<0.05$)	WVP (g/m s Pa) × 10^{-10}* ($p<0.05$)
PLA	0	0.171 ± 0.007	4.13 ± 0.13
PCO	0	0.178 ± 0.008	3.60 ± 0.22
PCOH0.25	0.25	0.188 ± 0.003	3.12 ± 0.33
PCOH0.5	0.5	0.196 ± 0.005	2.39 ± 0.28
PCOH1	1	0.202 ± 0.008	2.67 ± 0.23

*The results (n = 3) are represented as mean values ± standard deviation. The Tukey's test results of one-way ANOVA are given in appendix.

5.6.2.3 Thermogravimetric analysis (TGA) analysis

TGA analysis was done to study the thermal properties of the pristine PLA, PLA/CEO and PLA/CEO/NHNT bionanocomposites. The results are shown in Figs. 5.7a, and Table 5.3. The TGA thermographs revealed two step thermal degradation process of the polymer films. The first step of degradation take place at the temperature of around 74 – 160 ℃ which was mainly due to removal of water and volatile components from the samples. The second step of degradation occurs at around 315 – 0 ℃. The weight loss in this temperature range occurs due to chemical debonding/degradation of PLA chains. Risyon et al. also reported second step degradation temperature in the range of 330 – 350℃ (Risyon et al., 2020). Table 5.3 shows $T_{10\%}$, $T_{50\%}$, $T_{peak\%}$ and ash content (%) of all nanocomposite films. The TGA thermographs revealed that presence of CEO decreases the thermal stability of PLA. This might be due to plasticizing effect of the CEO. However, the incorporation of NHNT in PLA/CEO leads to the improvement in thermal stability of all nanocomposite films. This might be due to high thermal stability of NHNT (475 – 575℃). The highest thermal stability was observed for PCOH0.5 (0.5 wt% NHNT). The presence of homogeneously distributed NHNT formed a tortuous path, which acts as a heat barrier to PLA

films (Sharma et al., 2019). The tortuous path also hindered the diffusion of volatile decomposition material out of the PLA matrix that improved the maximum degradation temperature and ash residue. At high concentration of NHNT (PCOH1) the thermal stability of the nanocomposite film decreases in comparison to PCOH0.25 and PCOH0.5 due to agglomeration of the nanoparticles. The aggregation of the NHNT helps the volatile matter to escape from the nanocomposite films, thereby reducing the thermal stability and char formation. The pristine PLA and PCO showed $T_{10\%}$ at 323.2 and 311.6℃ respectively, while nanocomposites of CEO with NHNT (0.25, 0.5 and 1 wt%) had $T_{10\%}$ values of 342.5, 342.7 and 338.6℃ respectively. Maximum degradation temperature $T_{max\%}$ was obtained from DTG curve (Fig. 5.7b). The presence of NHNT enhanced the $T_{max\%}$ (PLA: 362℃, PCOH0.5: 374.4℃) of the nanocomposite films. Also, the residual weight/char value of the nanocomposite film containing NHNT is higher than pristine PLA. The higher amount of char formation and entrapment of decomposed product into the lumen of NHNT might be the possible explanation of the overall improvement of the thermal stability of nanocomposite films. These lumen act as a barrier for the diffusion of volatile matter. The entrapment of degraded product in lumen causes delay in the mass transport, thereby increasing thermal stability in presence of NHNT (De Silva et al., 2014).

Table 5.3. Thermal properties of PLA, PCO and PLA based nanocomposites with CEO and NHNT

Specimen	**$T_{10\%}$ (℃)**	**$T_{50\%}$ (℃)**	**T_{max} (℃)**	**Ash content (%) @ 500℃**
PLA	323.2	357.3	362.6	1.05
PCO	311.6	349.7	355.7	1.10
PCOH0.25	342.5	367.7	372.8	1.06
PCOH0.5	342.7	368.5	374.4	1.67
PCOH1	338.6	365.7	370.3	1.39

[**Note**: Degradation temperature for 10%, 50 % and, maximum weight loss (from DTG curve) are represented by- $T_{10\%}$, $T_{50\%}$ and $T_{max\%}$ respectively]

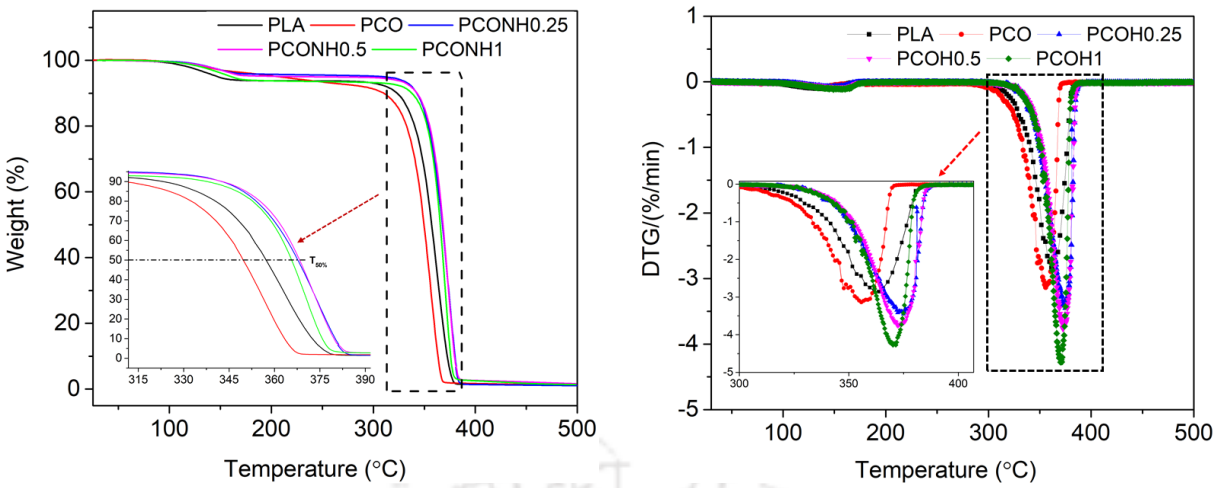

(a) (b)

Fig. 5.7. (a) TGA and (b) DTG curves of PLA and PLA based nanocomposite films

5.6.2.4 Mechanical properties

As already mentioned, one of the primary limitations of PLA based films in food packaging application is its brittle nature and low flexibility Therefore, developing packaging films with improved flexibility was one of the objectives of this research. The mechanical properties of pure PLA, PCO and PLA nanocomposite films with loadings of NHNT and CEO are presented in Fig. 5.8. In this study, the pristine PLA film showed a low elongation at break (EB) of about 2.8%, which is consistent with the values reported in the literature (Risyon et al., 2020). However, the flexibility of PLA films markedly increased after incorporation of CEO. As depicted in Fig.5.8d, up to 17-fold increase in the EB values (2.8 to 49.2 %) are obtained for PCO. This might be due to plasticizing effect of CEO. While, the incorporation of NHNT improves the elastic modulus and tensile strength of the nanocomposite films along with reduction in elongation at break. The result indicates that the loading of 0.5 wt% of NHNT gives maximum tensile strength (31.7 MPa) with elongation at break of 21.9%. Therefore, the toughness of the nanocomposite film was improved by loading of both NHNT and CEO.

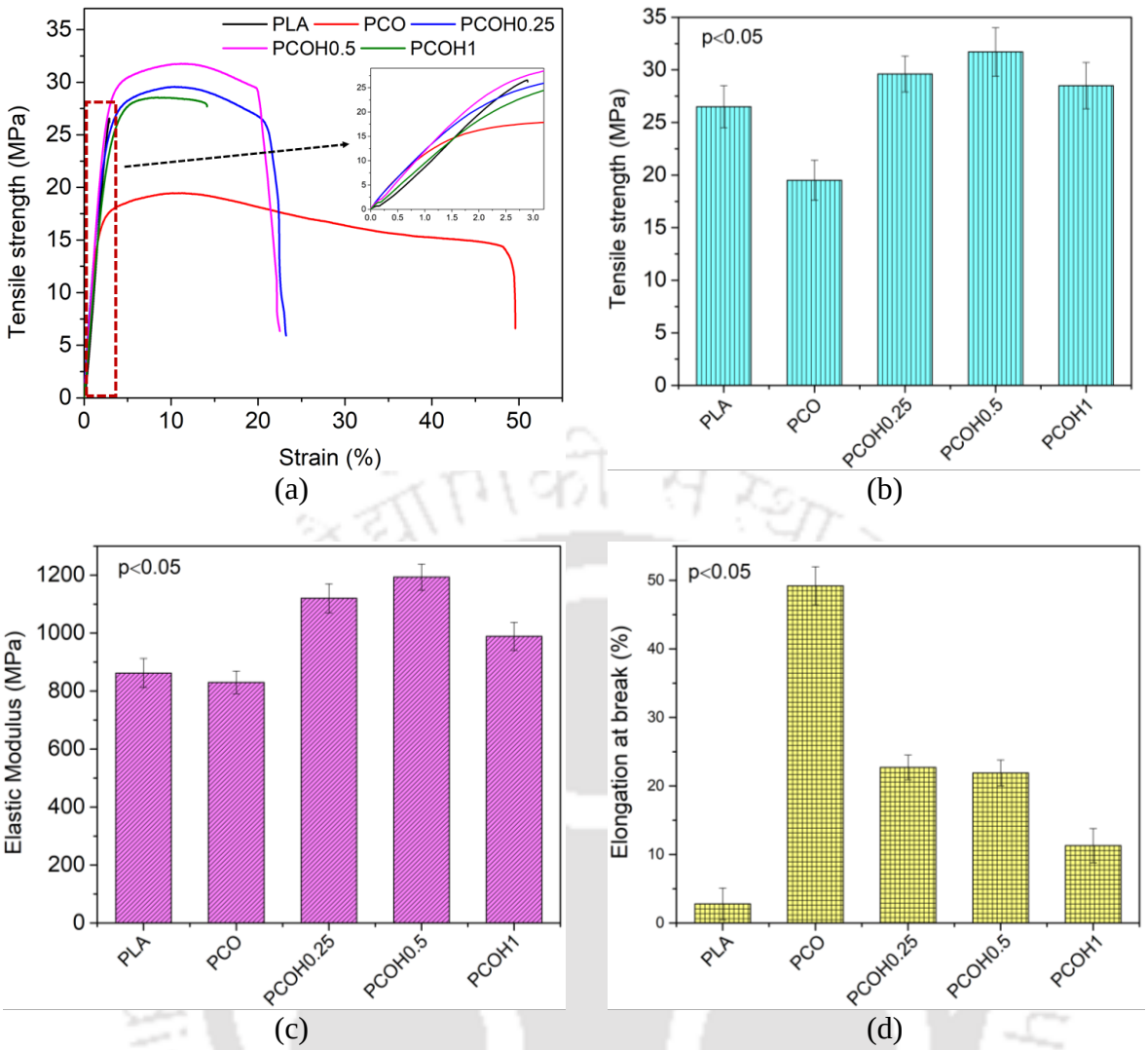

Fig. 5.8. Mechanical properties PLA, PCO and the nanocomposites. (a) Stress vs. strain curve, (b) Tensile strength, (c) Elastic modulus, and (d) Elongation at break. The results (n = 3) are represented as mean values ± standard deviation. The Tukey's test results of one-way ANOVA are given in supplementary material

5.6.2.5 Optical properties

The UV-barrier properties play an important role in food packaging to protect the food product from degradation on exposure to UV radiation. Some components of foods such as lipids, proteins and fats undergo oxidation when exposed to light and decreased food products shelf life. Therefore, the reduction in the transmittance value of the packaging material can be beneficial for the food packaging application. The optical properties (% transmittance, opacity and transparency) of the synthesized films is shown in Fig. 5.9. The results revealed that pristine PLA showed high transmittance in both visible and UV regions. In visible region (400 – 700 nm), PLA

has shown transmittance value of more than 90%. The transmittance value of PCO film in the UV range (250 – 400 nm) was significantly lower as compared to pristine PLA. The addition of NHNT on PCO matrix further decreased the transmittance value, which indicates high UV barrier property of the nanocomposite film.

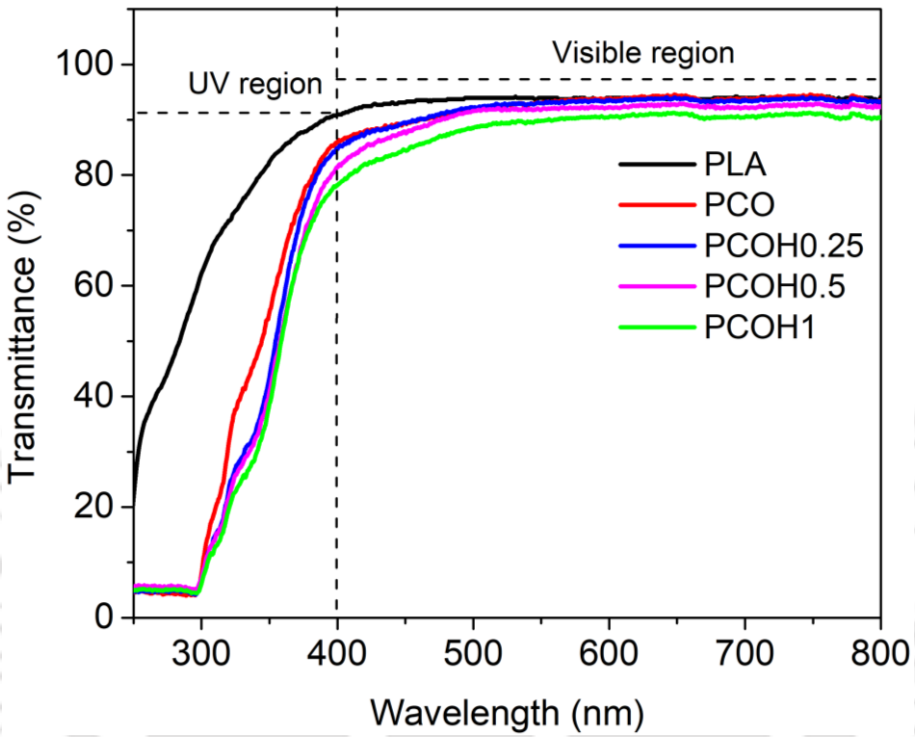

Fig. 5.9. UV-visible spectra of PLA, PCO and PLA based nanocomposite films

Table 5.4 depicts the transmittance value of the polymer films at UV-B (300 nm), UV-A (360 nm) and visible (600 nm). The transmittance values of neat PLA film at 300, 360 and 600 nm are 62.2, 85.4 and 95.1%, respectively, and transmittance value after incorporation of CEO (PCO) reduced to 7.9, 64.9 and 93.7%, respectively. The UV barrier property of films with CEO is due to presence of phenolic component of CEO, which absorbs the UV light. These findings matched with various studies, which also reported the UV barrier properties of CEO (M. Mulla et al., 2017; Sharma et al., 2020). Further, the addition of NHNT on PCO decreased the transmittance value. The maximum reduction in transmittance value was obtained for PCOH1. The transmittance values for PCOH1 at 300, 360 and 600 nm were 6.1, 51.9 and 90.5%, respectively.

The presence of nanoparticle NHNT in polymer matrix might diffract/block the UV-visible light which reduces the percentage transmittance at all wavelengths (Cui et al., 2021). It is noteworthy that addition of CEO and NHNT decreased the transmittance to greater extent in UV region as compared to visible region. Therefore, it is possible to obtain high UV barrier properties by preparing the nanocomposite films with PLA/CEO/NHNT without losing the transparency of the PLA films.

Table 5.4. Transmittance (%) of the PLA, PCO and PLA based nanocomposite films in UV and visible region

Specimen	% T UV-B (300 nm)	% T UV-A (360 nm)	% T Visible (600 nm)
PLA	62.2	85.4	95.1
PCO	7.9	64.9	93.7
PCOH0.25	7.1	57.1	93.4
PCOH0.5	7.1	52.7	92.3
PCOH1	6.1	51.9	90.5

5.7 Application of polymer nanocomposite films on fresh cut apples

5.7.1 Weight loss

The weight loss in fruits and vegetables during stoarge period hampers the quality of fresh produce. The harvested produce remains fresh as long as it contains water. Weight loss mainly occurs due to post harvest transpiration. Generally, a weight loss > 5% would cause a reduction in the market value of fruits and vegetables (Punia Bangar et al., 2022). The weight loss of cut apples stored in pure PLA, commercial polyethylene (PE) and nanocomposite packaging films were shown in Fig. 5.10a. For all packaging films, rise in weight loss was observed as the storage period increased from day 0 to day 6. This may be due to the continuous water evaporation from cut apples to the surroundings. The cut apples packaged with PE and pure PLA films showed weight loss of 5.53% and 5.60%, respectively up to day 6. The fruit packaged with PCO exhibited relatively lower weight loss (4.78%) as compared to PE and PLA films during storage period. Due to hydrophobicity, CEO enhanced the water vapor barrier ability of PLA based film to prevent loss of moisture. This can also be explained with the help of WCA analysis reported in earlier

section. The PLA has lower WCA than nanocomposite films. The addition of CEO forms a semi-permeable protective layer that allows passage of certain small molecules but acts as a protective barrier to decrease transpiration on the fruit surface and provide a physical barrier against moisture, O_2, CO_2, and solute movements (Punia Bangar et al., 2022). The PLA film reinforced with NHNT and CEO significantly lowered the weight loss with concurrent rise in storage period. The weight loss of 4.30%, 3.33% and 4.60% were obtained for PCOH0.25, PCOH0.5 and PCOH1, respectively. Among all nanocomposite films, PCOH0.5 exhibited minimum weight loss and preserved the freshness of the cut apples for longer period of time. Homogeneous dispersion of NHNT in PLA matrix created a tortuous path and hindered in the transport of gases (O_2, CO_2) and water vapor with atmosphere.

5.7.2 Total soluble solids (TSS)

The metabolic activity and respiration of cut apples during storage would lead to reduction in TSS for all compositions of nanocomposite films. The decrease in TSS values might be due to degradation of sugars and organic acid consumptions as the main respiratory substrates during storage. The TSS of cut apples stored in PE, PLA, PCO and PLA/CEO/HNT nanocomposites for day 0 to day 6 at room temperature have been shown in Fig. 5.10b. It could be seen that cut apples packed with PCO and PCOH0.5 maintain relatively higher amounts of TSS at room temperature as compared to PE and PLA at the end of 6-day storage. The lowest values of TSS 10.0 and 10.2 °Brix were obtained for PE and PLA respectively, while the highest value of TSS 11.0 °Brix was observed for PCOH0.5. Incorporation of CEO and NHNT in PLA helps in maintaining higher amounts of TSS by modification of internal atmosphere and delaying fruit respiration. The main role of TSS is in fruit flavour, and thus, maintanance of TSS in fruit produce is associated with fulfillment of consumer expectations. Hasheminejad et al. also reported higher values of TSS in nanocomposite films as compared to pristine polymer films (Hasheminejad & Khodaiyan, 2020).

5.7.3 Titratable acidity (TA) and pH

The presence of organic acids determines the final taste of fruit. The acidity in apple occurs due to high maleic acid content in under-ripe fruit. The quantity of maleic acid decreases, as the fruit attains full-ripe stage (Ghoshal & Chopra, 2022). TA depends on packaging type and storage temperature. Fig. 5.10c shows TA of cut apples during storage period. For all composition TA decreased with increasing storage period. The lower value of TA indicates maturation of fruit. The results demonstrated that cut apples packaged with PCOH0.5 film had shown the lowest rate of decreasing acidity followed by PCOH0.25, PCOH1, PCO, PLA and PE film. The results suggest that presence of CEO and NHNT delayed the ripening process by providing a protective barrier around the fruit against O_2 transport. The degradation of sugar and organic acid consumption during storage period could be the reason for decrease value of TA. Based on these results, the cut apples packaged with PCOH0.5 films could significantly maintain higher value of TA as compared to PE and PLA at day 6. The lowest level of TA (0.132 %) was recorded in PE, while the highest levels of TA (0.281 %) was obtained from cut apples stored in PCOH0.5 after 6-day storage period. Therefore, PCOH0.5 is found to be the most effective nanocomposite film for food packaging.

The pH value of apple juice significantly increased in control (PE and PLA) and all nanocomposite films as depicted in Fig.5.10d. The initial pH of juice at day 0 for PE and PLA were 3.87, 3.89, respectively, which increased up to 4.08 and 4.09 on day 6. In case of nanocomposite films at 0 day the pH values were 3.89, 3.86, 3.90 and 3.90, which increased up to 4.02, 3.95, 3.97 and 4.04 for PCO, PCOH0.25, PCOH0.5 and PCOH1, respectively on day 6. The changes of pH values depend on metabolic activities and respiration rate of the fruit. The results showed that PCOH0.5 was the most effective packaging film in maintaining the change of pH during storage period. This might be due to the lower respiration rate of cut apples packaged in PCOH0.5, which result into lower metabolic activities. Moreover, incorporation of CEO into PLA could probably modify the pattern of fruit respiration by possible interaction of CEO with cell

membranes, which in turn affect the fruit metabolic pattern and senescence. It was observed that during fruit ripening process the titratable acidity (TA) decreased and pH increased. Sadler and Murphy (2010) have discussed that TA gives only an estimation of the total acid content present in a food product as food contains many acids that cannot be distinguished through titration. TA does not give an exact idea of pH, since pH is a shared function of both titratable acid and conjugate base (Sadler et al., 2010).

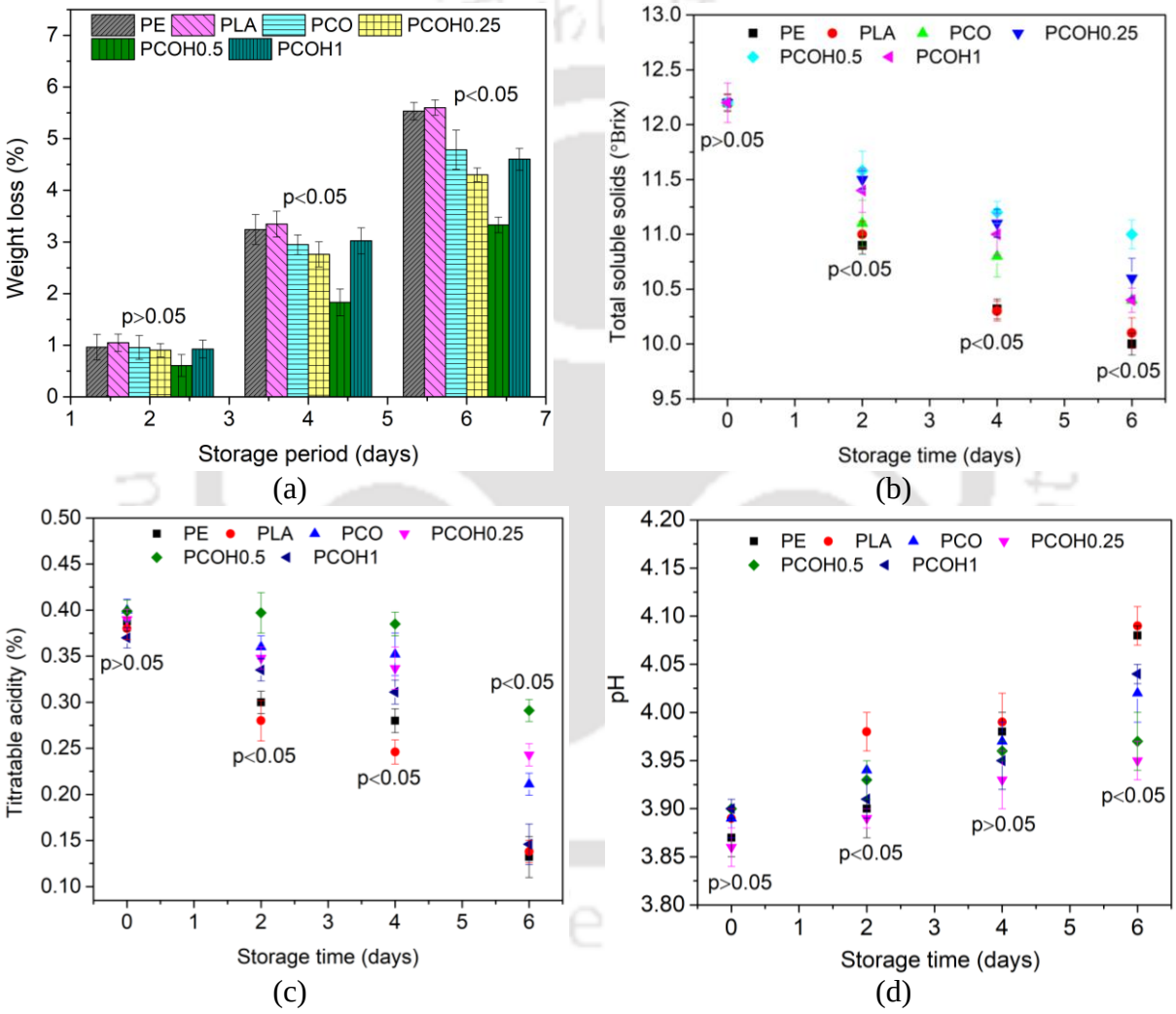

Fig. 5.10. Effect of PLA based nanocomposite films on (a) weight loss, (b) total soluble solids, (c) titratable acidity and (d) pH of cut apples stored for 6 days at room temperature. The results (n = 3) are represented as mean values ± standard deviation. The Tukey's test results of one-way ANOVA are given in appendix.

5.7.4 Fruit firmness

Firmness indicates the crispiness quality of fruits. It is an important parameter for consumer acceptability of the product. As shown in Fig. 5.11, the firmness of the cut apples decreases during storage period for all composite films. The weight loss that occurred during storage period causes the reduction in fruit firmness. The reduction in firmness (from day 0 to 6) of cut apples stored in packaging films were: PE = 2.73× (4.1 to 1.5 N), PLA = 3.5× (4.2 to 1.2 N), PCO = 2.56× (4.1 to 1.6 N), PCOH0.25 = 1.95× (4.1 to 2.1 N), PCOH0.5 = 1.62× (4.2 to 2.6 N) and PCOH1 = 2.47× (4.2 to 1.7 N). The results revealed that among all films, PCOH0.5 is the most efficient in maintaining the higher value of firmness during storage period. This might be due to tortuous path provided by NHNTs in nanocomposite film, which reduces the moisture loss from fruit. This finding was also supported by the low WVP value of PCOH0.5 as compared to PLA, PE and PCO as discussed in earlier section.

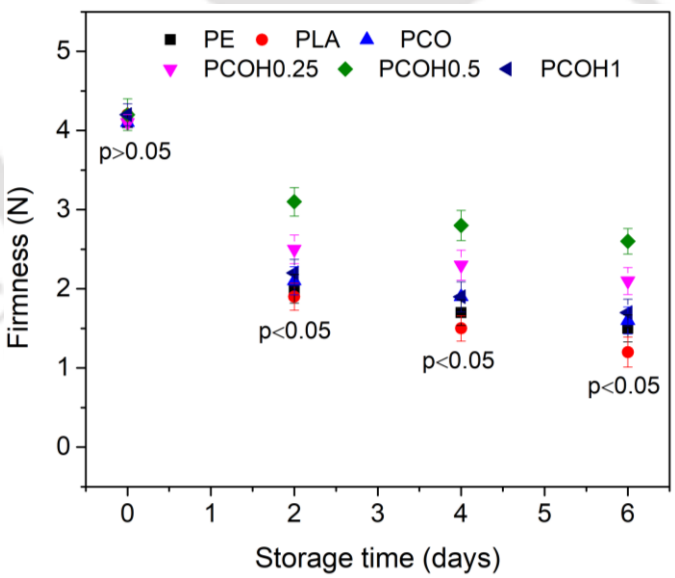

Fig. 5.11. Effect of PLA based nanocomposite films on firmness of cut apples stored at room temperature for 6 days. The results (n = 3) are represented as mean values ± standard deviation. The Tukey's test results of one-way ANOVA are given in appendix.

5.7.5 Microbial analysis

Microbial contamination is one of the main reasons for the spoilage, quality deterioration and unacceptability of vegetables and fruits. The microbial analysis of the stored and packaged cut apples was done in respect of aerobic mesophilic count. Fig. 5.12 and Fig. 5.13 show the total microbial count on fresh cut apples packaged with PLA, PE, PCO and nanocomposite films (PCOH0.25, PCOH0.5 and PCOH1) during the storage period. The total bacterial count gradually increased in all compositions during the storage period of 6 days. Initial bacterial count in control samples (PE and PLA) were 3.84 and 3.78 log (CFU/mL), which increased during storage period, reaching 5.77 and 5.58 log (CFU/mL), respectively, by day 6. Samples treated with PCO, PCOH0.25, PCOH0.5 and PCOH1 showed initial bacterial count of 3.3, 3.1, 3.0, 3.5 log (CFU/mL), which increased up to 5.52, 5.40, 5.36, and 5.48 log (CFU/mL) respectively. The results showed that the cut apples stored in PCOH0.5 films showed best antimicrobial properties as compared to others. This might be due to controlled release of CEO from nanocomposite films in the presence of NHNTs leading to better inhibitory effect.

Clove essential oil contains several bioactive components such as eugenol, eugenyl acetate, and β- caryophyllene etc. (Haro-González et al., 2021; Tarhan, 2021). The major component is eugenol (76%) which is primarily responsible for bacteriocidal activity (Lee et al., 2018; Lu et al., 2021). The interaction of bioactive components of CEO with cell wall and cell membrane causes structural damage by alteration of phospholipids and proteins in bacterial cells. After destruction of cell wall and membrane, CEO penetrates into the cytoplasm of bacterial cells and inhibits the function of DNA and protein synthesis necessary for the cell growth, which leads to the cell death (Arfat et al., 2018; Qin et al., 2017). Table 5.5 shows the comparison of the results of present study against previous literature on poly(lactic acid) based composites containing various essential oils and nanoparticles mainly for food packaging applications.

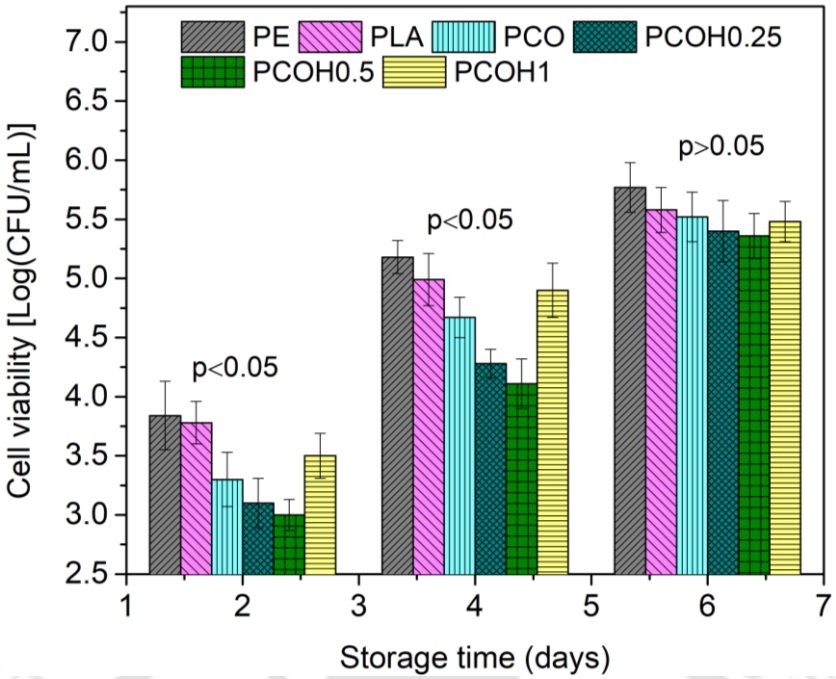

Fig. 5.12. Effect of different PLA based packaging films on total mesophilic count of cut apples stored at room temperature for 6 days. The results (n = 3) are represented as mean values ± standard deviation. The Tukey's test results of one-way ANOVA are given in appendix.

Days	PE	PLA	PCO	PCOH0.5
2	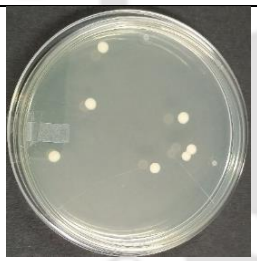	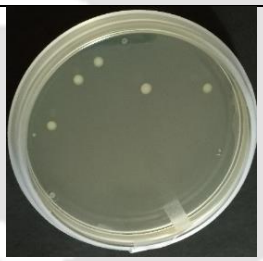	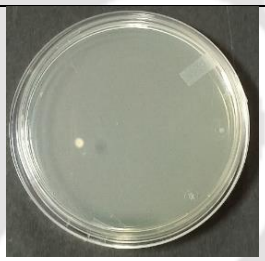	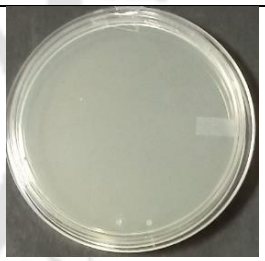
4	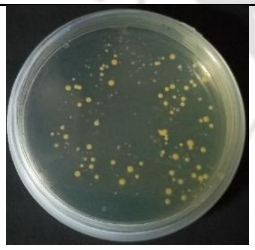	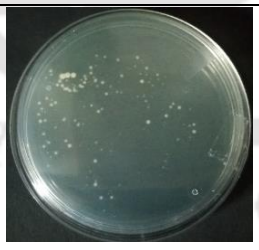		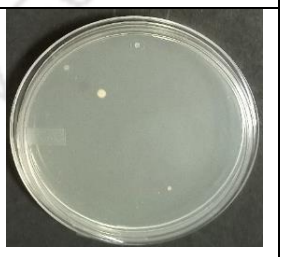
6	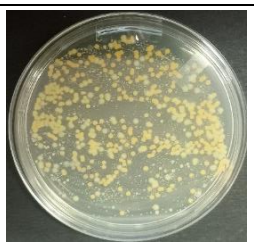	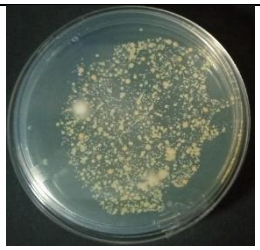		

Fig. 5.13. Photographs of spread plate method

Table 5.5. Literature comparison on PLA based biocomposites for food packaging applications

Components	Properties	Ref.
PLA/bergamot/TiO_2/Ag NPs	Reduction in weight loss by 44.6%, firmness is higher for nanocomposite films after storage period (PLA: 96.1N, PLA/bergamot/TiO_2/Ag NPs: 122.8N)	(Chi et al., 2019) [9]
Polylactide/graphene oxide nanosheets/clove essential oil	TS decreases by 22.2%, EAB increases by 133.2%, antimicrobial property: 7 log reduction of *s. aureus* and 6 log reduction of *E. coli* in 7 days.	(Arfat et al., 2018) [18]
PLA/clove oil/mesoporous silica	TS and EM decreases by 72.7% and 61.9% respectively, EAB and WVP increases by 1080.8% and 56.2% respectively, good antimicrobial properties against *E. coli* and *S. aureus.*	(Lu et al., 2021) [23]
Poly(lactide)-poly(butylene adipate -co-tereaphthalate)/clove oil/thyme oil	Film containing clove oil has shown 80% increase in UV blocking efficiency, TS decreases by 28.9% (clove oil) and 41.5% (thyme oil); clove oil and thyme oil inhibited *E. coli* biofilm by 93.43% and 82.30%, respectively.	(Sharma et al., 2020) [26]
PLA/bergamot, PLA/lemongrass, PLA/rosemary, PLA/clove oil	TS and EM reduce in all compositions as compared to PLA. PLA/rosemary exhibits the highest TS (29.2 MPa) and EM (1556.1 MPa), PLA/bergamot possessed the highest ε value (155.4%).	(Qin et al., 2017) [27]
PLA/Fenugreek essential oil (FEO)/curcumin	Hydrophobicity and TS improve by 15.4% and 21.53%, respectively; reduction in CFU for *E. coli* (as compared to PE): 89.2% reduction in weight loss (as compared to PE): 24%.	(Subbuvel & Kavan, 2022) [45]
PLA/HNT	TS (56.5%) and EM (110%) increase while EAB (38%) reduces; water vapor permeability decreases (21%); reduction in firmness (PLA: 25%, PLA/HNT:16%); weight loss (PLA: 2.8%, PLA/HNT:1.9%)	(Risyon et al., 2020) [47]
Poly(lactic acid)/ZnO/Zataria multiflora L. (ZEO)/ Mentha piperita L. (MEO)	TS reduces by 63% (ZEO) and 66.1% (MEO), EM reduces by 29.6% (ZEO) and 37.2% (MEO), EAB increases by 417.7% (ZEO) and 390% (MEO).	(Heydari-Majd et al., 2019) [55]
PLA/CEO/NHNT (This study)	Enhancement in properties as compared to PLA: surface hydrophobicity (20.2%), water vapor barrier (42.1%), EAB (682%), TS (20%), EM (38%), UV barrier property (62%), reduction in weight loss (40.5%) and mesophilic count (4.0%)	

[Note: TS = Tensile strength, EM = Elastic modulus, EAB = Elongation at break]

5.8 Conclusions

In this study PLA based nanocomposite films with alkali treated HNT and CEO were synthesized with solution casting method and various functional properties were assessed. The incorporation CEO and NHNT improved the surface hydrophobicity, water vapor barrier properties, thermal stability and mechanical properties (mainly elongation at break) of the PLA based nanocomposite films. The addition of 0.5 wt% of NHNT to PLA/CEO was found to be the optimum loading that provides best properties in terms of water vapor barrier, thermal properties among all other concentration of NHNT (0.25 and 0.5 wt%). The packaging results indicated that storage of cut apples for 6 days inside the pouches prepared from nanocomposites films delayed weight loss and retained firmness of the cut apples. Overall, the incorporation of NHNT and CEO in PLA matrix not only improves the physio-chemical properties but also impart antimicrobial properties which enhances the shelf life of the fruit. This study has thus demonstrated the potential of PLA films synthesized with functional filler NHNT and bioactive agent CEO for food packaging applications.

References

Acosta, S., Chiralt, A., Santamarina, P., Rosello, J., González-Martínez, C., & Cháfer, M. (2016). Antifungal films based on starch-gelatin blend, containing essential oils. *Food Hydrocolloids*, *61*, 233–240. https://doi.org/10.1016/j.foodhyd.2016.05.008

Akbari, V., Najafi, F., Vahabi, H., Jouyandeh, M., Badawi, M., Morisset, S., Ganjali, M. R., & Saeb, M. R. (2019). Surface chemistry of halloysite nanotubes controls the curability of low filled epoxy nanocomposites. *Progress in Organic Coatings*, *135*, 555–564. https://doi.org/10.1016/j.porgcoat.2019.06.009

Alizadeh-Sani, M., Moghaddas Kia, E., Ghasempour, Z., & Ehsani, A. (2021). Preparation of Active Nanocomposite Film Consisting of Sodium Caseinate, ZnO Nanoparticles and Rosemary Essential Oil for Food Packaging Applications. *Journal of Polymers and the Environment*, *29*(2), 588–598. https://doi.org/10.1007/s10924-020-01906-5

Arfat, Y. A., Ahmed, J., Ejaz, M., & Mullah, M. (2018). Polylactide/graphene oxide nanosheets/clove essential oil composite films for potential food packaging applications. *International Journal of Biological Macromolecules*, *107*, 194–203. https://doi.org/10.1016/j.ijbiomac.2017.08.156

Bao, Y., Gao, L., Feng, C., Ma, J., Zhang, W., Liu, C., & Simion, D. (2020). Sonochemical synthesis of flower-like ZnO assembled by hollow cones toward water vapor permeability and water resistance enhancement of waterborne film. *Journal of Industrial and Engineering Chemistry*, *82*, 180–189. https://doi.org/10.1016/j.jiec.2019.10.011

Batool, M., Abid, A., Khurshid, S., Bashir, T., Ismail, M. A., Razaq, M. A., & jamil, M. (2022). Quality Control of Nano-food Packing Material for Grapes (Vitis vinifera) Based on ZnO and Polylactic Acid (PLA) biofilm. *Arabian Journal for Science and Engineering*, *47*(1), 319–331. https://doi.org/10.1007/s13369-021-05361-9

Bhat, V. G., Narasagoudr, S. S., Masti, S. P., Chougale, R. B., & Shanbhag, Y. (2021). Hydroxy citric acid cross-linked chitosan/guar gum/poly(vinyl alcohol) active films for food

packaging applications. *International Journal of Biological Macromolecules*, *177*, 166–175. https://doi.org/10.1016/j.ijbiomac.2021.02.109

Boonsiriwit, A., Xiao, Y., Joung, J., Kim, M., Singh, S., & Lee, Y. S. (2020). Alkaline halloysite nanotubes/low density polyethylene nanocomposite films with increased ethylene absorption capacity: Applications in cherry tomato packaging. *Food Packaging and Shelf Life*, *25*, 100533. https://doi.org/10.1016/j.fpsl.2020.100533

Chaieb, K., Hajlaoui, H., Zmantar, T., Kahla-Nakbi, A. B., Rouabhia, M., Mahdouani, K., & Bakhrouf, A. (2007). The chemical composition and biological activity of clove essential oil, Eugenia caryophyllata (Syzigium aromaticum L. Myrtaceae): A short review. *Phytotherapy Research*, *21*(6), 501–506. https://doi.org/10.1002/ptr.2124

Chen, X., Ren, L., Li, M., Qian, J., Fan, J., & Du, B. (2017). Effects of clove essential oil and eugenol on quality and browning control of fresh-cut lettuce. *Food Chemistry*, *214*, 432–439. https://doi.org/10.1016/j.foodchem.2016.07.101

Chi, H., Song, S., Luo, M., Zhang, C., Li, W., Li, L., & Qin, Y. (2019). Effect of PLA nanocomposite films containing bergamot essential oil, TiO2 nanoparticles, and Ag nanoparticles on shelf life of mangoes. *Scientia Horticulturae*, *249*, 192–198. https://doi.org/10.1016/j.scienta.2019.01.059

Chu, Z., Zhao, T., Li, L., Fan, J., & Qin, Y. (2017). Characterization of Antimicrobial Poly (Lactic Acid)/Nano-Composite Films with Silver and Zinc Oxide Nanoparticles. *Materials*, *10*(6), Article 6. https://doi.org/10.3390/ma10060659

Cui, R., Zhu, B., Yan, J., Qin, Y., Yuan, M., Cheng, G., & Yuan, M. (2021). Development of a Sodium Alginate-Based Active Package with Controlled Release of Cinnamaldehyde Loaded on Halloysite Nanotubes. *Foods*, *10*(6), Article 6. https://doi.org/10.3390/foods10061150

De Silva, R., Pasbakhsh, P., Goh, K., Chai, S.-P., & Chen, J. (2014). Synthesis and characterisation of poly (lactic acid)/halloysite bionanocomposite films. *Journal of Composite Materials*, *48*(30), 3705–3717. https://doi.org/10.1177/0021998313513046

Falleh, H., Ben Jemaa, M., Saada, M., & Ksouri, R. (2020). Essential oils: A promising eco-friendly food preservative. *Food Chemistry*, *330*, 127268. https://doi.org/10.1016/j.foodchem.2020.127268

Gasti, T., Dixit, S., Hiremani, V. D., Chougale, R. B., Masti, S. P., Vootla, S. K., & Mudigoudra, B. S. (2022). Chitosan/pullulan based films incorporated with clove essential oil loaded chitosan-ZnO hybrid nanoparticles for active food packaging. *Carbohydrate Polymers*, *277*, 118866. https://doi.org/10.1016/j.carbpol.2021.118866

Ghoshal, G., & Chopra, H. (2022). Impact of apricot oil incorporation in tamarind starch/gelatin based edible coating on shelf life of grape fruit. *Journal of Food Measurement and Characterization*, *16*(2), 1274–1290. https://doi.org/10.1007/s11694-021-01234-9

Hadidi, M., Jafarzadeh, S., Forough, M., Garavand, F., Alizadeh, S., Salehabadi, A., Khaneghah, A. M., & Jafari, S. M. (2022). Plant protein-based food packaging films; recent advances in fabrication, characterization, and applications. *Trends in Food Science & Technology*, *120*, 154–173. https://doi.org/10.1016/j.tifs.2022.01.013

Haro-González, J. N., Castillo-Herrera, G. A., Martínez-Velázquez, M., & Espinosa-Andrews, H. (2021). Clove Essential Oil (Syzygium aromaticum L. Myrtaceae): Extraction, Chemical Composition, Food Applications, and Essential Bioactivity for Human Health. *Molecules*, *26*(21), Article 21. https://doi.org/10.3390/molecules26216387

Hasheminejad, N., & Khodaiyan, F. (2020). The effect of clove essential oil loaded chitosan nanoparticles on the shelf life and quality of pomegranate arils. *Food Chemistry*, *309*, 125520. https://doi.org/10.1016/j.foodchem.2019.125520

Heydari-Majd, M., Ghanbarzadeh, B., Shahidi-Noghabi, M., Najafi, M. A., & Hosseini, M. (2019). A new active nanocomposite film based on PLA/ZnO nanoparticle/essential oils

for the preservation of refrigerated Otolithes ruber fillets. *Food Packaging and Shelf Life*, *19*, 94–103. https://doi.org/10.1016/j.fpsl.2018.12.002

Javaherzadeh, R., Tabatabaee Bafroee, A. S., & Kanjari, A. (2020). Preservation effect of Polylophium involucratum essential oil incorporated poly lactic acid/ nanochitosan composite film on shelf life and sensory properties of chicken fillets at refrigeration temperature. *LWT*, *118*, 108783. https://doi.org/10.1016/j.lwt.2019.108783

Lee, M. H., Kim, S. Y., & Park, H. J. (2018). Effect of halloysite nanoclay on the physical, mechanical, and antioxidant properties of chitosan films incorporated with clove essential oil. *Food Hydrocolloids*, *84*, 58–67. https://doi.org/10.1016/j.foodhyd.2018.05.048

Lee, M. H., Seo, H.-S., & Park, H. J. (2017). Thyme Oil Encapsulated in Halloysite Nanotubes for Antimicrobial Packaging System. *Journal of Food Science*, *82*(4), 922–932. https://doi.org/10.1111/1750-3841.13675

Li, L., Fan, H., Wang, L., & Jin, Z. (2016). Does halloysite behave like an inert carrier for doxorubicin? *RSC Advances*, *6*(59), 54193–54201. https://doi.org/10.1039/C6RA09198A

Liu, M., Zhang, Y., & Zhou, C. (2013). Nanocomposites of halloysite and polylactide. *Applied Clay Science*, *75–76*, 52–59. https://doi.org/10.1016/j.clay.2013.02.019

Liu, Y., Ahmed, S., Sameen, D. E., Wang, Y., Lu, R., Dai, J., Li, S., & Qin, W. (2021). A review of cellulose and its derivatives in biopolymer-based for food packaging application. *Trends in Food Science & Technology*, *112*, 532–546. https://doi.org/10.1016/j.tifs.2021.04.016

Liu, Y., Wang, S., Zhang, R., Lan, W., & Qin, W. (2017). Development of Poly(lactic acid)/Chitosan Fibers Loaded with Essential Oil for Antimicrobial Applications. *Nanomaterials*, *7*(7), Article 7. https://doi.org/10.3390/nano7070194

Lu, W., Cui, R., Zhu, B., Qin, Y., Cheng, G., Li, L., & Yuan, M. (2021). Influence of clove essential oil immobilized in mesoporous silica nanoparticles on the functional properties

of poly(lactic acid) biocomposite food packaging film. *Journal of Materials Research and Technology*, *11*, 1152–1161. https://doi.org/10.1016/j.jmrt.2021.01.098

Lun, H., Ouyang, J., & Yang, H. (2014). Natural halloysite nanotubes modified as an aspirin carrier. *RSC Advances*, *4*(83), 44197–44202. https://doi.org/10.1039/C4RA09006C

Mohamad, N., Mazlan, M. M., Tawakkal, I. S. M. A., Talib, R. A., Kian, L. K., Fouad, H., & Jawaid, M. (2020). Development of active agents filled polylactic acid films for food packaging application. *International Journal of Biological Macromolecules*, *163*, 1451–1457. https://doi.org/10.1016/j.ijbiomac.2020.07.209

Mulla, M., Ahmed, J., Al-Attar, H., Castro-Aguirre, E., Arfat, Y. A., & Auras, R. (2017). Antimicrobial efficacy of clove essential oil infused into chemically modified LLDPE film for chicken meat packaging. *Food Control*, *73*, 663–671. https://doi.org/10.1016/j.foodcont.2016.09.018

Mulla, M. Z., Rahman, M. R. T., Marcos, B., Tiwari, B., & Pathania, S. (2021). Poly Lactic Acid (PLA) Nanocomposites: Effect of Inorganic Nanoparticles Reinforcement on Its Performance and Food Packaging Applications. *Molecules*, *26*(7), Article 7. https://doi.org/10.3390/molecules26071967

Popa, M. S., Frone, A. N., & Panaitescu, D. M. (2022). Polyhydroxybutyrate blends: A solution for biodegradable packaging? *International Journal of Biological Macromolecules*, *207*, 263–277. https://doi.org/10.1016/j.ijbiomac.2022.02.185

Punia Bangar, S., Whiteside, W. S., Ozogul, F., Dunno, K. D., Cavender, G. A., & Dawson, P. (2022). Development of starch-based films reinforced with cellulosic nanocrystals and essential oil to extend the shelf life of red grapes. *Food Bioscience*, *47*, 101621. https://doi.org/10.1016/j.fbio.2022.101621

Qin, Y., Li, W., Liu, D., Yuan, M., & Li, L. (2017). Development of active packaging film made from poly (lactic acid) incorporated essential oil. *Progress in Organic Coatings*, *103*, 76–82. https://doi.org/10.1016/j.porgcoat.2016.10.017

Riaz, A., Lei, S., Akhtar, H. M. S., Wan, P., Chen, D., Jabbar, S., Abid, M., Hashim, M. M., & Zeng, X. (2018). Preparation and characterization of chitosan-based antimicrobial active food packaging film incorporated with apple peel polyphenols. *International Journal of Biological Macromolecules*, *114*, 547–555. https://doi.org/10.1016/j.ijbiomac.2018.03.126

Risyon, N. P., Othman, S. H., Basha, R. K., & Talib, R. A. (2020). Characterization of polylactic acid/halloysite nanotubes bionanocomposite films for food packaging. *Food Packaging and Shelf Life*, *23*, 100450. https://doi.org/10.1016/j.fpsl.2019.100450

Saadat, S., Pandey, G., Tharmavaram, M., Braganza, V., & Rawtani, D. (2020). Nano-interfacial decoration of Halloysite Nanotubes for the development of antimicrobial nanocomposites. *Advances in Colloid and Interface Science*, *275*, 102063. https://doi.org/10.1016/j.cis.2019.102063

Sadeghi, A., Razavi, S. M. A., & Shahrampour, D. (2022). Fabrication and characterization of biodegradable active films with modified morphology based on polycaprolactone-polylactic acid-green tea extract. *International Journal of Biological Macromolecules*, *205*, 341–356. https://doi.org/10.1016/j.ijbiomac.2022.02.070

Sadler, G. D., & Murphy, P. A. (2010). pH and titratable acidity. In *Food analysis* (pp. 219-238). Springer, Boston, MA.

Saeed, K., Pasha, I., Jahangir Chughtai, M. F., Ali, Z., Bukhari, H., & Zuhair, M. (2022). Application of essential oils in food industry: Challenges and innovation. *Journal of Essential Oil Research*, *34*(2), 97–110. https://doi.org/10.1080/10412905.2022.2029776

Shankar, S., Kasapis, S., & Rhim, J.-W. (2018). Alginate-based nanocomposite films reinforced with halloysite nanotubes functionalized by alkali treatment and zinc oxide nanoparticles. *International Journal of Biological Macromolecules*, *118*, 1824–1832. https://doi.org/10.1016/j.ijbiomac.2018.07.026

Sharma, S., Barkauskaite, S., Duffy, B., Jaiswal, A. K., & Jaiswal, S. (2020). Characterization and Antimicrobial Activity of Biodegradable Active Packaging Enriched with Clove and Thyme Essential Oil for Food Packaging Application. *Foods*, *9*(8), Article 8. https://doi.org/10.3390/foods9081117

Sharma, S., Singh, A. A., Majumdar, A., & Butola, B. S. (2019). Tailoring the mechanical and thermal properties of polylactic acid-based bionanocomposite films using halloysite nanotubes and polyethylene glycol by solvent casting process. *Journal of Materials Science*, *54*(12), 8971–8983. https://doi.org/10.1007/s10853-019-03521-9

Subbuvel, M., & Kavan, P. (2022). Preparation and characterization of polylactic acid/fenugreek essential oil/curcumin composite films for food packaging applications. *International Journal of Biological Macromolecules*, *194*, 470–483. https://doi.org/10.1016/j.ijbiomac.2021.11.090

Tarhan, İ. (2021). A robust method for simultaneous quantification of eugenol, eugenyl acetate, and β-caryophyllene in clove essential oil by vibrational spectroscopy. *Phytochemistry*, *191*, 112928. https://doi.org/10.1016/j.phytochem.2021.112928

Vergis, J., Gokulakrishnan, P., Agarwal, R. K., & Kumar, A. (2015). Essential Oils as Natural Food Antimicrobial Agents: A Review. *Critical Reviews in Food Science and Nutrition*, *55*(10), 1320–1323. https://doi.org/10.1080/10408398.2012.692127

Vianna, T. C., Marinho, C. O., Marangoni Júnior, L., Ibrahim, S. A., & Vieira, R. P. (2021). Essential oils as additives in active starch-based food packaging films: A review. *International Journal of Biological Macromolecules*, *182*, 1803–1819. https://doi.org/10.1016/j.ijbiomac.2021.05.170

Villegas, C., Torres, A., Rios, M., Rojas, A., Romero, J., de Dicastillo, C. L., Valenzuela, X., Galotto, M. J., & Guarda, A. (2017). Supercritical impregnation of cinnamaldehyde into polylactic acid as a route to develop antibacterial food packaging materials. *Food Research International*, *99*, 650–659. https://doi.org/10.1016/j.foodres.2017.06.031

Wang, Q., Zhang, J., & Wang, A. (2013). Alkali activation of halloysite for adsorption and release of ofloxacin. *Applied Surface Science*, *287*, 54–61. https://doi.org/10.1016/j.apsusc.2013.09.057

Wei, Y., Liang, X., Wu, H., Cen, J., & Ji, Y. (2021). Efficient phosphate removal by dendrite-like halloysite-zinc oxide nanocomposites prepared via noncovalent hybridization. *Applied Clay Science*, *213*, 106232. https://doi.org/10.1016/j.clay.2021.106232

Yadav, S., Mehrotra, G. K., Bhartiya, P., Singh, A., & Dutta, P. K. (2020). Preparation, physicochemical and biological evaluation of quercetin based chitosan-gelatin film for food packaging. *Carbohydrate Polymers*, *227*, 115348. https://doi.org/10.1016/j.carbpol.2019.115348

Yuan, P., Tan, D., & Annabi-Bergaya, F. (2015). Properties and applications of halloysite nanotubes: Recent research advances and future prospects. *Applied Clay Science*, *112–113*, 75–93. https://doi.org/10.1016/j.clay.2015.05.001

CHAPTER 6

Conclusions and scope for future work

These chapter summarizes the major findings of the present research work and also provides the directions for future perspectives in the field of antimicrobial bio-based polymer nanocomposites for food packaging applications.

6.1. Conclusions

This thesis has presented the investigation in synthesis of PLA based nanocomposite films with antimicrobial properties for potential food packaging applications by incorporating different nanofillers (ZnO nanoflowers, functionalized ZnO, ZnO@HNT, HNT/clove essential oil). These nanocomposite films have been extensively characterized using standard techniques to determine their physiochemical properties. The synthesized nanocomposite films possess enhanced functional properties as compared to pristine PLA. The overall conclusions drawn from the major findings of the entire PhD work is shown in Table 6.1.

Table 6.1. Film properties of all the prepared PLA based bionanocomposites

Nanocomposites	Properties
PLA/flower shaped ZnO	PZ0.5 (0.5 wt% of ZnO) showed best properties: Increment as compared to PLA → tensile strength = 22%, percentage elongation = 62%, highest degradation temperature = 298 ℃, glass transition temperature = 52 ℃, reduction in UV transmittance (absorption edge 368 nm) = 95%. Moreover, it possesses excellent antimicrobial properties with >99 % reduction of both gram negative and gram positive bacteria (*Escherichia coli* and *Listeria. monocytogenes*) in just 12 to 18 h.
PLA/f-ZnO	In nanocomposites filled with ZnO and functionalized ZnO, highest tensile strength and elongation at break was obtained for PZF2 (TS = 42.7 MPa, EB = 5.7%). Nanocomposite films have excellent UV-barrier properties (% Transmittance for PZF2: 59% at 400 nm). The WCA of the neat PLA film was 65.4°, however, it increased significantly after formation of nanocomposite with pristine ZnO (WCA = 74.8°) and functionalized ZnO (WCA = 85.8°).
PLA/ZnO@HNT	The nanocomposite film PZH2 (consisting 2 wt% ZnO@HNT) showed the best properties with percentage increments over PLA as: surface hydrophobicity (16.5%), water vapor barrier (51.1%), flexibility (79.3%), tensile strength (38.9%), elastic modulus (507.1%), UV barrier property (95.3%), antimicrobial activity (R> 99%). The PZH2 films showed considerably improved results as follows: weight loss = 4.17%; total soluble solids = 10.9°Brix; firmness = 2.4 N; and pH = 4.0.
PLA/CEO/NHNT	Nanocomposite film PCOH0.5 (consisting 0.5 wt% NHNT and 200 µL CEO) possessed the best physical properties with percentage enhancements over PLA as: surface hydrophobicity (20.2%), water vapor barrier (42.1%), thermal stability (3.2%), flexibility (682%), tensile strength (20%), elastic modulus (38%), UV barrier property (62%). The PCOH0.5 films showed substantially improved results (as compared to PLA) as follows: weight loss (40.5%), mesophilic count (4.0%), firmness (116.6%), titratable acidity (110.8%), pH (2.9%) and total soluble solids (8.9%).

6.2. Scope for future work

- In current investigation, a simple ultrasound assisted solution casting method was used to prepare PLA based nanocomposites films for packaging applications. However, in order to realize the commercial potential of the current PLA based nanocomposite films, other processing technologies such as extrusion/blow/injection molding can be used.
- Application of developed nanocomposite packaging films on various food products including vegetables, dried foods etc. to check the effectivity of the films.
- Migration of nanoparticles on different food simulants can be studied for all synthesized nanocomposites.
- Biodegradation of the synthesized nanocomposites can be studied.
- In order to evaluate the environmental impact of PLA based active packaging as compared to other commercial packaging material (PET), life cycle assessment (LCA) can be conducted.

RESEARCH OUTPUTS

Publications from PhD work

1) **U. Boro**, A. Priyadarsini, V. S. Moholkar, Synthesis and characterization of poly (lactic acid)/clove essential oil/alkali-treated halloysite nanotubes composite films for food packaging applications, *International Journal of Biological Macromolecules*. 216 (2022) 927–939. https://doi.org/10.1016/j.ijbiomac.2022.07.209
2) **U. Boro**, N. Kashyap, V. S. Moholkar, Sonochemical Synthesis of Poly (lactic acid) Nanocomposites with ZnO Nanoflowers: Effect of Nanofiller Morphology on Physical Properties. *ACS Engineering Au*. 2 (2021) 46–60. https://doi.org/10.1021/acsengineeringau.1c00018
3) **U. Boro**, V. S. Moholkar, Antimicrobial Bionanocomposites of Poly (lactic acid)/ZnO Deposited Halloysite Nanotubes for Potential Food Packaging Applications. *Materials Today Communications*, (2022) 104787. https://doi.org/10.1016/j.mtcomm.2022.104787
4) U. Boro, V. S. Moholkar, Poly(lactic acid)/functionalized ZnO Nanocomposites for Antimicrobial Food Packaging Applications. (Under preparation)

Book Chapters

1) K. Ingtipi, **U. Boro**, V. S. Moholkar, Lignin in nanocomposite hydrogels. In *Micro and Nanolignin in Aqueous Dispersions and Polymers* 2022 (pp. 459–484). Elsevier. https://doi.org/10.1016/B978-0-12-823702-1.00002-5

Appendix

Table A1. Results of Tukey's test ($p<0.05$) (Physical properties of polymer nanocomposites). Letter 'S' indicate significant and 'NS' indicate Not significant.

Comparison	Tensile strength	Elastic Modulus	Elongation @break	WVP	Film thickness
PLA vs. PCO	S	NS	S	NS	NS
PLA vs. PCOH0.25	NS	S	S	S	S
PLA vs. PCOH0.5	S	S	S	S	S
PLA vs. PCOH1	NS	S	S	S	S
PCOH0.25 vs. PCOH0.5	NS	NS	NS	S	NS
PCOH0.5 vs. PCOH1	NS	S	S	NS	NS
PCOH0.25 vs. PCOH1	NS	S	S	NS	NS
PCO vs. PCOH0.25	NS	S	S	NS	NS
PCO vs. PCOH0.5	S	S	S	S	S
PCO vs. PCOH1	S	S	S	S	S

Table A2. Results of Tukey's test ($p < 0.05$) (Packaging test results). Letter 'S' indicate significant and 'NS' indicate Not significant.

(a)Firmness and weight loss

Comparison	Firmness			Weight loss		
	2 days	4 days	6 days	2 days	4 days	6 days
PE vs. PCO	NS	NS	NS	NS	NS	S
PE vs. PCOH0.25	NS	S	S	NS	NS	S
PE vs. PCOH0.5	S	S	S	NS	S	S
PE vs. PCOH1	NS	NS	NS	NS	NS	S
PLA vs. PCO	NS	NS	S	NS	NS	S
PLA vs. PCOH0.25	NS	S	S	NS	S	S
PLA vs. PCOH0.5	S	S	S	NS	S	S
PLA vs. PCOH1	NS	NS	S	NS	NS	S
PCOH0.25 vs. PCOH0.5	S	S	S	NS	S	S
PCOH0.5 vs. PCOH1	S	S	S	NS	S	S
PCOH0.25 vs. PCOH1	NS	NS	S	NS	NS	NS
PCO vs. PCOH0.25	NS	NS	S	NS	NS	S
PCO vs. PCOH0.5	S	S	S	NS	S	S
PCO vs. PCOH1	NS	NS	NS	NS	NS	NS

(b) pH and total soluble solids (TSS)

Comparison	pH			TSS		
	2 days	4 days	6 days	2 days	4 days	6 days
PE vs. PCO	NS	NS	S	NS	S	S
PE vs. PCOH0.25	NS	NS	S	S	S	S
PE vs. PCOH0.5	NS	NS	S	S	S	S
PE vs. PCOH1	NS	NS	NS	S	S	S
PLA vs. PCO	NS	NS	S	NS	S	S
PLA vs. PCOH0.25	S	NS	S	S	S	S
PLA vs. PCOH0.5	S	NS	S	S	S	S
PLA vs. PCOH1	S	NS	NS	S	S	NS
PCOH0.25 vs. PCOH0.5	NS	NS	NS	NS	NS	S
PCOH0.5 vs. PCOH1	NS	NS	S	NS	NS	S
PCOH0.25 vs. PCOH1	NS	NS	S	NS	NS	NS
PCO vs. PCOH0.25	S	NS	S	S	NS	NS
PCO vs. PCOH0.5	NS	NS	NS	S	S	S
PCO vs. PCOH1	NS	NS	NS	NS	S	NS

(c) Titratable acidity (TA) and microbial analysis

Comparison	TA			Microbial analysis		
	2 days	4 days	6 days	2 days	4 days	6 days
PE vs. PCO	S	S	S	S	S	NS
PE vs. PCOH0.25	S	S	S	S	S	NS
PE vs. PCOH0.5	S	S	S	S	S	NS
PE vs. PCOH1	S	NS	NS	NS	NS	NS
PLA vs. PCO	S	S	S	NS	NS	NS
PLA vs. PCOH0.25	NS	S	S	S	S	NS
PLA vs. PCOH0.5	S	S	S	S	S	NS
PLA vs. PCOH1	S	S	NS	NS	S	NS
PCOH0.25 vs. PCOH0.5	S	S	S	NS	NS	NS
PCOH0.5 vs. PCOH1	S	S	S	S	S	NS
PCOH0.25 vs. PCOH1	NS	NS	S	NS	S	NS
PCO vs. PCOH0.25	NS	NS	NS	S	NS	NS
PCO vs. PCOH0.5	S	S	S	NS	S	NS
PCO vs. PCOH1	NS	NS	S	NS	NS	NS